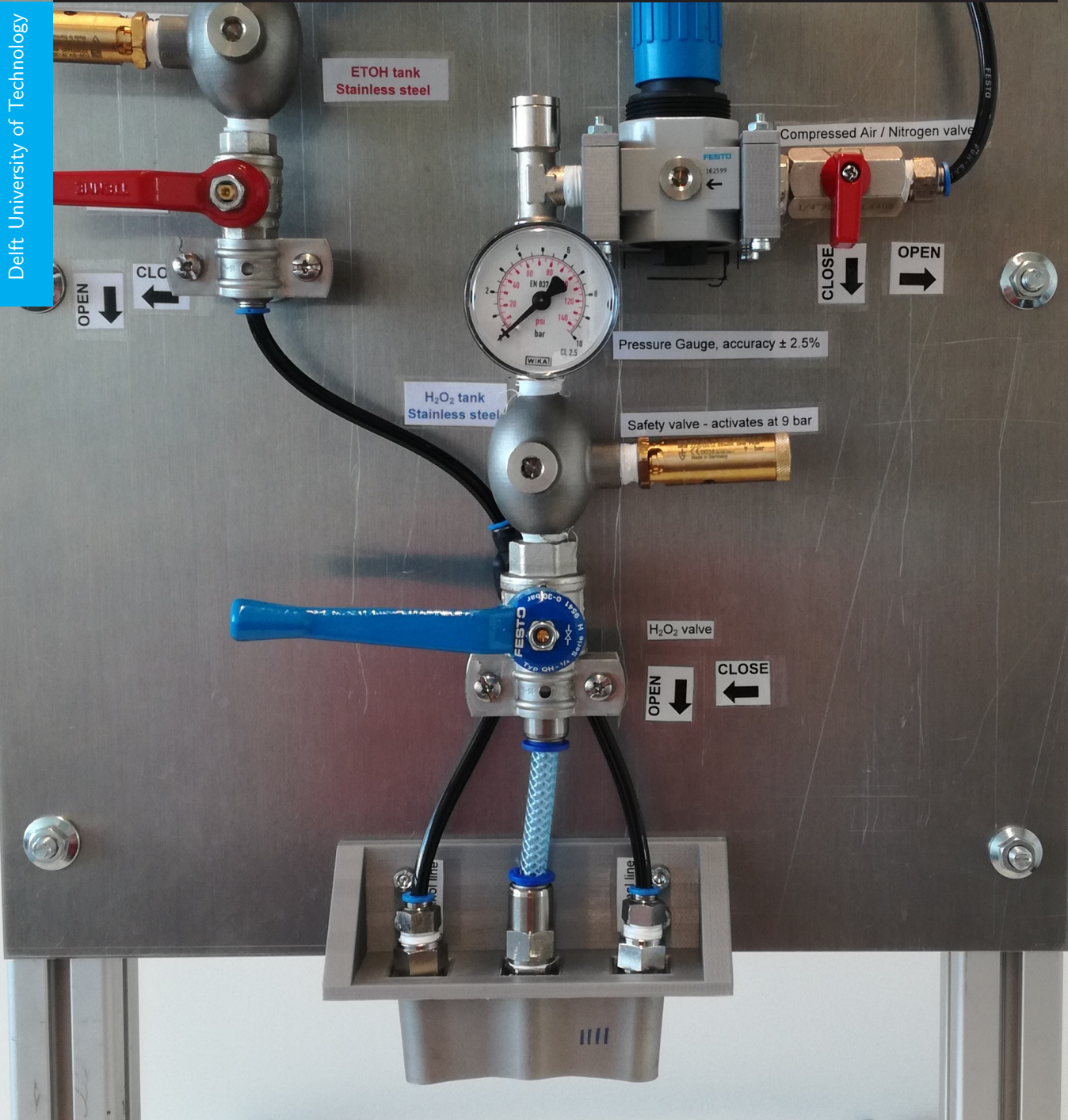


The design and testing of an injector for an advanced hypergolic dual-mode propulsion system

T. Borsboom 4289463

Date of Delivery April 28, 2021
Supervisors Jyoti Botchu Vara Siva

Delft University of Technology



The design and testing of an injector for an advanced hypergolic dual-mode propulsion system

Tommy Borsboom

CONFIDENTIAL

under embargo until 18-05-2022

This report is written to obtain a MSC degree in Aerospace Engineering from the Delft University of Technology. The thesis was conducted at SolvGE and was started on 1 September 2020 and completed at 18 May 2021. SolvGE is investigating a new hypergolic propellant combination, which can replace the current toxic propellant combinations. The goal of this thesis was to develop and test a dual-mode injector. This is the first hardware of a propulsion system that uses this new propellant combination.

Per ardua ad astra

Student number: 4289463
Thesis committee: Dr. B. V. S. Jyoti, TU Delft, supervisor
Prof. dr. E.K.A. Gill, TU Delft, chair
Ir. R. Noomen, TU Delft, external examiner

PREFACE

This report is written as part of the thesis for the master track Spaceflight with the profile Space Engineering of the Delft University of Technology. The thesis started on 1 September 2020 and is completed on 18 May 2021. The company SolvGE offered me the opportunity to get more experience in the design and testing process of a novel injector for a liquid propulsion system.

This report is intended for readers that are interested in the design and testing of an injector for a new hypergolic innovative propulsion system. A basic understanding of rocket propulsion is expected from the reader. For persons that are specifically interested in the design phase [Chapter 4](#) and [Chapter 5](#) are recommended. For those who are interested in the testing phase, [Chapter 6](#) and [Chapter 7](#) are recommended.

The results obtained during this thesis would not have been possible without a number of people. In no particular order, these are B.V.S. Jyoti for her excellent supervising and sharing her own experiences, the employees of the external company who has helped me to realize the different configuration of the injector and provide better understanding of the additive manufacturing process. Also I would like to thank D.P. Mainali Sharma for helping me in the lab and Jaime, Pranav, Pim and Nico who have contributed to the nice atmosphere at SolvGE. Not to be forgotten, I would also like to thank my friends, Ilse, William and Pepijn. They have always helped me with my challenges and provided the welcome distraction in these challenging COVID-19 times.

Delft April 2021
Tommy Borsboom

SUMMARY

The project aims to develop the injector of an advanced hypergolic propulsion system. A hypergolic propulsion system has several benefits. The most important benefit is the increased reliability due to the absence of an igniter system. The current hypergolic propellants are toxic, which is a large drawback. These toxic propellants are going to be banned and the space industry is looking for an alternative. An initial study has shown that hydrogen peroxide can be decomposed with thermal energy and can be used as a monopropellant. The decomposed products of hydrogen peroxide can also be ignited with ethanol, and thus having pseudo hypergolic propulsion behavior. This report focuses on the design and testing of an injector for this new propellant combination and is the next step in the investigation of an advanced hypergolic propulsion system.

Two injector types are selected for the injector design for an advanced hypergolic propulsion system to prevent typical problems associated with the dual-mode operation. To atomize the hydrogen peroxide, a swirl injector type is chosen because of the large spray angle. A large spray angle is required to optimize the use of a heating element. Hydrogen peroxide is the working liquid for the mono and dual-mode. To atomize the ethanol, a jet injector type injector was chosen and is only used for the dual-mode operation. The jet injector type ensures the injection of ethanol at the specific position, as required for the dual-mode operation. The dimensions of the injectors are optimized regarding the mass flow, SMD, and pressure drop. The injector was produced using additive manufacturing method. An external company offered to manufacture the different injector designs. This manufacturing method has many benefits, but several changes are required to produce the injector designs. The internal geometry was simplified and the dimensions were altered to provide more margin during the manufacturing process. The usage of a support structure is limited. In the initial design, a tolerance of ± 0.05 mm was required. However, this cannot be achieved with this manufacturing method since only a tolerance of ± 0.1 mm could be achieved. In total 4 configurations with the same swirl injectors and different jet injectors are designed to investigate the mixing process.

Several tests are conducted to validate the design and investigate the atomization behavior. A new test setup was made since the existing test setup did not meet the requirements of the desired mass flow and level of pressurization. The test setup used a pressure feed system to supply the propellant to the injectors. The designed test setup consists of a pressure regulator, tanks, and ball valves to control the propellant and pressurant gas. Compressed air is used as pressurant gas, due to the availability of compressed air and desired outlet pressure.

The literature described the different mechanism that occurs at an injector to form droplets that help the mixing and ignition process. A distinction was made between a sheet of liquid and a jet of liquid. For a sheet of liquid three mechanisms were identified: perforation, circumferential waves, and disintegration. For a jet of liquid also three mechanisms were described: axis-symmetric waves, asymmetric waves, and short waves. Deionized water is used as a working liquid for the first test to investigate the atomization behavior of the swirl and jet injector. A high-speed camera was used to capture this behavior. Observing collected data, several mechanisms are recognized that can be explained with the theoretical background. The variation of the mechanism was caused by a varying injection velocity, which is caused by pressure variations. The SMD and spray angle were investigated using hydrogen peroxide as working liquid for the swirl injector. The two observed patterns had an SMD of 0.4 mm, for an initial tank pressure of 3 bar. The SMD was underestimated by factor 5 during the design process. The pressure is increased to 7 bar and resulted in an SMD of 0.4 mm. A decrease in SMD was expected at an increase in the initial tank pressure. It is noticed that the injection velocity of the swirl injector was increased at an increase of pressure. However, this increase in injection velocity is not sufficient to decrease the SMD. The jet injector does not show the formation of droplets in the given resolution. The third test investigated the position of the mixing process. From this test, it was noticed that the pressure did not affect the mixing location. The inclination of the jet injectors did affect the mixing location. It is noticed that the droplets of the swirl and jet injector did not affect the atomization process of both injectors. Configuration 4 of the injectors had an inclined jet injector and led to the smallest combustion length. This configuration is used for further testing. The fourth test focused on the heating element. Three different configurations of heating elements were tested. According to the test results, the heating element configuration that had the most horizontal elements led to the best performance. The heating element is also used to improve the atomization process of the jet injector. A current of 2.5 A is required to evaporate the droplets of the swirl injector.

It is recommended to investigate means to achieve tighter tolerances so that the requirements of the SMD can be met. Also, the heating element can be modified that to optimize the supply of thermal energy and to aid the atomization process of the jet injector. Additionally, a testing location should be found where a hot firing test can be conducted. The test setup should be modified to include solenoid valves to accommodate the new testing location.

In conclusion, an injector that consists of a swirl injector with inclined jet injectors is the preferred configuration, because this leads to the shortest mixing distance and combustion chamber. The outlet diameter of the swirl injector is 1.6 mm and the swirl chamber diameter is 8.4 mm. The outlet diameter of the jet injector is 0.9 mm. The injectors are placed in a 5-degree inclination. This injector configuration was successfully tested to operate in mono and dual-mode operation with a heating element.

CONTENTS

Preface	v
Summary	vii
List of Figures.....	xi
List of Tables.....	xv
List of Symbols	xvii
List of Abbreviations.....	xix
1 Introduction.....	1
2 Theoretical atomization process.....	3
2.1 Atomization process in rocket engine	3
2.2 Jet atomization	4
2.3 Sheet atomization	5
2.4 Dimensionless criteria	5
2.5 Second disintegration and collision	7
3 Requirements	9
4 Initial design	11
4.1 Selection design options	11
4.1.1 Swirl injector selection	11
4.1.2 Jet injector selection	12
4.1.3 Material selection	12
4.1.4 Configurations	12
4.2 Design process	13
4.2.1 Swirl injector design	13
4.2.2 Jet injector design	16
4.3 Determining design parameters	17
4.3.1 Swirl injector design	18
4.3.2 Jet injector design	20
4.3.3 Connection swirl and jet injectors	21
4.3.4 Wall thickness	21
4.3.5 Tolerances	22
4.4 Hard start	22
4.5 Cooling	23
4.5.1 Methods of cooling	23
4.5.2 Film cooling	23
4.5.3 Incorporation injector design	23
4.6 Conclusion	24
5 Prototype design.....	27
5.1 Additive Manufacturing	27
5.1.1 Additive manufacturing for rocket propulsion	27
5.1.2 Power bed based manufacturing process	27
5.2 Alternation for the manufacturing method	28
5.3 Iterated design	29
5.3.1 Simplified internal geometry	29
5.3.2 Cross-section tubing	30
5.3.3 Connection swirl and jet injector	30
5.3.4 Geometric dimensions	30
5.3.5 Tolerances	31
5.4 Structural integrity	34
5.5 Manufacturing	35
5.6 Conclusion	36
6 Test setup	39
6.1 Existing test setups	39
6.1.1 Syringe pump	39
6.1.2 Pressurized propellant feed system	40
6.2 Design of propellant tanks	40
6.3 Selecting the pressurant gas	41
6.4 Test setup design	42
6.4.1 Diagram of test setup	42
6.4.2 Tubing	43
6.4.3 Pressure gauge	43
6.4.4 Pressure regulator	43
6.4.5 Safety valves	44
6.4.6 Threads	44
6.4.7 Test stand	44
6.4.8 Assembling	45

6.4.9	Overview test setup	46
6.5	Heating element	48
6.6	Safety	48
6.7	Conclusion	49
7	Experiments	51
7.1	Pressure differences	51
7.2	Atomized behaviour test	52
7.2.1	Swirl injector	52
7.2.2	Single jet injector	55
7.2.3	Comparison jet injectors different configurations	61
7.3	Atomized performance test	63
7.3.1	Swirl injector	63
7.3.2	Jet injector	68
7.4	Mixing test	72
7.4.1	Overview	72
7.4.2	Interaction jet and swirl	74
7.5	Heating element test	76
7.5.1	Mono propellant mode	76
7.5.2	Dual propellant mode	78
7.5.3	Electrical power	79
7.6	Conclusion	80
8	Conclusion and Recommendations	83
8.1	Conclusion	83
8.2	Recommendation	84
	Bibliography	87
A	Detailed calculations initial design	89
A.1	Detailed calculations swirl injector	89
A.2	Detailed calculations Jet injector configuration 2	91
B	Technical drawings	93
B.1	Initial design- configuration 1	93
B.2	Initial design- configuration 2	94
B.3	Initial design- configuration 3	95
B.4	Initial design- configuration 4	96
B.5	Prototype design- configuration 1	97
B.6	Prototype design- configuration 2	98
B.7	Prototype design- configuration 3	99
B.8	Prototype design- configuration 4	100
C	Python scripts	101
C.1	Initial design	101
C.1.1	Swirl injector	101
C.1.2	Jet injector	104
C.2	Design graphs	106
C.2.1	Massflow, SMD and pressure drop	106
C.2.2	Spray angle as function of filling factor	110
C.3	Tolerances analyses	114
C.3.1	Tolerances swirl injector	114
C.3.2	Tolerances jet injector	116
D	Mixing locations	119
D.1	Configuration 1	119
D.2	Configuration 2	120
D.3	Configuration 3	121
D.4	Configuration 4	122
E	Test procedures	125
F	Overview conducted experiments	129
F1	Atomization behaviour	129
F2	Atomization performance	130
F3	Mixing process	130
F4	Heating element	132

LIST OF FIGURES

1.1	Example of a test anomaly during SpaceX crew Dragon where a toxic hydrazine cloud is formed [1]	1
2.1	Different zones in the liquid rocket engine [2]	3
2.2	Graphical example of the different scenario's for the disintergration process [2]	4
2.3	Graphical example of the different scenario's for the disintergration of a liquid sheet. [2]	5
2.4	Classeficiation of the different mechanism as function of Reynolds and Ohnesorge numbers [3]	6
2.5	Graphical example of a parachute type [3]	7
2.6	Different collision possibilities [3]	8
3.1	Context diagram of the injector	9
4.1	Schematic overview of the location of the heating element	11
4.2	A schematic overview of the <i>general</i> lay out of the different configurations	13
4.3	An overview of the geometry and associated dimensions of a swirl injector [2]	13
4.4	A flow chart of the design process of the swirl injector	16
4.5	An overview of the geometry and associated dimensions of a jet injector [2]	17
4.6	Visual pressure drop, mass flow and SMD and outlet diameter	18
4.7	Filling factor and spray angle	19
4.8	A schematic, not on scale, overview of the dimensions of the swirl injector	20
4.9	A schematic, not on scale, overview of the dimensions for the configuration 2 jet atomizer	20
4.10	Graphical overview of the connector, tube and inlet port	21
4.11	An example of the film cooling principle [4]	23
4.12	An example of the made adjusmtents to accomendate for slots for the film cooling [5]	24
4.13	An example of slots used by film cooling located at the combustion chamber [6]	24
4.14	An overview of the exterior of the injector	25
4.15	The cutaway of the Catia model of the swirl and a jet injector	25
4.16	3D printed model of the swirl injector to a 4:1 scale	25
5.1	Classifications additive manufacturing methods [7]	27
5.2	Power bed based manufacturing process explained [8]	28
5.3	Definition of the void	28
5.4	Schematical example of the cross-section and support structure	29
5.5	Schematic overview of the changes in tubing orientation	30
5.6	Overview of the made changes to the geometry	30
5.7	Schematic overview of the logic for the script to determine the effect of the tolerances	31
5.8	Schematic overview of the logic for the script to determine the effect of the tolerances	32
5.9	The structural analysis, performed by the external company, of the injector when an inlet pressure of 10 bar is applied	35
5.10	Injector defects during manufacturing process in detail	36
5.11	Injectors before processing	36
5.12	The new design for the prototype	37
6.1	Information of the syringe pump and the associated volume flow [9]	39
6.2	Schematic overview of the test setup, where 1 is the Nitrogen valve, 2 is the Pressure reductor, 3 is the Low pressure nitrogen tank, 4 is the HTPfilling valve, 5 is the Safety valve, 6 is the HTP filter, 7 is Injection valve, 8 is the heater, 9 is the decomposition chamber, 10 is the Power supply and 11 is Thrust measurement device [10]	40
6.3	Structural analysis of the tank design performed by the external company	41
6.4	Diagram overview of the test setup	43
6.5	Section of the test setup for the compressed air feed line	44
6.6	Tüv safety valve that is used for the test setu [11]	44
6.7	The constructed test stand, including bracket to mount the injector	45
6.8	A CATIA image of the designed brackets	45
6.9	Test setup after assemblage	46
6.10	Overview of the placement of the test setup, high speed camera and external light source	47
6.11	Clamping of the heating element	47

6.12	Example of the different heating element configurations	48
6.13	Example of the used insulation for the clamps to position the heating element	49
7.1	Overview of the different regions of the atomization process of the swirl injector for injector configuration 1	52
7.2	Example of the mechanism where perforations occur for the swirl injector	53
7.3	Example of the mechanism where circumferential waves occur for the swirl injector	53
7.4	Example of the end-phase of the atomization process for the swirl injector	54
7.5	Spray pattern of the swirl injector	54
7.6	The first pattern for all configurations	55
7.7	Extrapolated graph of the Oh and Weber numbers	56
7.8	Example of the beginning and end-phase of the start up of the jet injector	57
7.9	Example of the axis-symmetric waves defining atomization mechanism 2 for the jet injector	57
7.10	Example of the asymmetric waves defining atomization mechanism 3 for the jet injector	58
7.11	Example of the formation of a cloud	58
7.12	End-phase of the atomization process of the jet injector	59
7.13	Detail asymmetric waves of mechanism III of the jet injector	59
7.14	Detail of the mechanism 2 where axis symmetric waves are shown for the jet injector	60
7.15	Details of the formed cloud during the atomization process of the jet injector	60
7.16	Spray pattern of the two jet injectors of configuration 4	60
7.17	Comparison between the different jet injectors for mechanisms 2	61
7.18	Comparison between the different jet injectors for mechanisms 3	61
7.19	Comparison between the different jet injectors for the formation of clouds	62
7.20	Example of the occurrence of a cloud and s-pattern	62
7.21	Example of the spray pattern of the jet injectors	63
7.22	Example of the two patterns for the HTP atomized flow for the swirl injector of configuration 4	63
7.23	Example of the increased clarity of a frame by adjusting the contrast	64
7.24	Example of the made threshold of a detail of the selected frame	64
7.25	Example of the two patterns for the HTP atomized flow at 7 bars	66
7.26	Ethanol and deionized water comparison axisymmetric wave	68
7.27	Ethanol and deionized water comparison asymmetric wave	69
7.28	Ethanol and deionized water comparison cloud	69
7.29	Symmetric pattern different configurations	70
7.30	Asymmetric mechanism comparisons ethanol different injectors	70
7.31	Axis symmetric at an initial tank pressure of 3 and 7 bar	71
7.32	Asymmetric symmetric at an initial tank pressure of 3 and 7 bar	71
7.33	Example of the raw and improved footage	72
7.34	Distance mixing process as function of different initial tank pressures	73
7.35	Measured spray angle of the swirl injector for different pressures	74
7.36	Dual-mode for configuration 2 at an initial tank pressure 3 bar	74
7.37	Dual-mode for configuration 2 at an initial tank pressure of 5 and 7 bar	75
7.38	Dual-mode for configuration 3 and at an initial tank pressure of 7 bar	75
7.39	Example of the heating element before and after the atomization process using configuration 1 of the heating element	76
7.40	Example of the heating element that droplets are moving through the injector	77
7.41	Example of droplets moving through the heating element	77
7.42	Example of the dual mode operation with a heating element 1	78
7.43	Comparison of different heating elements for a dual mode	78
7.44	Comparison of different current levels	79
7.45	Droplet formation on heating element during atomization process	79
7.46	Example of dual-mode with a heating element connected electrical power	80
B.1	Technical drawing of configuration 1 of the initial design	93
B.2	Technical drawing of configuration 2 of the initial design	94
B.3	Technical drawing of configuration 3 of the initial design	95
B.4	Technical drawing of configuration 4 of the initial design	96
B.5	Technical drawing of configuration 1 of the prototype design	97
B.6	Technical drawing of configuration 2 of the prototype design	98
B.7	Technical drawing of configuration 3 of the prototype design	99
B.8	Technical drawing of configuration 4 of the prototype design	100
D.1	Configuration 1 at an initial pressure of 3 bar	119

D.2	Configuration 1 at an initial pressure of 5 bar	119
D.3	Configuration 1 at an initial pressure of 7 bar	120
D.4	Configuration 2 at an initial pressure of 3 bar	120
D.5	Configuration 2 at an initial pressure of 5 bar	121
D.6	configuration 2 at an initial pressure of 7 bar	121
D.7	Configuration 3 at an initial pressure of 3 bar	121
D.8	Configuration 3 at an initial pressure of 5 bar	122
D.9	Configuration 3 at an initial pressure of 7 bar	122
D.10	Configuration 4 at an initial pressure of 3 bar	123
D.11	Configuration 4 at an initial pressure of 5 bar	123
D.12	Configuration 4 at an initial pressure of 7 bar	123

LIST OF TABLES

2.1	Overview of the different definitions of average diameter [2]	6
3.1	Overview requirements	10
4.1	Difference of injectors	12
4.2	Overview of the different fluid properties	18
4.3	Overview design parameters swirl injector	19
4.4	Overview design parameters jet injector	20
4.5	General guidelines to determine tolerances for technical drawings [12]	22
5.1	Overview of the effect of the tolerances	32
5.2	Overview of the effect of the tolerances of the swirl injector	33
5.3	Overview of the minimum and maximum values of the SMD for the different jet injectors configurations	33
5.4	Overview of the different configurations and the associated SMD	34
5.5	Overview of the new dimensions of the prototype	37
6.1	Overview pressurant gas proprieties	42
7.1	Results measured inlet pressure as function of the initial tank pressure	51
7.2	Overview of the properties of deionized water for different injector configurations	56
7.3	Overview of the measured SMD values for an initial tank pressure of 3 bar	65
7.4	Test conditions and associated expected performance	65
7.5	Measured SMD for an initial tank pressure of 7 bar	67
7.6	Test conditions and associated expected performance for an initial pressure of 7 bar	67
7.7	Overview of the measured injection velocity for the swirl injector	68
7.8	Overview of the measured distance where mixing process starts	72
7.9	Spray angle of the swirl injector for different pressures	73
E1	Overview of the conducted experiments to study the atomization behaviour	129
E2	Overview of the conducted experiments to study the atomization behaviour	130
E3	Overview of the conducted experiments to study the mixing process	130
E4	Overview of the conducted experiments to study the mixing process continued	131
E5	Overview of the conducted experiments to study the mixing process with the high-speed camera	131
E6	Overview of the conducted experiments to study the interaction between the atomized flow and heating element	132

LIST OF SYMBOLS

Symbol	Unit	Description
A	[-]	Defined by Equation 4.28
A_{cross}	[m^2]	Cross section area of the measured droplet
A_{outlet}	[m^2]	Cross section area of the tank outlet
B	[-]	Ratio of the swirl radius and inlet port
D	[mm]	Diameter droplet
d_0	[mm]	Outlet diameter
D_p	[mm]	Inlet port diameter
D'_p	[mm]	defined by
D_s	[mm]	Swirl radius
FN	[-]	Parameter defined by Equation 4.19
G	[kg/s]	Mass flow
h_0	[m]	Parameter defined by Equation 4.20
i	[-]	Number of inlet ports of the swirl injector
j_{safety}	[-]	Safety factor
j	[mm]	Timescale factor
K	[-]	Geometric constant for the swirl injector
K_λ	[-]	Corrected geometric constant for viscous effects
L	[mm]	Length of outlet
L_{port}	[mm]	Length of inlet port
L_p	[-]	Laplace number
M	[-]	Ratio between the density of the ambient air and liquid
\dot{m}	[kg/s]	mass flow
M_{gas}	[kg]	Mass of pressurant gas
N	[-]	Radio of dynamic viscosity
O/F	[-]	Oxidizer to fuel ratio
OH	[-]	Ohnesorge number
P	[Pa]	Pressure
P_0	[Pa]	Begin pressure in the pressurant tank
p_f	[Pa]	End pressure of the pressurant tank
P_t	[Pa]	Pressure in the propellant tank
Q	[m^3/s]	Volume flow
r	[mm]	radius
R	[mm]	Swirl radius
r_0	[mm]	Outlet radius
Re	[-]	Reynolds number
S	[-]	Dimensionless radius of the gas core in the outlet of the swirl injector
SMD	[μm]	Standard mean diameter
t	[m]	material thickness
T_0	[K]	Initial tank temperature
u_0	[m/s]	Injection velocity
V	[m/s]	Velocity
V_{prop}	[m^3]	Volume of the propellant tank
We	[-]	Weber number
We_{fj}	[-]	Weber number including the timescale parameter
α	[$degrees$]	Spray angle
γ	[-]	Heat capacity ratio
δ	[mm]	Film thickness for the swirl injector
ΔP	[Pa]	Pressure drop
ϵ	[-]	Filling factor for the swirl injector

Symbol	Unit	Description
θ	[degrees]	Spray angle jet injector
λ	[-]	Parameter which is a function of Reynolds number
μ	[-]	Discharge coefficient of the injector
μ_g	[Pas]	Dynamic viscosity ambient gas
μ_l	[Pas]	Dynamic viscosity liquid
ν	[m/s]	Kinematic viscosity
ρ_g	[kg/m ³]	Density of ambient gas
ρ_l	[kg/m ³]	Density of liquid
σ	[N/m]	Surface tension
σ_{stress}	[N/m ²]	Material stress
ϕ	[-]	Tolerance of design
ψ	[-]	Contraction coefficient

LIST OF ABBREVIATIONS

Abbreviation	Explanation
AWG	American wire gauge
DASML	Delft Aerospace Structures and Materials Laboratory
ETOH	Ethanol
fps	frames per seconds
HTP	High-test peroxide
LPBF	Laser Powder Bed Fusion
NASA	National Aeronautics and Space Administration
PUN	Polyurethane
PVC	Polyvinyl chloride
SMD	Sauter mean diameter

Overview of the chemical elements

Element	Name
CO_2	carbon dioxide
C_XH_Y	Hydrocarbon
H_2O	Water
N_2	Nitrogen
O_2	Oxygen

1

INTRODUCTION

An important topic in the field of rocket propulsion is the development of new green advanced hypergolic rocket propulsion system. A hypergolic system has the desired property of achieving ignition without the use of an ignition source. Hence, a reduced number of components is used by having a hypergolic system and thus the reliability is increased. Looking back at the history of spaceflight, the lunar module has used hypergolic propellants to ensure the operation of the rocket propulsion during crucial mission events. This is only one example of the benefits of a hypergolic propulsion system. The current hypergolic propellants, for example hydrazine, has one large drawback. This drawback is the toxic properties of the propellant. The toxicity imposes different challenges during the handling of the propellant. Also, if an anomaly happens during testing, a toxic cloud can be formed. For example, during testing of the SpaceX Crew Dragon capsule, an anomaly occurred forming this toxic cloud. This can be seen in [Figure 1.1](#). Currently, the European Union is looking into banning toxic hypergolic propellant, like hydrazine [13]. All this results in the quest to find a green, non-toxic, alternative for the currently used hypergolic propellant.



Figure 1.1: Example of a test anomaly during SpaceX crew Dragon where a toxic hydrazine cloud is formed [1]

An initial study investigated hydrogen peroxide as a possible oxidizer for a novel approach to achieve pseudo hypergolic ignition. Hydrogen peroxide is liquid under room temperature and ambient pressure and can decompose with thermal energy. Also, it is less toxic to handle than the current oxidizer. The initial study has mapped the temperature and associated concentration to achieve the decomposition of hydrogen peroxide. The decomposed products are suitable for mono-propellant operation, without requiring a catalyst bed. Furthermore, a combination of ethanol and hydrogen peroxide leads to combustion in appropriate condition. So, the hydrogen peroxide oxidizer is capable to be used in a bi-propellant mode with ethanol as a fuel. Ethanol is green and also liquid at room temperature and ambient pressure. The next step in this study to explore hydrogen peroxide as a green alternative for hypergolic propulsion is to development of the first hardware components. The injector has a crucial role in the performance of a liquid engine. Therefore, the first hardware component that has to be developed is the injector. The purpose of the master thesis is to design, manufacture, and show the capabilities of a novel injector to operate in both mono and bio-propellant mode.

The research objective of this master thesis is to investigate the dual-mode injector system for a thruster operating in both mono and bipropellant mode, where hydrogen peroxide is an oxidizer that decomposes with thermal energy. Based on the research objective, the main research question is formulated as: "What injector design can support the thruster that uses only thermal energy to decompose hydrogen peroxide in monopropellant mode and react with ethanol fuel for bipropellant mode?". To be able to answer this key research question, the following sub-questions formulated:

- What is the theoretical background of the atomization process of the liquid
- What atomize methods exist and which one is the most suitable for this application?
- How does the injector influence the decomposition process that only uses thermal energy?
- Which requirements have to be fulfilled by the injector?
- How can the injector support the thruster operation using the monopropellant and the bipropellant mode?

- How can the injector prevent a hard start?
- How can the injector be used to provide cooling for the rocket engine?
- How does additive manufacturing influence the design of an injector?
- What test set-up and test protocol will be required for experimental testing

This report has the following structure: in [Chapter 2](#) the theoretical atomization process is explained, focusing on the background of the atomization. In [Chapter 3](#), the requirements are determined that has to be fulfilled by injector design. The initial design of the injector is described in [Chapter 4](#). In this chapter, the hard start and the cooling possibilities are addressed. In [Chapter 5](#) discuss the optimized injector design for additive manufacturing. The test setup design process is described in [Chapter 6](#). The conducted tests and the results are explained in [Chapter 7](#). The conclusion and recommendations can be found in [Chapter 8](#).

2

THEORETICAL ATOMIZATION PROCESS

In this chapter the theoretical atomization process is discussed to better understand the testing results. It is typical for a rocket engine to distinguish between a liquid jet or liquid sheet atomization. In [Section 2.1](#) the general definition and explanation of the atomization process is given. The theoretical atomization process of a liquid jet is discussed in [Section 2.2](#), while in [Section 2.3](#) the sheet atomization process is described. In [Section 2.4](#) the dimensionless parameters are discussed which are related to the atomization process. The effect of a collision between droplets and the interaction of ambient gas is discussed in [Section 2.5](#).

2.1. ATOMIZATION PROCESS IN ROCKET ENGINE

Atomization is the process where a liquid disintegrated into droplets. This atomization process provides better mixing and distribution of propellant droplets, which essential for promising rocket engine performance. Sufficient atomization will set the right condition for propellant ignition and guarantees the rocket engine operation. The atomization occurs in the first zone of a liquid rocket engine. [Figure 2.1](#) shows the different zones of a liquid rocket engine [14].

Different methods exist to atomize the liquid flow. For rocket engines, the mechanism used to atomize the propellant is drag or wind-induced, impact-induced and swirl induced. The propellant drag or wind-induced will happen by the interaction of the ambient environment and the fluid. The impact-induced atomization occurs when the propellant collides with another propellant or a splash plate. The swirl inducement of the propellant is centripetal acceleration contributes to the atomization process. A different mechanism also exists to atomize the propellant, which is called oscillations. This mechanism can occur in a nozzle when a piezo crystal is used. Due to the vibration of the rocket engine, this mechanism can also occur. Another approach for propellant atomization is the usage of vapor pressure. When this happens in the droplet, the vapor bubbles will overcome the surface tension and helps with the breakup. [14].

The atomization process is influenced by many parameters. First of all, fluid atomization is affected by the liquid type. Secondly, the spray angle of the atomize propellant will influence the level of distribution of the propellant of the rocket engine. The droplet size will influence the combustion efficiency. When the droplet is smaller, a larger surface area exists (easier for vaporization) and this leads to higher efficiency. Also, the velocity of the atomized propellant will influence the required length of the combustion chamber. The reason for this is that the droplet should be evaporated in the combustion chamber [14].

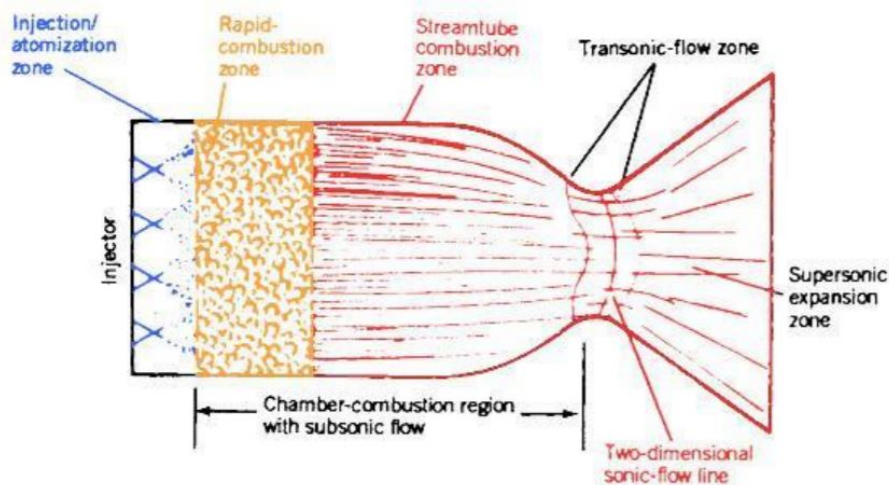


Figure 2.1: Different zones in the liquid rocket engine [2]

2.2. JET ATOMIZATION

According to Bayvel and Orzechowski [2], a jet will disintegrate into droplets based on injected fluid velocity. In general, three scenarios are distinguished based on different fluid injection velocities. The first and second scenario relate to the disintegration caused by axisymmetric and asymmetric waves. The third scenario describes that the jet breaking up into droplets due to aerodynamic forces. When the magnitude of this velocity is around 1 m/s, the jet fluid disintegrated by axisymmetric waves. At an injection velocity of 10 m/s, asymmetric waves will generate the droplets. At 100 m/s, injection velocity, the aerodynamic forces are the cause of the formation of droplets. See Figure 2.2 for a graphical example of these different scenarios.

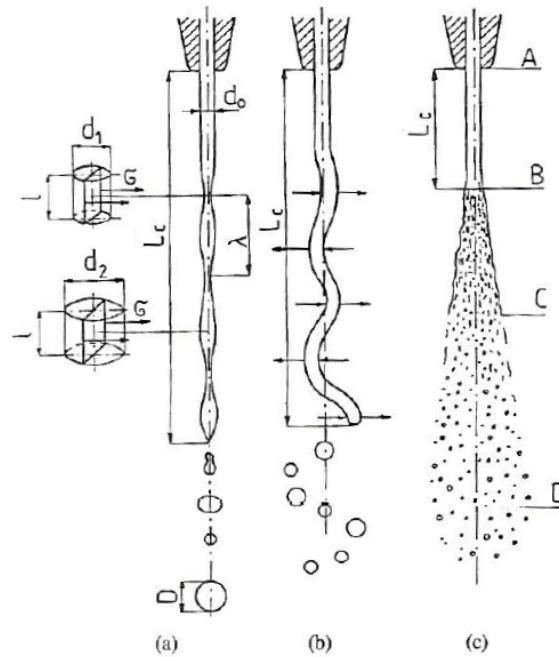


Figure 2.2: Graphical example of the different scenario's for the disintegration process [2]

The minor internal perturbations will cause narrow bands in a liquid jet. In these narrow bands, the pressure will increase, based on equilibrium condition for the forces of pressure and surface tension forces. From a narrow band, the liquid is strained in a wider band which will result in the formation of droplets. When the injection velocity is increased the jet will experience some aerodynamic forces. As a result of these perturbations, the jet will encounter some disturbances. Due to the varying shape of the liquid, as can be seen in Figure 2.2 in part b, negative and overpressure regions can be identified at some positions of the jet. This process is described as asymmetric waves. Due to the addition of aerodynamic forces, smaller droplets are generated than in the scenario of the axisymmetric scenario. If the injection velocity reaches around 100 m/s, the drag force will result in smaller droplets. As can be seen in Figure 2.2 in part c. For this scenario, also three regions can be identified. Part AB is the compact zone, where vibration will occur. The length of this zone will decrease at an increasing injection velocity. The part BC is called the disintegration zone, where small disturbances will happen. The part CD is referred to as the drop zone. The density (and thus pressure) influences the magnitude of the drag forces. When the atomization process will take place in a vacuum, the aerodynamic forces have a negligible magnitude. Also, the opposite can be said. At an increasing ambient pressure (and thus increase of density) the aerodynamic forces will increase and thus accelerate the formation of droplets [2].

The length of the compact jet is an important performance. It is influenced by the geometry of the outlet orifice, fluid properties, ambient conditions and injection velocity. A laminar flow is sensitive to disturbances which can lead to a reduction of the length of the compact jet. An increasing length of the outlet orifice will lead to an increase in the compact length. Finally, the viscosity will act as a means of damping the vibrations. This damping will lead to a delay in the droplet generation process. This principle can also be used to explain why viscous liquids experience more difficulties in the atomization process [2].

2.3. SHEET ATOMIZATION

When a sheet of liquid disintegrated, it will form several jets. These jets will then disintegrate in droplets. A sheet of liquid can form for several types of injectors, except for a single jet injector. When two or more jet injectors are used for liquids impingement, then a sheet of liquid can also form [2].

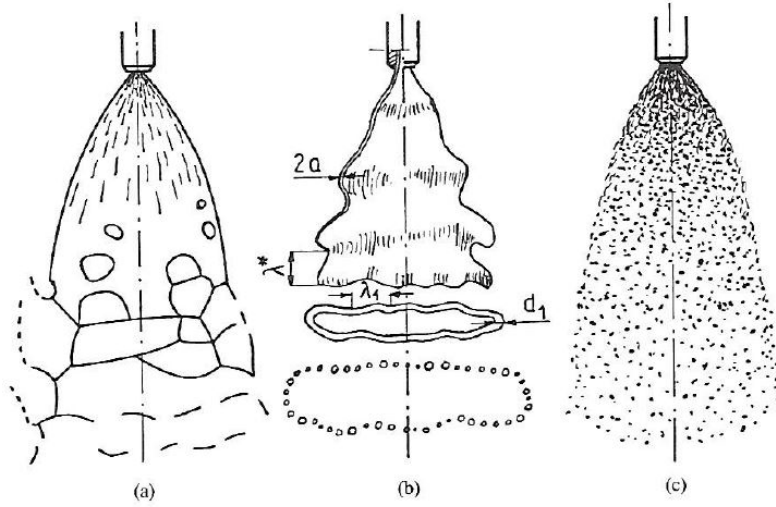


Figure 2.3: Graphical example of the different scenario's for the disintegration of a liquid sheet. [2]

Similar to Section 2.2, three scenarios can be noticed for the atomization process of a sheet of liquid. If the injection velocity is around a couple of m/s the atomization process is described by Figure 2.3 in part a. When the distance increases, the thickness of the sheet will decrease. At some point, some perforations will start. These perforations will start to grow and liquid jets start to form and then droplets will be formed. When the injection velocity increases the sheet will experience wave disturbances (as can be seen in Figure 2.3 in part b). As a result, annular and circumferential waves are generated. The annular waves have a longitudinal direction with respect to the discharge orifice. In these annular waves, jets are generated and these will convert into droplets. If the velocity is further is increased, short waves will form. The amplitude of these waves will increase and disintegrate the sheet to form droplets. This scenario can be seen in Figure 2.3 in c [2]. As a conclusion, a liquid sheet will always disintegrate into a number of liquid jets. The different transition scenartio from a sheet to a jet are discussed in Section 2.2.

2.4. DIMENSIONLESS CRITERIA

Often several dimensionless parameters are defined to compare different conditions to each other. This is also done for the atomization process. The size of the droplet diameter is affected by the following parameters: Diameter of the outlet orifice, initial velocity, surface tension, densities of liquid and ambient gas, the dynamic viscosity of liquid and gas, Weber number (see Equation 2.1), La place number (see Equation 2.2), ratio densities (as defined by Equation 2.3), ratio dynamic viscosity (see Equation 2.4. A different Weber number can also be identified. The difference between the two, is the usage of the density of the liquid instead of the gas. Which density is used is indicated by the subscript of the Weber number.[2].

$$We = \frac{\rho_g V^2 L}{\sigma} \quad (2.1)$$

$$Lp = \frac{\rho_l V^2 L}{\mu_g^2} \quad (2.2)$$

$$M = \frac{\rho_g}{\rho_l} \quad (2.3)$$

$$N = \frac{\mu_g}{\mu_l} \quad (2.4)$$

According to Christoph Heinzen, Andreas Berger, and Ian Marison, the different break-up options of a liquid jet can be classified into two parameters, Reynolds number and Ohnesorge numbers for a liquid in jet shape. In Figure 2.4, the classification and associated droplet formation mechanism based on the 2 parameters is shown [3].

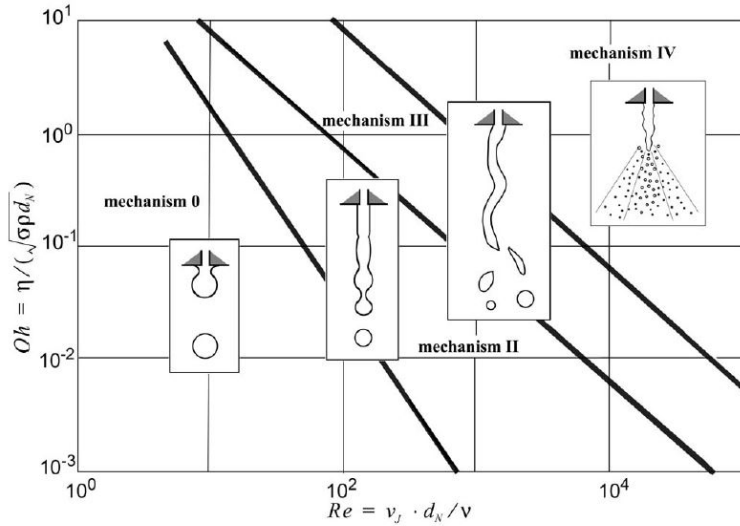


Figure 2.4: Classification of the different mechanism as function of Reynolds and Ohnesorge numbers [3]

Also, a different method of the classification exists determined by Lyshevskii. The definition of the Weber number is used to determine which scenario is applicable for the atomization process for a jet atomizer. Lyshevskii starts to identify a limiting Weber number, which is defined in Equation 2.5. From experiments, Lyshevskii has identified the limiting Weber number where the transition from the axisymmetric waves to asymmetric waves will take place, as can be seen in Equation 2.6. This is repeated for the transition point for the asymmetric waves and drag forces, as defined by Equation 2.7. The results of these experiments are only valid for a simple atomizer and the different scenarios as discussed in Section 2.2. Since a sheet of liquid will always atomize in a number of jets, the distinction is only made for the jet atomization [15].

$$We_{lim} = \frac{\rho_l V_{lim}^2 d_0}{\sigma} \quad (2.5)$$

$$We_{lim,II} = 16.6 Lp^{-3.02} M^{-1.05} \quad (2.6)$$

$$We_{lim,III} = 266 Lp^{-0.133} M^{-0.8} \quad (2.7)$$

There are many definitions to determine average droplet diameter. The difference is caused by using different calculation methods. Each definition has its specific applications, as can be seen in Table 2.1. The Sauter mean diameter (SMD) approach is suitable for many processes that include drop penetration or heat and mass transfer. [2].

Table 2.1: Overview of the different definitions of average diameter [2]

Definition mean diameter	Symbol	Application
Arithmetic	D_{10}	The average diameter considering the same number of droplets in data set
Surface	D_{20}	The average diameter considering the same number and surface in the data set
Volume	D_{30}	The average diameter considering the same volume and numbers in the data set
Relative surface	D_{21}	The average diameter considering the same total diameter and surface in the data set
Relative volume	D_{31}	The average diameter considering the same total diameter and volume in the data set
Volume - surface (SMD)	D_{32}	The average diameter considering the same total volume and surface in the data set

A classification based on the droplet diameter size exist and is given by Zanbergen [14]. First of all, coarse atomization is defined as a droplet diameter bigger than 1000 micrometer. Secondly, when the droplet size is smaller than 1000 and

larger 300 micrometer is referred to as semi coarse atomization. Thirdly, the classification of semi-fine atomization is applicable to a droplet diameter smaller than 300 micrometer and bigger than 100 micrometer. Fourthly, When the droplet diameter is bigger than 10 micrometer and smaller than 100 micrometer the droplet size is classified as fine atomization. Lastly, ultra-fine atomization is referred to as a droplet diameter smaller than 10 micrometer. According to Zhongtao Kang most droplets have a diameter of 100 micrometer for a typical swirl injector [16]. According to Kanmaniraja Radhakrishnan et al the SMD should be fine to have a right mixture between the propellants [17]. According to the classification of Zandbergen, fine atomization is when the diameter is lower than 100 micrometer [14]. This is in accordance with the found value of a typical swirl injector. Therefore, it is decided that the SMD of the designed injector should be lower than 100 micrometer.

2.5. SECOND DISINTEGRATION AND COLLISION

Aerodynamic forces have a secondary effect, namely causing secondary drop disintegration. The second disintegration level depends on the dynamic pressure, increase in droplet relative velocity, ambient gas, and ambient gas density. The secondary drop disintegration can be increased by increasing the ambient gas density. Another method is to increase the relative velocity of the droplet and ambient gas. Because of a relative velocity, a pressure distribution at the surface of the droplet will be generated and this will lead to disintegration. When the fluid has a high viscosity, shear forces will also contribute to the disintegration. A second mechanism exists, namely the collision with another droplet or a solid surface. However, this second mechanism will not always lead to disintegration. The critical Weber number is defined to determine the secondary droplet disintegration. The higher the Weber number (when it has exceeded the critical Weber number), the smaller the size of the secondary droplets. A great collection of experimental data exists regarding the critical Weber number, but the data is not consistent. An early explanation for this was measurements errors regarding the relative velocities. However, after reconsideration it was concluded that this process is very complex and can not only be described by the critical Weber number. In a range of 6 to 50 of the critical Weber number the following mechanism is applicable for the second drop integration:

- A non-uniform pressure distribution will occur at the surface of the droplet to cause the deformation.
- A boundary layer will develop at the surface of the droplet.
- The droplet will accelerate, caused by the ambient gas acting on its surface, leading to Taylor's instabilities to develop on the surface.

Two different principles explains the deformation of a droplet. These principles starts with the flattening of a droplet. Further distinction can be made for both principles, referred to the different modes. The different principles and modes are listed below:

- First principle
 - The first mode is the simple drop division. In this mode the droplet will deform in almost identical droplets.
 - The second mode is the parachute type. While the drop flattens it is blown out in the direction of the ambient gas and forms a shape of a parachute. Then, the droplet is disintegrated at the rim and the canopy part of the parachute. See [Figure 2.5](#) for a graphical overview of the parachute type.

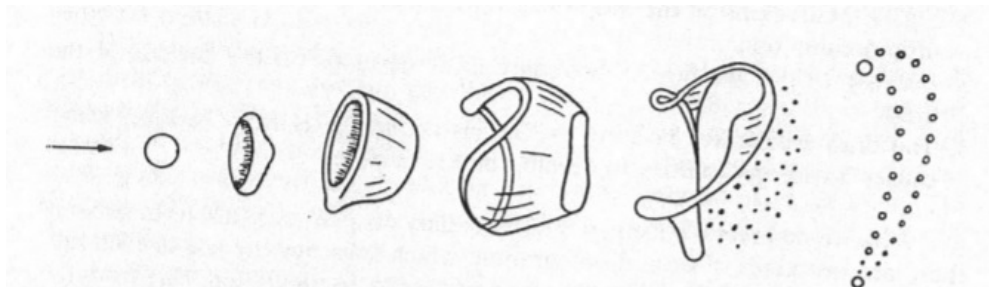


Figure 2.5: Graphical example of a parachute type [3]

- The third mode is the chaotic disintegration. In this mode several parachutes will develop at a single drop and this will disintegrate in small droplets with a varying shapes

- second principle

- The first mode is the shear mechanism, where the surface layer is torn off and this transforms in a cloud of droplets.
- The second mode is the burst disintegration. The disintegration process happens so fast, that the shearing is almost not noticeable.

From experimental data it is observed that not only the critical Weber number is important, but to describe the different options of secondary often the parameter $WeRe^{0.5}$ is used. In addition, the liquid viscosity, duration of contact of liquid and gas and the drop diameter has also an influence.

When droplets collide, this can lead to a second disintegration. A total of five characteristics options can be determined for collisions of drops in a stationary ambient gas, see figure [Figure 2.6](#) for a graphical overview. These different characteristics can be made based on the Weber number:

1. In the range $0.35 < We < 0.75$: because of the small relative velocities the droplets will bounce back without any effect. This is indicated in [Figure 2.6 in a](#).
2. In the range $1 < We < 7.5$: The smaller droplet can be absorbed by the large droplet to form 1 droplet. This larger droplet may be disintegrated. This characteristics can be seen in [Figure 2.6 part b](#).
3. In the range $7.5 < We < 20$: The smaller droplet will be absorbed to a larger one, but it will disintegrate in similar size as in the original position. This can be seen in [Figure 2.6 in part c](#).
4. In the range $We > 25$: The collision of droplets will result in puncture of the larger drop to form smaller droplets. This is shown in [Figure 2.6 in part d](#).
5. In the range $We > 50$: The collision of the 2 droplets will result in an explosive formation of smaller droplets. This situation is indicated in [Figure 2.6 in part e](#).

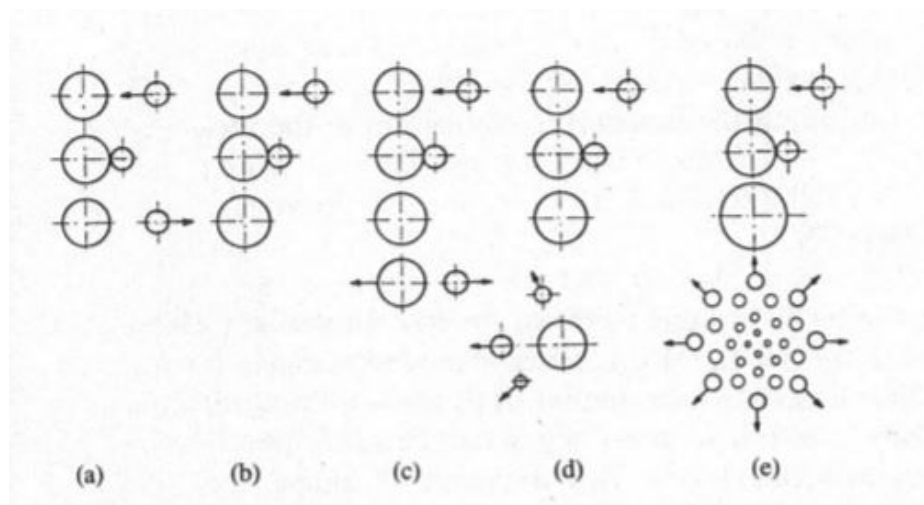


Figure 2.6: Different collision possibilities [3]

3

REQUIREMENTS

The requirements were determined to initiate the design process of the injector. A context diagram was made to aid the process of determining the requirements. First, the active and passive stakeholders were identified to draw the context diagram. The identified stakeholders for this thesis are listed below:

- **SolvGE:** this organization provides guidance to the design and testing process. As they are interacting with the injector SolvGE is an active stakeholder. Also, the results of this thesis are used in the future by this stakeholder to determine which next steps are required to further improve the advanced hypersonic propulsion system.
- **TU Delft:** this stakeholder has provided the required knowledge and experience to the stakeholder T. Borsboom. Also, this stakeholder provide guidance in the design and graduation process. This is classified as a passive stakeholder, since it does not interact with the injector.
- **T. Borsboom:** who is responsible to design the injector and perform all the required activities related to testing the injector. This stakeholder is the party that has the most interaction with the injector and is thus an active stakeholder.
- **External company:** who has helped to manufacture the injector and provide input for the design. However, this stakeholder is not actively interacting with the injector and is thus classified as a passive stakeholder
- **Chemical lab of DASML:** a partner who provides the test facilities. This stakeholder is not actively interacting with the injector, so this is a passive stakeholder.

By identifying the stakeholders, the context diagram is made and can be seen in [Figure 3.1](#).

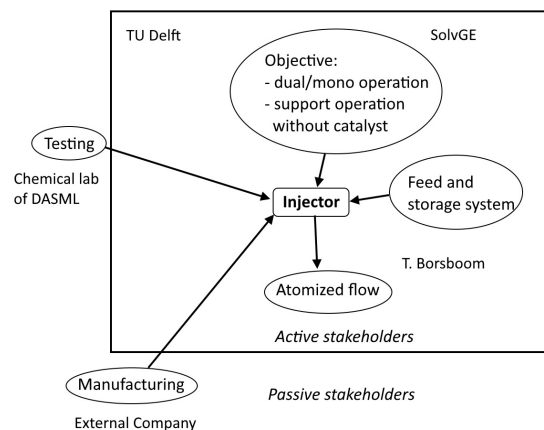


Figure 3.1: Context diagram of the injector

In this context diagram, the different parameters are shown which has an influence on the design of an injector and shall be described in a requirement. All the determine requirements can be found in [Table 3.1](#). These requirements are listed below:

- **Objective:** Several requirements are set to achieve the desired objective of the injector. As described in [Chapter 1](#), the objective of the injector is to support a propulsion system that uses thermal energy to decompose hydrogen peroxide for the mono-propellant operation made. Also, the injector shall be able to support the dual-mode operation, where ethanol is used as a fuel. The requirements related to the set objective have given the abbreviation OBJ and provide input to the injector design.
- **Atomized flow:** Several requirements are related to the atomized flow to support the objective of the injector. These requirements have the abbreviation ATOM. The atomized flow is the output of the injector.

- **Feed and storage system:** The feed and storage system imposes a number of requirements related to the interface between the injector and the feed and storage system. The abbreviation FFS is used to identify the requirements, which are used as an input for the injector design, related to this topic.
- **Testing:** It is desired to test the injector in order to validate the design. The testing facilities of the chemical lab of the Delft Aerospace Manufacturing Lab (DAMSL) can be used. A number of requirements are set when using these facilities, to guarantee a safe working environment. The related requirements to the testing subjects can be recognized with the abbreviation TST. This parameter forms an input to the injector design.
- **Manufacturing:** The chosen manufacturing method also imposes several requirements. SolvGE has a warm connection with an external company, that is experienced in the additive manufacturing method. A number of meetings were scheduled to understand what the possibilities and limitations are of this manufacturing method. The limitations are used to determine the requirements related to manufacturing and are identified with the abbreviation MANU. The manufacturing forms an input for the design.

Table 3.1: Overview requirements

Label	Requirement description
INJ-OBJ-1	The injector shall be able to run in monopropellant mode (using hydrogen peroxide) and bipropellant mode (using hydrogen peroxide and ethanol) to investigate the dual mode operation objective
INJ-OBJ-2	The atomized flow of hydrogen peroxide shall be decomposed with thermal energy
INJ-OBJ-3	The injector shall prohibit early decomposition inside the injector of HTP to prevent catastrophic failure
INJ-OBJ-4	The injector shall prevent a hard start to avoid catastrophic failure when operating in dual-mode,
INJ-OBJ-5	The injector shall maintain structural integrity during operation to prevent catastrophic failure
INJ-ATOM-1	The SMD of the atomized propellant shall be lower than 100 micrometer to provide the required quality of the atomized propellant
INJ-ATOM-2	The spray angle of the atomized flow shall be compatible with the ignition source to provide the required starting condition to achieve combustion
INJ-ATOM-3	The atomized flow of propellants shall support the combustion process
INJ-FSS-1	The injector shall provide inlet ports to accommodate the propellant flows of hydrogen peroxide and ethanol to be able to operate in mono mode and dual mode operation
INJ-FSS-2	The ethanol and HTP propellants shall be separated at all times to prevent catastrophic failure
INJ-TST-1	The injector shall be in microscale to be able to use the facilities of the chemical lab
INJ-TST-2	The propellant volume in the feed system shall be in the magnitude of microliters as a safety precaution
INJ-TST-3	The test setup of the injector shall fit within the geometric constants of a fumehood to have a safe working environment
INJ-MANU-1	Additive manufacturing supported by external company shall be used to limit the part numbers, cost and manufacturing time
INJ-MANU-1.1	Maximum dimension of injector shall be 30x 30 x40 cm to be able to be manufactured
INJ-MANU-1.2	The injector shall use only one type of material to be able to use additive manufacturing
INJ-MANU-1.3	The selected material for the injector shall be chosen from stainless steel or Inconel to be able to use the facilities of the external company

4

INITIAL DESIGN

In this chapter, the initial design of the injector is explained. Different choices have to be made during the design process of an injector. These choices are explained in [Section 4.1](#). The made choices effects how the design process is approached. An overview of the design process is given in [Section 4.2](#). The values of the design parameters are determined in [Section 4.3](#). In [Section 4.4](#) and [Section 4.5](#) a solution is suggested about the problems with cooling and a hard start that are encountered according to literature.

4.1. SELECTION DESIGN OPTIONS

Several choices related to the design have to be made before starting the actual design process. In [Subsection 4.1.1](#) the reasons are described for selecting a swirl type injector for the mono operation mode of the advanced hypergolic rocket propulsion system. In [Subsection 4.1.2](#) the motivation is given to choose the jet type of atomizer for the dual-mode operation. The selection of the material for the injector is given in [Subsection 4.1.3](#). It is desired to have several configurations that can be tested. These configurations are described in [Subsection 4.1.4](#).

4.1.1. SWIRL INJECTOR SELECTION

This thesis aims to design an advanced hypergolic propulsion system that uses a heating element to obtain thermal ignition of the propellant. An initial study [18] has revealed input parameters that are going to be used for the design of the injector. Two of the input parameters are the temperature and associated concentration of the hydrogen peroxide to achieve combustion. During the initial study, a heating plate is used in the test setup to determine the required temperature for combustion. The usage of a heating element will influence the selection of the type of injector, as the injector and heating element have to function together to provide a working ignition sequence.

The heating element cannot be placed inside the combustion chamber, since it blocks the inlet of the nozzle. Hence, the only option is to place the heating element in a cylindrical shape located at the outer radius of the chamber, to avoid blockage of the inlet of the nozzle. This can be seen in [Figure 4.1](#).

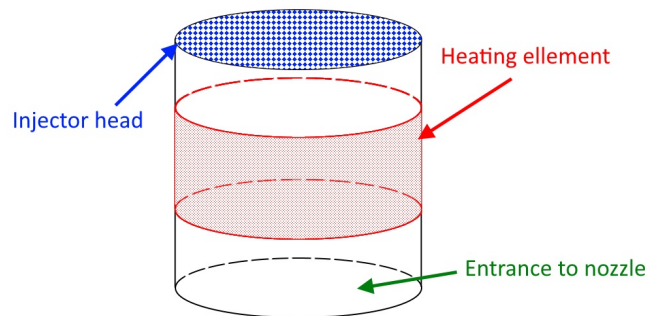


Figure 4.1: Schematic overview of the location of the heating element

One of the requirements (INJ-OBJ-1) of the injector states that the injector shall be capable of running in a monopropellant mode (using HTP), and in a dual-mode (using HTP and ethanol). An injector is designed for one type of liquid to prevent problems that occur at the transition from mono to bi-propellant caused by the difference in density [19]. Hence, it is not possible to use one injector type for dual-mode operation. Therefore, the design consist of two different injector types, one injector type per liquid.

Many injector types exist, all having its advantages and disadvantages. Based on the literature study performed before starting this thesis, the following types are typically used for rocket propulsion: jet injector, swirl injector, jet swirl injector and a pintle injector [20]. The advantages and disadvantages of those four injector types are shown in [Table 4.1](#) [2].

Table 4.1: Difference of injectors

Type of injector	Advantages	Disadvantages
Jet injector	Most simplest geometric of all type of injector	Small spray angle
Swirl injector	Large spray angle and good atomization quality	Limited useage for very viscous propellant and cannot cope with large changes in mass flow
Jet and swirl injector	Can generate full cone	More complex geometry
Pintle injector	Capable of having deep throttle capabilities	More complex internal geometry

A jet swirl injector has a large spray angle, which is desirable, however, it creates a full cone spray. While this is ideal when using a catalyst, it is not ideal when using a heating element that is located at the side. A full cone spray will waste a lot of HTP, because only a small fraction will come in contact with the heating element. The rest of the HTP will not be heated and therefore will not contribute to the combustion process. A pintle injector has great throttling capabilities, but this is not required for this engine. The jet atomizer has a very small spray angle and to still cover the whole surface of the heater, a high number of jet injectors must be used. This is undesirable since this will increase the costs, complexity and complicates the manufacturing process. The swirl injector has a large spray angle and a hollow cone of the atomized propellant, which is beneficial. The disadvantages of the swirl injector are irrelevant for this propulsion system since liquids will be used and the mass flow will not vary during operation.

4.1.2. JET INJECTOR SELECTION

In the mono mode operation, only hydrogen peroxide is used. Therefore only the swirl injector would be sufficient. However, in dual-mode operation, the ethanol is injected into the products of the decomposed HTP, requiring a second injector. The second injector atomizes the ethanol propellant. For these ethanol injectors, a small spray angle is desired, as it is required to aim the ethanol injectors at the specific area where the decomposed products of HTP are located. As only a jet injector is capable of producing a small spray angle, this type is selected to atomize the ethanol.

The injector that atomizes the HTP (see [Subsection 4.1.1](#)) is placed in the middle to use the large spray angle to its full potential. Therefore the jet injectors will be placed next to it. This research aims to demonstrate and understand the dual-mode operation of an advanced hypergolic propulsion system. Therefore, it is important to have a visual observation to understand the mixing process of the fuel and oxidizer. To not obstruct the imaging process during testing, only two jet injectors are used.

4.1.3. MATERIAL SELECTION

An external company is specialized in additive manufacturing, which is a manufacturing technique that is used for innovative products. SolvGe has contact with this company and this company is willing to provide their expertise to manufacturing the injector. This results in limited material options. Only Stainless steel 316L and Inconel are available. According to IS med Specilities, Inconel is not compatible with hydrogen peroxide [21]. However, Parabilis space technologies indicates that Inconel can be used in the case that the surface treatment is smaller than 10 percent [22]. Still, Inconel is not an option since the small inside diameter does not allow for surface treatment. Hence, stainless steel is the only option. The benefit of this material is that it is compatible with hydrogen peroxide and ethanol. Additionally, stainless steel is financially more attractive.

4.1.4. CONFIGURATIONS

To have a better understanding of the mixing of HTP and ethanol, four different configurations were designed. The schematic overview of the general layout of the injector configurations can be seen in [Figure 4.2](#). These four configurations varies in SMD and alignment of the jet and swirl injector to reveal the effect on the mixing. Below the four different configurations are explained:

- **Configuration 1:** SMD of the Jet injector is smaller than the swirl injector and placed under a 0 *degree* offset
- **Configuration 2:** SMD of the jet and swirl injector are roughly the same and placed under a 0 *degree* offset
- **Configuration 3:** SMD of the jet is larger than the SMD of the swirl injector and placed under a 0 *degree* offset
- **Configuration 4:** SMD of the jet and swirl injector are roughly the same and placed under a 5 *degree* offset

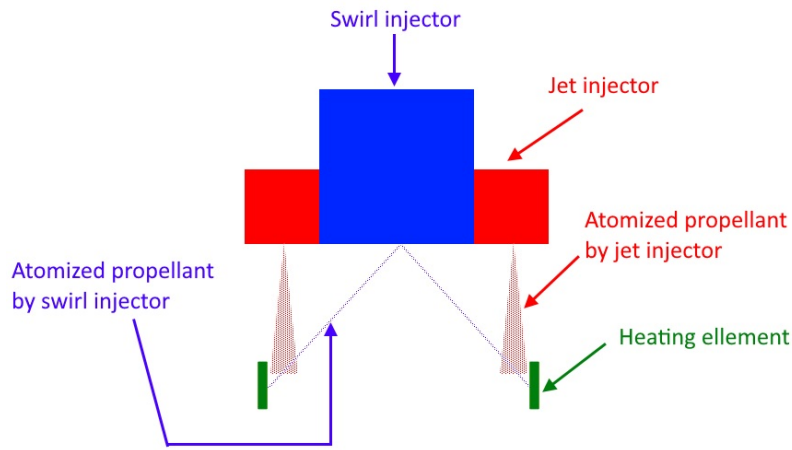


Figure 4.2: A schematic overview of the *general* lay out of the different configurations

4.2. DESIGN PROCESS

In this section, the design process is explained, related to a swirl and jet injector. In [Subsection 4.1.1](#), the design process of the swirl injector is explained in detail. The design process of the jet injector is described in detail in [Subsection 4.2.2](#). These subsections are the foundation of the design process and is used in [Section 4.3](#) to determine the values for the different design parameters.

4.2.1. SWIRL INJECTOR DESIGN

In this section, the theory to design and determine the performance of a swirl injector is discussed. A schematic overview of a swirl injector, including the different dimensions is shown in [Figure 4.3](#). It is typical for a swirl injector to define a geometric constant. This constant describes the characteristic parameters of a swirl injector. See [Equation 4.1](#) for the definition of the geometric constant represented by the parameter K . In this equation the swirl radius is represented by R in m , the outlet diameter has the symbol d_0 in m , the parameter i is the number of inlet ports and the diameter of the inlet port has the symbol d_p in m . A second definition of the geometric constant exists where only the filling factor is used, see [Equation 4.2](#). For this equation, the parameter ϵ represents the filling factor. This factor is a ratio between the gas and liquid core. This filling factor a design parameter and can be used to determine the value of the geometric constant. The inlet diameter can be determined when knowing the value of the geometric constant, swirl radius, and the outlet diameter [2].

$$K = \frac{2Rd_0}{id_p^2} \quad (4.1)$$

$$K = \frac{(1-\epsilon)\sqrt{2}}{\epsilon\sqrt{\epsilon}} \quad (4.2)$$

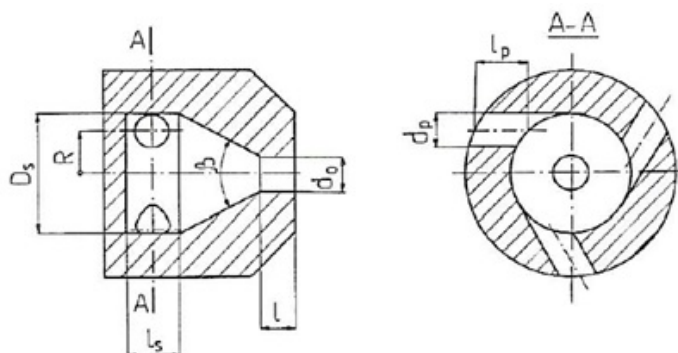


Figure 4.3: An overview of the geometry and associated dimensions of a swirl injector [2]

OUTLET DIAMETER AND SWIRL RADIUS

The outlet diameter is defined in Equation 4.3. In this equation, the mass flow is referred to the parameter G in kg/s , the parameter μ is the discharge coefficient, the density of the liquid is in kg/m^3 with the symbol ρ , and the pressure drop over the injector is in Pa (indicated with the parameter ΔP). The discharge coefficient is an indication of the loss of mass flow caused by flow separation or friction. To determine the discharge coefficient (which has the parameter μ) the filling factor has to be known, as can be seen in Equation 4.4. When the discharge coefficient is known, the outlet diameter can be determined. The swirl radius R can be determined by using Equation 4.5. In this equation, the parameter r_0 is the radius of the outlet, and the parameter $\frac{R}{r_0}$ refers to the ratio. According to L. Bayvel and Z. Orzechowski, this ratio has a value of 4 [2].

$$d_0 = \sqrt{\frac{4G}{\pi\mu\sqrt{2\rho\Delta P}}} \quad (4.3)$$

$$\mu = \epsilon \sqrt{\frac{\epsilon}{2-\epsilon}} \quad (4.4)$$

$$R = \frac{R}{r_0} r_0 \quad (4.5)$$

VISCOSITY EFFECT

The results of Equation 4.1 up to and including Equation 4.5 have assumed that the viscous effects can be neglected. Of course, this assumption has to be checked with, this can be done with Equation 4.6. If this equation is valid, the assumption can be made to neglect the viscosity. In this equation, the parameter B is defined by Equation 4.7, and the parameter ϕ represents a tolerance. Bayvel et al. recommends a tolerance of 5 percent, resulting in a value of 1.05 for the parameter ϕ . The number of inlet ports has the parameter i , and the K is referred to as the geometrical parameter of the swirl injector. The parameter λ is defined in Equation 4.8 and is a function of the Reynolds number. This Reynolds number is defined in Equation 4.9. In this equation, the parameter G refers to the mass flow in kg/s , the density of the liquid has the symbol ρ in kg/m^3 , ν is the kinematic viscosity in $Pa \cdot s$, the number of inlet ports has the parameter i , and the associated diameter is in m [2].

$$\frac{B^2}{i} - K \leq \frac{2}{\lambda} (\phi^{1.5} - 1) \quad (4.6)$$

$$B = \frac{R}{r_p} \quad (4.7)$$

$$\log(\lambda) = \frac{25.8}{(\log(Re))^{2.58}} - 2 \quad (4.8)$$

$$Re = \frac{4G}{\pi\rho\nu\sqrt{i}d_p} \quad (4.9)$$

When the result of Equation 4.6 is false, the geometric constant and the discharge coefficient have to be recalculated. The equation of the geometric constant with only the filling factor (Equation 4.2) remains valid, causing the filling factor to change. Consequently, the swirl radius (Equation 4.5) and the diameter for the outlet (Equation 4.3) have to be updated.

To determine the value of the geometric constant and discharge coefficient while taking into account the viscosity effects, Equation 4.10 and Equation 4.11 should be used. In Equation 4.10, the parameter B is defined by Equation 4.7 and the friction coefficient has the parameter λ , and is defined by Equation 4.8. The number of inlet ports has the symbol i .

$$K_\lambda = \frac{K}{1 + \left(\frac{\lambda}{2}\right) \left(\frac{B^2}{i} - K\right)} \quad (4.10)$$

$$\mu = \frac{1}{\sqrt{\frac{K_\lambda^2}{1-\epsilon} + \frac{1}{\epsilon^2}}} \quad (4.11)$$

GEOMETRIC DIMENSIONS

The length of the inlet port is defined by Equation 4.12. According to this equation, the inlet length is equal to a given ratio times the diameter port accent. Bayvel et al recommends a ratio with a minimum value of 1.5 and a maximum value of 3 for the inlet port length. The parameter diameter port accent is defined in Equation 4.13. In this equation, the parameter

d_p is the port diameter and the contraction coefficient has the symbol ψ . According to Bavyel, the contraction coefficient has a value of 0.875 [-].

The same method can be used to determine the outlet length. In this case, the outlet length equal to a ratio times the outlet diameter, as can be seen in Equation 4.14. A total of two definitions for this ratio exist. The first one is defined for a geometric constant that lower than 4. The the minimum value for this ratio is 0.5 and has a maximum value of 1. The second definition is applicable when the geometric constant is higher than 5. Then, a minimum value is 0.25, and a maximum value of 0.5 is recommended. [2]

$$L_{port} = (1.5 - 3.0)d_p' \quad (4.12)$$

$$d_p' = \frac{d_p}{\sqrt{\psi}} \quad (4.13)$$

$$\begin{aligned} L &= (0.5 - 1.0)d_0 \\ L &= (0.25 - 0.5)d_0 \end{aligned} \quad (4.14)$$

Equation 4.15 is used to determine the required dimensions of the swirl chamber. In this equation R is the swirl radius in m , the symbol d_p represents the inlet port diameter and the swirl chamber diameter has the symbol d_p . The height of the swirl chamber depends on the inlet port diameter. No specific relations exist to determine height, but Bayvel et all. have provided a general guideline that height is slightly larger than the inlet diameter. It is advised to have a minimum value of 60 degrees and a maximum of 120 degrees for the angle between the outlet and the swirl chamber.

$$D_s = 2R + d_p \quad (4.15)$$

SPRAY ANGLE

It is desired to also know the spray angle. For a swirl type injector, the spray angle can be calculated with Equation 4.16. In this equation, the spray angle has the symbol α , the parameter μ refers to the discharge coefficient, and the geometry constant has the symbol K. The parameter S is determined from Equation 4.17, where S is chosen such that the equation holds with the given geometric constant and discharge coefficient [2].

$$\tan\left(\frac{\alpha}{2}\right) = \frac{2\mu K}{\sqrt{(1+S)^2 - 4\mu^2 K^2}} \quad (4.16)$$

$$\mu = \sqrt{1 - \mu^2 K^2} - S\sqrt{S^2 - \mu^2 K^2} - \mu^2 K^2 \ln\left(\frac{1 + \sqrt{(1 - \mu^2 K^2)}}{S + \sqrt{S^2 - \mu^2 K^2}}\right) \quad (4.17)$$

SAUTER MEAN DIAMETER

Besides knowing the spray angle, it is also desirable to know the SMD value of the designed injector. To determine this parameter, Equation 4.18 is used, which is based on a rotary atomizer. The spray angle has the parameter α , the parameter h_0 is defined according to Equation 4.20, the surface tension has the symbol σ and has the units in cm . The density of the ambient gas and liquid has the symbols ρ_a and ρ_l , both expressed in g/cm^3 . The injection velocity is referred to as the parameter U_0 and has the units in cm/s . To determine the parameter h_0 , according to Equation 4.20, the outlet diameter has the parameter D_0 , the spray angle has the parameter α , the density of the liquid is referred ρ_l the parameter FN is defined by Equation 4.19. To determine this parameter, the mass flow (G), the density of the liquid (ρ_l) and the pressure drop across the injector ΔP are required. The injection velocity is defined by Equation 4.21. In this equation, the parameters ΔP and ρ_l refers to the pressure drop and the density of the liquid, respectively [23].

$$SMD = 0.9615 \cos(\alpha) \left(\frac{h_0^4 \sigma^2}{u_0^4 \rho_a \rho_l} \right) \left(1 + 2.6 \mu_l \cos(\theta) \left(\frac{h_0^2 \rho_a^4 u_0^7}{72 \rho_l^2 \sigma^5} \right)^{\frac{1}{3}} \right)^{0.2} \quad (4.18)$$

$$Fn = \frac{G}{\sqrt{\rho_l \Delta P}} \quad (4.19)$$

$$h_0 = \frac{0.00805 FN \sqrt{\rho_l}}{D_0 \cos \alpha} \quad (4.20)$$

$$U_0 = \sqrt{\frac{2\Delta P}{\rho_l}} \quad (4.21)$$

FILM THICKNESS

A final parameter that is desired to know is the generated film thickness of the atomized liquid. The ratio between the film thickness and the outlet radius is given by Equation 4.22. In this equation, the parameter $\frac{\delta}{r_0}$ is the ratio between the film thickness and outlet radius, the discharge coefficient is indicated with μ and the spray angle has the symbol α . When knowing this ratio and the outlet radius, the film thickness can be determined with Equation 4.23.

$$\frac{\delta}{r_0} = \frac{1 - \sqrt{1 - \mu \cos(\frac{\alpha}{2})}}{\cos(\frac{\alpha}{2})} \tag{4.22}$$

$$\delta = \frac{\delta}{r_0} r_0 \tag{4.23}$$

OVERVIEW DESIGN PROCESS

All the above-discussed equations are used in the design process. The first step in the design process uses Equation 4.1 up to and including Equation 4.5 to determine the geometric constant, discharge coefficient and swirl radius. Then, the assumption is checked if viscosity can be neglected with Equation 4.6. When it is required to take the viscosity into account, the geometric constant, discharge coefficient and the filling factor are corrected as defined by Equation 4.10 and Equation 4.11. The last step in the design process is to determine the theoretical performance (like spray angle, SMD and liquid film thickness) using Equation 4.18 up to and including Equation 4.23. A flow chart of design process is graphically shown in Figure 4.4.

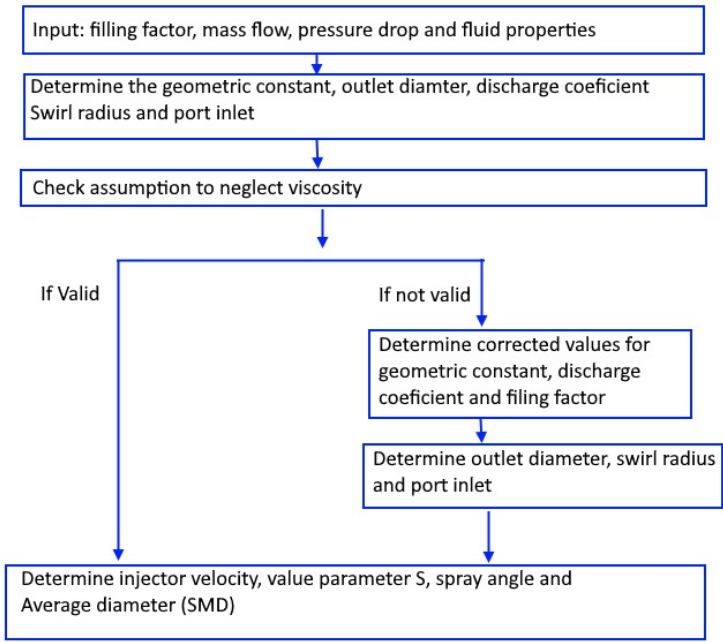


Figure 4.4: A flow chart of the design process of the swirl injector

4.2.2. JET INJECTOR DESIGN

In this section, the process of designing a jet injector is explained. In Figure 4.5 the schematic overview of this jet injector is shown. According to L. Bayvel and Z. Orzechowski, the discharge coefficient for a sharp edge jet injector can be calculated by Equation 4.24. In this equation the outlet diameter has the symbol d_0 in mm and the parameter Re_h is defined by Equation 4.25. This equation is valid when the Reynolds number is bigger than 100 but smaller than $1.5 \cdot 10^5$. The equation for the Reynolds number, the volume flow has the parameter Q in m^3/s , the outlet diameter has the symbol d_0 in m , and the kinematic viscosity (ν) in m^2/s . These two equation can be combined and after some algebraic manipulation has led to Equation 4.26 [2].

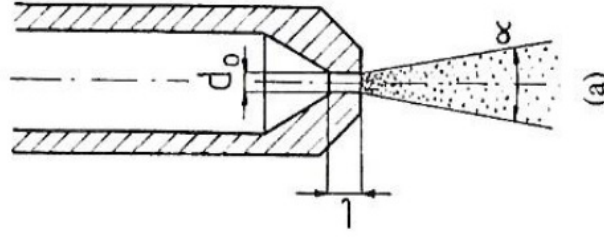


Figure 4.5: An overview of the geometry and associated dimensions of a jet injector [2]

$$\mu = \left(1.23 + \frac{58}{Re_h d_0} \right)^{-1} \quad (4.24)$$

$$Re_h = \frac{4Q}{\pi d_0 v \mu} \quad (4.25)$$

$$\mu = \left(1.23 + \frac{58}{\frac{4Q}{\pi d_0 v \mu} d_0} \right)^{-1} = \frac{1}{1.23 + \frac{58\pi v \mu}{4Q}} \rightarrow \frac{58\pi v \mu^2}{4Q} + 1.23\mu - 1 = 0 \quad (4.26)$$

The discharge coefficient can be determined using the above equations. Similar to the swirl injector design, the discharge coefficient is to determine the required outlet diameter by using Equation 4.27, and the spray angle is according to Equation 4.29. In this equation, the density of the ambient gas has the parameter ρ_g and is expressed in kg/m^3 . The density of the liquid has the symbol ρ_l and is in kg/m^3 . The parameter A, which is a coefficient, is often determined from experiments. However, this can be estimated by Equation 4.28, if the flow is turbulent. In this equation, the parameter L/D_0 is the length and diameter ratio [24].

$$d_0 = \sqrt{\frac{4G}{\mu\pi\sqrt{2\rho\Delta P}}} \quad (4.27)$$

$$A = 3 + \frac{L/D_0}{3.6} \quad (4.28)$$

$$\tan\left(\frac{\theta}{2}\right) = \frac{4\pi}{A} \sqrt{\frac{\rho_g}{\rho_l}} \frac{\sqrt{3}}{6} \quad (4.29)$$

The SMD is given by Equation 4.30. In this equation, the weber number is defined with Equation 4.32 and has the symbol We_{fj} . The parameter j represents the lengthscale. In the equation for the adjusted Weber number the parameter ρ_l represents the liquid density in kg/m^3 , the injection velocity is in m/s and has the symbol v and the surface tension (σ). The timescale is defined as a function of the outlet diameter according to Equation 4.31 [25].

$$SMD = We_{fj}^{-0.74} 133j \quad (4.30)$$

$$j = \frac{d_0}{8} \quad (4.31)$$

$$We_{fj} = \frac{\rho_l U_0^2 j}{\sigma} \quad (4.32)$$

4.3. DETERMINING DESIGN PARAMETERS

In this section the geometric dimensions and the theoretical performance of the swirl and jet injectors are provided. The required theory to determine these aspects is discussed in Subsection 4.2.1 and Subsection 4.2.2. The actual design of the swirl injector is described in Subsection 4.3.1. In Subsection 4.3.2 the design is made for the jet injector. How the injector is connected to the feed line is described in Subsection 4.3.3. The required minimum wall thickness is explained in Subsection 4.3.4. The selected tolerances that are used for the technical drawings are described in Subsection 4.3.5.

As discussed in previous sections, the swirl injector atomized the HTP propellant while the jet injector atomized the ethanol propellant. The properties of the different propellants form an input parameters. The required properties for the design process of HTP and ethanol are given in Table 4.2.

Table 4.2: Overview of the different fluid properties

Parameter	Value HTP	Value Ethanol
Density	1400 kg/m^3 [26]	789.40 [27] kg/m^3
Dynamic viscosity	1.25 cp [28]	$1.25 \cdot 10^{-3} Pa \cdot s$ [29]
Kinematic viscosity	8.92 m^2/s	$1.58 \cdot 10^{-6} m^2/s$
Surface tension	80 dyne/cm [30]	$22 \cdot 10^{-3} N/m$ [31]

Some general guidelines for certain geometrical dimensions are provided by Zandbergen. For example of the outlet diameters of the injectors, which should have a range that is higher than 0.5 mm and smaller than 3.0 mm. The lower limit is set to prevent clogging of the injector and limitations of manufacturing purposes. Also, a maximum of 1000 micrometer is set in SMD, as discussed in Chapter 2. These guidelines are used to determine the desired value for the mass flow and the set pressure drop for the design of the injectors.

4.3.1. SWIRL INJECTOR DESIGN

The input parameters for the design of the swirl injector are the filling factor, mass flow, pressure drop, and fluid properties (see Figure 4.4). A graph is made to explore the value of the SMD for a varying mass flow and pressure drop of the injector. A second graph is made to investigate the outlet diameter for a varying mass flow and pressure drop of the injector. The upper limit of the pressure drop of an injector is set to 10 bar as a safety precaution. The mass flow in the graphs is varied from 0.0001 kg/s to an upper limit 0.1 kg/s. For this graph, a filling factor of 0.5 is assumed. This graph is shown in Figure 4.6. As can be seen in this figure, a mass flow of 0.0001 kg/s results in an outer diameter smaller than 0.5 mm for a range of pressure drops of 0 to 10 bar. When a mass flow of 0.1 kg/s is selected, the outlet diameter is smaller than 3 mm for a pressure drop of 6 bar and higher. However, for this mass flow, the SMD is higher than 100 micrometers in the given pressure drop range. A mass flow of 0.01 kg/s results in an SMD smaller than 100 micrometer at a pressure drop of 1.75 bar and higher. For these reasons, the magnitude of the mass flow should be higher than 0.001 kg/s and smaller than 0.01 kg/s to comply in the desired range of the outlet diameter and SMD.

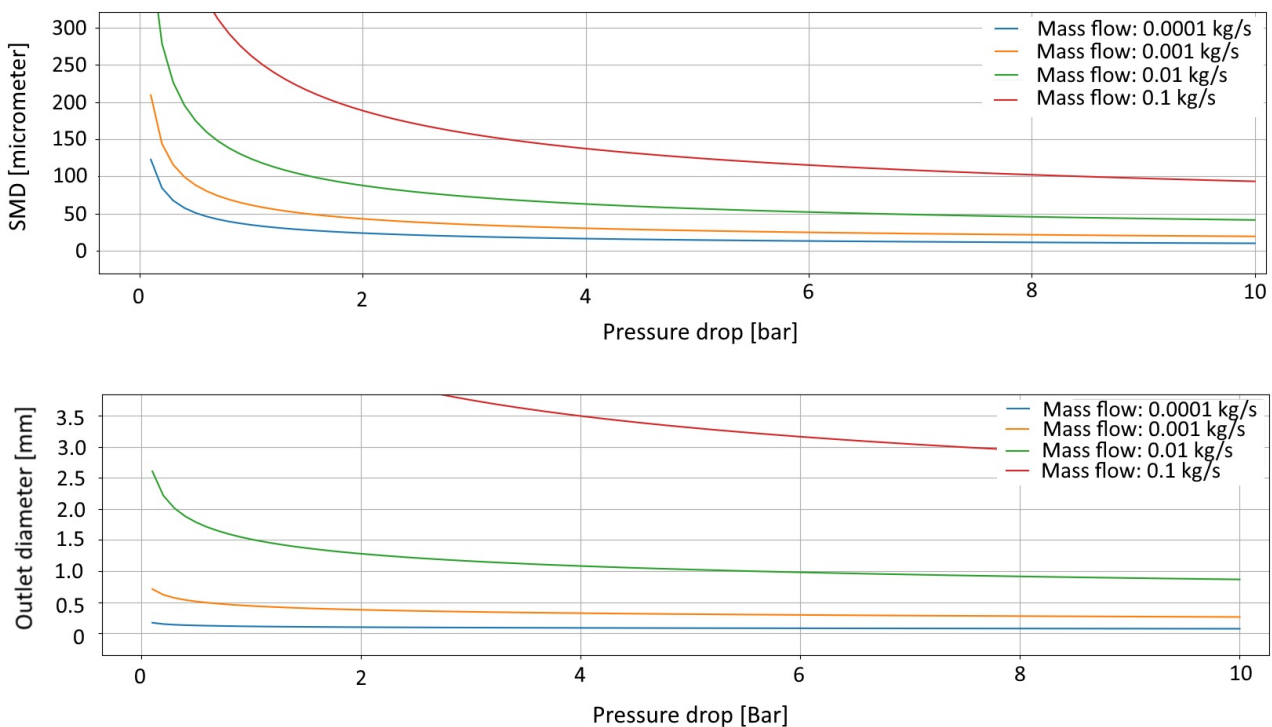


Figure 4.6: Visual pressure drop, mass flow and SMD and outlet diameter

The filling factor most dominantly influence the spray angle. To visualize the selected filling factor and the associated spray angle, a graph is made which can be seen in Figure 4.7. In this figure, it can be seen that at a filling factor around

0.75 the spray angle makes a jump. At this point, the assumption to neglect the viscosity is valid resulting in this jump.

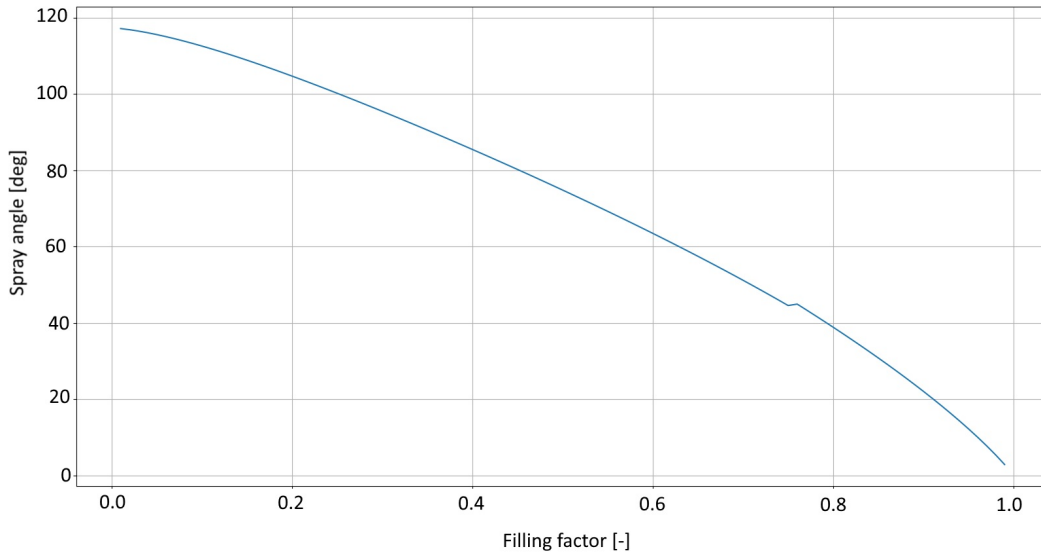


Figure 4.7: Filling factor and spray angle

The chosen spray angle affects the location of the heater and thus the decomposition process location. A larger spray angle decreases the distance between the injector and heater, imposing a higher thermal load at the injector. A smaller spray angle decreases the thermal load at the cost of a larger combustion chamber. As a starting point for this version of a design, it is chosen to have a spray angle of 90 degrees (and a filling factor of 0.5).

To aid the design process a python script is made to determine all the dimensions and performance parameters, as discussed in Section 4.2. It is chosen to have one inlet port, to have a more simple internal structure to test. As can be seen in Figure 4.6, the pressure drop can be increased after 2 bar, but there is no notable change in SMD and outlet diameter. For this reason, the pressure drop of 2 bar for the swirl injector is selected. Due to the unknown difference in theoretical and practical values, a margin of 40 percent is applied. So, an SMD value of 60 is desired. As a result, a mass flow of 0.005 kg/s is chosen. With these 2 parameters chosen, the filling factor is iterated until a spray angle is achieved of 90 degrees. Taking into account the viscosity effects, this results in a filling factor of 0.427 [-] and a spray angle of 90 degrees. Since the geometric constant is smaller than 4, a ratio of 0.75 is used to compute the length of the inlet port. The inlet port diameter is found to be equal to 1.2908 mm. Since the height of the swirl chamber must be slightly larger than the inlet port diameter (as a design guideline). For this reason, the height of the swirl chamber is set to 1.4 mm. All the associated calculations with these input parameters can be found in Appendix A, as well as the python code used for these calculations. An overview is given in Table 4.3 and the schematic dimensions.

Table 4.3: Overview design parameters swirl injector

Input parameter	Value	Unit	Output parameters	Value	Unit
Filling factor	0.427	[-]	Geometric constant	2.9	[-]
Mass flow	0.005	kg/s	Discharge coefficient	0.2	[-]
pressure drop	2	bar	Outlet diameter	1.1	mm
Number of inlets	1	[-]	Outlet length	0.8	mm
			Inlet diameter	1.3	mm
			Inlet length	3.1	mm
			Swirl chamber diameter	5.7	mm
			Spray angle	89.6	degrees
			SMD	58.5	micrometer
			Film thickness	0.06	mm
			Injection velocity	16.9	m/s

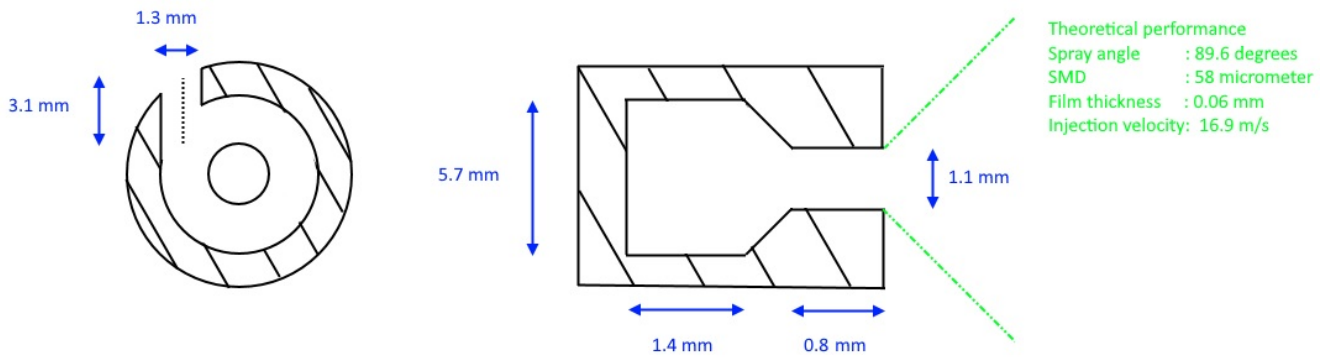


Figure 4.8: A schematic, not on scale, overview of the dimensions of the swirl injector

4.3.2. JET INJECTOR DESIGN

Now the swirl injector has been determined, the jet injector can be determined. Since the mass flow of the swirl injector is fixed, the mass flow for the jet injector can be determined with a given oxidizer to fuel ratio. According to Jaime Quesada Maña the optimal oxidizer to fuel ratio is equal to 4.403. Then, the mass flow for the jet injectors is given by Equation 4.33. In this equation, the mass flow is represented by \dot{m} , and the oxidizer to fuel ratio has the symbol O/F . The subscripts ox and fuel refers to the oxidizer and fuel. Having an oxidizer to fuel ratio of 4.403 results in a required mass flow for the jet injectors of $1.135 \cdot 10^{-3} \text{ kg/s}$. Since two jet injectors are used, mass flow for each jet injector is equal to $5.677 \cdot 10^{-4} \text{ kg/s}$. Similar to the swirl design, a python script is made to aid the design process. To obtain the difference in SMD, the pressure drop for each configuration is altered. An overview is given in Table 4.4 and a schematic overview can be found in Figure 4.9.

$$O/F = \frac{\dot{m}_{ox}}{\dot{m}_{fuel}} \quad (4.33)$$

Table 4.4: Overview design parameters jet injector

Parameter	Configuration 1	Configuration 2 and configuration 4	Configuration 3	Unit
Mass flow	0.00057	0.00057	0.00057	kg/s
Pressure drop	1	1.5	2.2	bar
Discharge coefficient	0.094	0.094	0.094	mm
Outlet diameter	0.78	0.70	0.64	mm
Length outlet diameter	3.91	3.54	3.21	mm
injection velocity	15.91	19.50	23.61	m/s
spray angle	3.73	3.73	3.73	degrees
SMD	85.5	61.7	45.3	micrometer

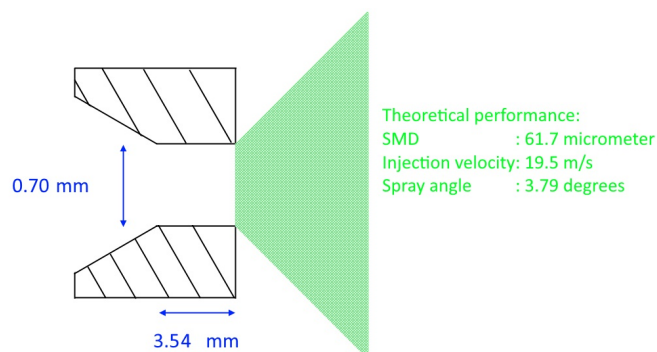


Figure 4.9: A schematic, not on scale, overview of the dimensions for the configuration 2 jet atomizer

4.3.3. CONNECTION SWIRL AND JET INJECTORS

It is important to incorporate the connection to the injector and the test setup in the initial design. The connector for the jet injector is placed at the top, as it is the most intuitive place to connect. The inlet port of the swirl injector is at the side of the swirl chamber. The small mass flow, which leads to the desirable range of SMD and outlet diameter, has one disadvantage. The small mass flow results in small dimensions of the swirl injector. Consequently, the connector will be lower than the injector head when connecting the feed line to the swirl injector. This causes two problems. Firstly, blockage of the atomize HTP can occur. Secondly, the HTP might thermally decompose prematurely in the connector. To avoid these two problems, the connector is placed at the top and be connected with through a tube to the inlet port of the swirl injector. This can be seen in Figure 4.10.

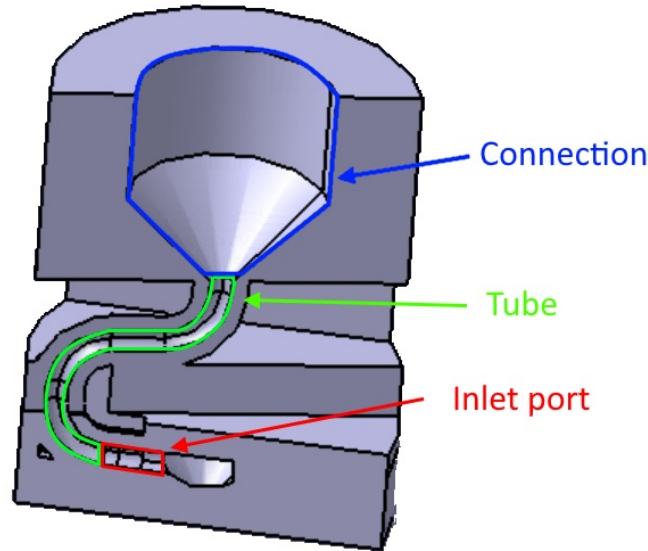


Figure 4.10: Graphical overview of the connector, tube and inlet port

There are additional benefits of placing the connector at the top of the swirl injector. Firstly, the amount of the inlet ports can be easily adapted while using one connector. Secondly, the thermal stand-off is higher which has a positive benefit on the thermal load to prevent thermal decomposition. Thirdly, the tube can also be used as the supply line for the slots in case film cooling is added in the future.

To prevent the possible mixup between the connectors of the swirl and jet injector, it is decided to use different thread size. The thread size of the swirl injector is G1/4, while the tread sizes of the injector is G1/8. The G thread is specific to be used for pressure connections and is according to ISO 228 norm.

4.3.4. WALL THICKNESS

When the material is selected, the required thickness can be determined. A quick method to do that is with the hoop stress that is given in Equation 4.34. In this equation σ is the stress in Pa, j is the safety factor, r is the radius in m and t is the thickness in m . The material is stainless steel 316L has a yield and ultimate of 205 and 505 MPa, respectively. The required thickness increases at an increasing radius. The thickness of the injector is determined for the largest radius. Which is 6 mm for the swirl injector and 4.4 mm for the jet injector. A safety factor of 5 is decided to be used. Both injectors should withstand a maximum pressure of 5 bar. Using these parameters Equation 4.34 results in a thickness of 0.073 mm and 0.05 mm for the swirl and jet injectors.

$$\sigma_{stress} = \frac{j_{safety}Pr}{t} \quad (4.34)$$

By using the hoop stress is a simplification and neglecting any stress concentrations. An external company has more experience in performing structural analysis and is willing to do this for the injector. During a meeting, an initial wall thickness of 5 mm is chosen. The results of the structural analysis and the implication of the design are given in the prototype section.

4.3.5. TOLERANCES

Technical drawings are made to realize the design. The tolerances of the dimensions are a crucial part of the technical drawings. A general guideline which tolerances should be selected is given in Table 4.5. Depending on the required accuracy of the dimensions the value of the tolerances is advised. The accuracy is classified into three magnitudes: fine, medium, and rough. It is decided to use the fine accuracy to the dimensions that influence the performance. For example, the outlet diameter, swirl radius, and outlet length affects the performance. Some dimensions, like the outer radius of the connector it is chosen to have the rough accuracy [12]. See Appendix A, for the technical drawing including the selected tolerances for each dimension.

Table 4.5: General guidelines to determine tolerances for technical drawings [12]

General guidelines values tolerances				
Dimensions		Value tolerances		
Bigger than [mm]	Including and smaller [mm]	Fine [mm]	Medium [mm]	Rough [mm]
0.5	3	± 0.05	± 0.10	± 0.15
3	6	± 0.05	± 0.10	± 0.20
6	30	± 0.10	± 0.20	± 0.50
30	120	± 0.15	± 0.30	± 0.80
120	315	± 0.20	± 0.50	± 1.20
315	1000	± 0.30	± 0.80	± 2.00

4.4. HARD START

The problem of a hard start was experienced during previous experimentation. This problem is not new, it was even experienced by Werner von Braun during the development of his W1 engine. A hard start occurs when the quantity of the propellants is too large before the ignition happens. As a result, the pressure increases rapidly, and in some cases, this leads to a structural failure. A hard start can be avoided by having the correct timing of opening valves related to the ignition. It is also possible to vary the oxidizer to fuel ratio to limit rapid pressure increase. Lastly, it possible to have an ignition source available. In general, a hard start can only occur with a liquid propellant since the quantity of gaseous propellant in a combustion chamber is limited. The reason for this is that gaseous propellant is vented through the throat of an injector (for a practical design), so the required condition cannot occur for a hard start [32].

The paper written by Hongjae Kang and et all. [33] also describes methods to prevent a hard start. It is mentioned that a hard start won't occur when it is prevented that the propellants are ignited with a long time interval. So, during the start-up phase, an oxidizer rich environment should be avoided. In this paper, two methods are described to achieve this environment. The first method is to have a fuel-rich environment at the ignition sequence by including a mass flow control device for the oxidizer. A cavitating venturi tube was selected by Hongje Kange et all. to be the mass flow controlling device. The benefit of the cavitating venturi tube is that it is passive, highly reliable, and inexpensive. The drawback is that it can only accommodate a small range in mass flow. The performance of this mass flow control device is not influenced by any pressure differences that happen in the combustion chamber, given that the downstream pressure remains under a critical value. It is given that this critical value is around 85 to 90 percent of the upstream pressure. The small-size cavitating venturi is often not used, because it easily gets choked when a high-pressure loss occurs. A second method to prevent a hard start is the usage of higher concentrations of Hydrogen peroxide. By using a higher concentration, the ignition delay time is decreased. By having a smaller ignition delay time, any excess of the propellant quantity cannot occur and thus a hard start is prevented. Even, if an oxidizer rich environment is used during the ignition process, the usage of a higher concentration can prevent a hard start.

For testing the configurations 1 to 4 the oxidizer is HTP with a concentration of 98 percent. According to Hongjae Kang and et all. this should already be sufficient to avoid the hard start problem. It is discovered that a hard start can still occur during a drop test while using 98 percent HTP. The explanation for this is that the drop test does not atomize the propellant at the same level as an atomizer is able to do. This leads to a larger ignition delay time when an injector is not used. The larger delay time is one of the main causes of the occurrence of a hard start. So, by using an injector and the high concentration HTP the hard start problem should not occur. The timing of the opening of the valves can be adjusted in the unlikely case that the hard start still occurs.

4.5. COOLING

High temperatures were measured during the drop test experiment that has been performed by the initial study. These temperatures were able to destroy several thermocouples, indicating a challenging thermal environment for the propulsion system. Therefore, methods of cooling are explored in [Subsection 4.5.1](#). The most promising method, film cooling, is explained in more detail in [Subsection 4.5.2](#). The effect of the film cooling method on the design is described in [Subsection 4.5.3](#).

4.5.1. METHODS OF COOLING

In general, 2 possible methods exist to cool a rocket engine. The first option is a passive method, which uses no energy-consuming devices. A couple of examples of this first method is to use a heat sink, ablative material, or radiation cooling. The design of the injector is not influenced when only passive means are used to cool the rocket engine [14]. The second method to cool a rocket engine is called active cooling. This method uses a device that transfers the heat away from the rocket engine. In general, a liquid or gas is used to cool the combustion chamber walls. This can be done by film or regenerative cooling. By regenerative cooling, the fuel or oxidizer is pumped in passages of the chamber wall to cool this section of the propulsion systems. Which propellant is consumed for the hyperbolic innovative propulsion system depends on the selected mode: dual or mono mode. The fuel ethanol is only used in dual mode, while hydrogen peroxide is used for both modes. As a result, the oxidizer hydrogen peroxide should be used when regenerative cooling is chosen. Otherwise, the fuel ethanol is wasted in the operation mode of mono propulsion, since it is required for cooling but is not used in the combustion process. However, hydrogen peroxide decomposes with thermal energy. So, using this oxidizer for regenerative cooling can have an explosive result in the chamber wall. Hence, this method is undesirable. Another method of active cooling is film cooling. This method consists that a liquid is injected around the injector to provide this sheet of protection to the high thermal environment. By choosing the method of film cooling the design of the injector is adjusted. In the section below a more detailed description of film cooling is given and the required injector adjustments are explained [14].

4.5.2. FILM COOLING

Film cooling is started by injecting the oxidizer or fuel through a set of holes or slots in the direction of the combustion chamber. The position of the injection can occur at the injector or the combustion chamber. When the combustion chamber has a small length, the film cooling can be used to cool the wall until the throat of the nozzle. When the film cooling layer evaporates, it is not diffused into the combustion process. So, the evaporated layer still protects against the high temperatures. Film cooling is an important aspect of the propulsion system since it has a large influence on the lifetime of the system [4].

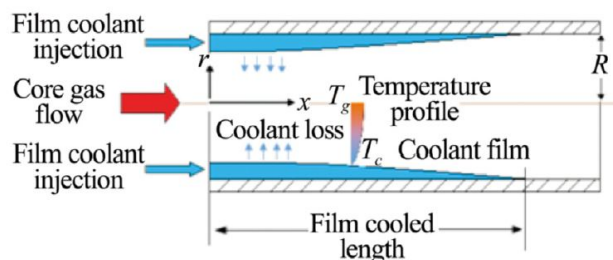


Figure 4.11: An example of the film cooling principle [4]

4.5.3. INCORPORATION INJECTOR DESIGN

The results of the paper written by R. Arnold, D. Suslov, and O. J. Haidn provide an example where the film cooling is incorporated in the design of the injector. Before any film cooling is used, the design of the injector can be altered by injector trimming. Injector trimming describes that the injector head outer layer, near the combustion chamber wall, has more fuel injectors or fewer oxidizer injectors. This leads to a more fuel-rich environment and a decrease in the thermal wall load. Unfortunately, similar to film cooling the injector trimming leads to a decrease in propulsion performance. In [Figure 4.12](#) an illustration is given of the design of an injector where slots are incorporated in the design of the injector. In this example, 15 jet orifices are used for the atomization of the propellant and 10 slots are used for the film cooling. These slots are tangential to the combustion chamber wall. The dimensions of the slot, such as height, width, and number of slots influences the effectiveness of the film cooling. Besides these geometrical aspects, the effectiveness of the film cooling is also influenced by the fluid mechanic properties. An example of this is the blowing ratio of momentum flux. During different experiments, the chamber pressures and the blowing ratio has been varied to investigate the minimal

temperature of the chamber wall. One of the conclusions was that the minimum wall temperature indeed has been decreased by using film cooling. However, the section of the wall more downstream had a less reduction in minimum temperature [5].

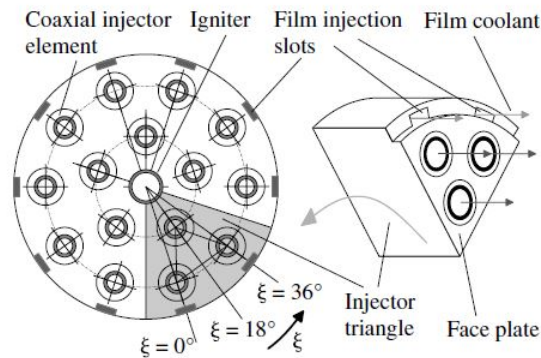


Figure 4.12: An example of the made adjustments to accommodate for slots for the film cooling [5]

It should be noted that it is also possible to have the slots for film cooling at the combustion chamber wall itself. An example of this is given in Figure 4.13. As can be seen in this figure, the locations of the slots are more downstream and with a separate feeding line. As a result, the design of the injector is not influenced by these slots [6].

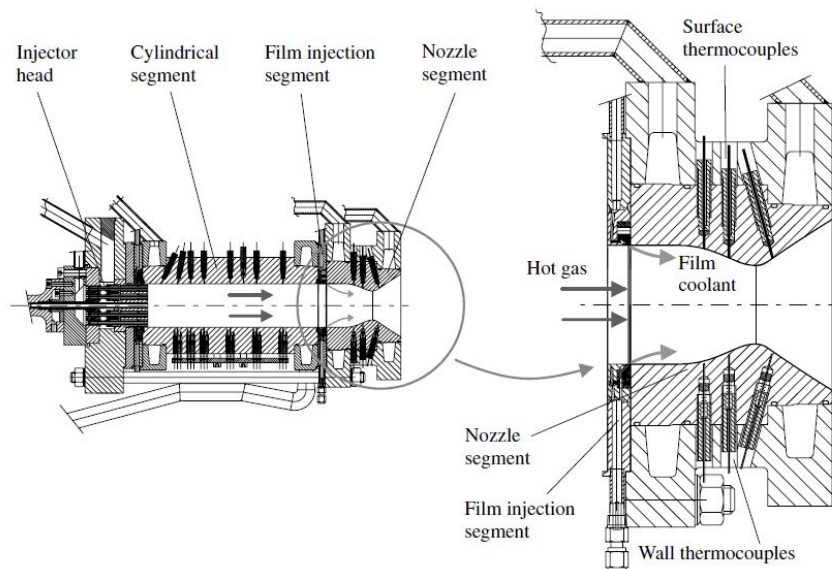


Figure 4.13: An example of slots used by film cooling located at the combustion chamber [6]

conclusion, several methods exist to protect the combustion chamber against the high temperatures during the ignition and combustion of the propellants. The design of the injector has to be adjusted in case if film cooling is chosen as a method to provide the required cooling. Then, the injector head can be used to provide slots where preferable, hydrogen peroxide is used as a coolant liquid. However, these slots can also be located at a specific point in the combustion chamber. The cooling of the combustion chamber is out of the scope of this thesis.

4.6. CONCLUSION

In total, four configurations of the injectors are designed. An example of one of the configuration can be seen in Figure 4.14. Each configuration consists of one swirl injector and two jet injectors. The swirl injector is used to atomize the HTP, while the jet is used to atomize the ethanol. The cross-section of these two injectors can be seen in Figure 4.15. The difference in the configurations is the change in the design of the jet atomizer and the alignment between the jet and swirl injector. The change in the design of the jet atomizer results in different SMD of the atomized ethanol and the SMD of the atomized HTP. The four configurations are used to investigate which configuration is the most suitable to be used for the dual-mode operation. To visualize the design, The swirl injector has been 3D printed to a 4 to 1 scale, as can be seen in Figure 4.16. This model can also be used in different meetings to discuss the manufacturing process.

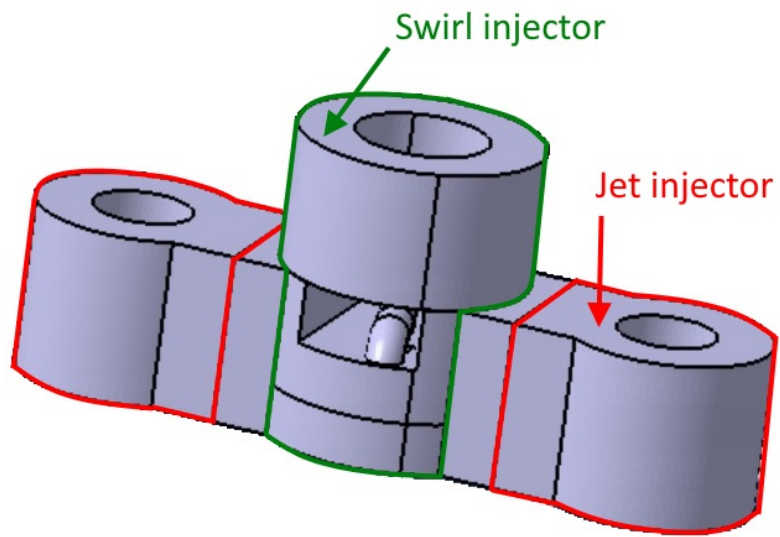


Figure 4.14: An overview of the exterior of the injector

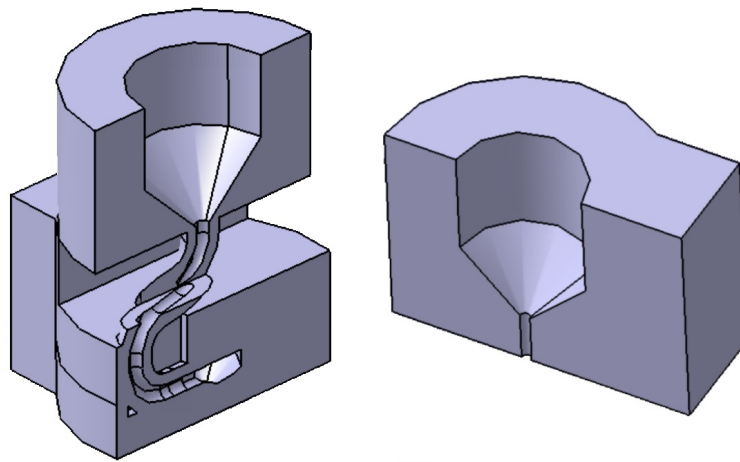


Figure 4.15: The cutaway of the Catia model of the swirl and a jet injector

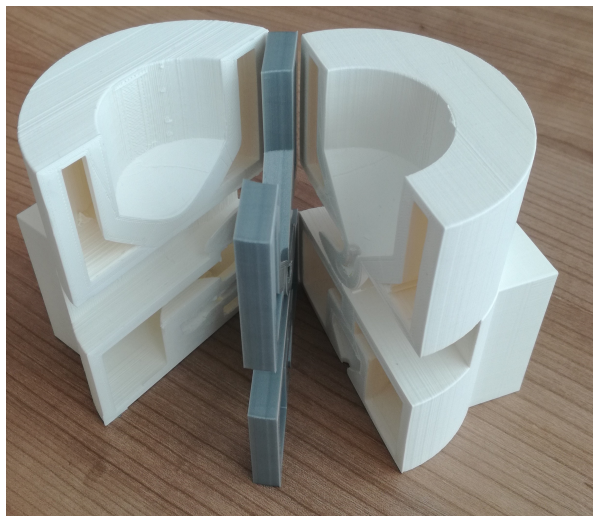


Figure 4.16: 3D printed model of the swirl injector to a 4:1 scale

5

PROTOTYPE DESIGN

This chapter presents the injector improvements from the initial design. The new design, known as the prototype design, is being manufactured by an external company. In [Section 5.1](#) the additive manufacturing process is explained to provide a theoretical background. The recommendations of this external company about the initial design are described in [Section 5.2](#), and the improvements are explained in detail in [Section 5.3](#). The overview of the prototype design is described in [Section 5.6](#)

5.1. ADDITIVE MANUFACTURING

The chosen manufacturing method of additive manufacturing imposes several modifications to optimize the initial design. [Subsection 5.1.1](#) covers the motivation to use additive manufacturing to manufacture components for rocket propulsion systems. In [Subsection 5.1.2](#), Laser Powder Bed Fusion (LPBF) is explained to understand this specific additive manufacturing method.

5.1.1. ADDITIVE MANUFACTURING FOR ROCKET PROPULSION

Additive manufacturing is more popular to construct new components for rocket propulsion systems. One reason that is additive manufacturing reduces the required number of components and the number of welds. A study by NASA has shown that the usage of additive manufacturing methods can lead to a reduction in production costs and a reduction in the manufacturing time. It should be noted that the percentage reduction also depends on the designed part [\[7\]](#).

Additive manufacturing is classified in different categories, like Power Bed based, Direct Energy Disposition and Solid state, as can be seen in [Figure 5.1](#). The company SolvGE has warm connections with an external company, which has the expertise and equipment in Laser Powder Bed Fusion (LPBF). This company has assisted in the manufacturing process of this thesis. For this reason, the LPBF is discussed in more detail below. The category which includes Powder Bed Fusion method is indicated in red, in [Figure 5.1](#).

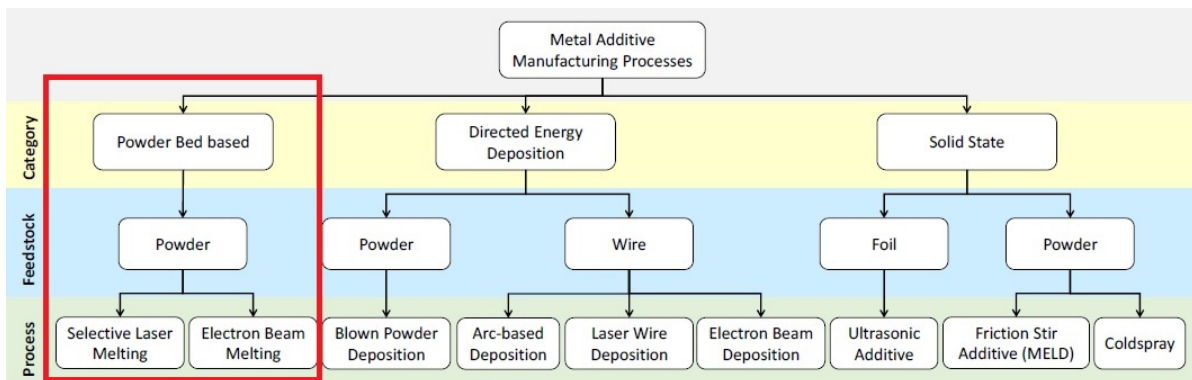


Figure 5.1: Classifications additive manufacturing methods [\[7\]](#)

5.1.2. POWER BED BASED MANUFACTURING PROCESS

The Power bed based manufacturing process uses a laser to melt the metal powder that is placed in a chamber. The desired part is manufactured is sliced in several 2D profiles that forms the input where the material has to melt. After melting the metal powder in the desired 2d profile, the build plate moves down to provide a new layer of metal powder. Then the next 2D profile is melted, and this process is repeated till the end of the manufacturing process. This process can be seen in [Figure 5.2](#). LPBF should not be confused with direct metal laser sintering (DMLS). The difference between LPBF and DMLS is that for LPBF is metal powder is melted, but for DMLS the metal powder is fused. . Similar to 3d printing of plastic material, a support structure can be used for overhanging structures. The support structure is removed during post-processing. This is challenging, as the main component and the support structure made of the same base material.

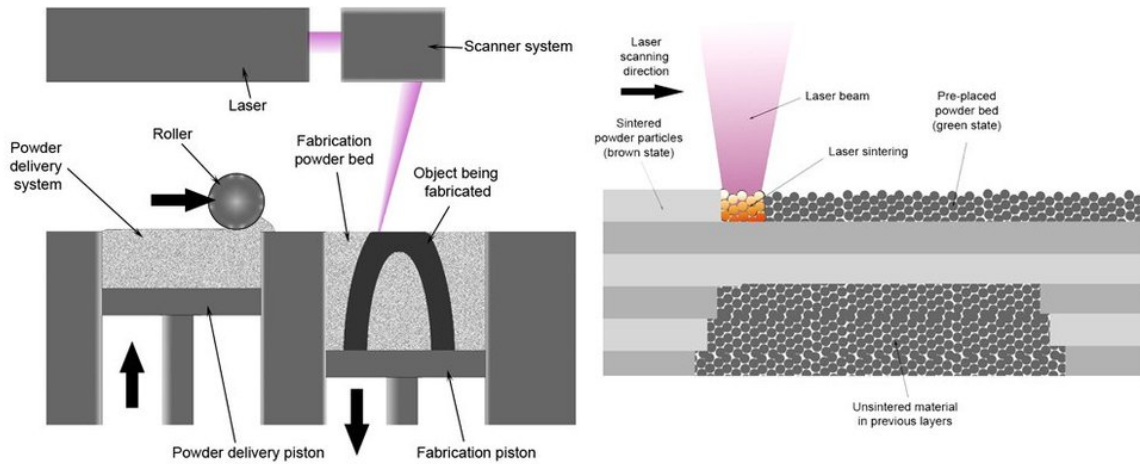


Figure 5.2: Power bed based manufacturing process explained [8]

The LPBF manufacturing method is ideal for complex structures that otherwise would be expensive or challenging to manufacture by other manufacturing methods. A second benefit is that a number of the same parts can be manufactured simultaneously. The drawback is the required knowledge and tools to realize the parts. Also, the parts should be adjusted for this manufacturing method, since otherwise it is an expensive process. The expertise of an external company is used to optimize the injector designs for the LPBF manufacturing method.

5.2. ALTERNATION FOR THE MANUFACTURING METHOD

The initial design was discussed in great detail with the external company. During several meetings feedback was given about the initial design in order to adjust the design for the LPBF. The feedback is summarized below:

- It is desired to have a simple geometry for an less time consuming manufacturing process. The initial design has a complex geometry by having an void between the connector and swirl injector. This region is indicated in Figure 5.3. It is required to fill this void.

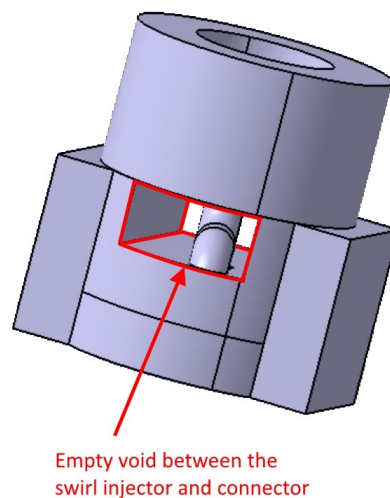


Figure 5.3: Definition of the void

- The angle between the flange and the tubing of the swirl connector is 90 degrees in the initial design. With this location of the tubing, the wall thickness has a minimal value in the order of 1 mm. This wall thickness is increased for the prototpye design.
- The required distance between the jet and swirl injector should be increased to fit certain components for testing purposes. Several changes are advised to ensure a sufficient fitting between the test setup and the injector

- The tubing that connects the swirl injector and the connector has a circular cross-section. It can be challenging to manufacture tubing with a circular cross-section using additive manufacturing. For tubing no support structure can be used, since it would block the internal flow. However support structure is needed to be able to print the overhanging surfaces. The overhanging structures can occur during the manufacturing of a circular shape. A possible solution for this is to not use a circular cross-section, but a cross-section that has the shape of a droplet. By doing so, a less steep angle is used compared to the circular cross-section and thus no support structure is required. A graphical overview of of the cross-section and the support structure can be seen in [Figure 5.4](#).

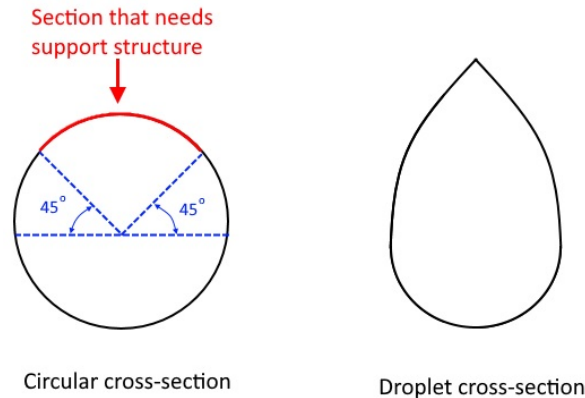


Figure 5.4: Schematical example of the cross-section and support structure

- The selected tolerances in the technical drawings of the initial design can not be achieved by LPBF only. The additive manufacturing process has a tolerance of ± 0.1 mm. To achieve the set tolerances of ± 0.05 mm the manufacturing method of electrospray can be used. When doing so, the set tolerances can be met but at the cost of requiring extra time to manufacture the injector configurations. The effect of the new tolerances on the performance is explained in [Subsection 5.3.5](#).
- Some material can be saved in the connection between the jet and swirl injector. This will reduce the cost of the manufacturing method.
- Some geometric dimensions have to be altered to accommodate for the additive manufacturing method, such as internal diameters and height.

5.3. ITERATED DESIGN

The feedback of the external company, as discussed in [Section 5.2](#), forms the input for the required changes to be made to the initial design. This new design is manufactured and tested. In [Subsection 5.3.1](#) improvements are made related to the feedback about the internal geometry. The made modifications related to support structure and tubing is described in [Subsection 5.3.2](#). The required geometric changes are explained in [Subsection 5.3.4](#). The effect of the new tolerances is discussed in [Subsection 5.3.5](#). The required change related to the feedback of the connection between the swirl and jet injector is described in [Subsection 5.3.3](#).

5.3.1. SIMPLIFIED INTERNAL GEOMETRY

It is desired to remove the empty void between the connector and the swirl injector to simply the internal geometry. Consequently, the manufacturing process is simplified. An additional benefit of simplifying the internal geometry is that the tubing is more protected during handling. Also, the orientation of the tubing has been altered to provide additional protection for the tube, as can be seen in [Figure 5.5](#). In the initial design, indicated in red, the tube was orientated in 90 degrees related to the flange. The new orientation, indicated in green, is in the same direction as the flange. Consequently, the wall thickness of the tube increases.

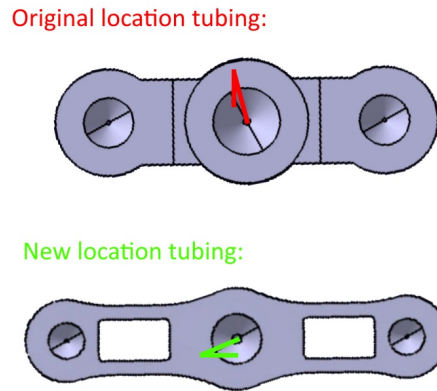


Figure 5.5: Schematic overview of the changes in tubing orientation

5.3.2. CROSS-SECTION TUBING

The inlet port geometry is crucial to provide the required starting condition to atomize the propellant, as specified in Subsection 4.2.1. For this reason, it is undesirable to alter this cross-section. The requirement was to avoid using a support structure for the cross-section of the tubing that connects the swirl injector and the connector. After consideration with the external company, it was concluded that no changes in cross-sections to be made to prevent the usage of a support structure, due to small cross-sections.

5.3.3. CONNECTION SWIRL AND JET INJECTOR

In the future, additional sensors could be used to measure data, for example the inlet pressure. These sensors were planned to be used, but this was not possible due to the budget constraints during this thesis. However, these sensors are taken into account during the current design to fully optimize the financial investment of manufacturing the current design. To connect these sensors, a 'T' joint is recommended. The distance between the jet and swirl injector is increased to be able to mount the different 'T' joint at the inlets of the swirl and jet injector. Increasing this distance demanded more material. According to the external company, some material could be saved in the connection between the jet and swirl injector. As a result, two cavities are included in the new design.

5.3.4. GEOMETRIC DIMENSIONS

In the injector, threads help to connect the feed lines to the injector. In the initial design, the inner diameter of the connectors is based on the required drill size. However, it is essential to have some extra material for margin. As a result, the internal diameter is decreased by 1 mm for the sections where a thread is required.

The height of the jet injector is increased to align with the swirl injector. As a result, the injector was able to be mounted to the test stand. It is essential to have a flat surface of both connectors to prevent any problems during the mounting of the injector. Additionally, a flat surface is needed for both the connectors for ease of injector mounting. The height of the swirl and jet injector was increased by 1 mm to machine a flat surface. Figure 5.6 shows the initial injector design modifications.

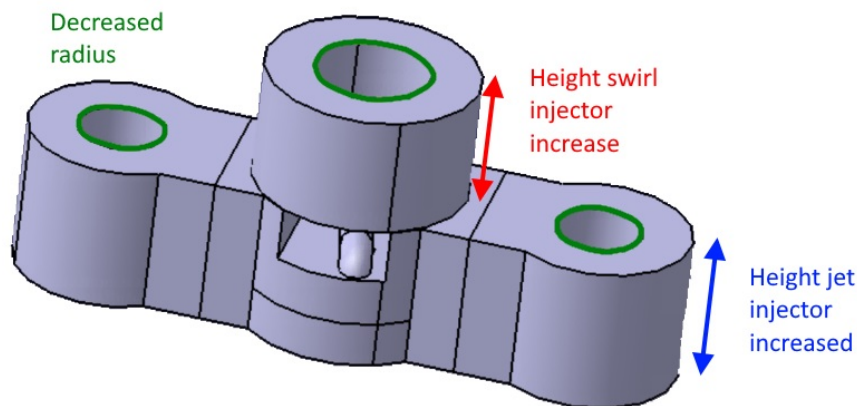


Figure 5.6: Overview of the made changes to the geometry

5.3.5. TOLERANCES

The effect of ± 0.1 mm tolerances on injector performance was investigated. For that, a new python script is written. In this python script, the geometric dimensions are used as an input to compute the performance. Figure 5.8 shows the schematic overview of the rewritten logic for this script. The discharge coefficient of the jet injector is an input parameter. This parameter value of 0.09 [-] has not changed from the initial design since the mass flow and kinematic viscosity have not changed. Only these parameter influences the value for the discharge coefficient. The used scripts are given in the Appendix C.

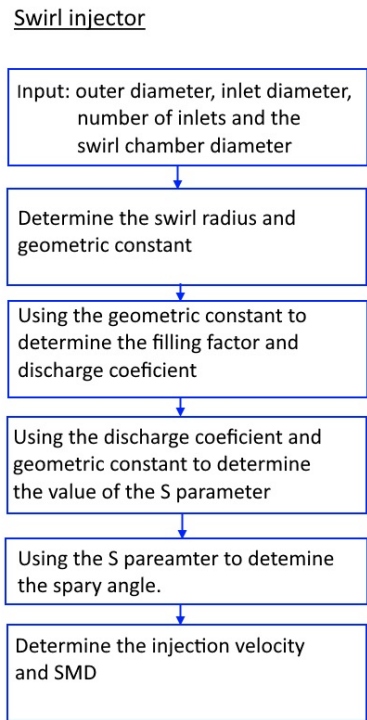


Figure 5.7: Schematic overview of the logic for the script to determine the effect of the tolerances

SWIRL INJECTOR

The performance of the initial design of the swirl injector is explored when the reduced tolerances are applied. As can be seen in Table 5.1, the modified script estimates the same theoretical performance as in described in Chapter 4. The reduced tolerances can lead to an increase of 0.1 mm in the outlet diameter. The effect of the increase in outlet diameter on the performance parameter (as SMD, spray angle and injection velocity) can be seen Table 5.1 in column "higher outlet diameter". A second possibility is the increase of the swirl chamber radius by relaxing the tolerances. The associated theoretical performance by an increase in swirl chamber diameter can be found Table 5.1 in the column "higher swirl radius". A third possibility of the relaxed tolerances is the increase in the inlet diameter. This change leads to a change in performance, as indicated in Table 5.1 in the column "higher inlet diameter". An increase of 0.1 mm of the outlet diameter, outlet length and inlet diameter simultaneously is also a possibility by having reduced tolerance. The associated theoretical performance can be found in Table 5.1 in the column "all dimensions higher". Besides an increase, it is also possible to have a decrease in the outlet diameter and length and the inlet length. The related performance can be found Table 5.1 in the column "All dimensions lower".

Table 5.1: Overview of the effect of the tolerances

	Original dimensions	Higher outlet diameter	Higher swirl radius	Higher inlet diameter	All dimensions higher	All dimensions lower
Outlet diameter [mm]	1.09	1.19	1.09	1.09	1.19	0.99
Swirl radius [mm]	5.67	5.67	5.79	5.67	5.77	5.59
Inlet diameter [mm]	1.29	1.29	1.29	1.39	1.39	1.19
Discharge coefficient [-]	0.23	0.21	0.21	0.25	0.23	0.21
Geometric constant [-]	2.90	3.16	2.97	2.44	2.72	3.20
Pressure drop [Bar]	2.00	3.16	2.07	1.56	1.30	3.20
SMD [micrometer]	58.50	63.35	57.15	69.61	73.00	45.40
Spray angle [deg]	90.00	92.14	90.53	85.60	88.40	91.00
R/r0 [-]	4.00	3.66	4.09	3.90	3.66	4.40
Injection velocity [m/s]	16.90	15.13	17.18	14.90	13.50	21.00

From [Table 5.1](#) it is clear that relaxing the tolerances has a serious effect on all performance parameters. For example, the pressure drop increases to a maximum value of 3.2 bar, which is 60 percent increase compared to the original design. This increase in pressure drop had to be taken into account for the test setup. Additionally, the SMD has a maximum value of 73 micrometers (25 percent increase) and a minimum value of 45.4 micrometers (22 percent decrease). Furthermore, it is seen that the spray angle increases to a value of 92 degrees (2 percent increase) and decreases to a value of 88.4 (2 percent decrease).

JET INJECTOR

In this section, the effect of relaxing the tolerances on the performance is explored for a jet injector with an outlet of 0.64 mm. A new python script was made to explore this effect and the overview of this script is provided in [Figure 5.8](#). To evaluate the modifications, the original dimensions are used as an input parameter, as seen in [Chapter 4](#). By relaxing the tolerances the outlet diameter can be increased by 0.1 mm. The effect of this change on the performance is given in the column of "outlet diameter higher" of [Table 5.2](#). A second possibility of relaxing the tolerances is the increase in the outlet length. The associated theoretical performance with this change can be seen in [Table 5.2](#) column "outlet length higher". A third possible scenario by relaxing the tolerances is that the outlet diameter and length is increased by 0.1 mm. The effect on the performance is indicated in the column "all dimensions higher" of [Table 5.2](#). The fourth possibility is that the outlet length and diameter is decreased by relaxing the tolerances. The performance of the decrease in dimensions can be seen in [Table 5.1](#).

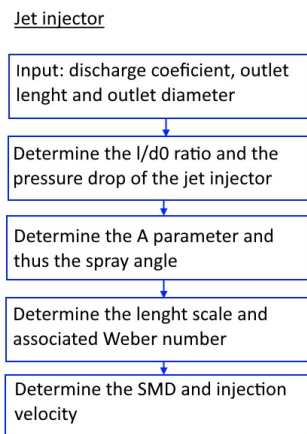


Figure 5.8: Schematic overview of the logic for the script to determine the effect of the tolerances

Table 5.2: Overview of the effect of the tolerances of the swirl injector

	Original Dimensions	Outlet diameter higher	Outlet length higher	All dimensions higher	All dimensions lower
Outlet diameter [mm]	0.64	0.74	0.64	0.74	0.54
Outlet length [mm]	3.21	3.21	3.31	3.31	3.11
Pressure drop [bar]	2.20	1.23	2.20	1.23	4.32
Spray angle [degrees]	3.73	3.89	3.69	3.86	3.56
SMD [micrometer]	45.32	72.20	45.32	72.20	29.00
Injection velocity [m/s]	23.60	17.60	23.60	17.60	33.11

From [Table 5.2](#), it is clear that relaxing the tolerances has a crucial consequence on the performance. For example, the pressure drop has a maximum value of 4.32 bar, which is a 96 percent increase. Furthermore, the SMD will vary to a maximum value of 72.2 micrometers (60 percent increase) and a minimum value of 29 micrometers (36 percentage decrease). Additionally, the spray angle has a maximum value of 3.89 degrees (4 percent increase) and a minimum value of 3.56 degrees (5 percent decrease).

The effect of the relaxed tolerances on the performance is repeated for all the jet configurations. The minimum and maximum SMD values, caused by the relaxed tolerances, are shown in [Table 5.3](#). From this table it is observed that the minimum value of the SMD from configuration 2 is lower than the maximum value of the SMD of configuration 1. This is also applicable for configuration 3. Hence, the relaxed tolerances introduced some overlap in the SMD parameter between the different configurations. The different jet configuration were selected to investigated how a different values for the SMD influencing the atomization process. This research objective was discussed in [Chapter 4](#). By introducing some overlap between the configuration, this research objective cannot be met.

Table 5.3: Overview of the minimum and maximum values of the SMD for the different jet injectors configurations

	Min SMD [micrometers]	Max SMD [micrometers]
Configuration 1	29	73
Configuration 2	38	95
Configuration 3	54	124
Configuration 4	38	95

RESULT RELAXING TOLERANCES

The research objective of the different configurations are not met by having relaxed tolerances. A possible solution to meet the research objective is to have stricter tolerances by using an different manufacturing process. However, this leads to an increase in manufacturing time and cost. So this option was discarded. Another option was to alter the dimensions to accommodate the tolerances of $\pm 0.1\text{mm}$. The benefit of this option is that, when the dimensions are modified, the different post-machining process can be used to experiment to achieve stricter tolerances. If the results of the experiment to achieve stricter tolerances are disappointing, the injector still can be used to achieve the set testing goals. For this reason, it is decided to modify the dimensions.

NEW DIMENSIONS

An iterated process was used to determine the best possible dimensions for the given tolerances of plus or minus 0.1mm to achieve the desired test goals. The new dimensions and associated performance per injector type are given below:

- **Swirl injector:**

The new dimensions are an outlet diameter of 1.6 mm, inlet diameter of 2.0 mm, a swirl radius of 8.41 mm. This leads to a pressure drop of 0.37 bar. Using these parameters results in an ideal case, an SMD of 139 micrometers. In the worst-case scenario, the SMD of the swirl injector varies, caused by the tolerances and has a minimum value of 117.8 micrometers and a maximum value of 163.1 micrometer

- **Jet injector - configuration 1:**

Having a pressure drop of 1.56 bar, results in an outlet length of 3.5 mm and an outlet diameter of 0.7 mm. These design parameters results in an ideal case an SMD of 59.7 mm. The SMD varies by applying the tolerances to the dimensions. Then, the SMD has a minimum value of 36.3 mm and a maximum value of 91.7 mm.

- **jet injector - configuration 2 and 4:**

A pressure drop of 0.57 bar, an outlet length of 4.5 mm and an outlet diameter of 0.9 mm leads, in an ideal case, to an SMD of 134 micrometers. In the worst-case scenario, the SMD has a minimum value of 91.7 micrometers and a maximum value of 188.5 micrometers.

- **jet injector - configuration 3:**

The new dimensions are: an outlet diameter of 1.1 mm, an outlet length of 5.5 mm results in a pressure drop of 0.256 bar. In an ideal case, this leads to an SMD of 256 micrometers. When the tolerances are applied to the dimensions results in a minimum value of 188 micrometers and a maximum value of 338.4 micrometers.

In [Table 5.4](#) the minimum and maximum values of the SMD for different injector configuration and types are listed. As can be seen in this table, the new dimensions ensure that for the first configuration, the SMD of the jet injector is always smaller than the SMD of the swirl injector, despite having relaxed tolerances. For the second and fourth configuration, the SMD of the jet and swirl injector is in the same magnitude. The SMD of the jet is always larger than the SMD of the swirl injector. Hence, with the new dimensions, relaxed tolerances can be used and still full fill the set test goals.

Table 5.4: Overview of the different configurations and the associated SMD

	Jet injector		Swirl injectors	
	<i>Min SMD</i> <i>[micrometers]</i>	<i>Max SMD</i> <i>[micrometers]</i>	<i>Min SMD</i> <i>[micrometers]</i>	<i>Max SMD</i> <i>[micrometers]</i>
Configuration 1	36.3	91.7	117.8	163.1
Configuration 2	91.7	188.5	117.8	163.1
Configuration 3	188.5	338.4	117.8	163.1
Configuration 4	91.7	188.5	117.8	163.1

5.4. STRUCTURAL INTEGRITY

The external company has performed a structural analysis with the new geometry of the different injectors. Finite elements are used to investigate the stresses inside the injector when a pressure of 10 bar is applied at the injector. A mesh of 228000 elements is used to compute the stresses when the injector is clamped to the test setup at the top surface. From these simulations, the maximum stress of 4.4 MPa is seen when an inlet pressure of 10 bar is applied. In [Figure 5.9](#) the stresses at the cross-section of the swirl injector is shown. This is much lower than the yield strength of 450 Mpa [34]. So, with the given geometry the injector is capable to withstand the pressure.

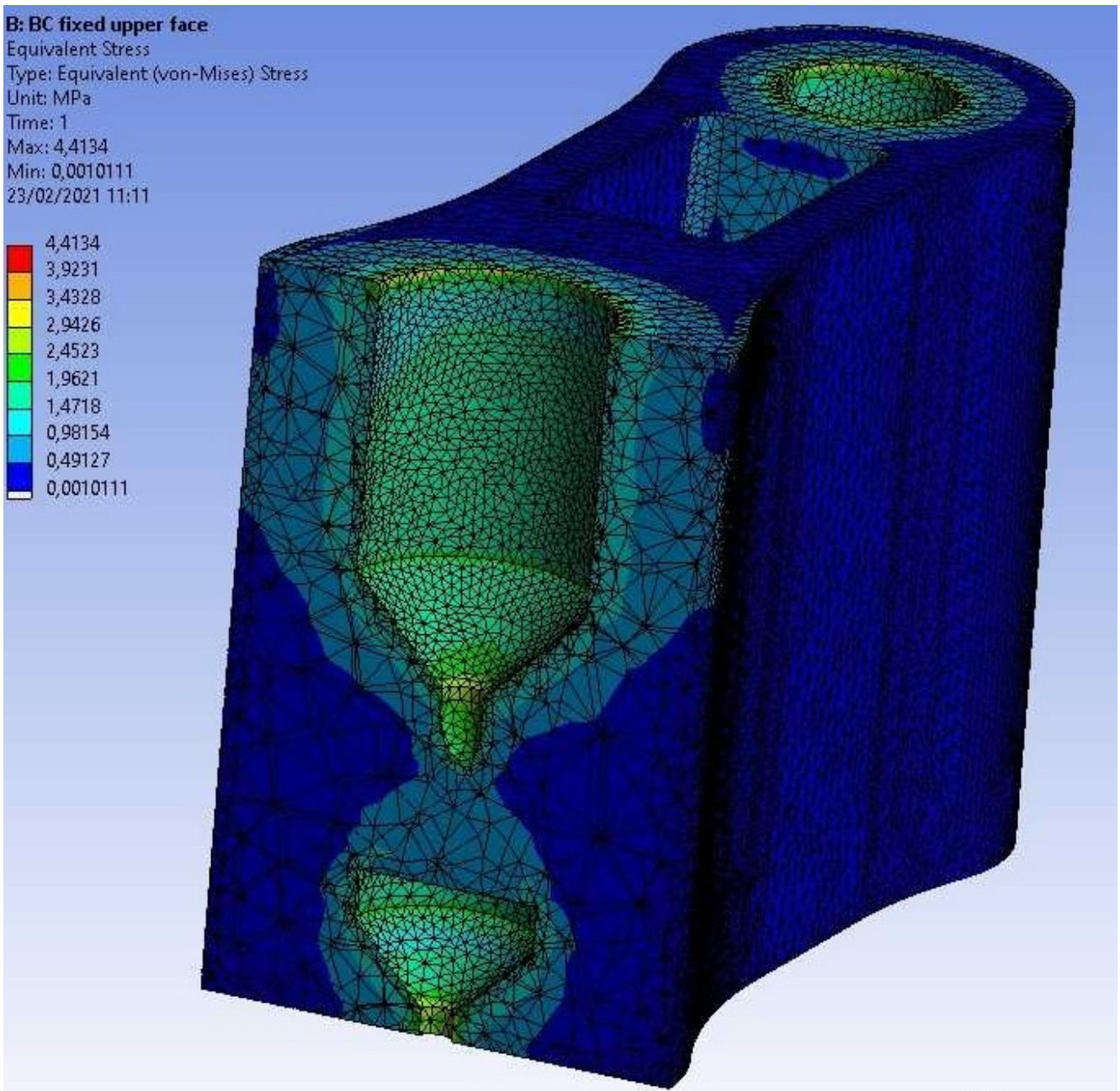


Figure 5.9: The structural analysis, performed by the external company, of the injector when an inlet pressure of 10 bar is applied

5.5. MANUFACTURING

The injector was placed in an inverted orientation, facing the outlets to the top. By using this orientation, no support structure in the outlets has to be removed during the post-processing, preventing additional challenges during the post-processing. An extra benefit of printing the different configurations in this orientation is that no support structure is needed when manufacturing the swirl chamber. In the current design, the swirl chamber has an inverted cone shape with a half-angle of 45 degrees. With the inverted orientation, an overhanging surface of the cone-shaped swirl chamber occurs, with also a 45-degree half-angle. An overhanging surface of 45 degrees half angle is the limit where no support structure is required. So, to avoid the usage of support structure for the swirl chamber, a minimum half angle of 45 degrees is required.

Some challenges were faced during the manufacturing process. Due to the COVID-19 crisis, the manufacturing facilities were used less frequently. This resulted in that the laser was unfocused, and the metal powder gained humidity. As a result, several injector defects can be seen in detail in [Figure 5.10](#) on the left side. Several injectors are printed to gain experience in manufacturing the different configurations, as seen in [Figure 5.10](#), on the right image.

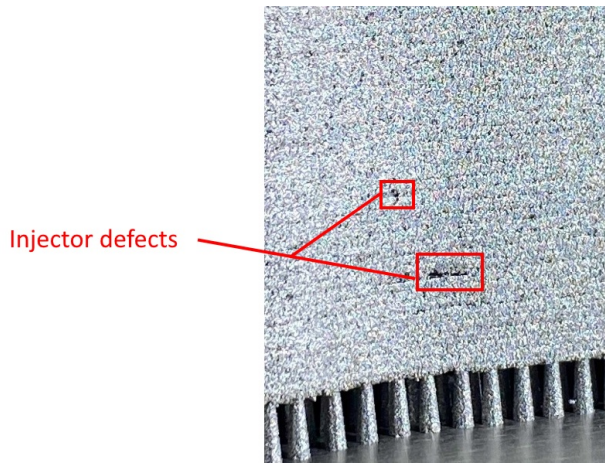


Figure 5.10: Injector defects during manufacturing process in detail

The LPBF additive manufacturing facilities were quickly repaired, and the injector was printed without any defects. To investigate whether, the tolerances were achieved, 3D scanning was planned. However, due to small dimensions, the 3D scanning method was not possible to be used. So, the holes are checked with different drill bits. For example, the outlet diameter of 0.7 mm is first checked if a drill bit of 0.8 mm fits, which did not. So, the outlet is smaller than 0.8 mm. The same process was repeated for a drill bit of 0.6 mm. These tests conclude that the tolerances of ± 0.1 mm were achieved. The manufactured injectors, before any post-processing, can be seen in Figure 5.11. In this figure, the printing orientation can be seen. It was decided to manufacture the injector upside down, to minimize the usage of support structure and manufacturing time.

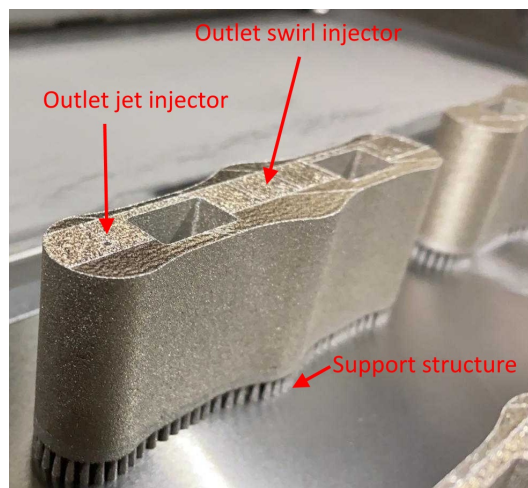


Figure 5.11: Injectors before processing

5.6. CONCLUSION

To summarize, several changes were made to adjust the initial design for the chosen additive manufacturing process. Several meetings were scheduled with the external company to determine the required modifications. The prototype design has a simplified internal structure which reduces the manufacturing time. After exploring the effect of relaxed tolerances, it was concluded that relaxing the tolerances has a severe consequence on the performance. As a result, the research objective was not met. Therefore, new geometric dimensions were determined, these new dimensions are shown in Table 5.5. Several changes ensure a good connection with the injector and the test setup. See Figure 5.12 for a graphical example of the new design and the machined threads. The technical drawings can be found in the Appendix B.

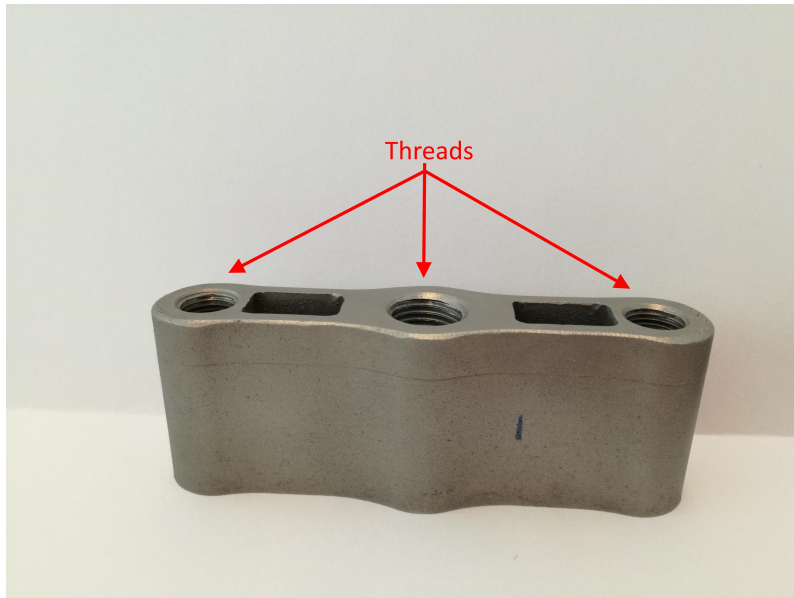


Figure 5.12: The new design for the prototype

Table 5.5: Overview of the new dimensions of the prototype

	Outlet diameter [mm]	Outlet length [mm]	Swirl radius [mm]	Inlet port diameter [mm]
Swirl injector	1.6	1.4	8.4	2.0
Jet injector- configuration 1	0.7	3.5	N/A	N/A
Jet injector - configuration 2 and 4	0.9	4.5	N/A	N/A
Jet injector - configuration 3	1.1	5.5	N/A	N/A

6

TEST SETUP

A test setup is required to test the different injector configurations, but no testing facilities for injectors existed at the DAMSL (Delft Aerospace Structures and Materials Laboratory) and SolvGE. So, a new test setup has to be designed and manufactured. The design process of this test setup is discussed in this chapter. Existing test setups are explored in [Section 6.1](#). The design of the propellant tanks is explained in [Section 6.2](#). In [Section 6.3](#), the pressurant gas is selected from the available options. The design process is explored in [Section 6.4](#). The safety of the test setup is described in [Section 6.6](#). A overview is made in [Section 6.7](#).

6.1. EXISTING TEST SETUPS

Existing test setups are investigated to aid the design process of the used test setup. The test setup that used a syringe pump to feed the propellant is explored in [Subsection 6.1.1](#). In [Subsection 6.1.2](#), a pressure-fed propellant feed system is investigated.

6.1.1. SYRINGE PUMP

The syringe pump NE-1000 from the company "New Era Pump systems INC" was used to feed the propellant during the initial investigation of the new propellant of hydrogen peroxide. According to the manufacture, the syringe pump is designed to pressurize the propellant. The maximum pressure depends on the used size of the syringe. For example, a 60 ml syringe can pressurize the propellant to 30 *psi*, equal to 2 *bar*. The syringe pump has also limited volume flow. Again, the minimum and maximum values of the volume flow depend on the selected syringe size. In [Figure 6.1](#) an overview is given of different syringe sizes and associate volume flows. As can be seen in this figure, the maximum value of the volume flow is 3470 mL/hr ($9.636 \cdot 10^{-7} m^3/s$) for a syringe size of 140 ml [9].

Syringe Size	Maximum Rate	Minimum Rate
0.5 μ L	25.49 μ L/hr	0.001 μ L/hr
1 mL	52.86 mL/hr	0.727 μ L/hr
3 mL	223.8 mL/hr	3.076 μ L/hr
5 mL	372.5 mL/hr	5.119 μ L/hr
10 mL	607.6 mL/hr	8.349 μ L/hr
20 mL	966.2 mL/hr	13.28 μ L/hr
30 mL	1260 mL/hr	17.32 μ L/hr
60 mL	2120 mL/hr	29.1 μ L/hr
140 mL	3470 mL/hr	47.7 μ L/hr



Figure 6.1: Information of the syringe pump and the associated volume flow [9]

The required mass flow for the HTP is 0.005 *kg/s*, as discussed in [Chapter 4](#). The maximum mass flow that the syringe pump is capable to supply to the injectors is $9.636 \cdot 10^{-7} m^3/s$. This was converted to the mass flow by multiplying the volume flow rate with the density of HTP ($1400 kg/m^3$). As a result, the maximum mass flow that can be obtained by the syringe pump for HTP is 0.00135 *kg/s*, while 0.005 *kg/s* is required by the design. Hence, the syringe pump is not capable to provide the required mass flow of 0.005 *kg/s*.

The syringe pump can only pressurize the propellant to a maximum value of 2.0 *bar*. The jet injector of the first configuration has a pressure drop of 1.56 *bar* when neglecting the geometric tolerances. The pressure drop could be increased to 2.89 *bar* if the tolerances on the geometrical dimensions were taken into account. Hence, the syringe pump is not capable of providing the required pressure. It is desirable to be able to vary the inlet pressure, leading to a higher level of tank pressurization than the 2.89 *bar*.

In conclusion, it is undesirable to use the syringe pump to feed the propellant to the injector, because the requirements of the mass flow and pressurization level cannot be met.

6.1.2. PRESSURIZED PROPELLANT FEED SYSTEM

A different method has to be used to feed the propellant to the injector since it is undesirable to use a syringe pump. The literature study provided the information that pressure feed setup commonly use for injector study [20]. An example of such a test setup is given in Figure 6.2. As can be seen, a pressurant gas is used to pressurize the propellant and feed to the injector. The usage of pressurant gas has additional benefits. For example, the mixture ratio is a design parameter which is not the case when using a syringe pump. So, it was chosen to use a pressure feed test setup to feed the propellant to the injector configurations. In the next section, all the design details of the test setup are discussed. The goal of this test setup is to investigate the injector performance and to provide a feasible test facility for SolvGE for future injector studies.

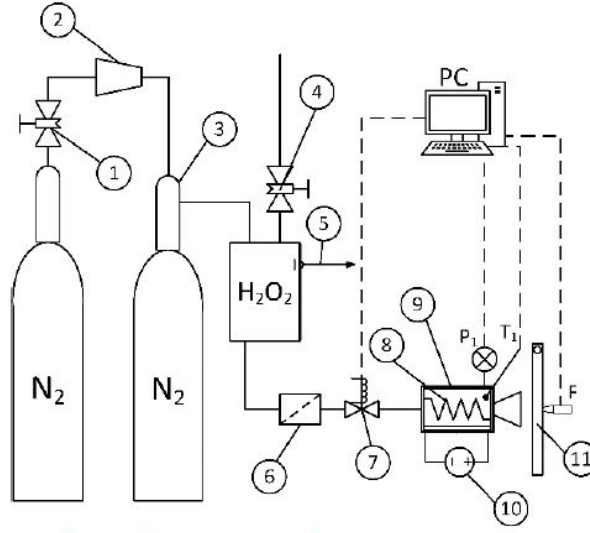


Figure 6.2: Schematic overview of the test setup, where 1 is the Nitrogen valve, 2 is the Pressure reductor, 3 is the Low pressure nitrogen tank, 4 is the HTP filling valve, 5 is the Safety valve, 6 is the HTP filter, 7 is Injection valve, 8 is the heater, 9 is the decomposition chamber, 10 is the Power supply and 11 is Thrust measurement device [10]

6.2. DESIGN OF PROPELLANT TANKS

Two tanks are required to store the propellant during testing operations. These tanks should be compatible with the used chemicals and can withstand a maximum pressure of 10 bar. In the chemical lab of the DAMSL, a glass tank is found with a volume of $2.6 \cdot 10^{-5} m^3$ and two outlet ports. One port can be used as an inlet port, to pressurize the propellant, while the second port can be used as an outlet port, going to the injector. While glass is compatible with the stored chemicals, but it is doubtful if glass can withstand a pressure of 10 bar. Hence, glass is not suitable for injector research. Also, the two outlet ports are located at the top of the glass tank. For injector application, an outlet port located at the bottom is desirable. To achieve the required mass flow, the outlet diameter has to be modified. Hence, a metal tank is more suitable than a glass tank for current research and it was decided to design a new propellant tank.

The volume of the designed tank is equal to the total volume of the glass tank. The mass flow needed for injector research is determined in Chapter 4. For the hydrogen peroxide tank and ethanol tank, a mass flow of $0.0005 kg/s$ and $0.000113 kg/s$ is required, respectively. Equation 6.1 and Equation 6.2 are used to determine the required outlet diameter and pressure of the tank. In these equations, the mass flow has the symbol \dot{m} in kg/s , the parameter ρ is the density of the propellant expressed in kg/m^3 , and the outlet area of the tank is in m^2 with the symbol A . The outflow velocity of the propellant is in m/s and is referred to the parameter V . The static pressure is equal to the level of pressurization of the propellant. The dynamic pressure depends on the velocity and the density of the liquid. The selected outlet diameter of the tank determines the velocity of the liquid.

$$\dot{m} = \rho A_{outlet} V \quad (6.1)$$

$$P = P_{static} + P_{dyn} = P_{static} + \frac{1}{2} \rho V^2 \quad (6.2)$$

For the hydrogen peroxide tank, an outlet diameter of $2 mm$ was selected. Having a density of $1400 kg/m^3$, an outlet diameter of $2 mm$, and a mass flow of $0.005 kg/s$ will result in a velocity of $1.14 m/s$. The static pressure at this velocity is

904.65 Pa. For the ethanol tank, an 1mm outlet diameter was selected. For this outlet diameter, a density of 789.4 kg/m^3 and a mass flow of 0.000114 kg/s will result in a velocity of 1.83 m/s . Therefore, the dynamic pressure is 1324 Pa . A precise pressure regulator is capable of regulating the pressure with an accuracy of $\pm 2.5 \text{ mbar}$, 250 Pa . In consultation with the external company, an oval shape was decided to be used. For an oval shape, no support structure has to be used and this is a suitable geometry that can withstand the required pressure. The external company helped to determine the required propellant tank wall thickness. Extra mass is added to increase the safety margin to withstand the pressure. According to the external company, the tanks have a burst pressure of 100 bar . Results of the simulations, like stress and deformation, can be found in Figure 6.3.

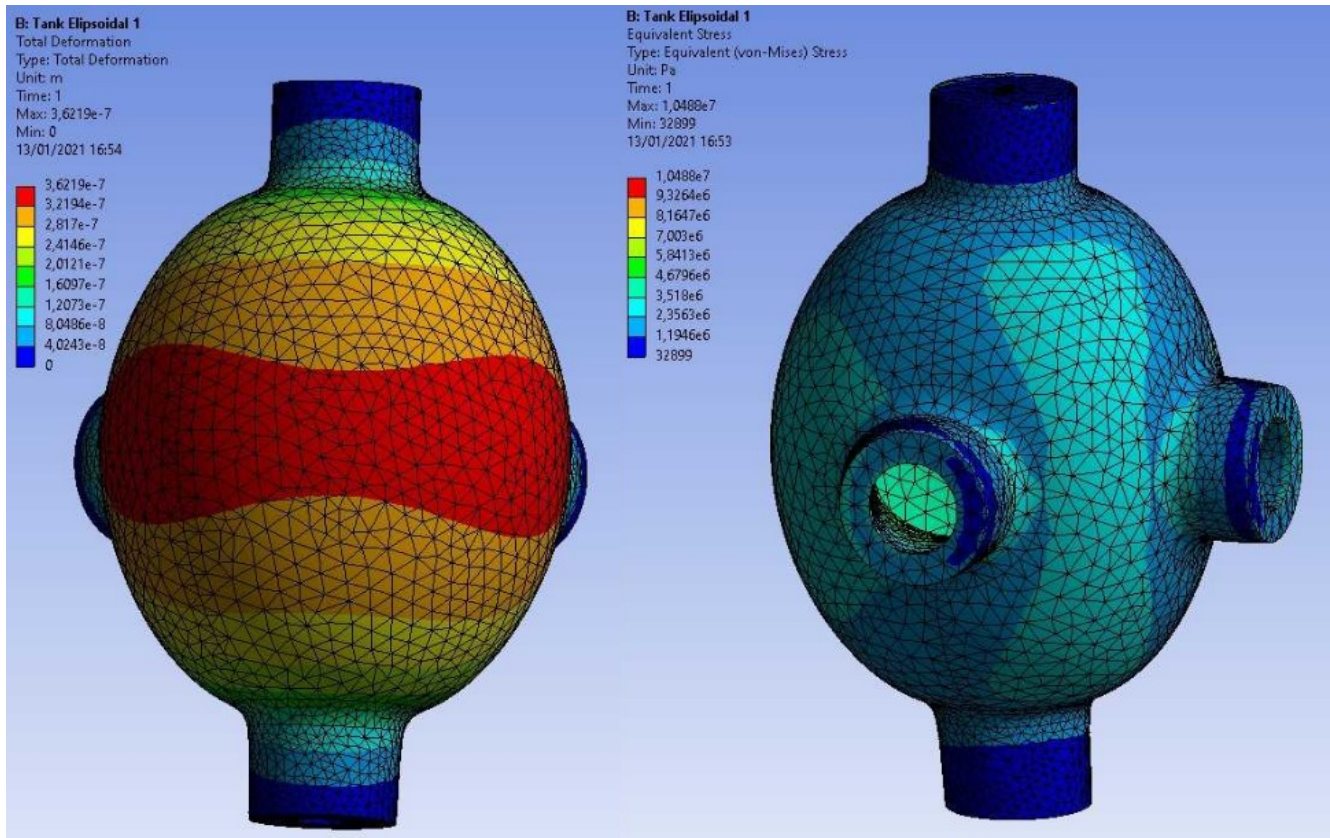


Figure 6.3: Structural analysis of the tank design performed by the external company

In conclusion, the outlet diameter of 2 mm for the hydrogen peroxide tank and 1 mm for the ethanol tank was selected to achieve the desired mass flow. The required dynamic pressure to obtain the desired mass flow can be achieved by a precise pressure regulator. The tank has two additional ports, one to fill the tank and one to connect the safety valve.

6.3. SELECTING THE PRESSURANT GAS

Nitrogen and compressed air are available in the DASML lab to pressurize the propellant tanks. Different options in the chemical lab exist to provide these gasses to the test setup. First, the required quantity of pressurant gas is determined before a selection is made which option is used to feed the pressurant to the test setup.

Equation 6.3 is used to determine the required quantity of the pressurant gas. In this equation, the tank pressure has the symbol P_t in Pa, R is the gas constant for the selected gas, the volume of the propellant tank is in m^3 and has the symbol V_{prop} . The beginning and end pressure of the pressure tank are indicated by p_0 and p_f respectively and both are in Pa. The volume of the propellant tank is equal to $2.657 \cdot 10^{-5} \text{ m}^3$. It is desired to conduct 100 tests with a single pressurant tank. Therefore, a propellant tank volume of $2.657 \cdot 10^{-3} \text{ m}^3$ is used in the calculations. The beginning pressure of the pressurant tank is 200 bar . An end pressure of 30 bar in the pressurant tank after 100 test firings is assumed. Using these parameters, the mass of the pressurant gas is determined for the cases where nitrogen and compressed air are used. When nitrogen is used, a total of 0.0372 kg is required. This can be converted to a total volume of 0.0304 m^3 . For compressed

air, a total of 0.038 kg is required or a volume of 0.0304 m³.

$$M_{gas} = \frac{\frac{2P_t}{RT_0 \left(1 + \frac{P_f}{P_0} \frac{1-\gamma}{\gamma}\right)} V_{prop}}{\left(1 + \frac{P_f}{P_0} \frac{1}{\gamma}\right)} \quad (6.3)$$

The first option is to use the nitrogen outlet from the fume hood. The gas nitrogen is suitable due to its inert nature and will not react with the propellant. The outlet pressure of the nitrogen gas is measured and has a value of 2.3 bar. The chemical lab cannot increase the pressure of the outlets that are located inside the fume hoods. So, the outlet pressure is slightly larger than the maximum pressure of the syringe pump. For this reason, the nitrogen outlet from the fume hood is discarded as an option to be used to pressurize the propellant tanks.

The second option is to use a separate nitrogen tank supplied by the Gassenteam of the TU Delft. The Gassenteam offers two qualities of nitrogen gas, in different tank sizes. A 10-liter tank size was recommended to be used, based on the determined quantity. Compressed air is used to compare the financial price to rent a nitrogen tank. The contamination and chemical properties of nitrogen and compressed air tanks can be found in [Table 6.1](#). As noticed in this table, Nitrogen 5.0 has less contamination and is thus more suitable to be used to pressurize the propellant.

Table 6.1: Overview pressurant gas properties

	Compressed air dry	Compressed air synthetic	Nitrogen 3.0	Nitrogen 5.0
Contamination	CO ₂ <500 vpm H ₂ O <25 vpm C _x H _y <5 vpm	H ₂ O <5 vpm C _x H _y <1 vpm	O ₂ <1000 vpm H ₂ O <1000 vpm	O ₂ <5 vpm H ₂ O <5 vpm C _x H _y <0.2 vpm
Density [kg/m³]	1.29	1.29	1.25	1.25
Molecular weight	28.96	28.96	28.01	28.01

By having a separate pressurant tank, the outlet pressure can be adjusted to any desired level. However, this option affects the financial budget. The Gassenteam charges 46.42 Euro to rent a 10-liter nitrogen 5.0 tank and 42.02 Euro to rent a 10 liter compressed air tank. The financial resources are limited to manufacturing the injector and propellant tanks. Also, this option requires some planning to have the requested tank at the right time. For these reasons, this option is also discharged.

The third option is to use compressed air as pressurant gas. The chemical lab has several outlets for compressed air and has a suitable pressure of 8.5 bar, in contradiction to the nitrogen outlet in the fume hood. The drawback of this option is that the hydrogen peroxide sensitive to compressed air impurity. The test setup exposes hydrogen peroxide for a short time duration to compressed air, so this drawback acceptable. The benefit of this option is the required outlet pressure and economical.

6.4. TEST SETUP DESIGN

This section discusses the test setup and the diagram is presented in [Subsection 6.4.1](#). The selection of the used tubing is explained in [Subsection 6.4.2](#). The choice of selecting the pressure gauge and pressure regulator are described in [Subsection 6.4.3](#) and [Subsection 6.4.4](#). [Subsection 6.4.6](#) explains which thread type was used. In [Subsection 6.4.5](#) it is described why a Tüv safety valve is selected. The overall test stand is explained in [Subsection 6.4.7](#). The assembling process of the test setup is described in [Subsection 6.4.8](#). The total overview of the constructed test setup is provided in [Subsection 6.4.9](#).

6.4.1. DIAGRAM OF TEST SETUP

To separately test the mono-mode and the dual-mode, the two propellant tanks pressurize individually using two feed-lines. As a result, it was possible to pressurize only one tank for the mono-propellant mode or two tanks for the dual-mode operation. A pressure regulator is placed in the feed line before the pressurant gas enters the tanks and enables to adjust the pressure in the propellant tank to the required pressure. The pressure gauge is located at the top of each tank to monitor the tank's pressure and a ball valve in each line controls the flow of the pressurant gas. Each tank is equipped with a

safety valve to ensure the safety of the test setup. A second ball valve is added below the tank to control propellant feed to the injector. An overview of the components described in the diagram, shown in [Figure 6.4](#).

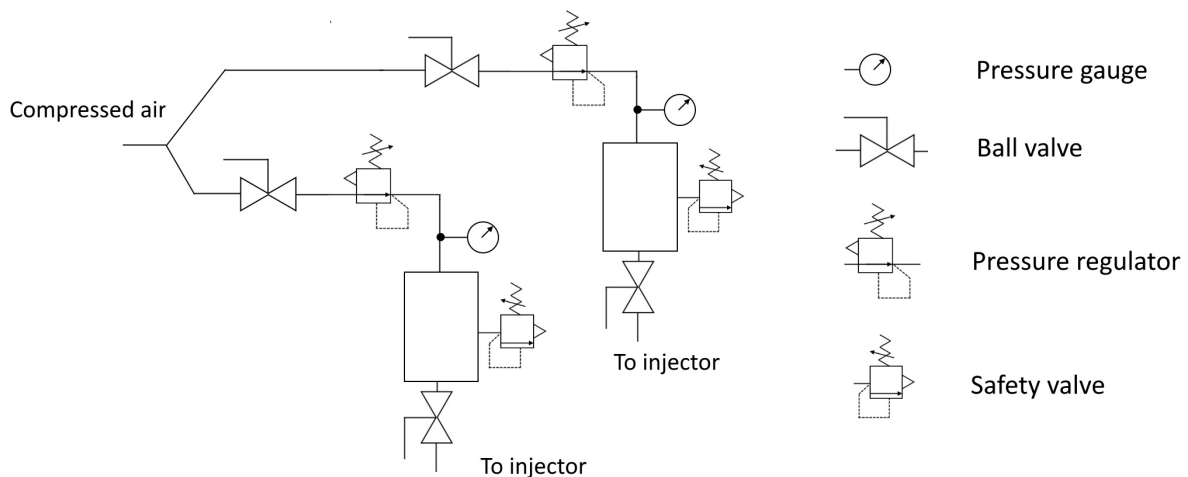


Figure 6.4: Diagram overview of the test setup

6.4.2. TUBING

Tubing is used to connect different components of the test setup. Compressed air is compatible with a wide range of materials, and the PUN hosing is available from the DASML lab. According to the specifications of the tubing, this tubing can withstand a maximum pressure of 10 bar. The maximum pressure of compressed air is 8.5 bar, so this specific tube can safely be used.

The ball valve and injector were connected with tubing to control the propellant flow to the inlet of the injectors. By doing so, an extra margin is generated when assembling the test stand and ensuring the correct fitting between the different parts. The benefit of using tubing is the flexibility to connect different types of injectors in the future. It is required to look into the compatibility of the tubing material when feeding hydrogen peroxide. The PVC material is compatible with hydrogen peroxide and was used [21]. A braiding material has to be used to withstand the maximum operating pressure of 8 bar. Hence, PVC tubing with fabric braiding of the company Landefeld was selected. This specific type of tubing can withstand a maximum pressure of 31 bar at a temperature of 20 degrees Celsius. To feed the ethanol to the inlet of injectors, PUN tubing was used to connect the ball valve. This material is conditionally resistant to ethanol [35].

The different components of the test setup will be assembled and disassembled a number of times, since it is an experimental test setup. Quick disconnect were used to generate the connection between the tubing and the thread of the connected component. Quick disconnects made it very easy to assembly and disassemble the different components. The quick disconnects can withstand a maximum pressure of 20 bar.

6.4.3. PRESSURE GAUGE

Different classes of pressure gauges with different accuracy exist to measure the pressure. For the current experiment, a 2.5 class pressure gauge (2.5 percent accuracy) was selected and connected to the feed line with a "T-joint". The applied tank pressure was adjusted with the help of a pressure regulator.

6.4.4. PRESSURE REGULATOR

It is essential to adjust the pressure in the propellant tank with a high accuracy and therefore a high-precision pressure regulator is required. With the limited financial budget for this thesis, it was decided to use a different pressure regulator, namely the pressure regulator LR-1/8-D-MINI manufactured by Festo. This pressure regulator has an inlet port that can withstand a maximum pressure of 16 bar. The outlet of the pressure regulator is connected to several "T-joints" to connect the pressure regulator and provide an extra venting point of the test setup. The venting point can be opened or closed by inserting or removing a plug. The section consisting of the pressure regulator, pressure gauge, ball valves, and "T-joints" of the test setup can be seen in [Figure 6.5](#).



Figure 6.5: Section of the test setup for the compressed air feed line

6.4.5. SAFETY VALVES

Safety valves are used to relieve the excess pressure. The PUN hosing has the lowest limit, namely 10 bar and the outlet pressure of the compressed air supply line is 8 bar. So, it was decided to use a safety valve that operates at an activation pressure of 9 bar. The first reason is that hydrogen peroxide may start to decompose, causing an increase in pressure. Then, the safety valve immediately activates to relieve the pressure. The second reason is the possibility that the outlet of the tank is blocked, generating an increase in pressure. By placing the safety valve at the tank, this situation is prevented. Moreover, if the injector is blocked, the pressure starts to increase up to the tank. Again, the tank will experience an over-pressurization, and this pressure is relieved by the safety valve. The safety valve of the company Landefeld is ordered and can be seen in [Figure 6.6](#).



Figure 6.6: Tüv safety valve that is used for the test setu [11]

6.4.6. THREADS

Different thread types are used at the test setup. A G1/4 thread type is commonly used for the selected components. This thread type can be combined with the R1/4 thread type. The difference between those types is the tapered section that the thread R1/4 has. As a result, only a male R1/4 can be safely connected to a G1/4 thread. This combination of threads was used for the different "T-joints" and the outlet port of the pressure regulator. A connection element was used to connect the pressure regulator and the ball valve, since both connections had a female connection.

6.4.7. TEST STAND

After selecting the components, different options were explored to design a test stand. It is desired that the test stand has some flexibility for future testing operations. Also, the test stand should be able to stand on a table, prohibiting the usage of clamps to attach the external frame located inside the fume hood. As a result, the test stand is a portable system as desired.

Aluminum profiles with four grooves are used to full fill the requirement of a flexible system. The four grooves in the profile and the associated bolts enable to have a flexible location where the bolts are placed. The aluminum profile is used to construct two L-shapes. The two L-shapes are connected by a metal sheet to provide the required rigidity. These specific bolts are also used to attach a metal sheet. The metal sheet is used to mount the different components to the test stand. The dimensions of the metal sheet are 400 mm by 500 mm. These dimensions are sufficient to mount all the components and still have some margin. The height of the metal sheet can be adjusted by placing the top two bolts 25 cm lower than the top plate. The constructed test stand is shown in [Figure 6.7](#)



Figure 6.7: The constructed test stand, including bracket to mount the injector

The pressure regulator and the propellant tanks are the heaviest components. For this reason, these two components are mounted to the metal sheet by a bracket. A 3D printed bracket was developed to mount the pressure regulator to the metal sheet. The propellant tank was connected with a pipe clamp. A different bracket was used to mount the injector to the test setup. The alignment of the bracket and the injector is guaranteed by 3D printing. The designed brackets for the injector and pressure regulators can be found in [Figure 6.8](#).

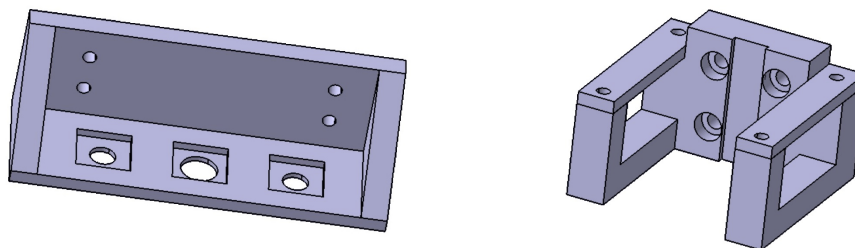


Figure 6.8: A CATIA image of the designed brackets

6.4.8. ASSEMBLING

The injector configurations and the propellant tanks were checked after arriving at SolvGE. The different injectors configurations had no defects related to the threads, outlet, and inlet diameters. One tank had a non-circular inlet for the compressed air, caused by some difficulties in clamping the part during the post-processing. This diameter is not a critical parameter for the testing operation, so this defect is acceptable. Some threads of the tanks had small manufacturing defects making it difficult to connect the safety valve and closing plug to the propellant tank. The safety valves are only connected once, while the closing plugs are connected every time during the filling operation. For this reason, the less well-manufactured threads were used to connect the safety valves. The tanks and injectors configurations are cleaned

with deionized water and dried with compressed air before installing the components to the test setup. Teflon tape is used to prevent any leakage between the different parts. The test setup is pressurized after connecting all the components and a soap mixture was used to identify possible leakage. Any detected leakage was fixed and resulted in the correct operation of the test setup. See [Figure 6.9](#) for the test setup after assemblage.

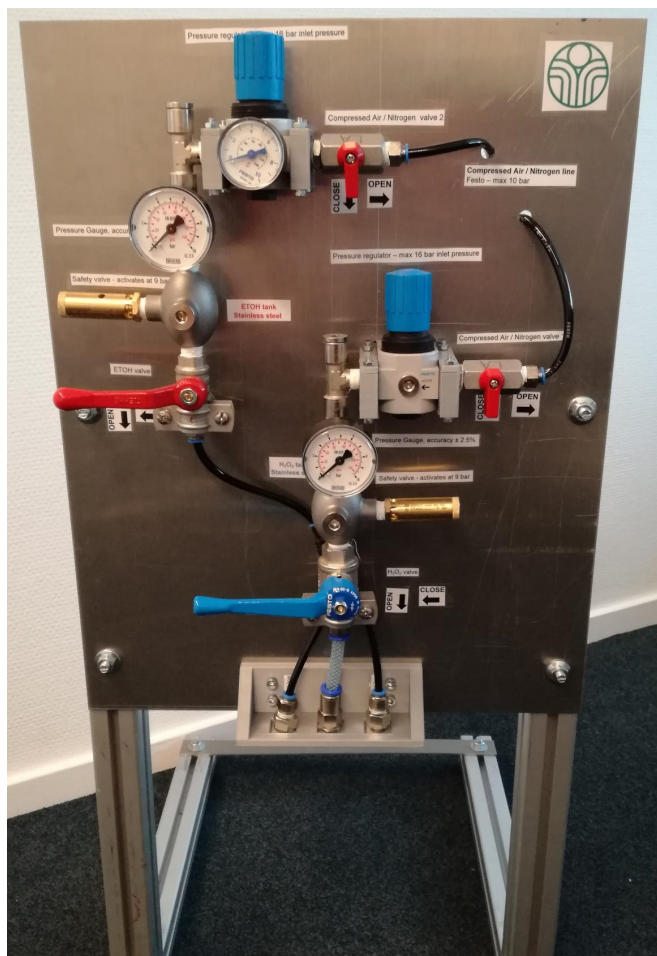


Figure 6.9: Test setup after assemblage

6.4.9. OVERVIEW TEST SETUP

The test setup is placed inside the fume hood on a table. The fume hood provided a safe testing environment when using hydrogen peroxide and ethanol. A high-speed camera is used to observe the atomization process for the different injector configurations. The DAMSL has a black and white Photron FastCAM mini AX200 high-speed camera that could be used. The high-speed camera is equipped with a separate desktop computer to operate the high-speed camera and to store the footage. Also, an external light source is required to provide sufficient light to visualize the atomization behavior with the high speed camera. The computer, external light source, and the high-speed camera were placed outside the fume hood. With this placement, the test setup can be operated while standing outside the fume hood. In [Figure 6.10](#) the overview of the test setup can be seen. When using chemicals, safety glass is placed in between the test setup and the desktop, so that the operator of the test setup is protected in the case of any splashes of hydrogen peroxide. The heating element is clamped with a metal rod and can be placed at any desired place. The clamping method of the heating element is shown in [Figure 6.11](#).



Figure 6.10: Overview of the placement of the test setup, high speed camera and external light source



Figure 6.11: Clamping of the heating element

6.5. HEATING ELEMENT

A heating element is used to supply the thermal energy to decompose the atomized propellant by the swirl injector. Different materials can be selected to construct a heating element. A wire of Nichrome 80/20 with a thickness of 24 AWG (0.51 mm) was available at SolvGE and was used as material to construct the heating element. This wire has a resistance of $5.6 \Omega/meter$ and can achieve a maximum temperature of 1200 degrees Celsius. The applied current and resistance at the heating element determine the applied energy to the heating element. The generated heat from the heating element is transferred by convection and radiation to the ambient environment, resulting in an outflow of energy. The difference in incoming and outgoing energy increases the temperature of the heating element. In conclusion, the current is a parameter that can be easily adjusted to achieve a specific temperature. Since the heating element has a specific length the total resistance of the value is specified. The required power and current can be supplied by a power supply and a multi-meter is used to measure the consumed electrical current and power. For this test setup, the power supply model ES030-10 from Delta Elektronika was used.

Different configurations of a heating element can be made. For example, the length, width, and number of horizontal segments can be varied. In total three different configurations of the heating elements were made. All configurations that are made have a constant length. Configuration 1 had a width of 4 cm and a total height of 6.5 cm. It had 6 horizontal segments and the distance between these segments was 1.5 cm. Configuration 2 had the largest height of the different configurations and had a height of 10 cm and a width of 1 cm. Configuration 2 had 10 horizontal segments with a spacing of 1 cm. The third configuration had the shortest spacing between the horizontal segments. Configuration 3 had 10 horizontal elements with a spacing of 0.5 cm. Configuration three had a height of 7 cm and a width of 2 cm. The end of the heating element is bent 90 degrees and connected to the power supply. In Figure 6.12 the different configurations of these heating elements are shown. The best configuration of the heating element was selected by analyzing the test results. The testing results is discussed in the next chapter.

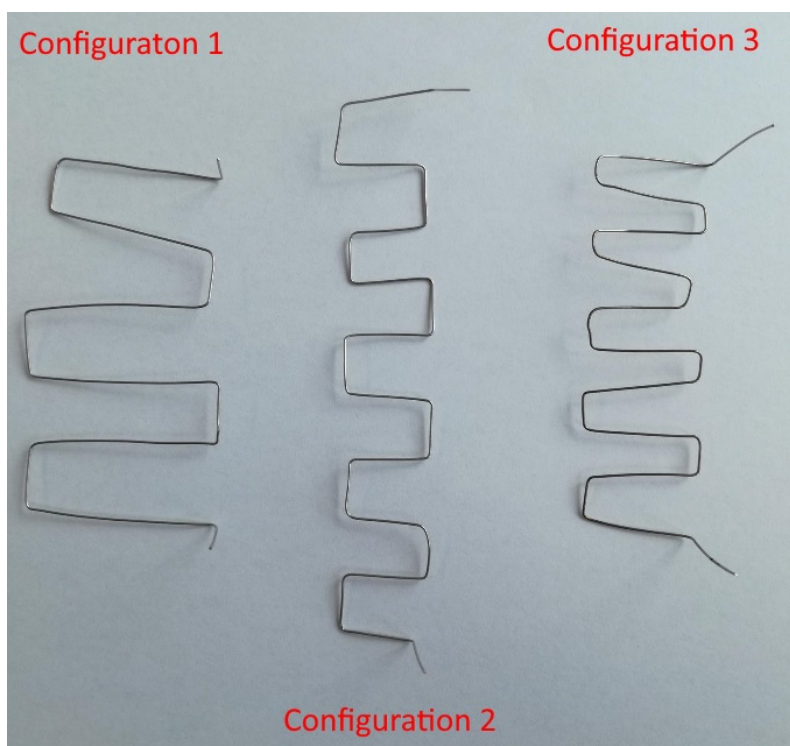


Figure 6.12: Example of the different heating element configurations

6.6. SAFETY

Several design choices of the test setup were made to guarantee safety during testing operations. The selection of ball valves is an example of this. For example, smaller handles of the ball valves were selected to control the compressed air feed lines. To indicate the different propellant feed lines, distinctive colors for the handles are used. The color red is used for the fuel (ethanol) and blue for the oxidizer (hydrogen peroxide). As a result, the handles of using the different ball valves correspond to the different functions of the ball valves.

A syringe was used to fill the tank with propellant. This reduces the risk of spilling during the filling operation. Reducing the risk of spilling is important, especially when handling hydrogen peroxide. The test setup is placed on a table that is

covered with aluminum sheets, which protects the table in case of spillage of hydrogen peroxide. To reduce the consequences of spillage, deionized water should be present to dilute the hydrogen peroxide in case of spilling

Labels are applied to the test setup to distinguish the different components. It also helps to specify which ball valve has to be operated for the testing procedures and thus decreasing the risk of an operator error. Several checks are included in the testing procedures. First of all, it is checked if all ball valves were closed before the propellant tanks were filled. Before the testing operations were started, it was checked if the ball valve for the compressed air was opened. These checks are summarized in the testing procedures. The testing procedures can be found in [Appendix E](#)

When a heating element is connected to a power supply, it is checked if any conduction occurs between the test setup and the environment. Different means are used to prevent the conduction to the environment. For example, a plastic connection between the power supply and the heating element was used. An insulated clamp is used to hold the heating element at the desired position. Also, duct tape is applied at the end of the metal rods to insulate, as can be seen in [Figure 6.13](#). Before starting the experiment, it was measured if any current flow from the test setup to the environment as a final check.

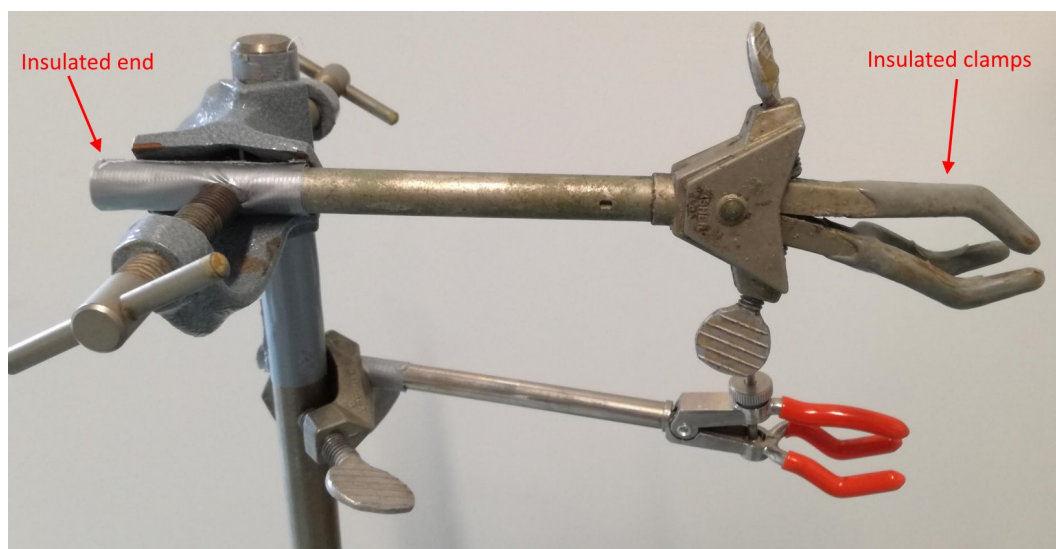


Figure 6.13: Example of the used insulation for the clamps to position the heating element

6.7. CONCLUSION

A pressure-fed test setup is selected to feed the propellant to the different injector configurations. The designed test setup meets the mass flow and pressurization requirements. Custom propellant tanks were designed and manufactured by the external company. This test setup can also be used in the future, because of the usage of flexible tubing and is a portable system. So, new testing facilities have been added to the testing capabilities of SolvGE.

7

EXPERIMENTS

Different experiments are conducted to characterize the atomized flow for the different injector configurations. In this chapter, the results of these experiments are discussed. Different test objectives were defined to validate the injector configurations. The first test objective is to investigate the pressure drop between the tank outlet and the inlet of the injector, which is discussed in [Section 7.1](#). The second test objective is investigate the atomized behavior for the swirl and jet injector which is provided in [Section 7.2](#). The performance of the injector is investigated during the third test objective which is discussed in [Section 7.3](#). In [Section 7.4](#) the fourth test objective, which is the investigation of the mixing between the atomized flow of the jet and swirl injector, is discussed. In [Section 7.5](#) the fifth and final test objective, which is investigation into the interaction between atomized flow and heating elements, is discussed. A conclusion of all these tests is drawn in [Section 7.6](#).

7.1. PRESSURE DIFFERENCES

The pressure drop between the initial tank pressure and the inlet of the injector is explored to better understand the functioning of the test setup. This is executed for the ethanol and hydrogen peroxide feed lines and for varying initial tank pressures. The initial tank pressure started at 1 bar and is increased to 8 bar with an increment of 1 bar. Compressed air was used to pressurize the test setup and to determine the pressure drop. A pressure gauge of class 2.5 was used to measure the inlet pressures. Therefore, a measurement error of 2.5 percent is associated with the measured inlet pressures. In [Table 7.1](#) the measured inlet pressures and associated pressure drops as obtained from experiments are provided for different initial tank pressures. These experimental results shows that no pressure drop occurs for both feed lines up to an initial pressure of 5 bar. This can be seen in [Table 7.1](#). For initial tank pressure higher than 6 bars, a pressure drop was measured. Although the feed line is longer for ETOH compared to the HTP, the pressure difference for the ETOH feed line is less than for the feedline of HTP. Also, for the HTP feed line, the measured pressure is higher than the initial pressure. This is different than expected since a pressure drop was expected. This probably due to the error of the pressure gauge since the difference is within 5 percent. This resembles the maximum difference in pressure of 5 percent observed for the HTP line.

Table 7.1: Results measured inlet pressure as function of the initial tank pressure

Initial tank pressure [bar]	HTP feed line		ETOH feed line	
	Measured inlet pressure [bar]	Pressure drop [bar]	Measured inlet pressure [bar]	Pressure drop [bar]
1	1.00	0.00	1.00	0.00
2	2.00	0.00	2.00	0.00
3	3.00	0.00	3.00	0.00
4	4.00	0.00	4.00	0.00
5	5.00	0.00	5.00	0.00
6	6.20	+ 0.20	5.90	- 0.10
7	7.25	+ 0.25	6.75	- 0.25
8	8.4	+ 0.4	7.75	- 0.25

In conclusion, up to an initial tank pressure of 5 bar no pressure difference is measured between the inlet and initial tank pressure for both feedlines. When the pressure is increased, some differences are measured. However, these differences is within 5 percent. So, the pressure loss between the inlet and initial tank can be neglected. As a result, a pressure gauge

located on the inlet of the tank can be used for future testing objective, without using an additional pressure gauges at the inlets of the injectors.

7.2. ATOMIZED BEHAVIOUR TEST

It is essential to understand how the different injector configurations atomize the liquid, before the performance parameters are investigated. Since this injector test was performed for the first time, deionized water was used as a test fluid [14]. The benefit of deionized water is that it is safe to handle, economical, and ease of availability. The atomization process is captured with a high-speed camera. An A4 paper is used to capture the spray pattern. The absorbent effect of A4 paper was taken into account during the analysis of these spray patterns. In Subsection 7.2.1 the swirl injector is analyzed in great detail, while in Subsection 7.2.2 the jet injector of configuration 4 is reported. In Subsection 7.2.3 the different injector configurations are compared.

7.2.1. SWIRL INJECTOR

In this section, the atomization process of the swirl injector is investigated. The high-speed camera is set at 6400 frames a second and has sufficient resolution to provide a better understanding of the atomization process of the swirl injector. It is seen that large droplets are generated, near the injector outlet from the captured footage of the two experiments of the first injector configuration at an initial tank pressure of 3 bar. A small swirl motion of the liquid was observed before the development of the hollow cone shape. The hollow cone has a constant spray angle for some time interval. When the tank is almost depleted the mass flow is decreased. This resulted in a decrease in the spray angle. These three regions can be distinguished in the hollow cone, as seen in Figure 7.1:

- **First region - thin sheet** Directly after the outlet of the swirl injector, a thin sheet is formed where the generated swirl motion can be seen.
- **Second region - break up** Moving more downstream of the liquid sheet, the second region is identified. In this region, it is perceived that the thin sheet starts to break up in the shape of long droplets.
- **Third region - spreading** The third region is identified where the second region starts to spread, increasing the distance between the droplets.

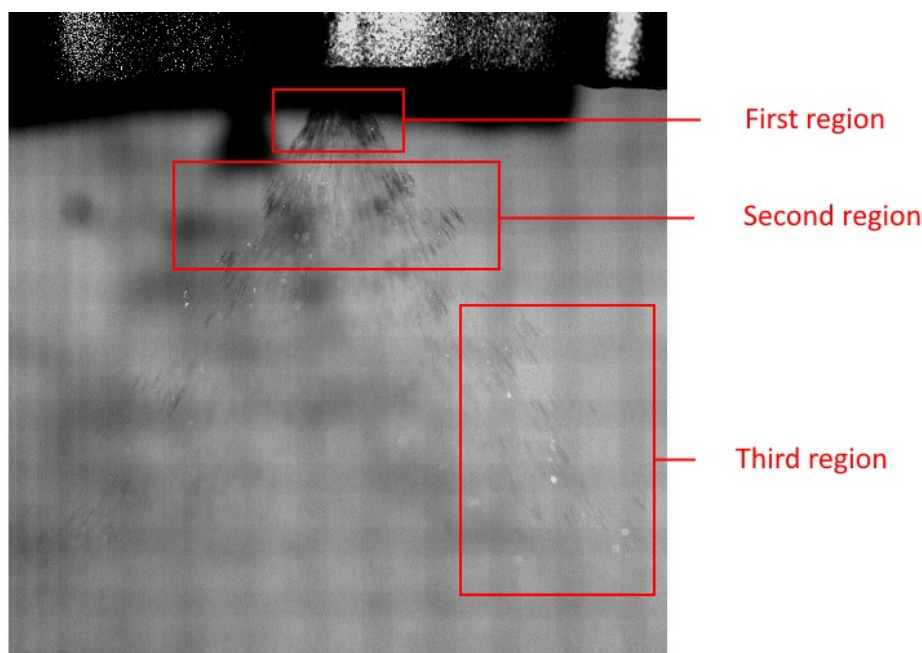


Figure 7.1: Overview of the different regions of the atomization process of the swirl injector for injector configuration 1

The third region indicated a promising atomizing behavior. It also shows that the atomized liquid motion is too fast for the selected frame rate. For this reason, the frame rate of the high-speed camera is increased. The high speed camera has a limited memory capacity. So, increasing the frame rate results in a decrease in resolution. Hence, a region has to be identified where the close-up at a higher frame rate is focused. It is determined to focus on the outlet of the swirl injector to fully understand how the swirl injector operates.

More details were noticed when the atomization process is captured at a frame rate of 67500 frames a second. This confirms that a frame rate of 6400 frames a second is more suitable to observe the general mechanisms with the increased resolution, but is not suitable for the microscopic details. It is seen that during the start-up, the swirl motion had already occurred. It is also detected that the formation of the hollow cone operates smoothly. Just after developed the hollow cone, a mechanism can be distinguished that has been described in [Chapter 2](#). This mechanism is described that some perforations are started in the liquid sheet. These perforations tend to grow and start to form droplets. This pattern indicates an injection velocity of a couple of m/s and can be seen in [Figure 7.2](#).

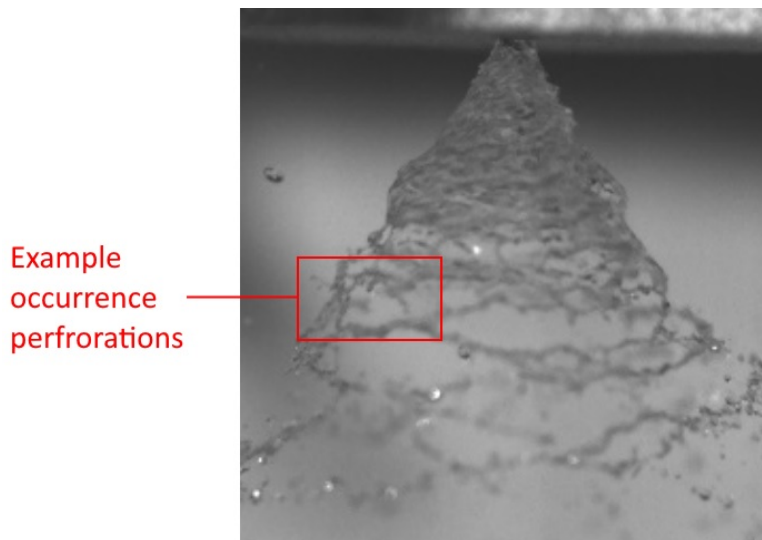


Figure 7.2: Example of the mechanism where perforations occur for the swirl injector

A second mechanism is also recognized. In this new mechanism, circumferential waves are formed. According to the theory [2], this indicates that the injection velocity has been increased compared to the first mechanism. When these circumferential waves move more downstream, it breaks up into different droplets. At some time intervals, it seems that the second pattern of the circumferential waves transforms back to the first pattern of the perforations and then back to the second pattern. However, the second pattern is less clear to recognize during the start-up phase. This indicates that injection velocity varies, but that the injection velocity never decreases back to the velocity experienced during start-up.

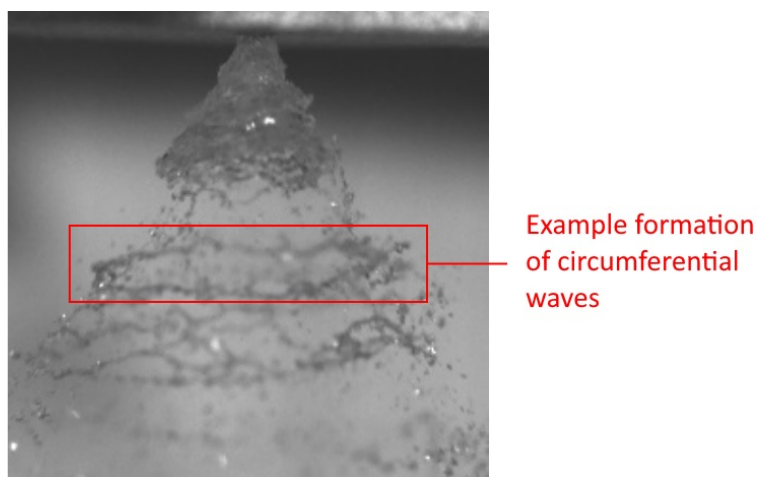


Figure 7.3: Example of the mechanism where circumferential waves occur for the swirl injector

The end-phase started when the hollow cone shape cannot be sustained and is identified when the spray angle starts to decrease. In this end-phase, droplets are still generated. At a regular interval, the liquid velocity increased for a small time interval. It is suspected that the combination of compressed air and liquid caused this increase in velocity. In the tanks, no anti-vortex elements were included to prevent gas entering the feed lines. Before the end phase, no gas can enter the feed line since the tank has not been depleted to a certain level. The acceleration of the liquid leads also to the formation of more droplets. However, these droplets are larger than the droplets before the end phase. See [Figure 7.4](#) for an example of the footage of the end phase of the swirl injector.

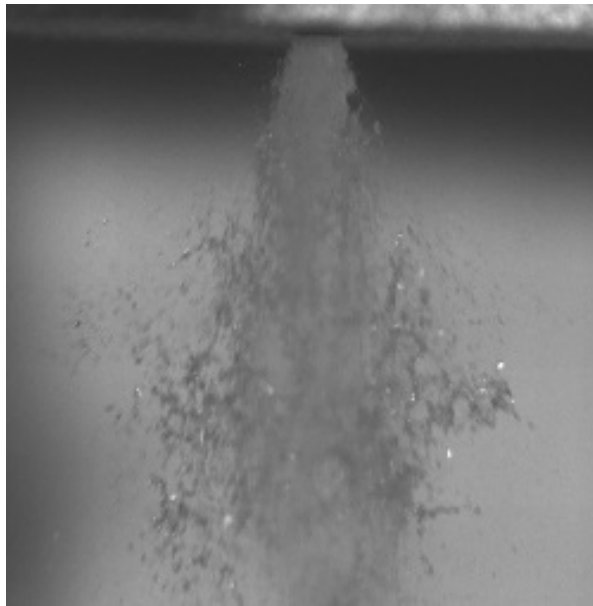


Figure 7.4: Example of the end-phase of the atomization process for the swirl injector

The high-speed camera capture footage can also be linked to the generated swirl injector spray pattern on the A4 paper. The absorbed behavior of A4 paper leads to an increase in spray patterns with time. So, the spray patterns can only be used as an indication of the performance and are less reliable than the made observations of the high-speed camera. Two regions are identified from the spray pattern. The first region is the outer ring. This region is due to the hollow cone and indicating a proper manufactured injector since it is a full circle. The second region is the inner ring. It is suspected that at the end-phase when the spray angle decreases could be the reason for the second pattern. The spray pattern of the swirl injector can be seen in [Figure 7.16](#).

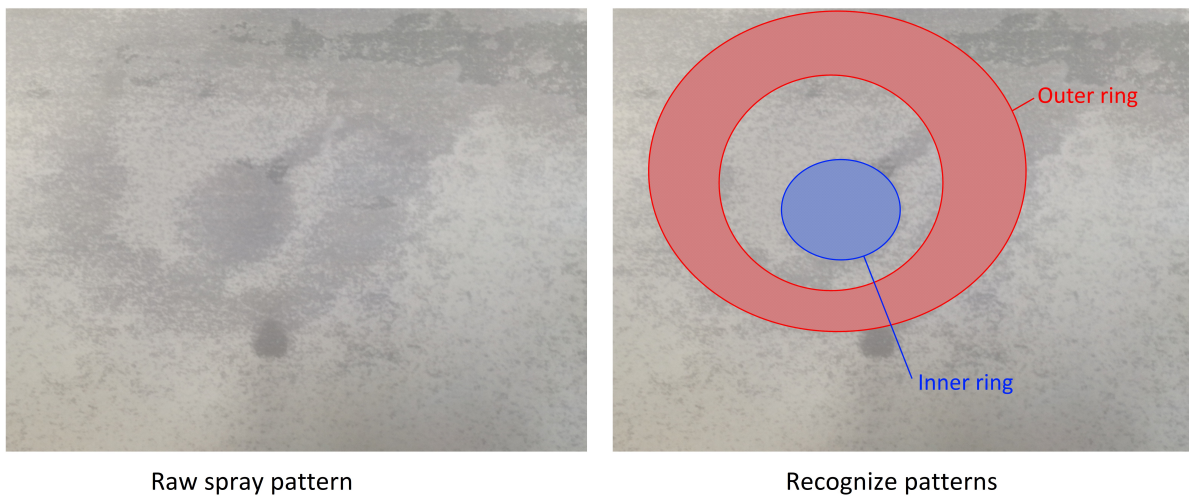


Figure 7.5: Spray pattern of the swirl injector

The swirl injector has the same design for all the different injector configurations. So theoretically, the performance of the swirl injector should be the same. All the swirl injectors are tested with deionized water to investigate if the theory matches the reality. The same patterns, as described above, are recognized after analyzing the footage of all the swirl injectors configurations. An example is given in [Figure 7.6](#). The same spray pattern is also recognized. For these reasons, it is concluded that the swirl injectors of the different configurations have the same performance, as expected. Hence, only one swirl injector has to be tested for future testing.

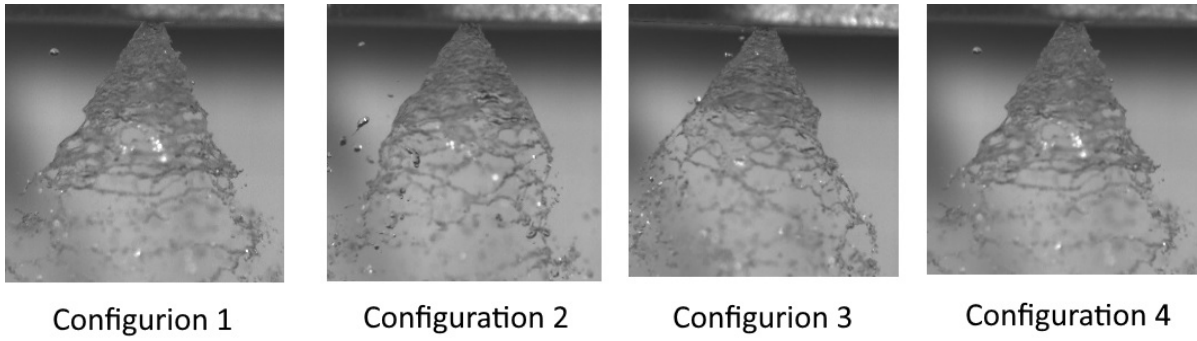


Figure 7.6: The first pattern for all configurations

7.2.2. SINGLE JET INJECTOR

In this section, the atomization behavior of the jet injector of configuration 4 is investigated in detail. First, the atomized behavior is predicted using the theory that has been discussed in Chapter 2. Then, the footage is analyzed to understand how the jet injector atomizes the liquid.

PREDICTIONS

A prediction is made which mechanism is used by the jet atomizer to atomize the deionized water. As discussed in Chapter 2, different mechanisms exist how a jet injector atomizes the liquid. Based on the Reynolds number and Ohnesorge number, a prediction can be made using the associated graph. These different numbers are determined for all the configurations of the jet injectors. The Reynolds number is defined in Equation 7.1, where the density of the liquid has the symbol ρ_l in kg/m^3 , the parameter v_j is the injection velocity in m/s , the parameter d_j is the outlet diameter of the injector in meters and the dynamic viscosity has the symbol μ . The Weber number, as is defined in Equation 7.2, is required to determine the Ohnesorge number. In Equation 7.2, the parameter v_g is the gas velocity in m/s and the surface tension is in N/m and has the symbol σ . The Ohnesorge number is a function of the Weber and Reynolds number and is defined by Equation 7.3.

$$Re = \frac{\rho_l v_j d_j}{\mu} \quad (7.1)$$

$$We = \frac{\rho_l (v_g - v_j)^2 d_j}{\sigma} \quad (7.2)$$

$$OH = \frac{\sqrt{We}}{Re} \quad (7.3)$$

The properties of deionized water have to be known to predict which mechanism is applicable for the different configurations. The surface tension is 72.2 dyn/cm [36] and the dynamic viscosity is 0.001002 kg/ms [37]. deionized water has a density of 1000 kg/m^3 [38]. In Chapter 4 the injection velocity of the jet injector is determined for the fuel ethanol. Since this test uses deionized water and not ethanol, the injection velocity has also be determined using the properties of deionized water. Also, the tolerances of $\pm 0.1 \text{ mm}$ are taken into account. See Table 7.2 for the determined value of Reynolds, Weber and Ohnesorge numbers for the different configurations. As it is observed, the minimum and maximum values for the Reynolds number are $6.4 \cdot 10^3$ [-] and $1.28 \cdot 10^4$ [-]. From this table, it is also seen that the minimum and maximum values for the Ohnesorge number are $3.407 \cdot 10^{-3}$ [-] and $4.81 \cdot 10^{-3}$ [-], respectively.

The computed numbers for the given configurations and using deionized water did not fit within the given range of the Ohnesorge and Weber numbers. For this reason, the data from this graph has been extrapolated. This extrapolated graph is presented Figure 7.7. A prediction was made using this graph and the computed values of the Reynold, Weber and Ohnesorge numbers. In Figure 7.7, the minimum and maximum values of the Reynolds and Ohnesorge number are plotted. The plotted points are within the region of mechanism 2. The minimum value applies to configuration 3 and the maximum value for configuration 1. So, it is expected for all configurations to have the second mechanism of atomizing behavior.

Table 7.2: Overview of the properties of deionized water for different injector configurations

Configuration	Tolerance plus 0.1 mm	Tolerance minus 0.1 mm
1	injection velocity: 12.03 m/s $Re = 9.60 \cdot 10^3$ $We = 1603$ $Oh = 4.18 \cdot 10^{-3}$	injection velocity= 21.38 m/s $Re = 1.28 \cdot 10^4$ $We = 3798$ $Oh = 4.81 \cdot 10^{-3}$
2 and 4	injection velocity = 7.6989 m/s $Re = 7.67 \cdot 10^3$ $We = 820$ $Oh = 3.73 \cdot 10^{-3}$	injection velocity = 12.03 m/s $Re = 9.60 \cdot 10^3$ $We = 1603$ $Oh = 4.17 \cdot 10^{-3}$
3	injection velocity = 5.45 m/s $Re = 6.40 \cdot 10^3$ $We = 475$ $Oh = 3.41 \cdot 10^{-3}$	injection velocity = 7.70 m/s $Re = 7.67 \cdot 10^3$ $We = 820$ $Oh = 3.73 \cdot 10^{-3}$

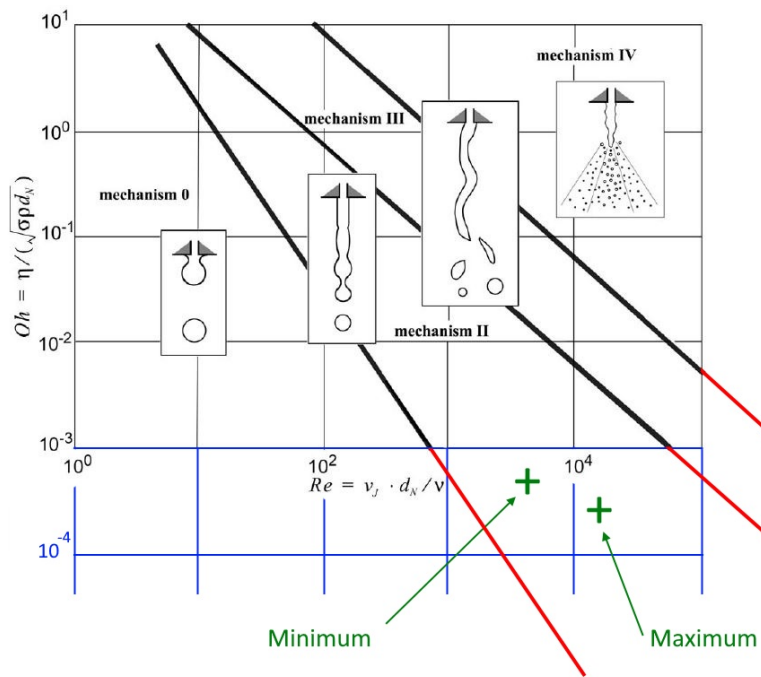


Figure 7.7: Extrapolated graph of the Oh and Weber numbers

OVERVIEW ATOMIZED PROCESS

First, the jet injectors are investigated at a frame rate of 6400 frames a second to investigate how the jet injectors atomize the deionized water. The start-up phase is given in figure Figure 7.8. From Figure 7.8 it is noticed that the right jet injectors start earlier with the atomization process than the left injector. However, the time difference between the atomization process for both injectors is small and is measured to be 1.41 ms, with an error of ± 0.2 ms. While the left injector starts a fraction later, it continues to provide a steady stream of liquid. This is different concerning the right injector, where an interval in the atomized liquid is observed. Because of this interval, the left injector is the first injector to fully achieve the operation phase. From the footage of the high-speed camera, the time difference between achieving atomized flow is 3 ms, with an error of ± 0.2 ms. The start-up phase of configuration 1 is also studied. For this configuration, the time difference between the left and right injector to achieve the atomized flow is measured to be 8.6 ms, with an error of ± 0.2 ms. For this configuration, the right injector does not experience an interval in atomized liquid in a time interval of the

atomized flow. In a conclusion, the start-up phase is a very dynamic process and different observations are made. The largest time interval between the start-up phase of the atomization for jet injectors is 8.6 ms.

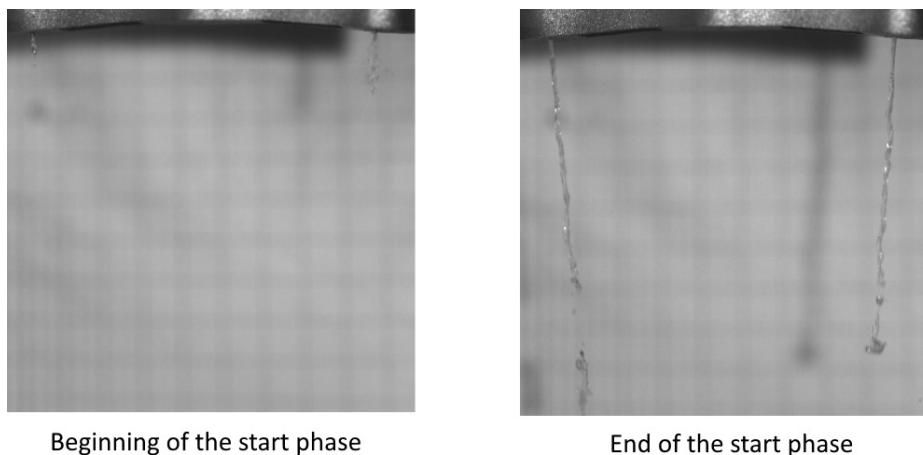


Figure 7.8: Example of the beginning and end-phase of the start up of the jet injector

After the atomized liquid is developed, different mechanisms are recognized in the footage filmed at 6400 frames a second. The first mechanism that is recognized is the axis-symmetric waves, which are described in [Chapter 2](#). As it is observed, the jet diameter will decrease at different sections of the atomized jet. This decreased diameter in jet diameter will then form ligaments, which then will form droplets. This pattern corresponds with mechanism 2 and is predicted to occur. An example of this pattern can be seen in [Figure 7.9](#). The second mechanism is related to the asymmetric waves, which are also described in [Chapter 2](#). This mechanism is recognizable by a small s pattern that is observed after the decrease in jet diameter and corresponds to mechanism III. According to the theory, this indicates that the injection velocity has been increased compared to the first pattern. An example of the observed second pattern can be seen in [Figure 7.10](#). The third recognized mechanism is identified when a large cloud of droplets occurs. The occurrence of this cloud happens near the injector head, where smaller droplets has generated. This pattern has similar characteristics as mechanism IV, where the injection velocity is fuhrer increased compared to mechanism III. An example of this can be seen in [Figure 7.11](#). As can be seen in the three figures, the left and right jet injectors do not show the same patterns at the same time instance of the filmed footage. This indicates that the occurrence of the observed mechanism is a dynamic process.

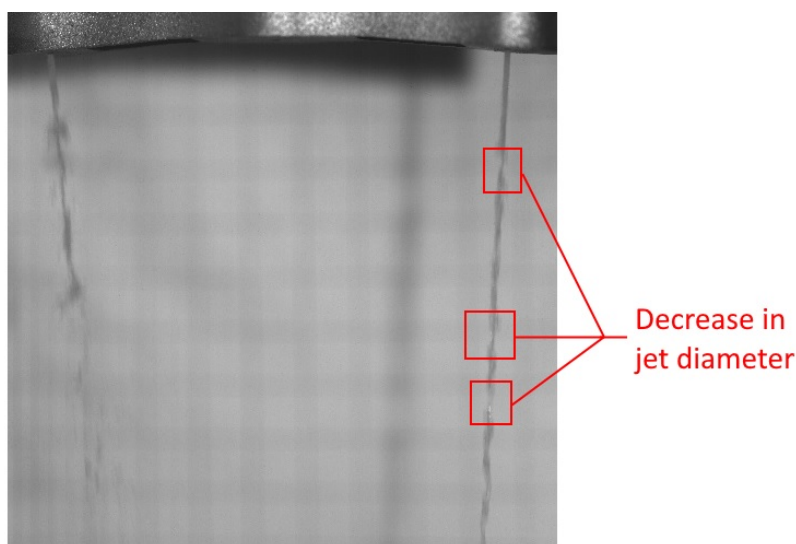


Figure 7.9: Example of the axis-symmetric waves defining atomazation mechanism 2 for the jet injector

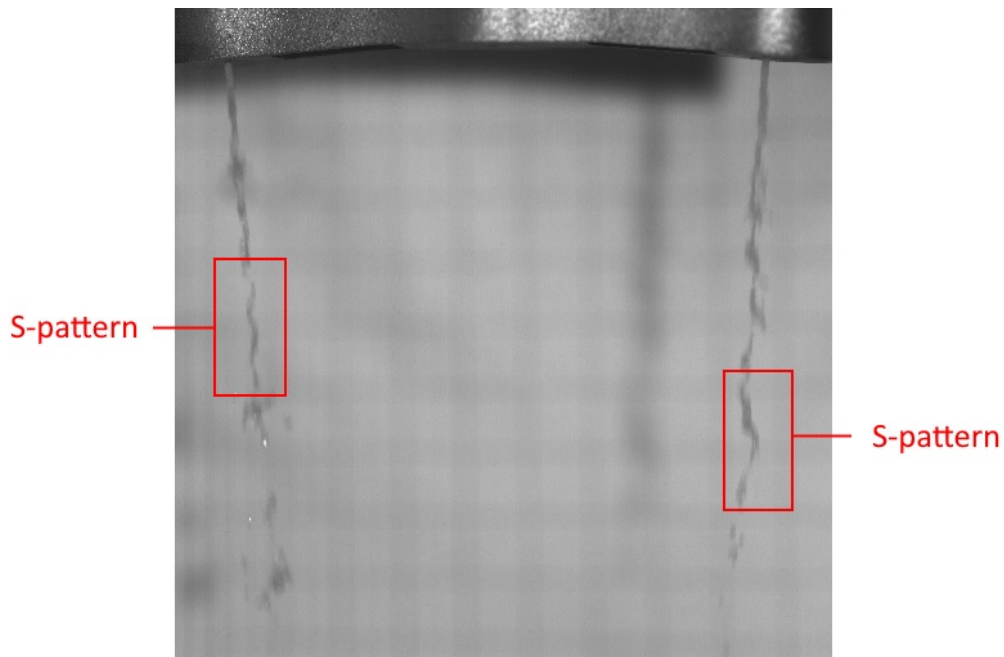


Figure 7.10: Example of the asymmetric waves defining atomization mechanism 3 for the jet injector

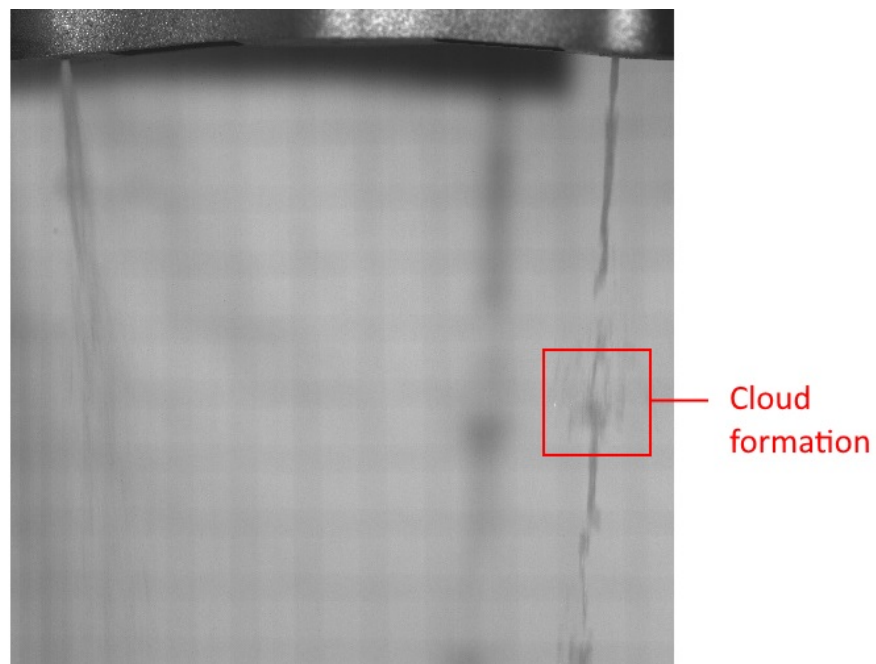


Figure 7.11: Example of the formation of a cloud

The end phase of the atomization process is started when the propellant tank is nearly depleted. The end phase of the injector is noticed when the spray angle is increased and the liquid is less visible as seen in [Figure 7.12](#). The increase in spray angle is due to the combination of compressed air and deionized water that has entered the jet injectors. This mixing of compressed air and deionized water has also occurred for the swirl injector. This has shown that mixing of compressed air and deionized water does not only occur for a specific design of the injector and is caused by the design of the test setup.

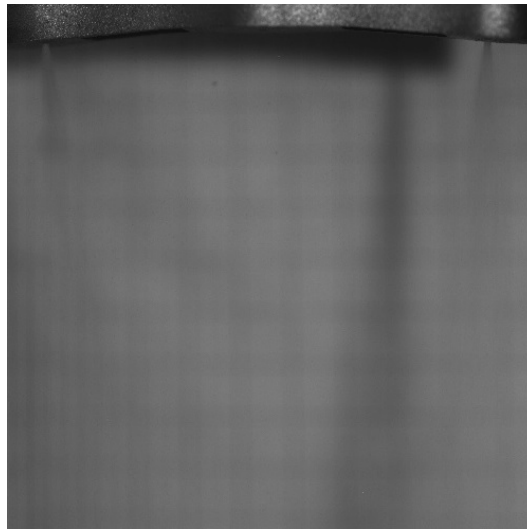


Figure 7.12: End-phase of the atomization process of the jet injector

To capture the details of atomization process for the jet injector, the high-speed camera frame rate is increased to 67500 frames/second. The increase in frame rate results in a smaller resolution, caused by the memory limitations of the high speed camera. For this reason, only one jet injector could be observed at one time. The same three mechanisms observed in the slower frame rate are recognized at increase frame rate. Figure 7.13 shows the beginning of the asymmetric pattern. Due to the limited resolution, only the start phase of this pattern was noticed. In Figure 7.13, it is seen that deionized water has no s-pattern at the outlet nozzle. A small decrease in the jet diameter is noticed. After this change in diameter a change a small s-pattern is recognized. The amplitude of the s-pattern is increased when the distance of the injector head is increased. The surface tension of the deionized water is sufficient to follow this s-pattern for the observed resolution. According to the theory, the further increase in amplitude causes the formation of droplets.

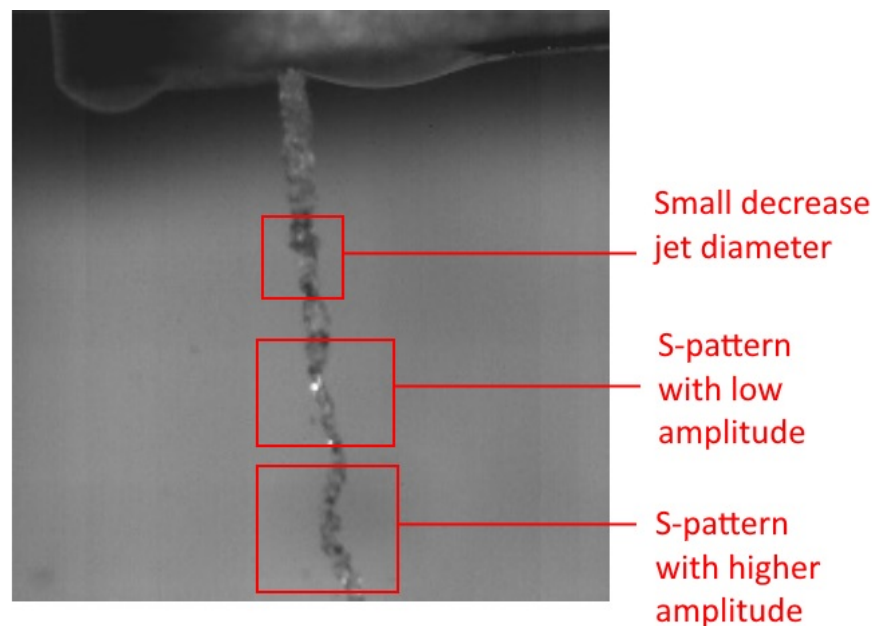


Figure 7.13: Detail asymmetrix waves of mechanism III of the jet injector

At this increased frame rate, different versions of mechanism II can be seen. In the first version, the jet diameter starts to decrease with no sign of ligament formation. The second version is that the diameter has decreased sufficiently and ligaments are formed. Figure 7.14 shows both versions. According to the theory, the second version will form droplets. Due to the limited resolution, this is not seen in this higher frame rate.

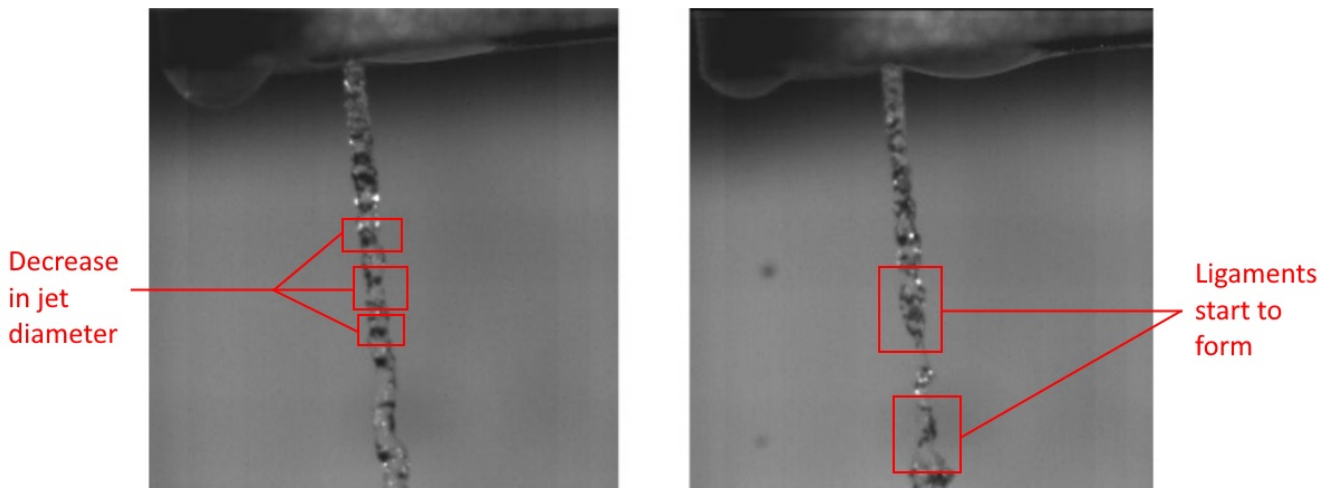


Figure 7.14: Detail of the mechanism 2 where axis symmetric waves are shown for the jet injector

At a higher frame rate it is noticed that the diameter of the liquid jet has decreased after the cloud of deionized water. Compared to the other mechanism, this decrease in jet diameter is larger than earlier observed. It is also seen that the cloud will form a number of droplets. One explanation for this phenomenon is that the injection velocity is temporarily increased and resulted in that mechanism IV of the atomized propellant is approached. A different explanation could be that compressed air is temporarily mixed with the deionized water, similar to the observed process during the end-phase. As a result, the combination of two processes resulted in the cloud mechanism.

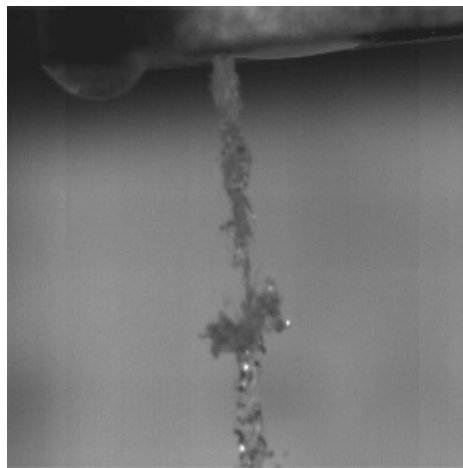


Figure 7.15: Details of the formed cloud during the atomization process of the jet injector

The generated spray pattern of the jet injectors is also observed. As can be seen in [Figure 7.16](#), a large sport is generated. This is different than the swirl pattern, where a large circle is generated with in the center a smaller circle. This difference is due to the jet injector forms a full cone of the atomized liquid instead of a hollow cone of the swirl injector. Because of the inclination of the two jet injectors, an oval shape is generated.



Figure 7.16: Spray pattern of the two jet injectors of configuration 4

7.2.3. COMPARISON JET INJECTORS DIFFERENT CONFIGURATIONS

In this section, the difference in the atomization behavior is explored for the different jet injector configurations. Again, deionized water is used as a liquid. The different configurations performance are observed with a high-speed camera with a selected frame rate of 67500 frames/second to fully understand the differences. For configurations 1, 2 ,and 3 it was possible to recognize the three mechanisms, as discussed earlier.

AXIS SYMMETRIC MECHANISM

First, the mechanism that describes the axis-symmetric waves is discussed in detail for the different configurations. Configuration 1 has the smallest outlet diameter. According to the theory, this results in the smallest SMD. From Figure 7.17, it is clear that only configuration 1 has created a ligament in the given resolution. Configuration 3 has the largest outlet diameter. For this configuration, it can be seen that the diameter of the jet has been decreased several times with ligament initiation. Configurations 2 and 4 have the same outlet diameter, with a change the inclination of the jet injector. Configuration 2 has also a decrease jet diameter, similar to configuration 3. The difference in the generated droplet size, which for configuration 3 is the largest, is caused by the larger outlet diameter. The imaged footage of this pattern for configuration 2 and 4 are not entirely the same. The jet of configuration 4 travels a longer path in the same resolution, due to the inclination of 5 degrees. The traveled path is an important parameter that defines the atomizing process, as explained in Chapter 2.

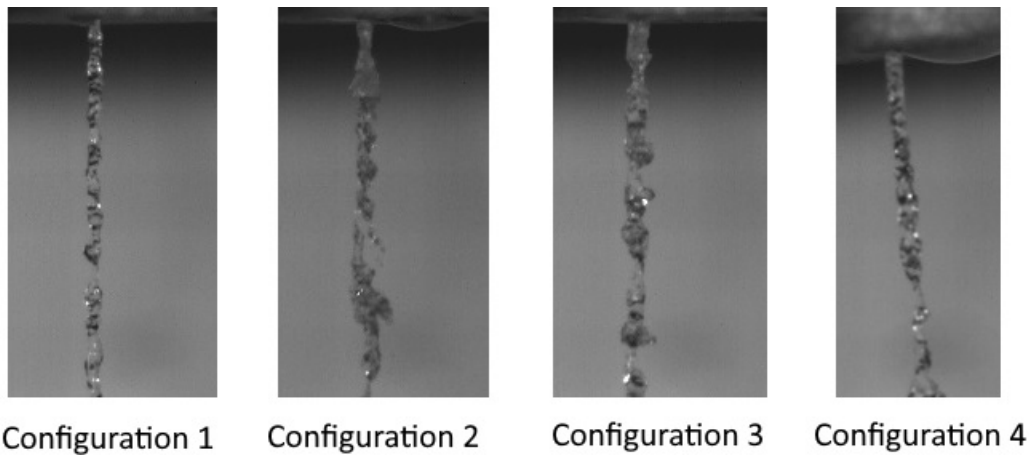


Figure 7.17: Comparison between the different jet injectors for mechanisms 2

ASSYMETRIC WAVES

The second mechanism that was observed for all the configurations is that of the asymmetric waves. The injection velocity is higher in configuration 2 than configuration 3, caused by the difference in outlet diameter. So, configuration 2 has a more recognizable s-pattern than configuration 3. Since configuration 1 has the smallest outlet diameter and thus the highest injection velocity, it is expected that the s-pattern can be seen more clearly than configuration 2. However, this is not the case as noticed in Figure 7.18. Also, for configuration 1 the s-pattern occurs less frequently than at configurations 2, 3, and 4.

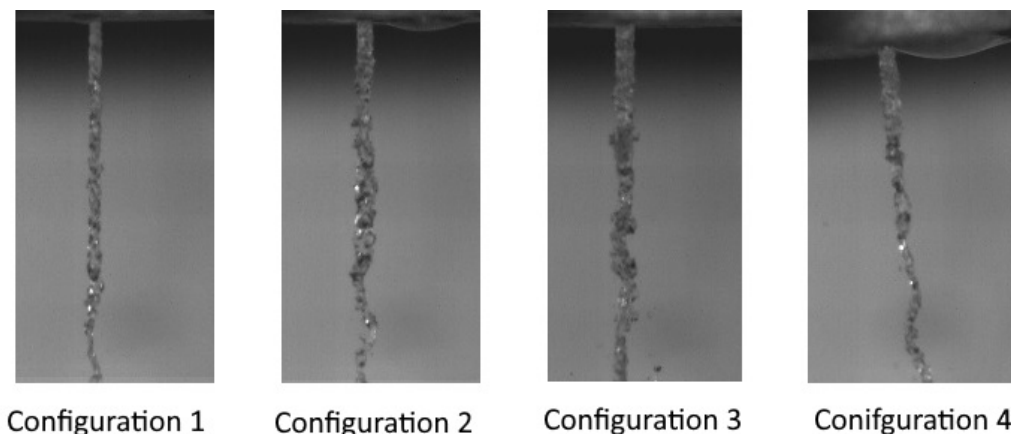


Figure 7.18: Comparison between the different jet injectors for mechanisms 3

CLOUD PATTERN

The cloud pattern was observed for all four configurations. As a result, the formation of clouds is independent of the outlet diameter with variation in the cloud size due to variance in the outlet diameter. It is also seen that the cloud formation is more deformed for configurations 2, 3, and 4 than for configuration 1, which could be due to increased interactions with the ambient air.

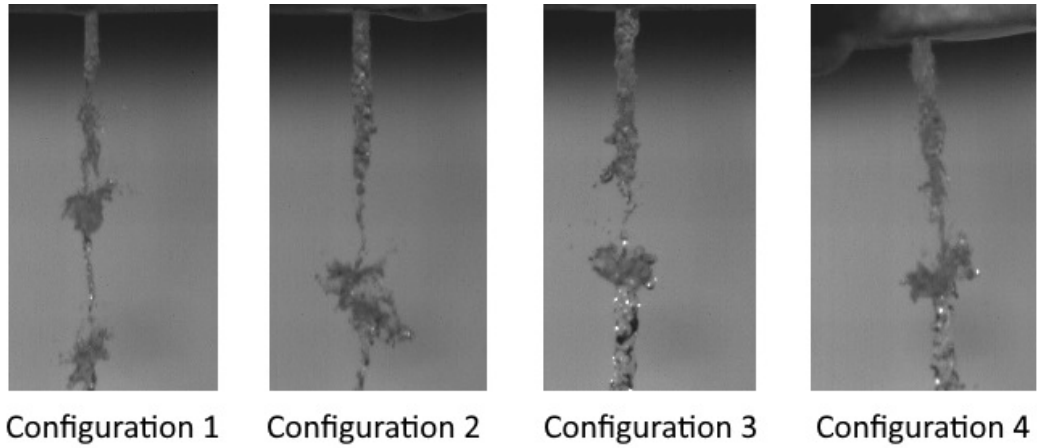


Figure 7.19: Comparison between the different jet injectors for the formation of clouds

FREQUENCY OCCURRENCE PATTERN AND CONFIGURATIONS

In the above sections, the patterns are discussed in detail, but not in which frequency this occurs. A conclusion about the frequency is made, after analysing the footage of two test runs for each injector configuration. First, it is seen that the cloud pattern formation occurs less for configuration 1 than for configurations 2, 3, and 4. Second, an s-pattern is observed after a cloud pattern has occurred. An excellent example is given in Figure 7.20. This confirms that the injection velocity has been temporally increased during the clouds formation. After the formation of the s-patter, the atomization process returns to the behavior described by mechanisms 1, as the theory describes. This process repeats several times during the atomization process. By observing the spray pattern, the difference between configurations 4 and 1,2, and 3 is visible. The spray pattern of configuration 1,2 and 3 has a similar pattern, namely two dots. An example of this spray pattern can be seen in Figure 7.21. Each jet injector will develop a full cone of atomized flow and this corresponds with a dot. When the jet injectors has an inclination, the two dots are combined to a single shaped oval.

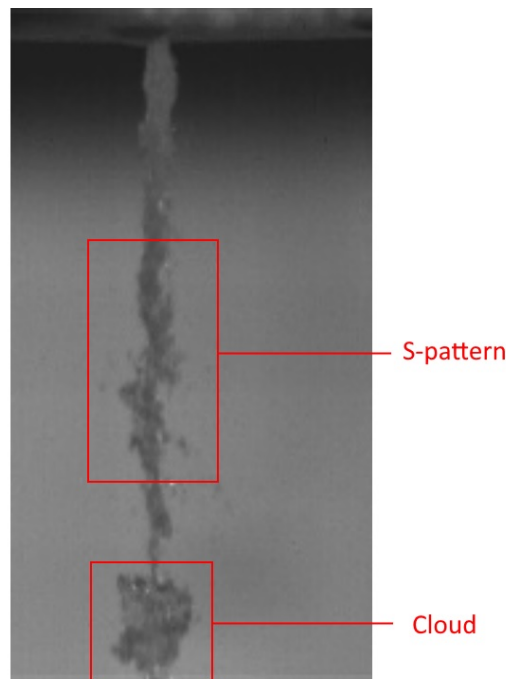


Figure 7.20: Example of the occurrence of a cloud and s-pattern



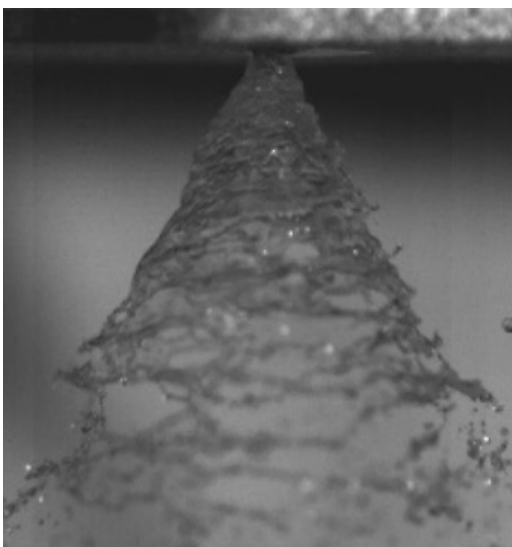
Figure 7.21: Example of the spray pattern of the jet injectors

7.3. ATOMIZED PERFORMANCE TEST

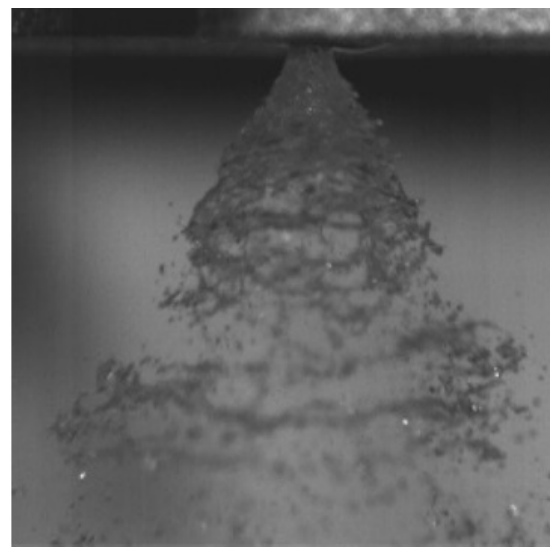
After understanding the atomization behaviour, the performance of the jet and swirl injector is investigated in this section. In [Subsection 7.3.1](#) and [Subsection 7.3.2](#) the performance of the swirl and the jet injectors for the different injector configurations are discussed.

7.3.1. SWIRL INJECTOR

Hydrogen peroxide was used as a working liquid for the swirl injector performance tests. It is the first time test was performed with hydrogen peroxide. Therefore a 34 percent concentrated hydrogen peroxide was used, considering safety protocols. It was expected to see similar mechanisms as observed from the deionized water testing, since 66 percent of the HTP mixture is deionized water. A general understanding of the atomization process has already been achieved with previous studies. Therefore the current test focuses on the details of the atomization process. So, the HTP flow atomization process was captured at 67500 frames a second. The high-speed camera is focused on the outlet of the swirl injector to compare the deionized water test to the HTP. The same two mechanisms were observed as with deionized water and at an initial tank pressure of 3 bars. See [Figure 7.22](#) for an example of these two patterns for the swirl injector of configuration 4.



Peforations pattern



Circumferential waves

Figure 7.22: Example of the two patterns for the HTP atomized flow for the swirl injector of configuration 4

EXPLANATION SMD ESTIMATION PROCESS

The high-speed camera footage is used to estimate the SMD of the atomized HTP liquid. To perform the SMD estimation, footage has to be used where the details of the atomization process can be seen. So, this leads to selection of the frame rate of 67500 frames. The determination of the SMD is made two times for each observed mechanism. After a detailed investigation, a frame with the most promising atomization behavior was selected for the SMD study. The ImageJ program was used to determine the cross-section area of the droplets. The outlet diameter is known and can be seen in the observed footage. Therefore, this diameter was used to set the scale in the Image J program. After the scale is set, the contrast of the frame is modified. It will increase the clarity of the cross-sections of the droplets, which helps to the estimation of the SMD. See Figure 7.23 for an example of the improved clarity. A section of the frame was selected to analyze the cross-sections of the droplets that lead to threshold generation. It was found that the bandpass filter leads to the best conversion from a frame to a threshold. See Figure 7.24 for an example of the conversion from the frame to the generated threshold. From this threshold, the cross-section of the droplets are determined.

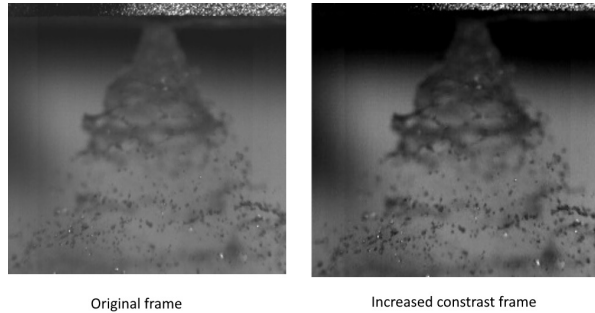


Figure 7.23: Example of the increased clarity of a frame by adjusting the contrast

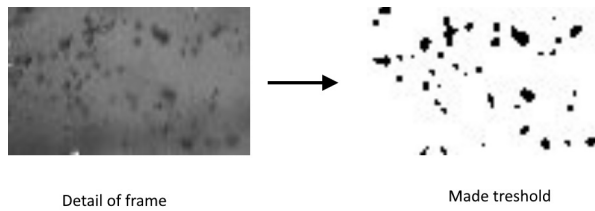


Figure 7.24: Example of the made threshold of a detail of the selected frame

A simplification is made to estimate the SMD from the determined cross-sections of the droplets. This simplification relates the diameter to a spherical cross-section to Equation 7.4. The SMD can then be determined knowing the diameter for each droplet using Equation 7.5. In this equation, D is the diameter in mm and the parameter Δn is the quantity of the droplets of this specific diameter. This is set to 1, when the SMD is computed for each droplet.

$$D = \sqrt{\frac{4A_{cross}}{\pi}} \quad (7.4)$$

$$D_{32} = \frac{\sum D^3 \Delta n}{\sum D^2 \Delta n} \quad (7.5)$$

SMD ESTIMATION AT INITIAL TANK PRESSURE 3 BAR

The SMD is determined for both the atomized mechanisms, using the described approach. For each pattern, the SMD is determined twice from different frames and this provided four data points of a single test run for both atomization mechanism. Two test runs are executed for the swirl injector with an initial tank pressure of 3 bar. The computed SMD for both test runs and pattern can be seen in Table 7.3. The measured scale, in pixel per mm, provides information of the measurement error for each data point. The computer program works with pixels and this forms the limiting factor in the measurement and therefore introduced some measurement errors. Since this SMD determination is a manual process, the measuring scale can also provide information on how well this process is executed. This table shows that the measurement scale has a minimum value of 7.29 pixels per mm and a maximum value of 8.75 pixels per mm. This indicates a difference of fewer than 2 pixels, which is an acceptable difference. Hence, no major mistakes are made within the manual process. This measured scale leads to a measurement error of 0.125 mm. It is observed that there is a small

difference between the measured and average values of SMD for the different mechanisms. However, this difference is within the measurement error. In conclusion, the atomized flow has the same estimated SMD for both mechanisms. It should be noted that the measurement error is a large uncertainty, compared to the average value. This is caused by the low resolution of the footage, which is related to the high frame rate. As already mentioned, a high frame rate is required to capture the small details of the atomization process to estimate the SMD.

Table 7.3: Overview of the measured SMD values for an initial tank pressure of 3 bar

Pattern	Test	Measured SMD [mm]	Measurement error [mm]	Measured scale [pixel/mm]
Circumferential waves 1	1	0.497	0.137	7.292
Circumferential waves 2	1	0.501	0.117	8.542
Circumferential waves 1	2	0.406	0.121	8.281
Circumferential waves 2	2	0.44	0.125	7.969
Average circumferential wave		0.461	0.125	8.021
Perforations 1	1	0.473	0.133	7.501
Perforations 2	1	0.454	0.120	8.33
Perforations 1	2	0.362	0.116	8.646
Perforations 2	2	0.393	0.114	8.75
Average perforations		0.421	0.120	8.306

The estimated value of the SMD is compared to the computed value of the design, where the testing conditions and tolerances has been taken into account. In the design process, a mass flow of 0.005 kg/s for the swirl injector was considered. A syringe is used for the filling operation of the tank. It simplified the filling operation and enabled to measure the quantity of the used propellant during the test. This information is used to determine the mass flow of the test conditions. The footage of the high speed camera provides information on the start and end of the atomization process. The start is visible, but the end of the operation is difficult to observe. This is caused by the mixing of compressed air and hydrogen peroxide and could be due to the mixing of compressed air and hydrogen peroxide. For this reason, the end of the atomization process is taken into account when the end pattern is no longer observed. With this method, the mass flow of the testing condition is computed. This method is straightforward but has simplified the testing conditions. Because of the mixture with compressed air and HPT, the mass flow will vary, but this approach eases the mass flow to a constant value. The computed mass flow are shown in [Table 7.4](#). As can be seen, the mass flow is in the same magnitude of the 0.005 kg/s but has not the same value due to the less-precision pressure regulator. The selection of a less-precision pressure regulator was due to the financial budget limit for this thesis. The computed mass flow at the testing conditions is used to update the performance calculations. The tolerances are taken into account when the SMD is computed and resulted in minimum and maximum values for the SMD parameter. See [Table 7.4](#) for the updated performance parameters. From [Figure 7.22](#) the spray angle is measured for the first test to be 57 degrees and for the second test 58 degrees.

Table 7.4: Test conditions and associated expected performance

Parameter	Test 1	Test 2
Mass flow [kg/s]	0.0095	0.0080
Min SMD [mm]	0.078	0.087
Max SMD [mm]	0.105	0.118
Min injection velocity [m/s]	13.16	11.08
Max injection velocity [m/s]	17.56	14.78
Min spray angle [deg]	80.40	80.40
Max spray angle [deg]	81.00	81.90

When the results of [Table 7.4](#) and [Table 7.3](#) are compared, it is observed that the SMD is underestimated by a factor

around 5 during the design process. A possible explanation for this underestimation is that the ambient pressure is not used during the design process when the SMD is computed. The interaction between the ambient air provided also a mechanism that helps the atomization process, as described in [Chapter 2](#). Because of the required frame rate and thus the limited resolution, it is difficult to observe if the generated droplets by the swirling process are further atomized when the droplets moved more downstream. The spray angle is also overestimated by 20 degrees. Again, the ambient pressure is also not taken into account during the spray angle computation. Additionally, 30 droplets are used to determine the SMD for every pattern. As a result, the measured SMD is an estimation of the achieved SMD during testing. When a larger quantity of droplets is analyzed, the measurement will be more reliable. Unfortunately, this is not possible with the current high-speed camera available during testing.

The initial tank pressure has also been increased to 7 bars to investigate how this influences the atomization process. The same two patterns, as earlier discussed, are observed again at the increased initial pressure. The only difference is that the atomization process starts more upstream compared to the 3 bar. It is observed that the spray angle of the swirl not changed when the initial tank pressure increased to 7 bar. See [Figure 7.25](#) for an example of the two mechanisms at an initial tank pressure of 7 bar.

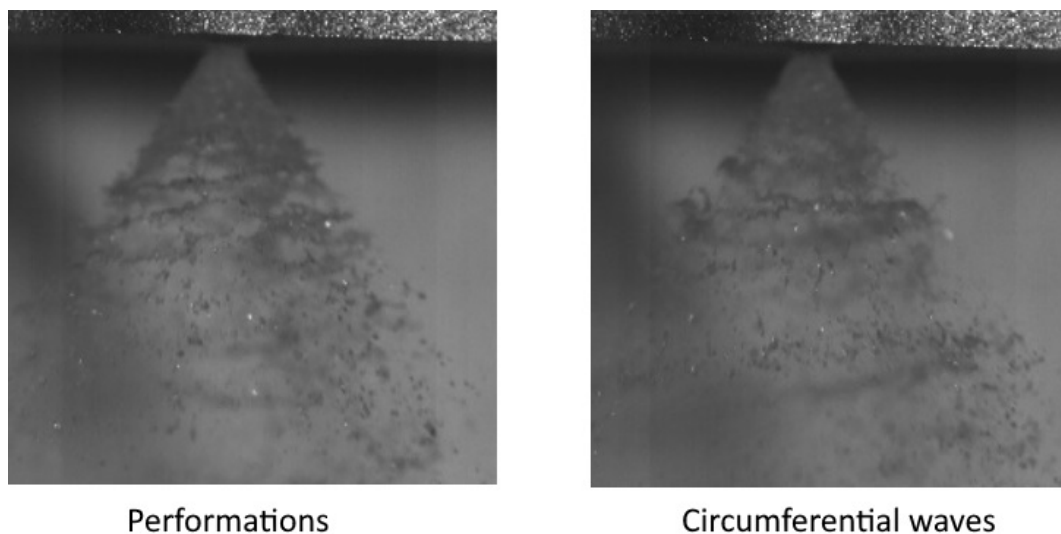


Figure 7.25: Example of the two patterns for the HTP atomized flow at 7 bars

SMD ESTIMATION AT INITIAL TANK PRESSURE 7 BAR

The same process that is discussed above is used to estimate the SMD of the working liquid through the swirl injector for an initial tank pressure of 7 bar. The results of these measurements, including the measurement error, are given in [Table 7.5](#). The same measurement error is applicable for the conducted measurements at an increased pressure of 7 bar. The reason for this is that the same frame rate and resolution settings are used. It is clear that the manual process for SMD estimation was done correctly. Because of the increase in pressure, the injection velocity increase, and a decrease of SMD was expected. Because of the increase in pressure, it is expected that the injection velocity is increased, and thus that the SMD is smaller than at an initial tank pressure of 3 bar. However, no change observed in the SMD average value for the mechanism perforation, when compared to lower initial pressure. The average value of the SMD of the circumferential waves measured at 7 bar is smaller than the value measured at 3 bar. The estimated SMD of circumferential wave 1 measurement at test 2 is much lower compared to the other measurements. Hence, this measurement is less reliable and is discarded. As a result, the average value is 0.417 mm, and comparable to the test at 3 bar with measurement error consideration.

Table 7.5: Measured SMD for an initial tank pressure of 7 bar

Pattern	Test	Measured SMD [mm]	Measurement error [mm]	Measured scale [pixel/mm]
Circumferential waves 1	1	0.412	0.121	8.281
Circumferential waves 2	1	0.429	0.125	7.969
Circumferential waves 1	2	0.191	0.123	8.125
Circumferential waves 2	2	0.410	0.117	8.542
average Circumferential wave		0.360	0.122	8.229
Perforations 1	1	0.460	0.120	8.333
Perforations 2	1	0.457	0.132	7.578
Perforations 1	2	0.451	0.123	8.125
Perforations 2	2	0.410	0.119	8.438
Average perforations		0.445	0.123	8.118

Again, the measured SMD values are compared to the estimated performance during the design process, while the testing conditions and tolerances are considered. The computed mass flow and estimated performance for the tests at increased initial tank pressure can be seen in [Table 7.6](#). The mass flow is closer to the targeted 0.005 kg/s, but the SMD was over-estimated during the design process. However, the factor has been decreased from 5 to 3.5 at the increased initial tank pressure. From [Figure 7.25](#), the measured spray angle for the first and second tests were 64 and 61 degrees. This value is similar to the previous test at 3 bars.

Table 7.6: Test conditions and associated expected performance for an initial pressure of 7 bar

Parameter	Test 1	Test 2
Mass flow [kg/s]	0.0062	0.0058
Min SMD [mm]	0.103	0.110
Max SMD [mm]	0.139	0.149
Min spray angle [deg]	80.4	80.4
Max spray angle [deg]	81.0	81.9
Min injection velocity [m/s]	8.6	8.0
Max injection velocity [m/s]	11.5	10.7

The injection velocity was studied to investigate the negligence in a decrease in SMD when an increase in pressure. The footage of the high-speed camera is used for this purpose. To determine the injection velocity, the time required to achieve a hollow cone is measured. The start phase is chosen because the hollow cone formation is quite clear and the measurement is more reliable. In [Table 7.7](#) the measured time interval is shown. The outlet diameter is known and is visible in the frames. As a result, the distance between the injector head and the frame can be measured, which in turn helps to determine the injection velocity. From this table, it is clear that the time required to form a hollow cone is decreased with an increase in pressure. As a result, the injection velocity is increased, as expected. For a higher initial tank pressure, the time required to form a hollow cone only difference is 1.2 ms, while at lower pressure this difference is increased to 6.2 ms. However, the measured injection velocities are lower than anticipated. This indicates that the pressure drop of the injector is different. As a result, the discharge coefficient and thus filling factor are different. This explains the difference between the expected and measured spray angle and SMD.

Table 7.7: Overview of the measured injection velocity for the swirl injector

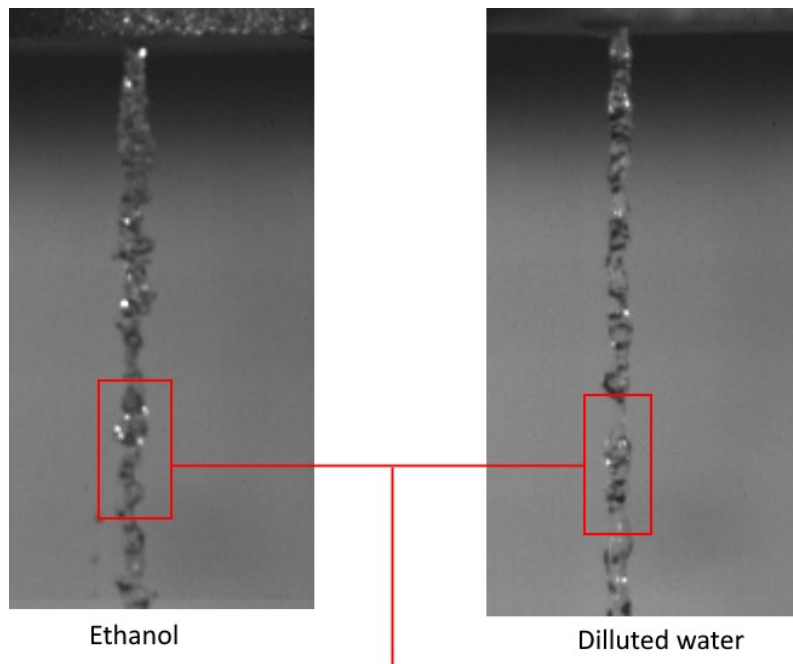
Initial tank pressure	Time to form hollow cone [ms]	Measured injection velocity [m/s]
3 bar - test 1	8.47	2.52
3 bar - test 2	14.89	1.29
7 bar - test 1	5.33	4.42
7 bar - test 2	6.55	2.88

7.3.2. JET INJECTOR

Ethanol (ETOH) is used as a working liquid to assess the performance of the jet injectors. The jet injectors of different configurations are tested with an initial tank pressure of 3 bars and are compared with the atomized test behavior results. Since the global understanding of this process is achieved, the high-speed camera is set to 67500 frames a second to investigate in detail how the jet injectors atomize the ETOH. The same patterns that are recognized during the deionized water tests are spotted for the ethanol. The initial tank pressure is also increased to 7 bars to explore how this increase influences the atomization process.

COMPARISON TO WATER

The footage of configuration 1 is used to investigate the difference in atomized behavior of deionized water and ethanol. In Figure 7.26 the axisymmetric pattern is compared for ethanol and deionized water. The surface tension of ethanol is less than for deionized water. As a result, axis-symmetric wave generates smoothly for ethanol and benefit the atomization process. But the formation of small segments is not visible in this resolution.



Increased number of decrease in jet diameter

Figure 7.26: Ethanol and deionized water comparison axisymmetric wave

The effect of the reduced surface tension is also visible for the third mechanism. The s-shape pattern, which is a distinguished pattern for the asymmetric wave mechanism, starts earlier when using ethanol and can be seen in Figure 7.27. Also, the amplitude of the s-pattern is increased when ethanol is used, which improved the atomization process.

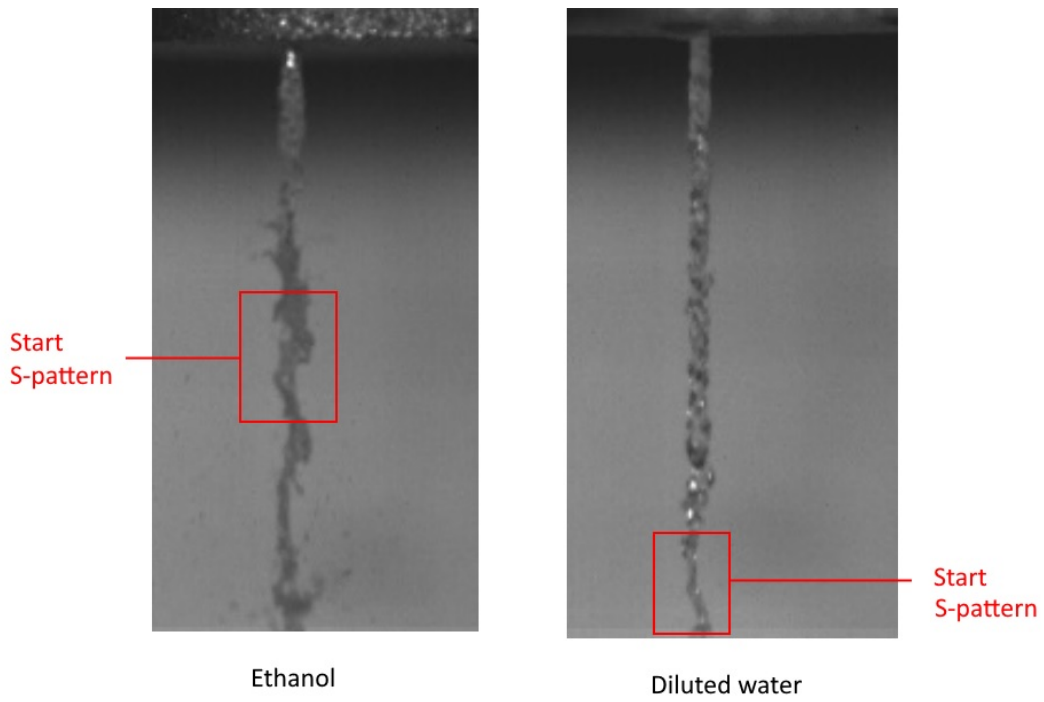


Figure 7.27: Ethanol and deionized water comparison assymmetric wave

The formation of clouds is also observed, when ethanol is used. Again, after the formation of a cloud, a s-pattern is observed. This confirms that the injection temporarily increased when a cloud is formed, as discussed earlier. In conclusion, because of the decreased surface tension of ethanol, the atomization process is improved. This is seen for the axis and asymmetric mechanism.

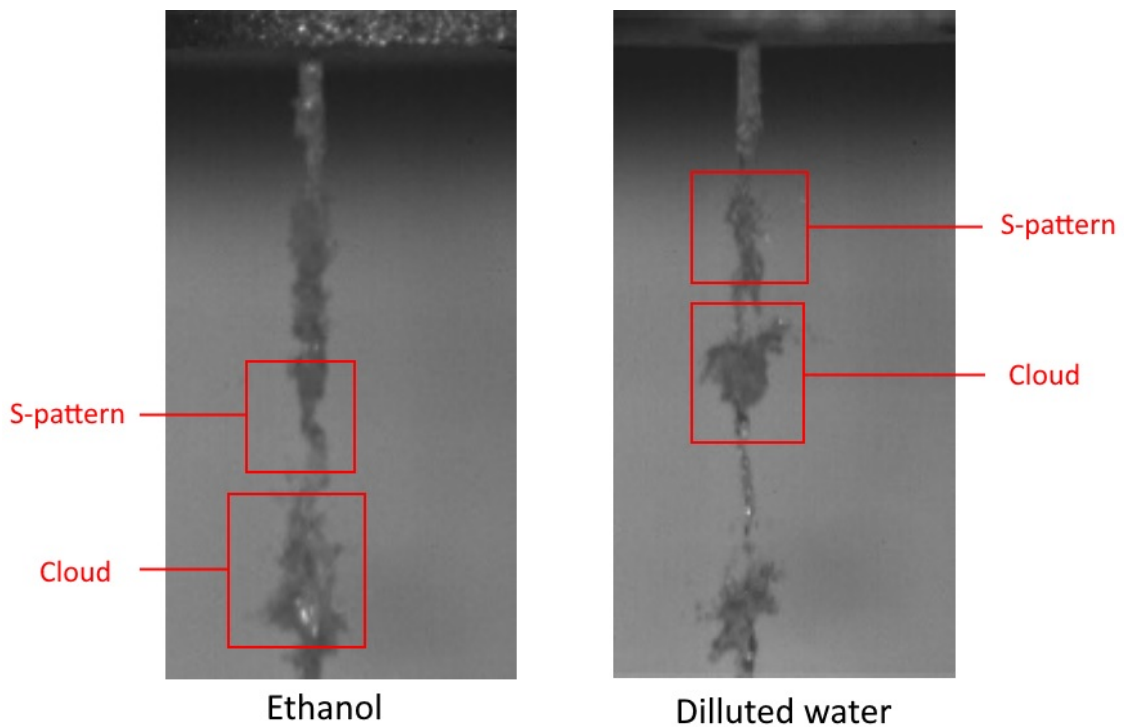


Figure 7.28: Ethanol and deionized water comparison cloud

COMPARISON CONFIGURATION INJECTORS

The jet injectors show a different atomization behavior, while investigating the difference in using ethanol and deionized water as a working liquid. For this reason, the atomization mechanism are studied for the different injector configurations using ethanol. In [Figure 7.29](#) the axis-symmetric mechanism of the different configurations is shown. Configuration 1 shows the most promising atomization, because of the smallest outlet diameter. Configurations 2 and 3 show that the decrease in jet diameter is less when the outlet diameter is increased. Unfortunately, due to the resolution issue, the droplet formation was unable to capture.

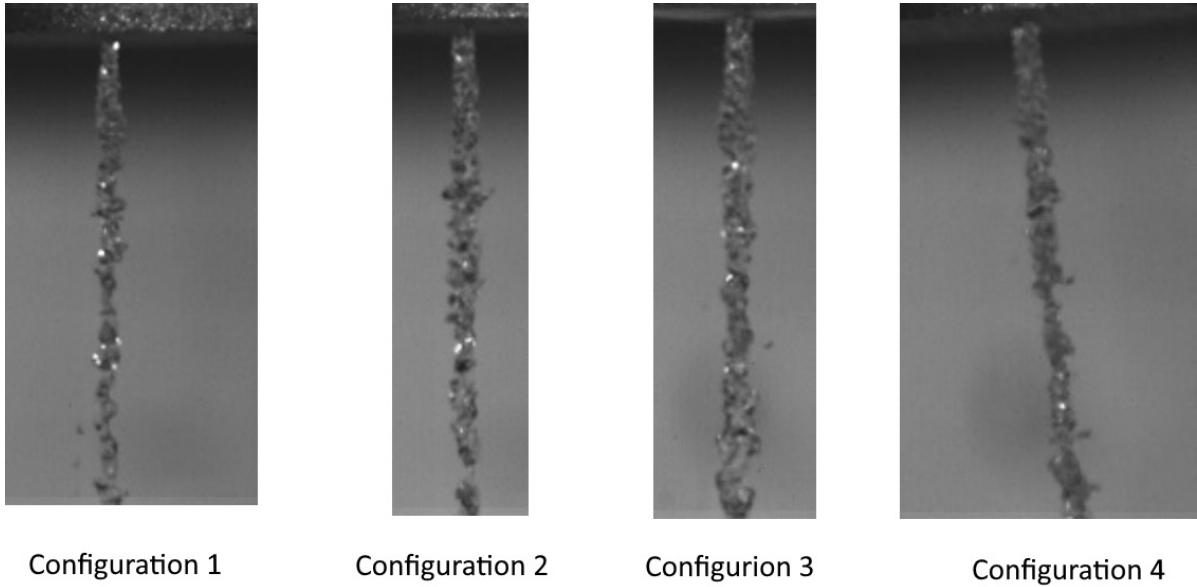


Figure 7.29: Symmetric pattern different configuraions

In [Figure 7.30](#) the comparison is made for the different configurations for the asymmetric patterns. Configuration 1 shows the most promising automation behavior. When the outlet diameter increases, the s-pattern becomes less recognizable, as seen in configurations 2 and 3. There is a small difference in configurations 2 and 4, despite the same outlet diameter. It is due to an increase in the traveled path by the inclination of 5 degrees. Similar to the axis-symmetric waves, no droplets formed for asymmetric waves. From [Figure 7.29](#) and [Figure 7.30](#) it is seen that no droplets were observed for both patterns in the limited high-speed camera resolution. As a result, it is impossible to estimate the SMD for jet injectors. It is possible that the droplet formation occurred further downstream. This possibility is checked during the upcoming test objective studying the mixing process.

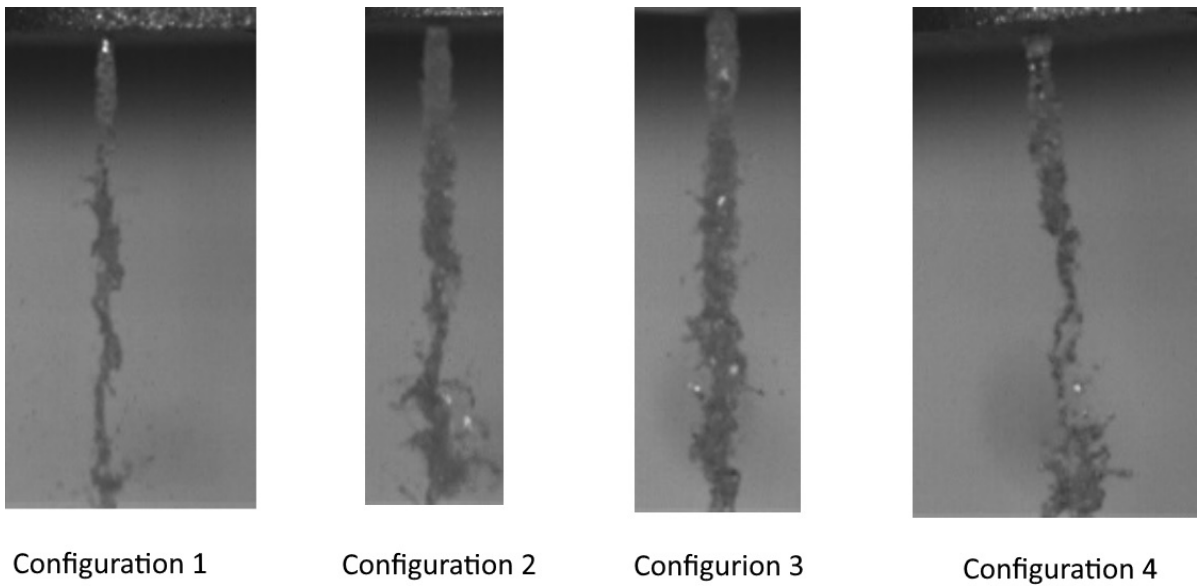
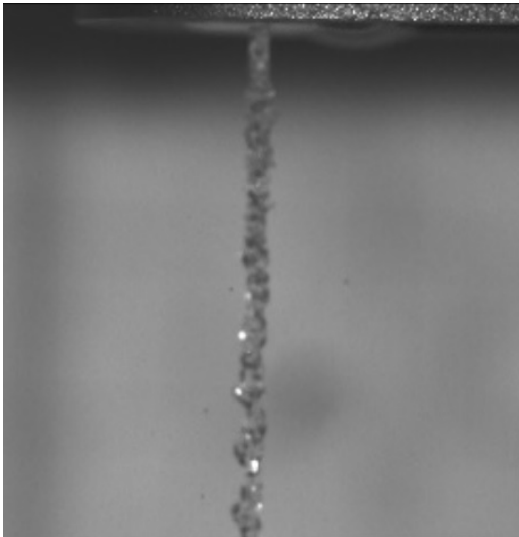


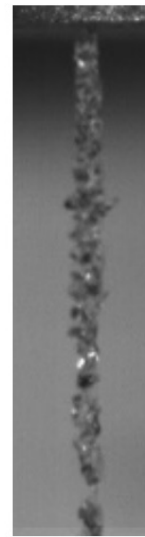
Figure 7.30: Assymmetric mechansim comparisions etoh diffent injectors

INCREASED PRESSURE

The initial tank pressure is increased to 7 bar for configuration 2 to investigate if any change in the atomization process occurs. Fewer cloud formations were noticed with increasing pressure. As a result, the asymmetric patterns occur less, and thus fewer s-patterns are observed. The increase in initial tank pressure leads to an observed change in axis-symmetric waves, as can be seen in Figure 7.31. From the captured footage, it was observed that an increased pressure did not lead to the formation of individual droplets. From Figure 7.31, it is clear that the decrease in jet diameter occurs more often at a higher pressure, especially moving more downstream. An s-pattern is expected, after a cloud of ethanol was formed. However, this s-pattern is less recognizable. Furthermore, the s-shape is longer compared to at low pressure and is clear from Figure 7.32.

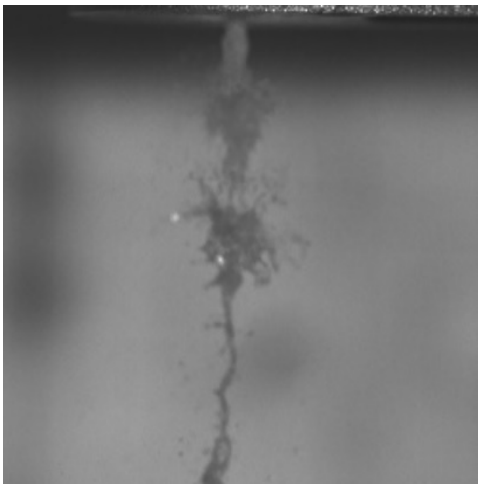


7 bar- axis symmetric



3-bar axis symmetric

Figure 7.31: Axis symmetric at an initial tank pressure of 3 and 7 bar



assymmetric waves - 7 bar



assymmetric waves - 3 bar

Figure 7.32: Assymmetric symmetric at an initial tank pressure of 3 and 7 bar

7.4. MIXING TEST

In this section the mixing properties between the jet and swirl atomizer are investigated. In [Subsection 7.4.1](#), the location where the mixing process occurs is investigated for different initial tank pressures. How the atomized flow of the jet and swirl injector interacts is explored in [Subsection 7.4.2](#).

7.4.1. OVERVIEW

In this section, the working fluid mixing location of the dual-mode is investigated. A P600 Nikon camera is used to image the mixing process. This camera has a frame rate of 25 Hz, which is sufficient to provide information on the mixing location. Color dye is mixed with the propellant to increase the footage clarity. The red color is added to the deionized water for the jet injectors, while blue is added for the swirl injector. A black surface is used to increase the contrast with the color dye. The pressure is varied from 3 to 7 bar, with an increment of 2 bars to investigate the effect of the increase of pressure on the mixing location. The mixing location is defined where the swirl crosses the jet spray. According to the theory, the spray angle of the swirl injector is not a function of the pressure. So, it is expected that the pressure has the least influence on mixing location.

The ball valves of the jet and swirl injector have to be open manually and timing of opening the valves is essential. In some cases, the timing was poor, resulted in that the full potential is not imaged. To compensate for the poor timing, an imaging editing program is used to compute where the mixing zone would be located if the timing was sufficient. To provide extra clarity in the images, the outlines swirl spray pattern were highlighted with two blue lines, and the outline of the jet spray pattern were highlighted with the two red lines. The origin is set to the injector head of the swirl injector and is the same for all the configurations. The start of the mixing location is indicated with a yellow line. The width of the injector was also marked with a yellow lines. This will make it easier to correlate the measured distance of the mixing process on the footage. An example of the raw footage and the one improved for clarity can be seen in [Figure 7.33](#).

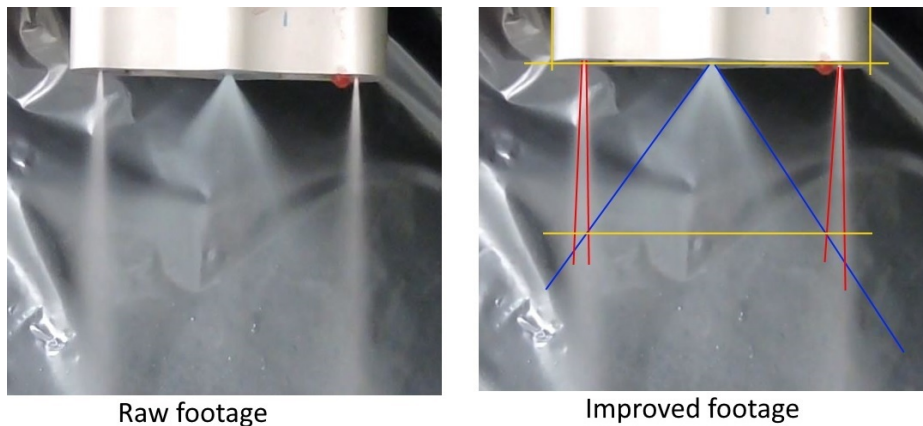


Figure 7.33: Example of the raw and improved footage

The distance was measured for all the configurations with the improved footage and these experiments are repeated twice. This data, included the average, can be seen in [Table 7.8](#). It is clear from the table that the average of configurations 1,2 ,and 4 varies within 1 mm for the different pressures. For configuration 3 the average fluctuates more than 1 mm. The reason for this that configuration 3 has an asymmetry in the mixing process. This asymmetry is only observed at a pressure of 5 and 7 bar.

Table 7.8: Overview of the measured distance where mixing process starts

Pressure [bar]	Distance mixing zone swirl injector head [mm]											
	Config 1			Config 2			Config 3			Config 4		
	#1	#2	avg	#1	#2	avg	#1	#2	avg	#1	#2	avg
3	48.6	53.4	51.0	49.7	52.9	51.3	49.5	54.9	44.7	44.7	47.7	46.2
5	54.2	50.1	52.2	51.3	54.5	52.9	59.7	57.7	58.7	46.7	45.7	46.2
7	51.5	49.6	50.6	53.0	50.5	51.8	57.5	57.5	57.5	47.6	47.6	47.6

The average data is also plotted in Figure 7.34. An error margin was applied at the data points. The pressure gauge has an accuracy of 2.5 percent, and this margin has been used for the x-axis. The distance has been measured with an accuracy of 1 mm of the image. It translates to a distance of 2 mm in real life, with a 5 percent compared to the results of the distances. So, a 5 percent error has been applied at the y axis. The reason for this is that the images have been modified with the hand, resulted in larger errors.

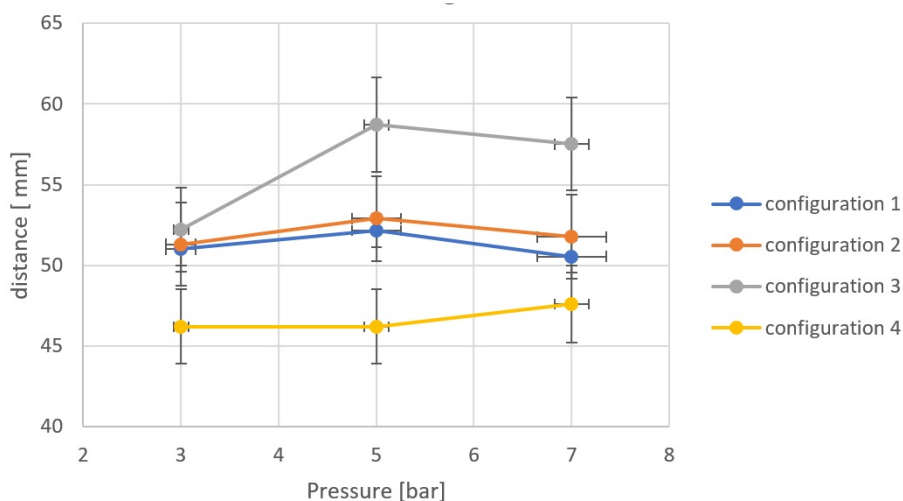


Figure 7.34: Distance mixing process as function of different initial tank pressures

As can be seen in Figure 7.34, configuration 1 and 2 has a similar distance where the mixing process occurs. Because of the observed symmetry in the mixing location of configuration 3 at a pressure of 3 bars, this data point is within the error range of configuration 2. The data points of configuration 3 for pressure 5 and 7 are less reliable, because of the asymmetric locations. It is also seen that the mixing distance of configuration 4 is smaller configurations 1, 2, and 3. This is caused by the inclination of the jet injectors. While there are some variances of the distance of the mixing process of a pressure increase, this variance is within the measurement error and observed for all configurations. So, a change in pressure does not influence the position of the mixing process. It is suspected that the spray angle is not a function of the pressure as the theory describes. To further investigate the influence of the swirl spray angle of the pressure, the spray angle is also measured, see table Table 7.9. For each configuration, the test was repeated twice. From these tests, the average value is determined. As can be seen in this table, the average spray angle of the swirl injector varies with a maximum of 3 degrees for all the configurations.

Table 7.9: Spray angle of the swirl injector for different pressures

Pressure [bar]	Spray angle swirl [deg]											
	Config 1			Config 2			Config 3			Config 4		
	#1	#2	avg	#1	#2	avg	#1	#2	avg	#1	#2	avg
3	70.0	68.0	68.8	72.0	70.0	70.5	70.0	68.0	69.9	73.0	70.0	71.5
5	69.0	73.0	71.0	68.0	72.0	69.8	67.0	67.0	67.0	70.0	70.0	70.0
7	71.0	72.0	71.5	73.0	66.0	69.5	67.0	67.0	67.0	70.0	70.0	70.0

The measured spray angles are plotted to provide a graphical overview. In this overview, the errors are taken into account. The pressure has an error bar of 2.5 percent since a pressure gauge of class 2.5 is used. A geo triangle is used to determine the spray angle of the swirl injector of the improved footage. This method has an error of 1 degree. Based on the average measurement of 70 degrees, a 1-degree error complies with a percentage error of 2 percent. See Figure 7.35 for the graph where the error bars are included. As can be seen in this graph, the variance in swirl angle is within the error bars and that confirmed the spray angle of the swirl injector does not vary with the pressure. For this reason, the position where the mixing starts is then also constant for a varying pressure.

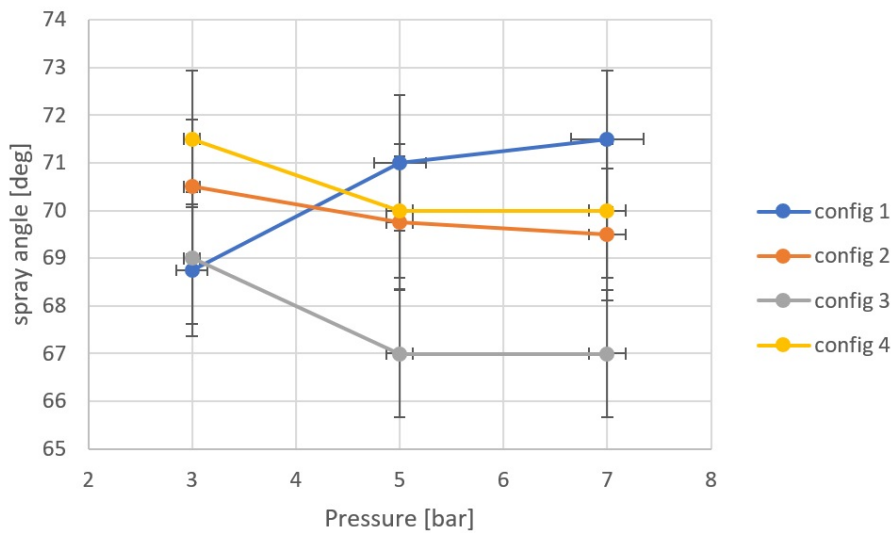


Figure 7.35: Measured spray angle of the swirl injector for different pressures

By investigating the swirl angle and the associated measurement errors, it is concluded that configuration 4 has the smallest distance when the mixing process is initiated, due to the inclined jet injectors. It is desired to use configuration 4, to minimize the combustion chamber length of the rocket engine.

7.4.2. INTERACTION JET AND SWIRL

In this section, it was investigated how the atomized liquid of the jet and swirl injectors interact at varying initial tank pressures. The theory describes that different scenarios as a function of the Weber number exist to explain the interactions between the droplets. However, the mixing occurs at a certain distance of the injector head. This makes it difficult to accurately predict how the atomized flow of the swirl and jet injector has mixed. Therefore, the high-speed camera is used to image and investigate the mixing process. A frame rate of 6400 frames a second is chosen since this is the best compromise between the frame rate to observe the details and to have sufficient resolution to provide the overview. It is important to have the overview of how the injector operates in the dual-mode, especially for a black and white image provided by the high-speed camera. The same color dye is used for the swirl (blue) and jet (red) injector, to increase the contrasts of the dual-mode operation

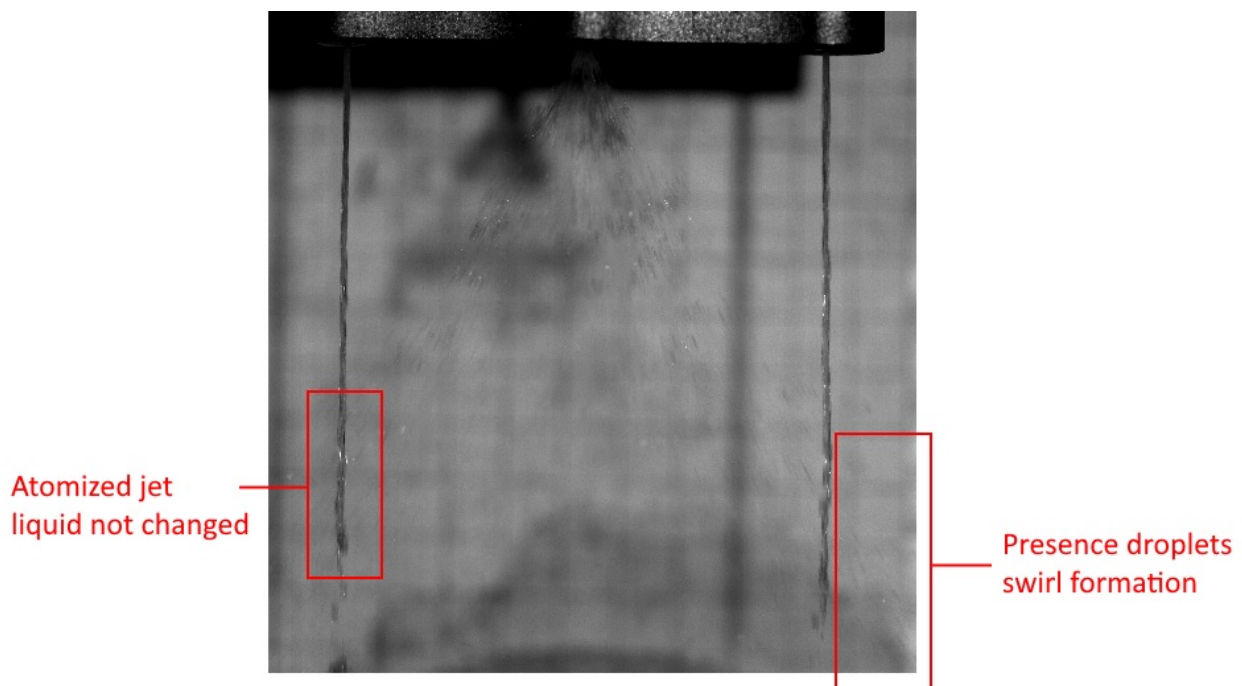
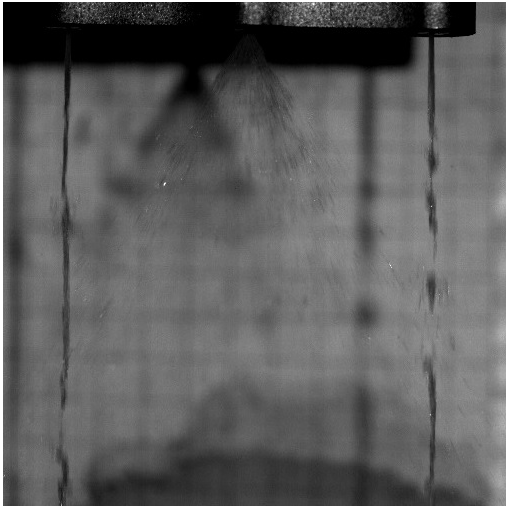


Figure 7.36: Dual-mode for configuration 2 at an initial tank pressure 3 bar

First, the dual-mode of configuration 2 is observed at an initial tank pressure of 3 bars. See [Figure 7.36](#) of an example of the observed footage. Several observations are made from this figure. The first observation is the presence of droplets at the swirl injector to the right-hand side of the right injector. This implies that the droplets of the swirl injector are not influenced by the jet injector. The reason for this is that the jet injector has a very small spray angle and only two jet injectors are equipped for a single injector configuration. The second observation is that the atomization process of the jet injector is not affected by the droplet shape, since this same pattern is observed before and after the intersection. The third observation is that the atomized liquid is not fully developed to droplets at the point where the mixing occurs. The same observations are made when the initial tank pressure is increased to a pressure of 5 and 7 bars. The only difference is observed that the velocity of the droplets is increased, caused by the pressure increase. In figures [Figure 7.37](#) the mixing process of configuration 2 and an initial tank pressure of 5 bar and 7 bar are shown. When the inclination is of the jet injectors is changed, by using configuration 4, the same observations are made for the same pressure range as shown in [Figure 7.38](#). In conclusion, the atomized flow of the jet and swirl injector did not influence the atomized behaviour and this is also not effected by the initial tank pressure.



Configuration 2
initial tank pressure 5 bar



Configuration 2
initial tank pressure 7 bar

Figure 7.37: Dual-mode for configuration 2 at an initial tank pressure of 5 and 7 bar



Configuration 2
Initial tank pressure 7 bar



Configuration 4
Initial tank pressure 7 bar

Figure 7.38: Dual-mode for configuration 3 and at an initial tank pressure of 7 bar

7.5. HEATING ELEMENT TEST

In this section the interaction between the injector and the heating element is explored. Since configuration 4 shows the most promising behaviour to achieve the smallest combustion length, this configuration is used for this test objective. For these tests, an initial tank pressure of 5 bar was used. During previous tests, it is observed that a minimum quantity of 6 ml results in an acceptable atomization process. In the chemical lab, only a quantity of microliters is allowed to use for any hot firing tests. So, deionized water is used. In [Subsection 7.5.1](#) the monopropellant operation mode is simulated, while in [Subsection 7.5.2](#) the dual-mode is simulated. From this simulation test, the most promising heating element configuration is selected. This selected heating element is then electrically powered, and the evaporation of the dual-mode operation is investigated as explained in [Subsection 7.5.3](#).

7.5.1. MONO PROPELLANT MODE

First, the three possible heating elements are assets using only the swirl injector, and thus the monopropellant operation mode is simulated. No electrical power is applied to the heating element, since first the interaction with this heating element is investigated. The high-speed camera is set to 6400 frames/second to provide an overview of how the swirl injector interacts with the heating element. From the footage of every heating element, it is seen that the droplets of the swirl injector have collided with the horizontal lines of the heating element. When the deionized water in the propellant tanks is depleted, the collection of droplets at the heating element is visible, as can be seen in [Figure 7.39](#).

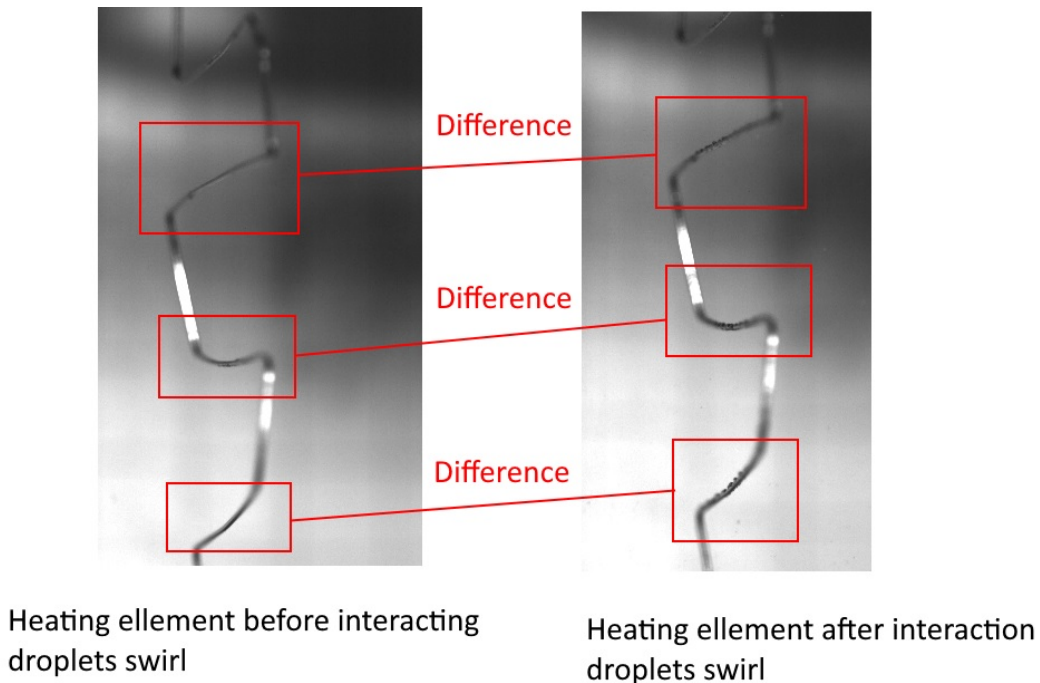


Figure 7.39: Example of the heating element before and after the atomization process using configuration 1 of the heating element

After all the footage of the different heating elements is observed, it is seen that the atomized droplets of the swirl injector passes the open section of the heating element, as can be seen in [Figure 7.40](#). This indicates that the swirl injector is more than capable to spread the droplets to the heating element. It also shows that the distance between the heating element and swirl injector can be further increased, based on the requirement. It also shows the drawback of the current heating element. Since openings in the heating element exist, it is possible that not all the hydrogen peroxide is decomposed. Therefore the full potential of the thermal decomposition process is not used.

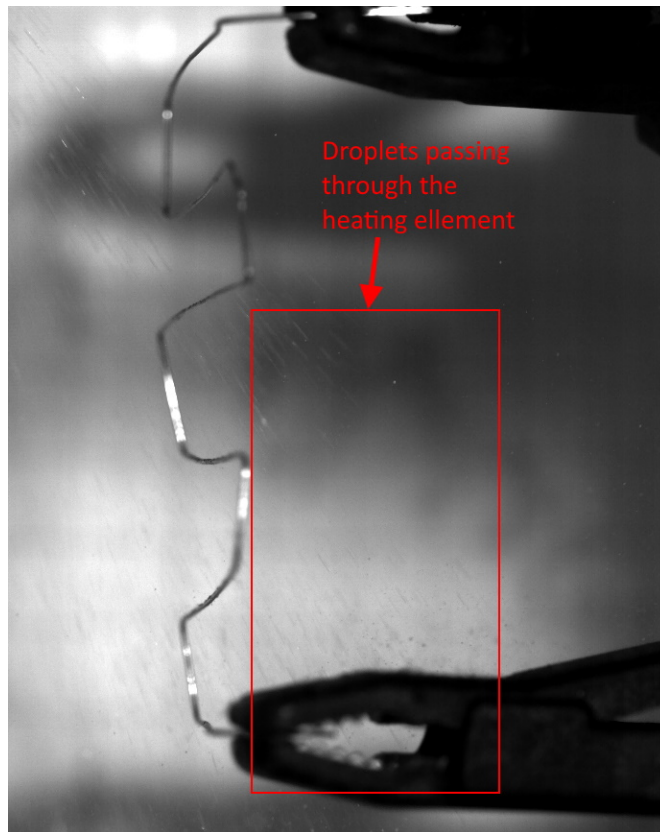


Figure 7.40: Example of the heating element that droplets are moving through the injector

In [Figure 7.41](#) the comparison is made with the different injector configurations. To objectively compare the different heating elements, the comparison is made just after the propellant tank has been depleted. As noticed, the configuration with the most horizontal elements is preferable, due to most interaction with the swirl droplets. Therefore, configuration 3 of the heating element makes the optimum use of the atomized propellant of the swirl injector. [Figure 7.40](#) and [Figure 7.39](#), clearly shows this. Additionally, the vertical elements do not contribute to provide thermal energy to the atomized droplets. The length of the heating element can play a role, depending on how the swirl and jet droplets interact and is investigated in [Subsection 7.5.2](#). For the monopropellant mode, the third configuration of the heating element is the most promising since it has the most horizontal elements.

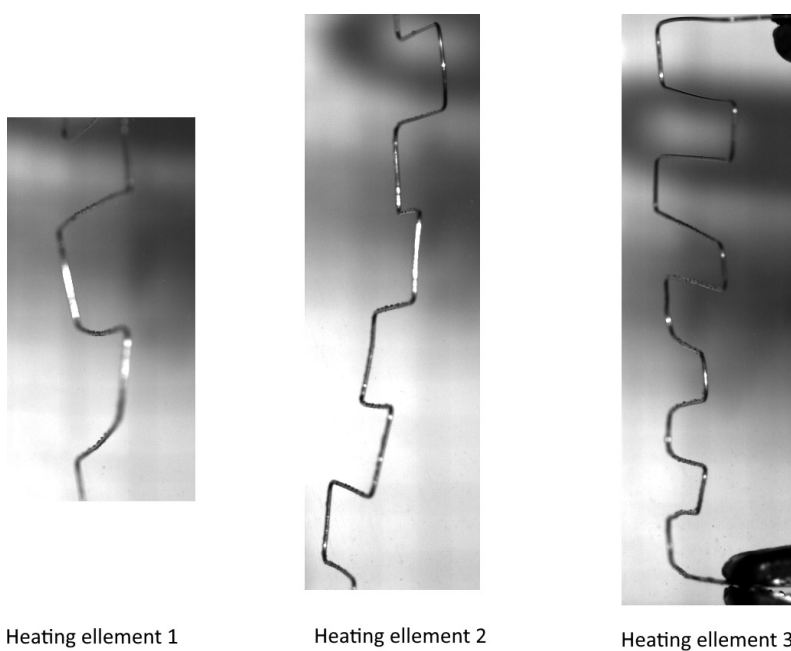


Figure 7.41: Example of droplets moving through the heating element

7.5.2. DUAL PROPELLANT MODE

After the mono-propellant operation mode is investigated, the dual propellant mode was tested. The same settings of the high-speed camera and deionized water are used for these tests. Not only the heating element is tested, but also the atomization properties of the jet injector at an increased distance from the injector head. After all the footage of the different configurations of the heating element was observed, the following observations are made. An example of this observation can be seen in Figure 7.42. First, the droplets of the swirl still reach the heating element, while the jet injector atomizes the propellant. Secondly, the same pattern of jet atomization is seen, as previously described. This indicates that the swirl droplets did not interact with the atomization process of the jet injector. The third observation is that the atomization behavior of the jet injector has not changed by observing the mixing location. This is a disappointing observation. The different heating elements are also compared, as can be seen in Figure 7.43. Again, it is observed that the horizontal elements are the most important sections of the heating elements. Because no interaction is observed between the droplets of the swirl and jet injector, the height of the heating element is not an important parameter. This would be different, when the interaction between the droplets would deform the traveled path. This would make it difficult to measure the start of the mixing zone. Because of the absence, it is possible to have a specific starting point for the mixing zone. So, the third configuration of the heating element has the most horizontal elements and is thus the preferred configuration.

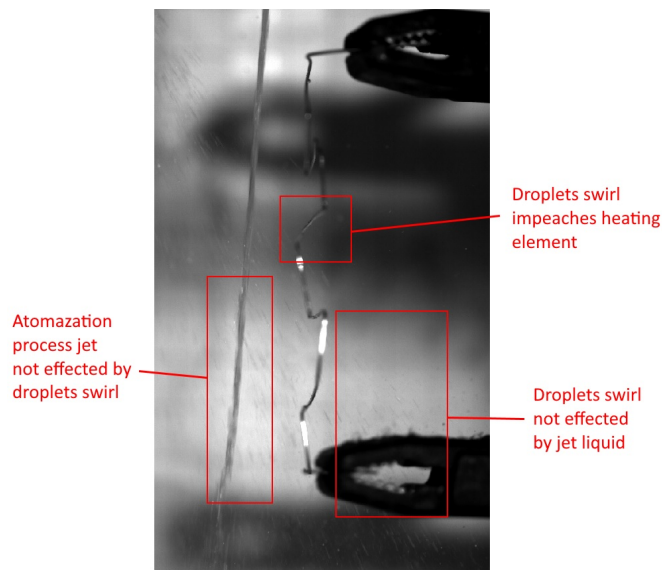


Figure 7.42: Example of the dual mode operation with a heating element 1

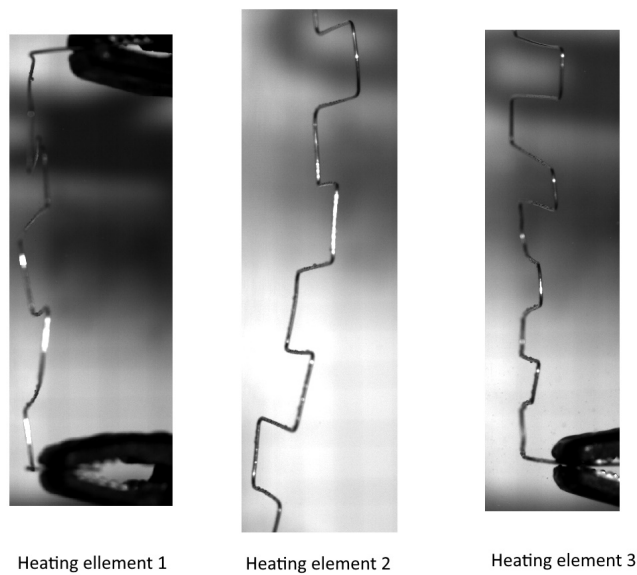


Figure 7.43: Comparison of different heating elements for a dual mode

7.5.3. ELECTRICAL POWER

The next tests focus on the amount of power is required to provide the thermal energy to evaporate the droplets of the atomized flow. As previously explained, the current will influence the temperature of the heating element. First, the required current is determined for the monopropellant mode. The current is started at 1.50 A and is increased to 3 A, with steps of 0.5 A. In Figure 7.44, the heating element after the atomization process has been finished, observed, and compared for different current levels. From this figure, it is noticed that at a current level of 2.5 A or higher no droplets are visible at the heating element. When the current level is 2.0 A or lower, the droplets are still observed. From this, it is concluded that a current level of 2.5 A is sufficient to provide thermal energy to evaporate the deionized water. This heating element requires a voltage of 4.67 V, which is measured by a multimeter tool. It results in a required power of 11.8W. In Figure 7.45, it is also seen that no droplets are formed during the atomization process at the heating element for a current level of 2.5 A, while at a current of 1.5 A the droplets are indeed seen. It indicates that the droplets are evaporated during the atomization process, validating the monopropellant mode.

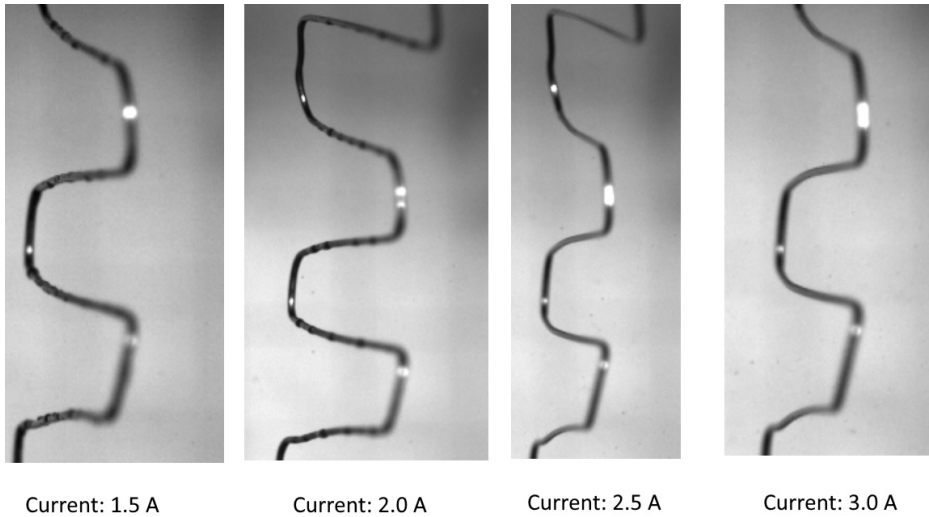


Figure 7.44: Comparison of different current levels

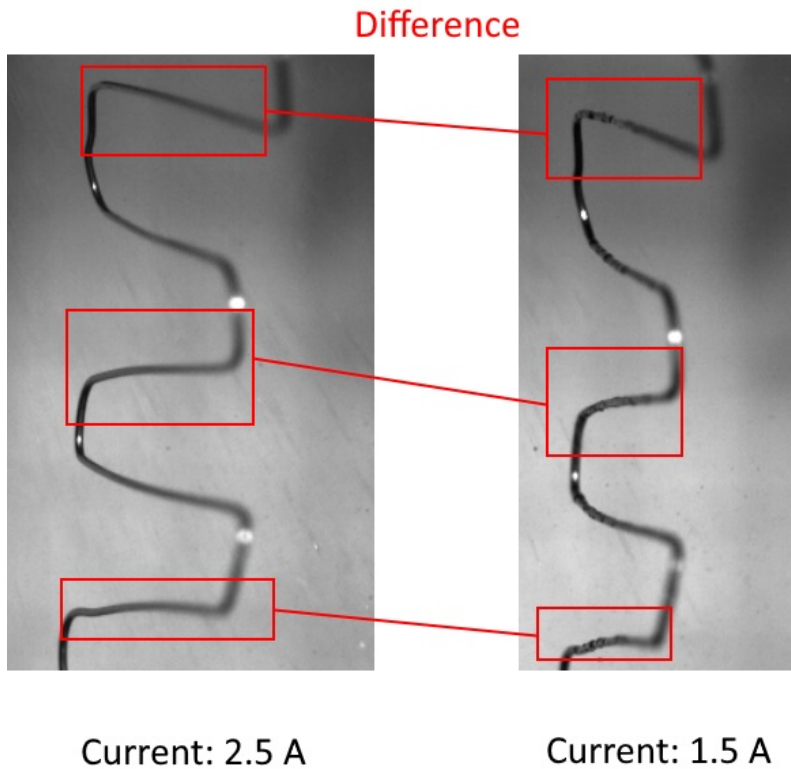


Figure 7.45: Droplet formation on heating element during atomization process

The next test objective is to test the dual-mode operation with a heating element that has electrical power. The heating element is also used to provide an impingement method to further improve the atomization behavior of the jet injector. From the monopropellant tests, a current level of 2.5 A is suitable to evaporate the droplets. This current level corresponds to a temperature of 350 degrees Celsius of a straight wire [39]. The impingement point of the jet is roughly at the same point where the droplet of the swirl comes in collision with the heating element, which helps to mix the oxidizer and fuel for the dual-mode operation. This can be seen in Figure 7.46. While the impingement occurs, the droplets are still be seen at the right-hand side of the heating element, similar to the monopropellant mode tests. Because the heating element is used as an impingement mean, vibrations of the heating element are introduced by the jet injector, especially after a cloud is formed. This confirms that an increase in injection velocity occurs when a cloud pattern is formed . No droplets are formed at the horizontal elements, implying that the droplets of the swirl injector are evaporated. It validates the dual-mode operation.

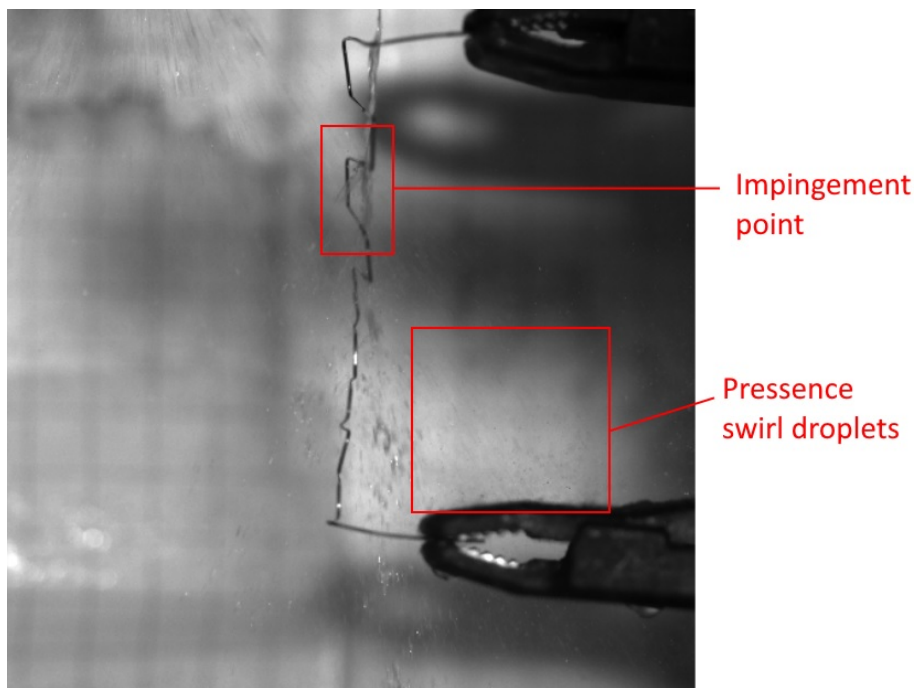


Figure 7.46: Example of dual-mode with a heating element connected electrical power

7.6. CONCLUSION

In this section, a conclusion is made from all the conducted tests. In Appendix F an overview is provide for every conducted experiment. First, the pressure drop is investigated between the outlet of the tank and the inlet of the injector. No pressure drop is measured for an initial tank pressure up to 5 bar. At a pressure of 6 bar, a pressure drop is measured, but this value is within 5 percent. This is within the measurement error of the two pressure gauges, which have each a 2.5 percent measurement error.

The atomization behavior for the swirl and jet injectors is investigated during the second test. Two mechanisms are recognized for the swirl injector: the perforation and circumferential waves. Three patterns are recognized for the jet injector: axis-symmetric waves, asymmetric waves, and the formation of clouds. All these patterns are according to the theory. During the end phase, the mixing of compressed air and the liquid occurs for both types of injectors.

The SMD and the spray angle are determined from the two observed mechanisms of the swirl injector. The perforations mechanism has an average SMD value of 0.461 mm. The SMD has a value of 0.391 mm for the circumferential waves, Both SMD estimations have an error of 0.12 mm. The test condition are used to update the expected design performance. Using the geometric tolerances leads to a minimum and maximum value of the SMD, which are 0.105 mm and 0.118 mm, respectively. As a result, the SMD has been underestimated by a factor of 5 for a pressure of 3 bar. The initial tank pressure has been increased to 7 bar, and then the SMD has a value for perforations of 0.445 mm and 0.417 mm. For the given test condition the expected SMD has a minimum value of 0.103 mm and 0.149 mm, respectively. The injection velocity at the start has been computed to investigate the reason why the SMD has not been decreased at increased initial tank pressure. The maximum injection velocity that is computed is 4.4 m/s and this is lower than anticipated. As a result, the SMD and spray angle is different than expected. The performance of the jet injector is also investigated. Unfortunately, no droplets were observed in the given resolution, so the SMD cannot be determined. Since the resolution is limited, it is also possible that the droplets are formed more downstream and will be investigated in a different test.

The position where the mixing between the jet and swirl injector occurs is investigated for a range of initial tank pressure. It is seen that the location is constant since the spray angle of the swirl injector is constant for varying initial tank pressure. The inclination of the placement of the jet injector does influence the location where the mixing starts. The atomization process of both injectors is not influenced by the mixing process. The only change of the increased initial tank pressure is the observed increased injection velocity.

Three different configurations of the heating elements are tested for the mono and dual-mode to investigate the interaction between the atomized flow and heating element. From these tests, it is observed that the horizontal elements have the most contact with the droplets of the swirl injector. Also, the swirl injector is efficient in providing the right mixing condition to interact with the heating element. The drawback of the current heating element is that it has open sections, where the atomized hydrogen peroxide passes through and is not contributing to the decomposition process. It is found that a current of 2.5 A is sufficient to evaporate the generated droplets. Also, the heating element can be used to impinge the jet injector, which improves the atomization behavior.

In conclusion, the different tests showed that the injector configurations have an atomization behavior as described in the literature. The predicted performance of the SMD is overestimated for the swirl injector but is within the predicted magnitude. The functional operation of the different modes in combination with the heating element is also discussed. The heating element is introduced to the atomized jet stream, which improves the atomization behavior of the jet injector. The overall testing results provide a solid understanding of the operation of the injector configuration and this foundation can be used for the next steps of this project.

8

CONCLUSION AND RECOMMENDATIONS

This report describes the development of an injector for an advanced hypergolic propulsion system. In this section, the main question "What injector design can support the thruster that uses only thermal energy to decompose hydrogen peroxide in monopropellant mode and react with ethanol fuel for bipropellant mode?" is answered.

8.1. CONCLUSION

The advanced hyperbolic propulsion system operates in two modes. The first mode is the monopropellant mode that uses only hydrogen peroxide and the second mode is the dual-mode operation of hydrogen peroxide and ethanol. The most promising solution to operate a propulsion system in two modes is by making use of two types of injectors. Several types of injectors exist that can atomize a liquid propellant. The swirl injector is selected to atomize the hydrogen peroxide because this injector type has a large spray angle. Additionally, a large spray angle decreases the combustion chamber length, which is beneficial for the overall mass of the propulsion system. Another benefit of the swirl injector is the formation of a hollow cone. A hollow cone makes it possible to place the heating element at the circumferential shape of the combustion chamber without blocking the inlet of the nozzle. Lastly, a single swirl injector is sufficient to atomize the hydrogen peroxide. A jet injector is chosen to atomize the ethanol, because of the small spray angle. The small spray angle will direct the ethanol to a specific location, which is required for the dual-mode operation.

Different requirements were set that had to be fulfilled by the design of the injector. In the requirements, not only the performance is addressed, but also the manufacturing and testing aspects. Based on these requirements, the geometric dimensions of the swirl and jet injector were determined. In total, four different injector configurations were made to investigate the mixing process. Each configuration has the same swirl injector design. The swirl injector had an outlet of 1.1 mm and a swirl chamber diameter had a value of 5.7 mm, resulting in an SMD of 58 micrometers and a spray angle of 90 degrees. Each configuration has a different outlet diameter of the jet injectors. Configuration 1, 2, and 3 had a jet injector outlet diameter of 0.78 mm, 0.70 mm, and 0.64 mm respectively. Configuration 4 had the same outlet diameter as configuration 2, but the jet injectors were placed under an angle of 5 degrees. The SMD of the jet injector for configurations 1, 2, and 3 is 85.5 micrometers, 61.7 micrometers, and 45.3 micrometers, respectively. As can be seen, the SMD of the jet for the different configurations is higher, equal, or lower than the SMD of the swirl injector. This is preferred to investigate the mixing process. The tolerances have to be within ± 0.05 mm to achieve the performance requirements.

The injectors are produced with an additive manufacturing method. Additive manufacturing has the benefits of reducing the number of components, reducing manufacturing costs, and reducing manufacturing time. An external company offered to provide the knowledge and experience for this manufacturing process. To comply with this manufacturing method, the initial design has to be altered. The geometry of the swirl was simplified and the dimensions were modified to have sufficient material margin for the post-processing operation to machine the different threads and flat surfaces. The dimension of the tubing for the swirl injector was sufficient to be manufactured without a support structure. However, the orientation of this tubing is changed to increase the wall thickness of the swirl injector. The desired tolerances of ± 0.05 mm cannot be achieved with additive manufacturing, as the smallest tolerance is ± 0.1 mm. As a consequence, a second design iteration was required. This resulted in an outlet diameter of 1.6 mm for the swirl injector and a diameter of 8.4 mm for the swirl chamber. Furthermore, the jet diameter for configuration 1, 2, and 3 are 0.7 mm, 0.9 mm and 1.1 mm respectively. Still, the SMD of the jet injector is smaller, equal, or larger for the different configurations, as it was intended. Due to this second iteration, all manufacturing requirements were met, only the SMD requirement is unfulfilled.

This injector design atomizes the propellant into sufficiently small droplets such that a hard start can be prevented. In combination with the high concentration of hydrogen peroxide (>98%) the ignition delay time is decreased, which helps the prevention of a hard start. Additionally, the timing of opening the propellant valves can be adjusted to prevent an oxygen-rich environment. Furthermore, the cooling of the propulsion system is taken into account in the design. After exploring different options, film cooling is selected. Film cooling is initiated at two positions: near the injection head or near the combustion chamber. Slots are included at these positions to accommodate film cooling. As hydrogen peroxide is used for all operation modes, this liquid is used to generate the film coolant. In the design of the swirl injector, a small tubing is added. In the future, this tubing can feed the hydrogen peroxide to the slots to cool the propulsion system.

For the validation of the injector design, testing is required. As no test setup was available, one has to be designed and manufactured. The test setup consists of two pressure regulators and two propellant tanks. Ball valves were used to

control the flow of the propellant and pressurant gas. Compressed air is used as pressurant gas since this has the desired pressure and fits within the financial budget. As a result, the propellant can be fed to the injectors with a maximum pressure of 8 bars. Custom tanks were designed to accommodate the desired mass flow and volume since off-the-shelf tanks are expensive and the outlet had to be adjusted to achieve the desired mass flow.

The validation of the design of the injectors is based on four different tests. First, the atomization behavior was investigated with deionized water. The experimental results are in line with the mechanism described in the literature. The swirl injector produces a sheet of liquid. Literature specifies three mechanisms: perforation, circumferential waves, and short waves. The first two mechanisms were observed for the swirl injector during the tests. This indicated that the injection velocity fluctuates. Three different mechanisms are specified for a liquid jet: axis-symmetric waves, asymmetric waves, and aerodynamic forces. For the jet injector, the first two mechanisms were observed during the tests. This indicates that the injection velocity varies. The second test focuses on the performance of the jet and swirl injector. Hydrogen peroxide was used as a working liquid to be atomized with the swirl injector. The SMD of the perforations mechanism was equal to $0.42 \text{ mm} \pm 0.12 \text{ mm}$ and the SMD of the circumferential waves was equal to $0.46 \text{ mm} \pm 0.12 \text{ mm}$ at an tank pressure of 3 bar. This is larger than expected. The reason for the higher SMD can be found by investigation of the injection velocity. It is found that the injection velocity is lower than intended, resulting in higher SMD. During the tests, it was also observed that the spray angle is smaller, which has the same reason. For the jet injector, no droplets of the atomized flow of ethanol were observed due to the limited resolution of the high-speed camera. Furthermore, the test reveals an improved atomization process, which is caused by the lower surface tension of ethanol, compared to deionized water. Based on these two types of tests, it is concluded that the swirl and jet injectors are validated. The observed atomized behavior is in line with the mechanism described by the theory.

The next type of test focuses on the investigation of the dual-mode operation, influencing the design parameters and implementation of a heating element. In the third test, the mixing location of the dual-mode operation is investigated for the different injector configurations and different tank pressures. The testing revealed that the mixing location is independent of an initial tank pressure between 3 and 7 bar. The mixing location is independent of the design parameters, except for the inclination of the jet injectors. Therefore, configuration 4, with the inclined jet injectors, provided the shortest distance to start the mixing process. It is also noticed that no interaction occurs between the droplets of the swirl and jet injector. In the fourth test different configurations of a heating element are investigated. The droplets of the swirl are capable of reaching the heating element and the behavior of the droplets is not influenced by the heating element. Furthermore, it was seen that not all droplets are vaporized, due to the openings of the heating element. From this test, it is noticed that the heating element that has the most horizontal segments evaporates the largest amount of droplets and therefore this configuration is preferred. The heating element is used as an impingement point to accelerate the atomization process of the jet injector. A current of 2.5 A is sufficient to evaporate deionized water, consuming 11 W of power.

In conclusion, a swirl injector is used to atomize the hydrogen peroxide and the observed test results correspond to the described mechanism by the theory. The heating element with a current of 2.5 A is capable to evaporate the droplets. The jet injector atomizes the ethanol and should be placed under an inclination to have the shortest mixing distances. This configuration of the injector is the best design to support the operation of a thruster that can operate in mono and dual-mode operation using hydrogen peroxide and ethanol.

8.2. RECOMMENDATION

Several recommendations are made from the design, manufacturing, and testing process:

- **Hot firing test** From all the conducted tests, it is noticed that milliliters of propellant is required to achieve the desired atomization behavior. As a result, no hot firing was conducted since the chemical lab only allows to use of microliters of propellant for any hot firing tests. A different testing location has to be found to conduct hot firing tests. It should be noted that a different test location has to be found to execute this test. By moving to a different test location, the selection of pressurant gas should be reconsidered. The gassenteam of the TU Delft could be contacted to explore these possibilities. Also, the ball valves should be replaced by solenoid valves to safely operate the test setup. A possible location is a grass field behind the parking lot of the Fellowship. If this location is used, special care has to be taken to collect the atomized hydrogen peroxide and ethanol to prevent spilling it into the environment.
- **Modifications test setup** Modifications are recommended to be made to the test setup to conduct the hot firing test. First of all, mass flow measurement equipment is recommended to be able to measure the mass flow during the testing operation. Also, it is desired to be able to understand how the inlet pressure varies during the atomization process to provide further insights into the formation of the clouds. By using pressure transducers, the pressure drop across the injector configurations can be measured, which forms a critical design parameter. Also, the ball valves that control the propellant should be replaced by the solenoid valves.

- **Heating element** The current heating element is capable of supply thermal energy to the atomized droplets. However, several improvements can be made to this heating element. The used heating element has open spaces between the horizontal segments, resulting in limited evaporation of the atomized hydrogen peroxide. It is recommended to investigate the design and manufacturing of a heating element that has no open spaces between the horizontal elements. Also, it can be investigated the influence of the heating element on the atomization behavior of the jet injector
- **Swirl injector** Now that a solid understanding of the performance of the swirl injector is understood, the atomization behavior swirl injector can be investigated in detail. It is recommended to observe the swirl injector at 67500 frames a second at different downstream positions. This is a time-consuming process since at this frame rate the resolution is limited. When moving to different downstream positions the ability to check the focus of the high-speed camera and to be able to have a scale should be considered.
- **Stricter tolerances** In this report is shown that tolerance of ± 0.1 mm has a large effect on the performance of the atomizer. For the next iteration of the injector, it can be investigated how stricter tolerances can be achieved. One method that can achieve smaller tolerances is the electroerosion. The external company has connections with a company that has electroerosion capabilities. The increased manufacturing time and costs should be considered when using this method to achieve stricter tolerances.

During this investigation, the first hardware of an advanced hypergolic propulsion system is developed. Although the development of the injector is still in early stage, already huge progress is made in the realization of this thruster. The initial design is validated by numerous testings. The usage of swirl and jet injector combination shows promising results to achieve the set goal of mono and dual-mode operation using green propellant.

BIBLIOGRAPHY

- [1] J. Waymer, *SpaceX's Crew Dragon fire sent hazardous chemical compounds into the environment*, <https://eu.floridatoday.com/story/news/local/environment/2019/04/25/spacexs-crew-dragon-incident-sent-hazardous-chemicals-into-environment/3548180002/> (2019).
- [2] L. Bayvel, Z. Orzechowski, *Liquid atomization* (Taylor & Francis, 1993).
- [3] Christoph Heinzen, Andreas Berger, Ian Marison, *Use of Vibration Technology for Jet Break-Up for Encapsulation of Cells and Liquids in Monodisperse Microcapsules*, (2014).
- [4] S.R. Shinen, MS.ShriNidhi, *Review on film cooling of liquid rocket engines*, Propulsion and Power Research (2016).
- [5] R. Arnold, D. Suslov, O. J. Haidn, *Circumferential Film Cooling Effectiveness in a LOX H2 Subscale Combustion Chamber*, JOURNAL OF PROPULSION AND POWER (2009).
- [6] R. Arnold, D. Suslov, O. J. Haidn, *Film Cooling of Accelerated Flow in a Subscale Combustion Chamber*, JOURNAL OF PROPULSION AND POWER (2009).
- [7] Paul Gradl, Sandy E. Greene, Christopher Protz, Brad Bullard, James Buzzell, James Hulka, Robin Osborne, *Additive Manufacturing of Liquid Rocket Engine Combustion Devices: A Summary of Process Developments and Hot-Fire Testing Results*, 54th AIAA/SAE/ASSEE Joint Propulsion Conference 2018 (2018).
- [8] Kamran Saeidi, Farid Akhtar, *Microstructure-Tailored Stainless Steels with High Mechanical Performance at Elevated Temperature*, https://www.researchgate.net/figure/Schematic-of-the-selective-laser-melting-process_fig1_330972447 (2019).
- [9] I. New Era Pump Systems, *NE-1000 Programmable Single Syringe Pump*, <http://www.syringepump.com/NE-1000.php> (2021).
- [10] Lukasz MEZYK, Zbigniew GUT, Przemyslaw PASZKIEWICZ, Piotr WOLANSKI, Grzegorz RARATA, *Possibility of using thermal decomposition of hydrogen peroxide for low thrust propulsion system application*, 54th AIAA/SAE/ASSEE Joint Propulsion Conference 2018 (2017).
- [11] Landefeld, *Safety valve valve G 1/4*, <https://www.landefeld.com/artikel/en/t-v-safety-valve-g-14-dn8-900-bar-brass/SV2014208-920MS> (2021).
- [12] Arnoud Breedveld, *Producttekenen en -documenteren van 3d naar 2d* (BIM Media bv, Den Haag, 2011).
- [13] E. Parlinment, *Impact of REACH legislation on European space industry*, https://www.europarl.europa.eu/doceo/document/E-8-2016-003827_EN.html (2016).
- [14] Ir. B.T.C. Zandbergen, *Theram1 Rocket Propulsion (version 2.07)* (Tu Delft, 2018).
- [15] Lyshevskii, *Processes of Fuel Atomization in Diesel Nozzles*, (1963), in russian.
- [16] Zhongtao Kang, Zhen-guo Wang, Qinglian Li, Peng Cheng, *Review on pressure swirl injector in liquid rocket engine*, Acta Astronautica (2017).
- [17] Kanmaniraja Radhakrishnan, Min Son, Keonwoong Lee, Jaye Koo, *Effect of injection conditions on mixing performance of pintle injector for liquid rocket engines*, Acta Astronautica (2017).
- [18] Jaime Quesada Mañas, *Propellant grade hydrogen peroxide production and thermo pseudo hypergolicity investigation for dual mode green propulsion systems*, Tu Delft (2020).
- [19] Hongjae Kang, Hyuntak Kim, Sejin Kwon, *Difficulties in Dual-Mode Operation of Nontoxic Hypergolic Thruster Using Decomposition of H2O2*, JOURNAL OF PROPULSION AND POWER (2019).
- [20] T. Borsboom, *Investigating into injectors, decomposition using only thermal energy and dual-mode operation*, Tu Delft (2020).
- [21] I. M. specialties, *Hydrogen Peroxide Material Compatibility Chart*, Document (2015).
- [22] ParaBilis, *H2O2 Handling Safety Overview*, Powerpoint (2015).
- [23] P.-K. Wu, L.-K Tseng, G. M. Faeth, *Primary Breakup in Gas/Liquid Mixing Layers for Turbulent Liquids*, American Institute of Aeronautics and Astronautics (1992).
- [24] R. D. Reitz, F. B. Bracco, *On the Dependence of Spray Angle and Other Spray Parameters on Nozzle Design and Operating Conditions*, Society of Automotive Engineers (1979).
- [25] H. S. Couto, J. A. Carvalho Jr., D. Bastos-Netto, *Theoretical Formulation for Sauter Mean Diameter of Pressure-Swirl Atomizers*, JOURNAL OF PROPULSION AND POWER (1997).
- [26] U. Technologies, *Density H2O2*, <https://www.h2o2.com/technical-library/physical-chemical-properties/physical-properties/default.aspx?pid=11&name=Density-of-H2O2-Solutions> ().
- [27] D. GmbH, *Density ethanol*, <http://ddbonline.ddbst.de/DIPPR105DensityCalculation/DIPPR105CalculationCGI.exe> ().
- [28] E. Europa, *Dynamic viscosity Tension H2O2*, <https://echa.europa.eu/registration-dossier/-/registered-dossier/15701/4/23s>.

- [29] D. GmbH, *Dynamic viscosity Tension H2O2*, http://www.ddbst.com/en/EED/PCP/VIS_C11.php ().
- [30] U. Technologies, *Surface H2O2*, <https://www.h2o2.com/technical-library/physical-chemical-properties/physical-properties/default.aspx?pid=19&name=Surface-Tension-of-H2O2-Solutions> ().
- [31] D. GmbH, *Surface Tension of Ethanol*, http://www.ddbst.com/en/EED/PCP/SFT_C11.php ().
- [32] NPR, *INTRODUCING PROPELLANT INTO A COMBUSTION CHAMBER*, <http://nprcet.org/e20content/Misc/e-Learning/Mechanical/III20year/ME1303-GAS20DYNAMICS20AND20JET20PROPULSION.pdf>.
- [33] Hongjae Kang, Eunkwang Lee, Sejin Kwon, *Suppression of Hard Start for Nontoxic Hypergolic Thruster Using H2O2 Oxidizer*, JOURNAL OF PROPULSION AND POWER (2017).
- [34] MetalCor, *Data sheet 1.4462*, <http://www.metalcor.de/en/datenblatt/21/f> (2021).
- [35] C. Parmer, *Chemical Compatibility Database*, <https://www.coleparmer.com/chemical-resistance> (2021).
- [36] E. toolbox, *Surface Tension of Water in contact with Air*, https://www.engineeringtoolbox.com/water-surface-tension-d_597.html (2021).
- [37] E. toolbox, *Water - Dynamic and Kinematic Viscosity*, https://www.engineeringtoolbox.com/water-dynamic-kinematic-viscosity-d_596.html (2021).
- [38] E. toolbox, *Water - Density, Specific Weight and Thermal Expansion Coefficient*, https://www.engineeringtoolbox.com/water-density-specific-weight-d_595.html (2021).
- [39] Omega, *Resistance Heating Wire Nickel-Chromium Alloy*, <https://assets.omega.com/pdf/cable-and-wire/heating-wire/NI80.pdf> (2021).

A

DETAILED CALCULATIONS INITIAL DESIGN

In this section the detailed calculation of the initial design of the required dimensions and the associated theoretical performance is shown. The theory behind these equations and the made design choices are explained in [Chapter 4](#).

A.1. DETAILED CALCULATIONS SWIRL INJECTOR

In this section the detailed calculation of the design of the swirl injector is shown.

Input parameters

As it is explained in [Chapter 4](#), the following values are used as input parameters for the design process of the swirl injector. See [Chapter 4](#) for the explanation why these values are chosen.

Initial filling factor: 0.343 [-]	Contraction coefficient (ψ): 0.9 [-]
Mass flow: 0.005 kg/s	Is ratio: 2.0 [-]
Density ambient gas: 1.225 kg/m^3	Density HTP: 1400 kg/m^3
Pressure drop: 2 Bar	Dynamic viscosity: 1.249 CP
Number of inlet ports: 1 [-]	Kinematic viscosity: $8.9214 \cdot 10^{-7}$
Ratio between swirl radius and outlet radius: 4 [-]	Surface tension: 80 dyne/cm
Tolerances (ϕ): 1.05 [-] (5 percent tolerance)	

Determining the Geometric constant, discharge coefficient, outlet diameter, inlet diameter and swirl radius

Geometric constant:

$$K = \frac{(1-\epsilon)\sqrt{2}}{\epsilon\sqrt{\epsilon}} = \frac{(1-0.343)\sqrt{2}}{0.343\sqrt{0.343}} = 4.625$$

Discharge coefficient

$$\mu = \epsilon\sqrt{\frac{\epsilon}{2-\epsilon}} = 0.343\sqrt{\frac{0.343}{2-0.343}} = 0.156$$

Outlet diameter:

$$d_0 = \sqrt{\frac{4G}{\pi\mu\sqrt{2\rho\Delta P}}} = \sqrt{\frac{4 \cdot 0.005}{\pi \cdot 0.156 \cdot \sqrt{2 \cdot 1400 \cdot 2 \cdot 10^5}}} = 1.313 \cdot 10^{-3} \text{ m} = 1.313 \text{ mm}$$

Swirl radius:

$$R = \frac{R}{r_0} = 4 \cdot 0.5 \cdot 1.313 = 2.626 \text{ mm}$$

Inlet diameter:

$$K = \frac{2Rd_0}{id_p^2} \rightarrow 4.625 = \frac{2 \cdot 2.626 \cdot 10^{-3} \cdot 1.313 \cdot 10^{-3}}{1 \cdot d_p^2} \rightarrow d_p = 1.221 \cdot 10^{-3} \text{ m} = 1.221 \text{ mm}$$

Check assumption viscosity

Viscosity:

$$Re = \frac{4G}{\pi\rho v\sqrt{id_p}} = \frac{4 \cdot 0.005}{\pi \cdot 1400 \cdot 8.9214 \cdot 10^{-7} \sqrt{1 \cdot 1.221 \cdot 10^{-3}}} = 4174.5$$

Kappa:

$$\log(\lambda) = \frac{25.8}{(\log(Re))^{2.58}} - 2 = \frac{25.8}{(\log(4174.5))^{2.58}} - 2 = -1.067 \rightarrow \lambda = 0.0857$$

B parameter

$$B = \frac{R}{r_p} = \frac{2.626 \cdot 10^{-3}}{0.5 \cdot 1.221 \cdot 10^{-3}} = 4.301$$

Check assumption

$$\frac{B^2}{i} - K \leq \frac{2}{\lambda}(\phi^{1.5} - 1) \rightarrow \frac{4.301^2}{1} - 4.625 \leq \frac{2}{0.0857}(1.05^{1.5} - 1) \rightarrow 13.874 \leq 1.772$$

As can be seen, this equation does not hold. This means that the viscosity has to be taken into account!

Correction viscosity

corrected geometric constant:

$$K_\lambda = \frac{K}{1 + \left(\frac{\lambda}{2}\right)\left(\frac{B^2}{i} - k\right)} = \frac{4.625}{1 + \left(\frac{0.0857}{2}\right)\left(\frac{4.301^2}{1} - 4.625\right)} = 2.9$$

Corrected filling factor:

$$K = \frac{(1-\epsilon)\sqrt{2}}{\epsilon\sqrt{\epsilon}} \rightarrow 2.9 = \frac{(1-\epsilon)\sqrt{2}}{\epsilon\sqrt{\epsilon}} \rightarrow \epsilon = 0.427$$

An iterative approach is used to determine the associated value of the filling factor

corrected discharge coefficient:

$$\mu = \frac{1}{\sqrt{\frac{K_\lambda^2}{1-\epsilon} + \frac{1}{\epsilon^2}}} = \frac{1}{\sqrt{\frac{2.9^2}{1-0.427} + \frac{1}{0.427^2}}} = 0.222$$

Updating swirl radius, outlet diameter and inlet diameter

Outlet diameter:

$$d_0 = \sqrt{\frac{4G}{\pi\mu\sqrt{2\rho\Delta P}}} = \sqrt{\frac{4 \cdot 0.005}{\pi \cdot 0.222 \cdot \sqrt{2 \cdot 1400 \cdot 2 \cdot 10^5}}} = 1.101 \cdot 10^{-3} m = 1.101 mm$$

Swirl radius:

$$R = \frac{R}{r_0} r_0 = 4 \cdot 0.5 \cdot 1.101 = 2.202 mm$$

Inlet diameter:

$$K = \frac{2Rd_0}{i d_p^2} \rightarrow 2.9 = \frac{2 \cdot 2.202 \cdot 10^{-3} \cdot 1.101 \cdot 10^{-3}}{1 \cdot d_p^2} \rightarrow d_p = 1.293 \cdot 10^{-3} m = 1.293 mm$$

Determining the outlet length, inlet length and diameter chamber

Define parameter D port':

$$d'_p = \frac{d_p}{\sqrt{\psi}} = \frac{1.293}{\sqrt{0.85}} = 1.382 mm$$

Determine inlet length

$$L_p = 2.25 d'_p = 2.25 \cdot 1.382 = 3.11 mm$$

Determine outlet length for geometric constant that is smaller than 5:

$$L = (0.75) d_0 = 0.75 \cdot 1.1 = 0.825 mm$$

Determine the diameter of the swirl chamber:

$$D_s = 2R + d_p = 2 \cdot 2.202 + 1.293 = 5.697 mm$$

Determining the spray angle

Determine parameter S:

$$\mu = \sqrt{1 - \mu^2 K^2} - S \sqrt{S^2 - \mu^2 K^2} - \mu^2 K^2 \ln \left(\frac{1 + \sqrt{(1 - \mu^2 K^2)}}{S + \sqrt{S^2 - \mu^2 K^2}} \right) \rightarrow$$

$$0.222 = \sqrt{1 - 0.222^2 \cdot 2.9^2} - S \sqrt{S^2 - 0.222^2 \cdot 2.9^2} - 0.222^2 \cdot 2.9^2 \ln \left(\frac{1 + \sqrt{(1 - 0.222^2 \cdot 2.9^2)}}{S + \sqrt{S^2 - 0.222^2 \cdot 2.9^2}} \right) \rightarrow$$

$$S = 0.827$$

An iterative approach is used to determine the value of the S parameter.

Determine spray angle:

$$\tan\left(\frac{\alpha}{2}\right) = \frac{2\mu K}{\sqrt{(1+S)^2 - 4\mu^2 K^2}} = \frac{2 \cdot 0.222 \cdot 2.9}{\sqrt{(1+0.827)^2 - 4 \cdot 0.222^2 \cdot 2.9^2}} = 0.993 \rightarrow \alpha = 89.6[\text{degrees}]$$

Determining SMD

Determine FN parameter:

$$Fn = \frac{G}{\sqrt{\rho_l \Delta P}} = \frac{0.005}{\sqrt{1400 \cdot 2 \cdot 10^5}} = 2.988 \cdot 10^{-7}$$

Determine parameter h_0

$$h_0 = \frac{0.00805 FN \sqrt{\rho_l}}{D_0 \cos 0.5\alpha} = \frac{0.00805 \cdot 2.988 \cdot 10^{-7} \sqrt{1400}}{1.101 \cdot 10^{-3} \cos(0.5 \cdot 89.6)} = 1.152 \cdot 10^{-4} \text{ meter}$$

Determine injector velocity:

$$U_0 = \sqrt{\frac{2\Delta P}{\rho_l}} = \sqrt{\frac{2 \cdot 2 \cdot 10^5}{1400}} = 16.9 \text{ m/s}$$

Convert some parameters to the correct dimensions for the equation of D_l :

$$h_0 = 1.152 \cdot 10^{-4} \text{ meter} = 1.152 \cdot 10^{-2} \text{ cm}$$

$$U_0 = 16.9 \text{ m/s} = 1690 \text{ cm/s}$$

$\sigma = 80 \text{ dyn/cm}$ (is not required to be changed)

dynamic viscosity = 1.249 cp (is not required to be changed)

Determine D_l parameter:

$$D_l = 0.9615 \cos(0.5 \cdot \alpha) \left(\frac{h_0^4 \sigma^2}{u_0^4 \rho_a \rho_l} \right) \left(1 + 2.6 \mu_l \cos(\theta) \left(\frac{h_0^2 \rho_a^4 u_0^7}{72 \rho_l^2 \sigma^5} \right)^{\frac{1}{3}} \right)^{0.2}$$

$$D_l = 0.9615 \cos(0.5 \cdot 89.6) \left(\frac{(1.52 \cdot 10^{-2})^4 \cdot 80^2}{1690^4 \cdot 1.225 \cdot 10^{-3} \cdot 1400 \cdot 10^{-3}} \right)^{\frac{1}{6}} \left(1 + 2.6 \cdot 1.249 \cos(0.5 \cdot 89.6) \left(\frac{(1.152 \cdot 10^{-2})^2 (1.225 \cdot 10^{-3})^4 \cdot 1690^7}{72 \cdot (1400 \cdot 10^{-3})^2 80^5} \right)^{\frac{1}{3}} \right)^{0.2}$$

$$D_l = 3.09 \cdot 10^{-3} \text{ cm} = 3.09 \cdot 10^{-5} \text{ m}$$

Determine SMD:

$$SMD = 1.89 D_l = 1.89 \cdot 3.09 \cdot 10^{-5} = 5.8 \cdot 10^{-5} \text{ meter} = 58 \mu\text{meter}$$

Film thickness

Determine ratio film thickness and outlet radius

$$\frac{\delta}{r_0} = \frac{1 - \sqrt{1 - \mu \cos\left(\frac{\alpha}{2}\right)}}{\cos\left(\frac{\alpha}{2}\right)} = \frac{1 - \sqrt{1 - 0.222 \cos\left(\frac{89.6}{2}\right)}}{\cos\left(\frac{89.6}{2}\right)} = 0.116[-]$$

Film thickness:

$$\delta = \frac{\delta}{r_0} r_0 = 0.116 \cdot 0.5 \cdot 1.101 = 0.064 \text{ mm}$$

A.2. DETAILED CALCULATIONS JET INJECTOR CONFIGURATION 2

In this section the detailed calculation of the required diminutions and the associated theoretical performance of the a jet injector configuration 2 is discussed.

Input parameters:

Density ambient gas: 1.225 kg/m³

Density ethanol: 789.4 kg/m³

Pressure drop: 1.5 Bar

Dynamic viscosity: 1.25 * 10⁻³ Pa s

L_0/d_0 ratio: 5.0 [-]

Kinematic Viscosity: 1.58348 * 10⁻⁶ m/s²

Mass flow: 0.00056779 kg/s

Surface tension: 22 * 10⁻³ n/m

Determining discharge coefficient and outlet diameter

Discharge coefficient:

$$\mu = \frac{58}{1.23 + \frac{4Q}{\pi v \mu d_0}} \rightarrow \frac{58\pi v \mu^2}{4Q} + 1.23\mu - 1 = 0$$
$$\frac{58\pi \cdot 1.583 \cdot 10^{-6} \mu^2}{4 \cdot \frac{0.00056779}{789.4}} + 1.23\mu - 1 = 0 \rightarrow 100.255\mu^2 + 1.23\mu - 1 = 0 \rightarrow \mu_1 = 0.0939 \text{ v } \mu_2 = -0.106$$

So, 2 possible values are found. A negative discharge coefficient is not possible in reality. So, a discharge coefficient of 0.0939 [-] is selected.

outlet diameter:

$$d_0 = \sqrt{\frac{4G}{\mu \pi \sqrt{2\rho \Delta P}}} = \sqrt{\frac{4 \cdot 0.00056779}{0.0939 \cdot \pi \sqrt{2 \cdot 789.4 \cdot 1.5 \cdot 10^5}}} = 7.073 \cdot 10^{-4} = 0.707 \text{ mm}$$

Check assumption previous equation:

$$Re_h = \frac{4Q}{\pi d_0 v \mu} = \frac{4 \cdot \frac{0.00056779}{789.4}}{\pi \cdot 0.707 \cdot 10^{-3} \cdot 1.583 \cdot 10^{-6} \cdot 0.0939} = 8714.3$$

The equation for the discharge coefficient is only valid for Reynolds numbers lower than $1.5 \cdot 10^5$. Since 8714 is smaller than $1.5 \cdot 10^5$, the used method to determine the discharge coefficient is valid.

Determine spray angle

Determine parameter A

$$A = 3 + \frac{LD_0}{3.6} = 3 + \frac{5}{3.6} = 4.389$$

Determine spray angle:

$$\tan\left(\frac{\theta}{2}\right) = \frac{4\pi}{A} \sqrt{\frac{\rho_g \sqrt{3}}{\rho_l}} = \frac{4\pi}{4.389} \sqrt{\frac{1.225 \sqrt{3}}{789.4}} = 0.0325 \rightarrow \theta = 3.73$$

Injection velocity

Injection velocity:

$$U_0 = \sqrt{\frac{2\Delta P}{\rho_l}} = \sqrt{\frac{2 \cdot 1.5 \cdot 10^5}{789.4}} = 19.5 \text{ m/s}$$

Determine SMD

Determine time scale factor:

$$j = \frac{d_0}{8} = \frac{0.707 \cdot 10^{-3}}{8} = 8.8375 \cdot 10^{-5}$$

Determine We_{fj}

$$We_{fj} = \frac{\rho_l U_0^2 j}{\sigma} = \frac{789.4 \cdot (19.5)^2 \cdot 8.8375 \cdot 10^{-5}}{22 \cdot 10^{-3}} = 1205.8$$

Determine SMD:

$$SMD = We_{fj}^{-0.74} 133j = 1205.8^{-0.74} \cdot 133 \cdot 8.8375 \cdot 10^{-5} = 6.17 \cdot 10^{-5} \text{ meter} = 61.6 \text{ micrometer}$$

B.2. INITIAL DESIGN- CONFIGURATION 2

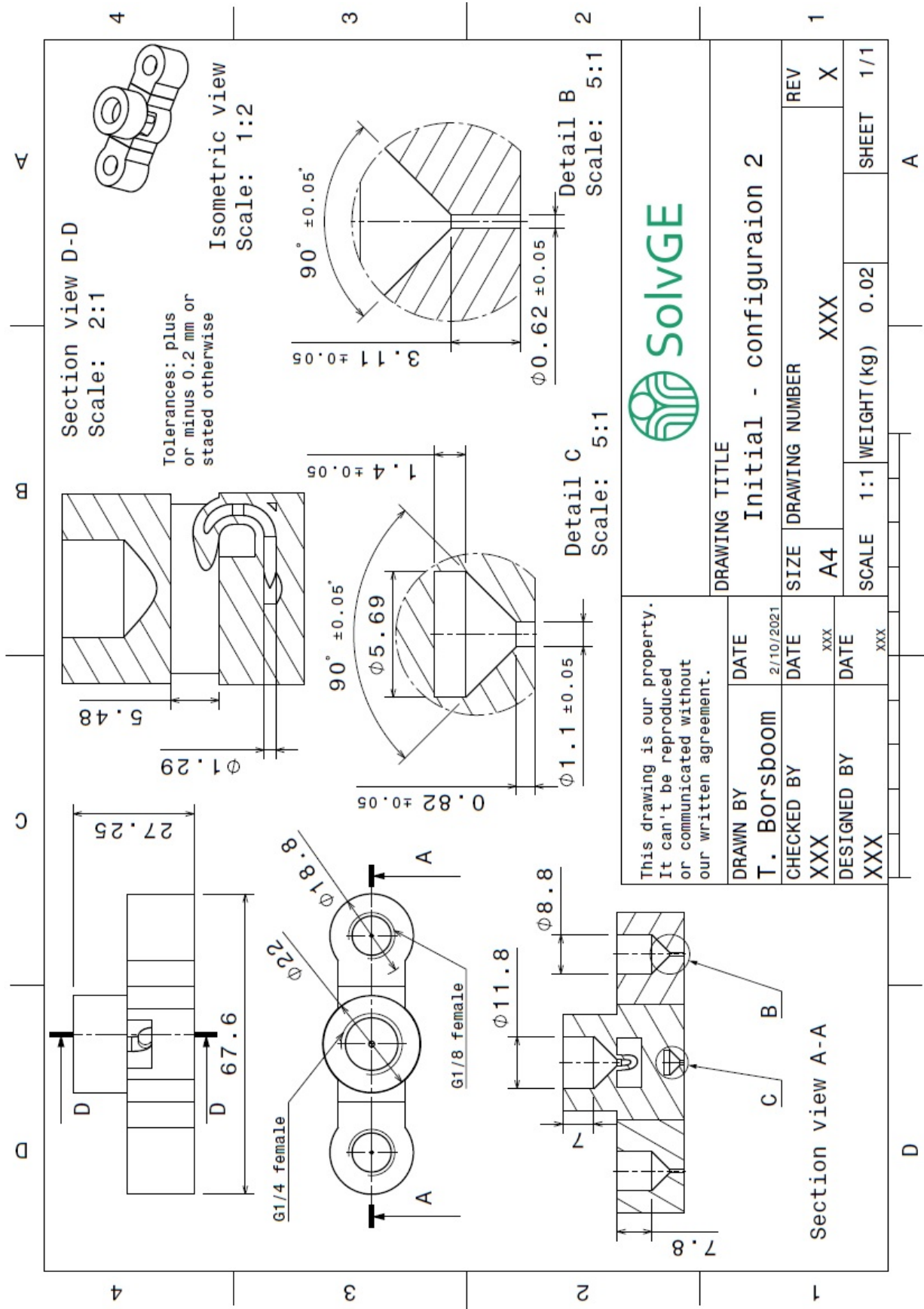


Figure B.2: Technical drawing of configuration 2 of the initial design

B.3. INITIAL DESIGN- CONFIGURATION 3

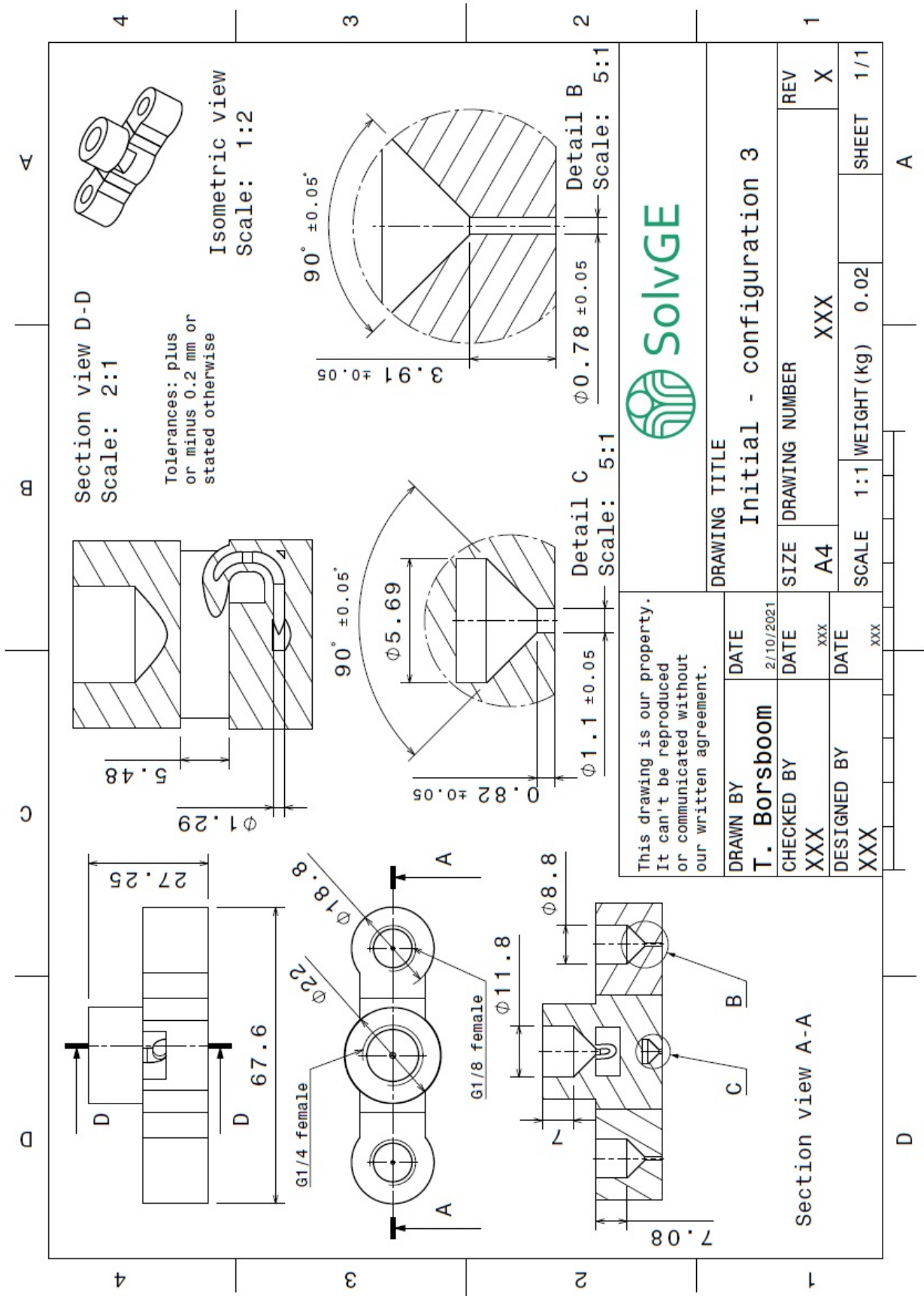


Figure B.3: Technical drawing of configuration 3 of the initial design

B.5. PROTOTYPE DESIGN- CONFIGURATION 1

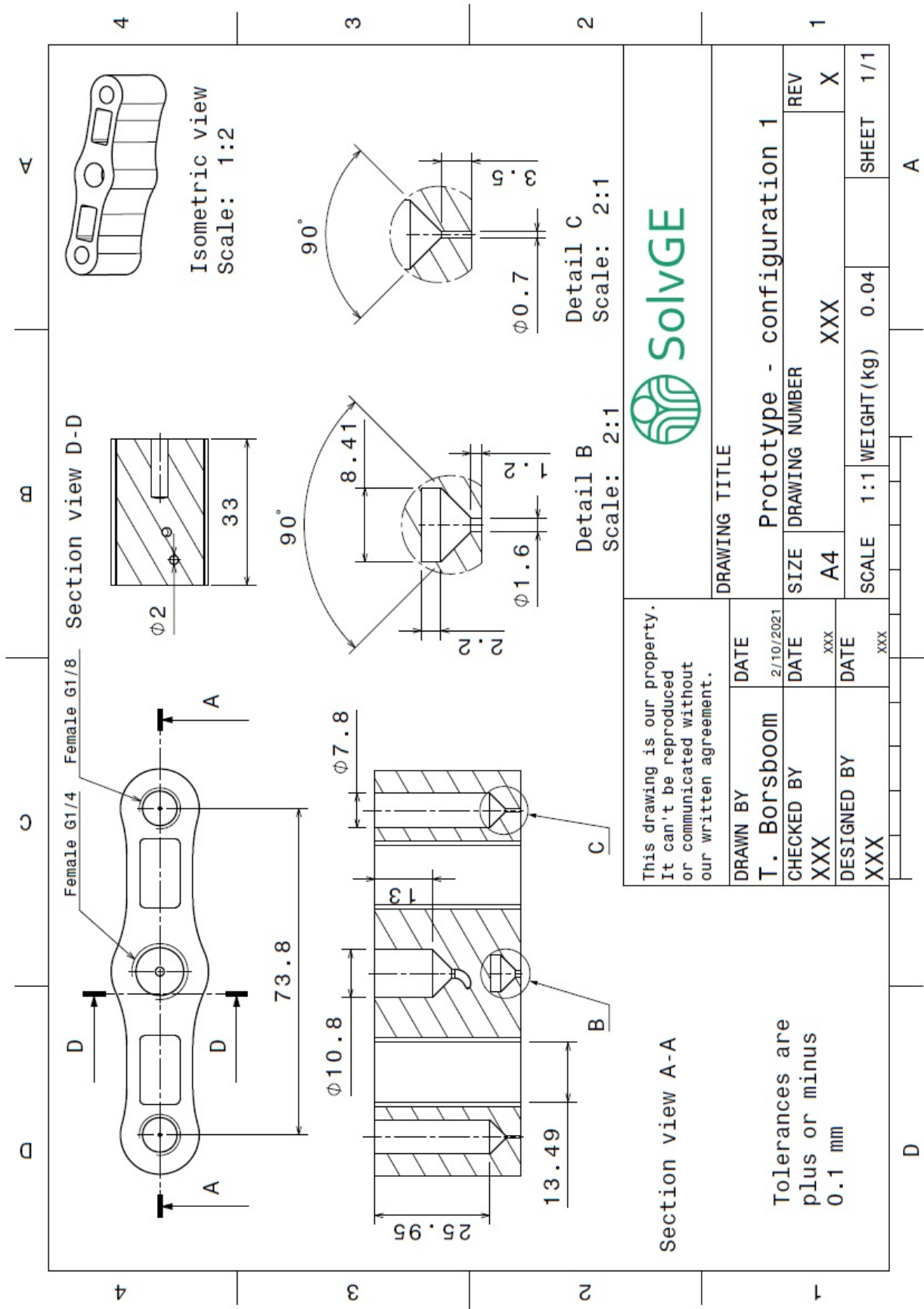


Figure B.5: Technical drawing of configuration 1 of the prototype design

B.6. PROTOTYPE DESIGN- CONFIGURATION 2

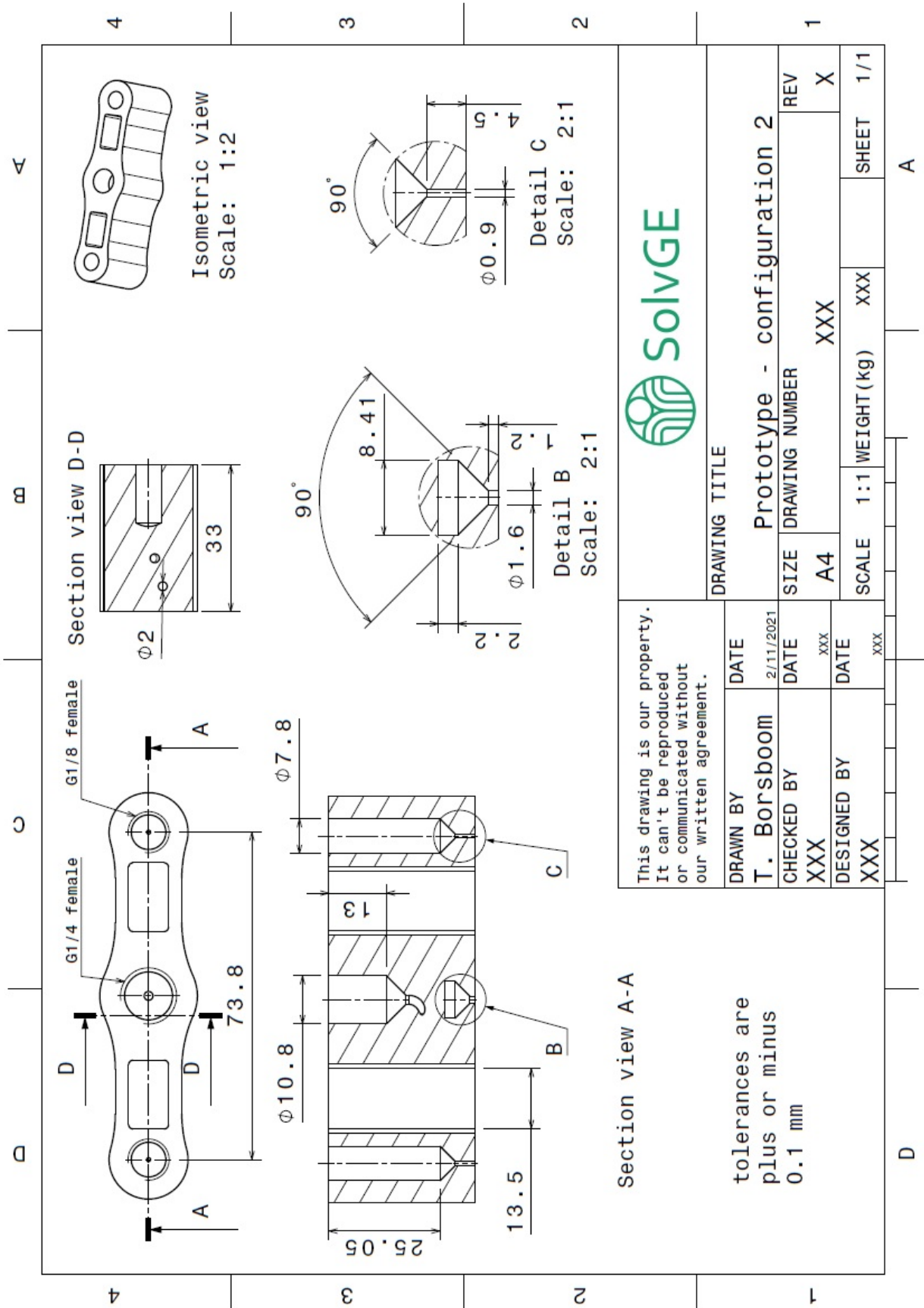


Figure B.6: Technical drawing of configuration 2 of the prototype design

B.7. PROTOTYPE DESIGN- CONFIGURATION 3

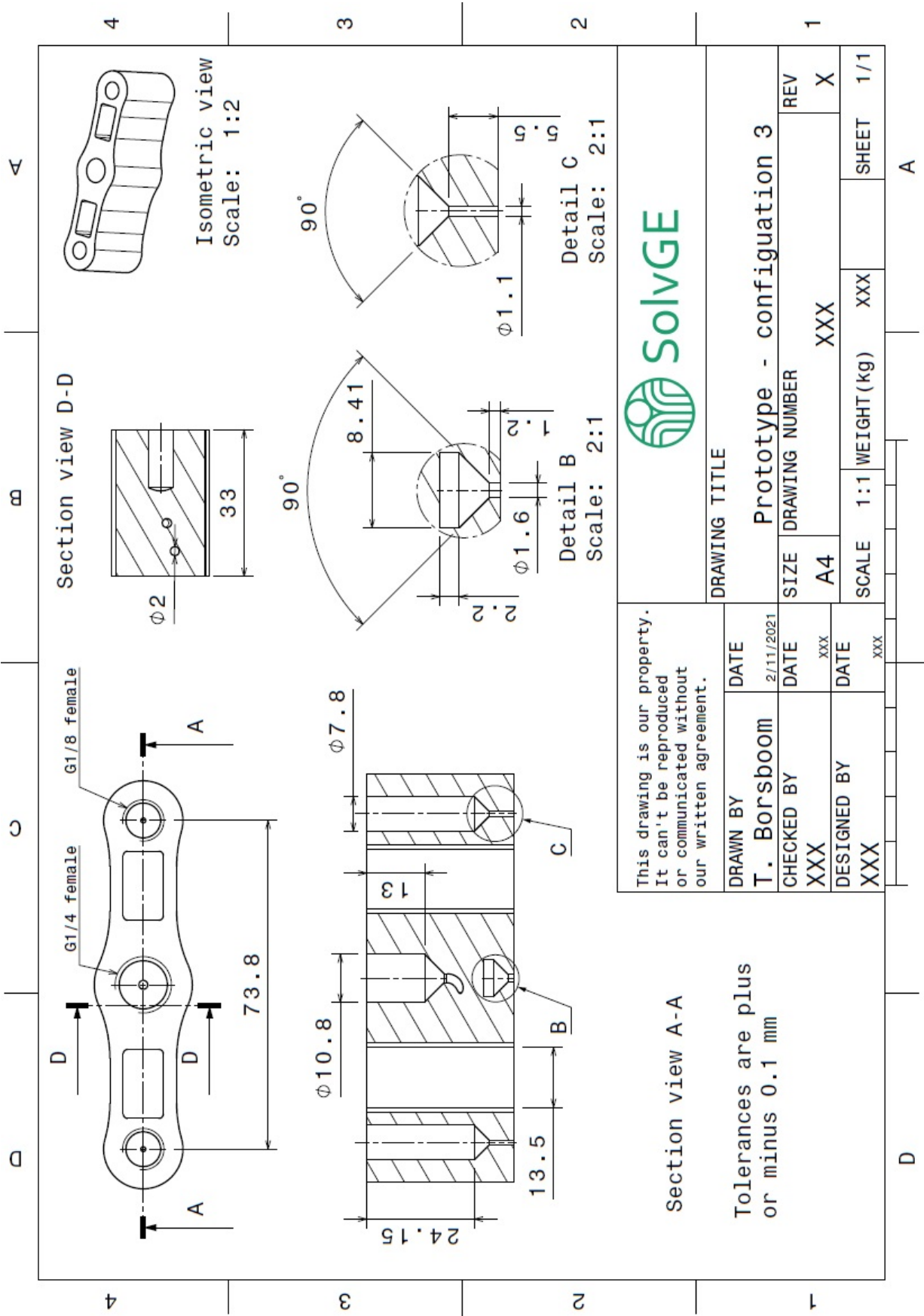


Figure B.7: Technical drawing of configuration 3 of the prototype design

B.8. PROTOTYPE DESIGN- CONFIGURATION 4

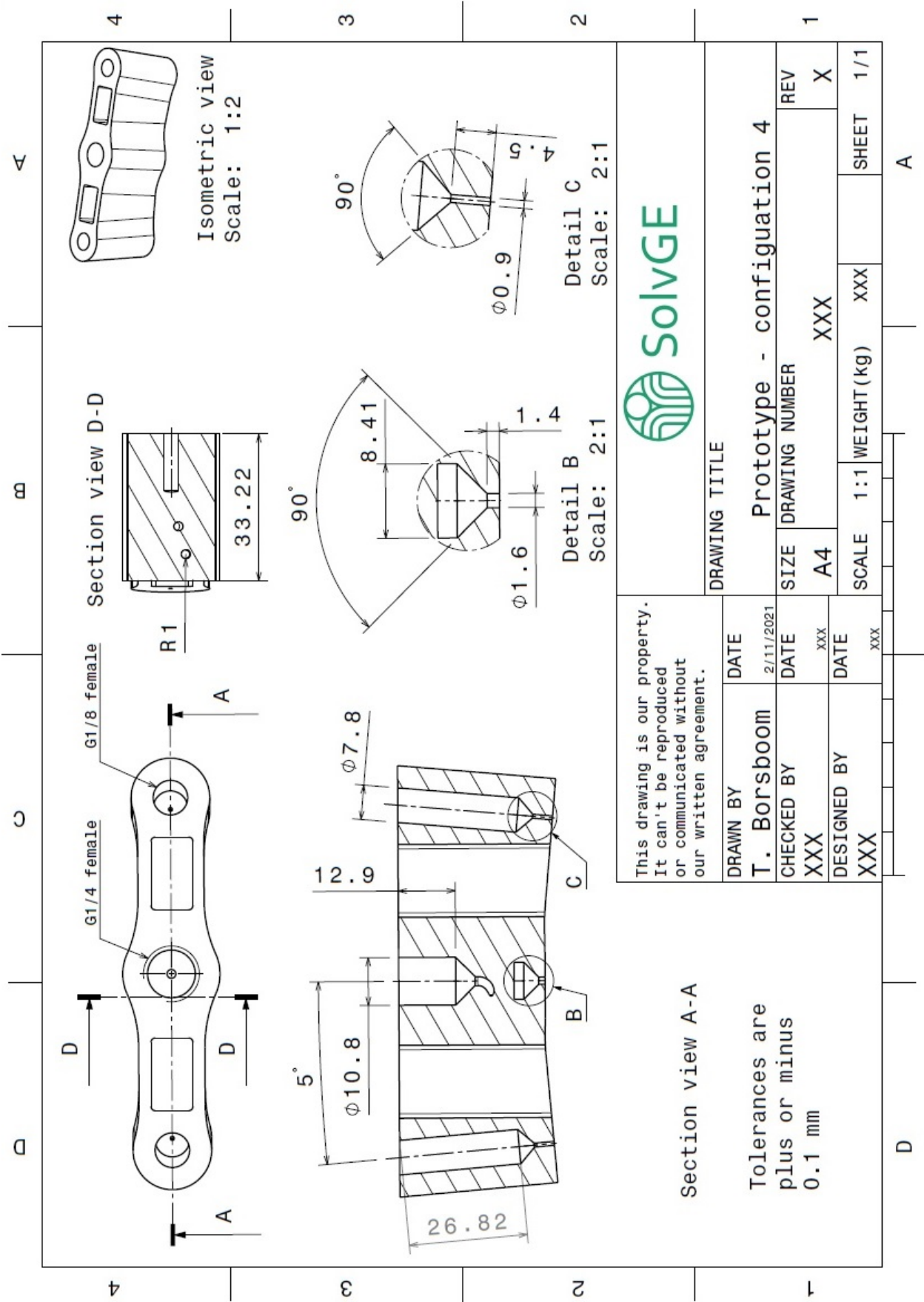


Figure B.8: Technical drawing of configuration 4 of the prototype design

C

PYTHON SCRIPTS

In this section the python scripts that have been used during the design process can be found

C.1. INITIAL DESIGN

C.1.1. SWIRL INJECTOR

In this section the python script is provided to design the swirl injector.

```
"""
Written by T. Borsboom at 02-10-2020
script will determine geometrical and performance parameters for
a pressure simplex swirl injector.
"""
from math import *
import numpy as np

#=====FLUID PROPERTIES=====
"""
WATER:
rho_l=997                                #density
    liquid in kg/m^3
v=1.004*10**-6                            #kinematic
    viscosity in m^2/s
mu_l=1.002                                #dynamic
    viscosity in cp
sigma=72.75                                #
    surface tenstion dyne/cm
"""
rho_l=1400                                #density
    liquid in kg/m^3
v=8.9214*10**-7                            #kinematic
    viscosity in m^2/s
mu_l=1.249                                #dynamic
    viscosity in cp
sigma=80                                    #surface
    tenstion dyne/cm

#=====DESIGN PARAMETERS=====
e= 0.343                                    #efficiency
    of filling [-]
G= 0.005                                    #mass flow
    inkg/s
rho_a=1.225                                #density
    ambient gas (air) kg/m^3
dp=2*10**5                                  #Pressure
    drop in pa
i=1                                         #number in
    inlets[-]
ratio1=4                                    #factor
    between R and r0
```

```

phi=1.05 #ratio of
    viscous and ideal flow
cc=0.875 #
    contraction coefficient
ls_ratio=2.25 #ratio of
    the length of the port and dport1 var

#=====FIRST DESIGN STEP=====
K=((1-e)*sqrt(2))/(e*sqrt(e)) #K factor
print(K)
mu=e*sqrt((e)/(2-e)) #discharge coeficeint mu

d0=sqrt((4*G)/(mu*pi*sqrt(2*rho_l*dp))) #outlet
    diameter in meter
R=ratio1*0.5*d0 #swirl
    radius in meter
dport=sqrt((2*R*d0)/(i*K)) #inlet
    diameter in meter

print(e)
#=====CHECK VISCOSITY=====
B=R/(0.5*dport) #determine
    the B factor
Re=(4*G)/(pi*rho_l*v*sqrt(i)*dport) #determine
    the Reynolds number
labda=10**(25.8/(log10(Re))**2.58-2) #determine
    labda
K_labda=K/(1+(labda/2)*(B**2/i-K))
c2=(2/labda)*(phi**1.5-1) #check 2
c1=(B**2/i-K) #check 1

if c1<c2: #case
    viscosity can be neglected
    condition=1
elif c1>c2: #case
    viscosity has to be taken into account
    condition=2
    K=K_labda #corrected

#=====DETERMINE NEW EPSILON VALUE=====
K_ant=K_labda
e_step=0.000001
K=((1-e)*sqrt(2))/(e**1.5)
error_previous=K_ant-K

run=True
while run==True:
    e=e+e_step
    K=((1-e)*sqrt(2))/(e**1.5)
    error=K-K_ant
    #print(error)
    if abs(error)>abs(error_previous):
        e_step=e_step*-1
    if abs(error)<0.0001:
        run=False
        e_best_guess=e
        error_previous=error

e=e_best_guess
K=K_labda
mu=1/(sqrt(K**2/(1-e)+1/e**2)) #corrected

```

```

        discharge coefficient
d0=sqrt((4*G)/(mu*pi*sqrt(2*rho_l*dp))) #corrected
        outer diameter
R=ratio1*0.5*d0 #corrected
        swirl radius in meter
dport=sqrt((2*R*d0)/(i*K))
        #corrected inlet diameter in meter
print(dport)

#=====DETERMINE S VALUE=====
S=1 #guess
    value S
mu_ant=sqrt(1-mu**2*K**2)-S*sqrt(S**2-mu**2*K**2)-(log((1+sqrt(1-mu**2*K**2))/(S+sqrt(S**2-mu
**2*K**2))))*mu**2*K**2
error_previous=mu-mu_ant
step=0.00001
run=True
while run==True: #iteration
    S=S+step
    mu_ant=sqrt(1-mu**2*K**2)-S*sqrt(S**2-mu**2*K**2)-(log((1+sqrt(1-mu**2*K**2))/(S+sqrt(S
**2-mu**2*K**2))))*mu**2*K**2
    error=mu-mu_ant
    if abs(error)>abs(error_previous):
        step=step*-1
    if abs(error)<0.00001:
        run=False
        S_best_guess=S
        error_previous=error

#=====DESIGN STEP 2=====
alpha=2*np.rad2deg(atan((2*mu*K)/(sqrt((1+S_best_guess)**2-4*mu**2*K**2)))) #spray
        angle in degrees
ds=R*2+dport #diameter
        swirl chamber in meter
dport1=dport/sqrt(cc) #define parameter dport'
print("dport", dport)
ls=ls_ratio*dport1 #length of
        inlet in meters
if K_labda<4.5: #if
    K_labda<4.5 a ratio of 0.75 is used
    l=0.75*d0 #length of
        outlet in meter
elif K_labda>4.5: #if
    K_labda>4.5 a ratio of 0.375 is used
    l=0.375*d0 #length of
        outlet in meter

#=====DETERMINE SMD=====
theta=np.deg2rad(0.5*alpha) #determine
        half angel in rad
Fn=G/sqrt(rho_l*dp) #Determine
        Fn parameter
h0=(0.00805*Fn*sqrt(rho_l))/(d0*cos(theta)) #Determine
        h0 parameter in meter
U0=sqrt((2*dp)/rho_l) #determine
        injection velocity
print("h0",h0)
#convert to different units->
U0=U0*100 #from
        meter to cm

```

```

h0=h0*100 #from
    meter to cm
rho_l=rho_l*10**-3 #from kg/m
    ^3 to g/cm^3
rho_a=rho_a*10**-3 #from kg/m
    ^3 to g/cm^3
DI=((h0**4*sigma**2)/(U0**4*rho_l*rho_a))*(1/6)*cos(theta)*0.9615)*(((h0**2*rho_a**4*U0**7)
/(72*rho_l**2*sigma**5))*(1/3)*cos(theta)*2.6*mu_l+1)**0.2)

print("DI",DI)

DI=DI/100 #to meter
SMD=1.89*DI #SMD in
    meter

#convert back to si units->
U0=U0/100 #from cm
    to meter
h0=h0/100 #from cm
    to meter
rho_l=rho_l*10**3 #from g/cm
    ^3 to kg/m^3
rho_a=rho_a*10**3 #from g/cm
    ^3 to kg/m^3

#DETERMINE LIQUID SHEET THICKNESS=
ratio_t_r0=(1-sqrt(1-mu*cos(np.deg2rad(alpha*0.5))))/(cos(np.deg2rad(alpha*0.5))) #determine
    ratio thickness and r0
Delta=ratio_t_r0*0.5*d0 #determine
    sheet thickness in meter

print(ratio_t_r0)

#=====PRINT RESULTS=====
print("===_Data_DESIGN_SWIRL_INJECTOR_===");
print("value_filling_factor:_",round(e,3), "[-]");
print("used_pressure_drop:_",round(dp*10**-5,4), "[bar]");
print("value_K_factor:_", round(K,4), "[-]");
print("value_discharge_coeficient:_",round(mu,4), "[-]");
if condition==1:
    print("Viscosity_can_be_neglegted")
elif condition==2:
    print("Viscosity_has_to_be_taking_into_account")
print("outlet_diameter:",round(d0*1000,4), "[mm]");
print("length_of_the_outlet:_",round(l*1000,4), "[mm]");
print("number_of_inlets:",i, "[-]");
print("inlet_diameter:",round(dport*1000,4), "[mm]");
print("length_of_the_inlet:_",round(ls*1000,4), "[mm]");
print("swirl_chamber_diameter:_",round(ds*1000,4), "[mm]");
print("spray_angle:",round(alpha,4), "[degrees]");
print("value_of_SMD:_",round(SMD*10**6,4), "[micrometer]");
print("thickness_of_the_atomized_sheet", round(Delta*1000,4), "[mm]");
print("injection_velocity:_",round(U0,4), "[m/s]");

```

C.1.2. JET INJECTOR

The pythonscript that has been used to determine the dimensions and theoretical performance of the jet injector is given below:

```

from math import *
import numpy as np
import matplotlib.pyplot as plt
#====FLOW PROPERTIES=====
rho_l=789.4 #kg/m^3
v=1.58348*10**-6 #m^2/s
mu_l=1.25*10**-3 #Pa s
sigma=22*10**-3 #n/m

#====DESIGN PARAMETERS=====
G=0.00056779 #kg/s
dP=1.5*10**5 #Pa
#mu=0.3247
mu_g=18.13*10**-6 #kg/m^3 ambient
rho_a=1.225
l_d0_ratio=5 #length over d0 ratio

dt=0.001 #time step
t=0.001 #start time
Ta=293 #ambient temp

#==DETERMINE DISCHARGE COEFFICIENT==
Q=G/rho_l
a=(58*pi*v)/(4*Q)
b=1.23
c=-1

D=sqrt(b**2-4*a*c)
cd_1=(-b+D)/(2*a)
cd_2=(-b-D)/(2*a)
if cd_1>0:
    cd_sel=cd_1
elif cd_2>0:
    cd_sel=cd_1
else:
    message="help!"

#====FUTURE DESIGN STEPS=====
d0=sqrt((4*G)/(cd_sel*pi*sqrt(rho_l*2*dP))) #outer diameter
A=3.0+l_d0_ratio/3.6 #coefficient for spray angle
theta=2*np.rad2deg(atan((4*pi)/A*sqrt(rho_a/rho_l)*sqrt(3)/6)) #spray angle
l_nozzle=d0*l_d0_ratio #length nozzle
j=d0/8 #length scale
U_l=sqrt(2*dP/rho_l)
We_fj=(rho_l*U_l**2*j)/sigma
print(We_fj)
SMD=We_fj**-0.74*133*j
#====check assumptions=====
Re_h=(4*Q)/(pi*d0*v*cd_sel)
print(Re_h)
if Re_h<(1.5*10**5):
    message1="The_assumptions_for_the_discharge_coefficients_equations_are_valid_"
else:
    message1="Error_1:_computed_discharge_coefficient_is_not_valid"

Re=(U_l*d0)/v
if Re>3500:
    message2="the_assmption_for_the_time_scale_is_valid"
else:

```

```

    messag2="Error_2:_time_scale_computation_is_invalid"
#=====SHOW RESULTS=====
print("===_DESIGN_DATA_JET_ATOMIZER===")
print("mathically_options_of_the_discharge\ncoefficient:", round(cd_1,4), "and", round(cd_2,4)
)
print("selected_discharge_coefficient:", round(cd_sel,4), "[--]")
print("Pressure_drop", dP*10**(-5), "bar")
print("outlet_diameter", round(d0*1000,4), "[mm]")
print("outlet_length", round(l_nozzle*1000,4), "[mm]")
print("Injection_velocity", round(U_1,3), "[m/s]")
print("spray_angle", round(theta,2), "[deg]")
print("SMD", round(SMD*10**6,4), "[micrometer]")
print(message1)
print(message2)

#=====SPRAY PENETRATION=====
S_list=[]
t_list=[]
while t<0.2:
    S=3.01*(sqrt(dP/rho_a)*d0*t)**0.5*(295/Ta)**0.25
    S_list.append(S*1000)
    t_list.append(t*1000)
    t=t+dt

plt.plot(t_list, S_list)
plt.ylabel('spray_penetration_[mm]')
plt.xlabel('time_[msec]')
#plt.show()

```

C.2. DESIGN GRAPHS

Two graphs are made to aid the design process. These python scripts are provided in this section.

C.2.1. MASSFLOW, SMD AND PRESSURE DROP

A python script is used to make a graph where the SMD and outlet length is given as a function of the pressure drop and mass flow. This python code is given below:

```

"""
Written by T. Borsboom at 08-10-2020
script will show the SMD and diamter orrifice
for different delta pressure and mass flows for
a pressure simplex swirl injector.
"""
from math import *
import numpy as np
import matplotlib.pyplot as plt
G_list=[0.0001,0.001,0.01,0.1]
dp_list=[]
SMD_list_0=[]
d0_list_0=[]
SMD_list_1=[]
d0_list_1=[]
SMD_list_2=[]
d0_list_2=[]
SMD_list_3=[]
d0_list_3=[]

for j in range(0,4,1):
    for loop is used to vary the mass flow
#

```

```

G=G_list[j]
print("Start_calculations_for_mass_flow_of",G_list[j],"kg/s")
dp=0.1*10**5 #
    Starting pressure drop
deltadp=0.1*10**5; #
    Step in pressure drop
while dp<10.1*10**5: #
    while loop is used to vary the delta p
    print(dp)
    #=====FLUID PROPERTIES=====
    rho_l=1400 #
        density liquid in kg/m^3
    v=8.9214*10**-7 #
        kinematic viscosity in m^2/s
    mu_l=1.249 #
        dynamic viscosity in cp
    sigma=80 #
        surface tenstion dyne/cm

    #=====DESIGN PARAMETERS=====
    e= 0.5 #
        efficiency of filling [-]
        #mass
        flow inkg/s
    rho_a=1.225 #
        density ambient gas (air) kg/m^3
        #Pressure
    drop in pa
    i=1 #
        number in inlets[-]
    ratio1=4 #
        factor between R and r0
    phi=1.05 #
        ratio of viscous and ideal flow
    cc=0.875 #
        contraction coefficient
    ls_ratio=2.25 #
        ratio of the length of the port and dport1 var

    #=====FIRST DESIGN STEP=====
    K=((1-e)*sqrt(2))/(e*sqrt(e)) #K
        factor
    mu=e*sqrt((e)/(2-e)) #
        discharge coeficeint mu
    d0=sqrt((4*G)/(mu*pi*sqrt(2*rho_l*dp))) #
        outlet diameter in meter
    R=ratio1*0.5*d0 #
        swirl radius in meter
    dport=sqrt((2*R*d0)/(i*K)) #
        inlet diameter in meter

    #=====CHECK VISCOSITY=====
    B=R/(0.5*dport) #
        determine the B factor
    Re=(4*G)/(pi*rho_l*v*sqrt(i)*dport) #
        determine the Reynolds number
    labda=10**(25.8/(log10(Re))**2.58-2) #
        determine labda
    K_labda=K/(1+(labda/2)*(B**2/i-K))
    c2=(2/labda)*(phi**1.5-1) #

```

```

    check 2
c1=(B**2/i-K) #
    check 1
if c1<c2: #
    case viscosity can be neglected
    condition=1
elif c1>c2: #
    case viscosity has to be taken into account
    condition=2

K=K_labda #
    corrected

#=====DETERMINE NEW EPSILON VALUE=====
K_ant=K_labda
e_step=0.000001
K=((1-e)*sqrt(2))/(e**1.5)
error_previous=K_ant-K

run=True
while run==True:
    e=e+e_step
    K=((1-e)*sqrt(2))/(e**1.5)
    error=K-K_ant
    #print(error)
    if abs(error)>abs(error_previous):
        e_step=e_step*-1
    if abs(error)<0.001:
        run=False
        e_best_guess=e
        error_previous=error

e=e_best_guess
K=K_labda #
    corrected K
mu=1/(sqrt(K**2/(1-e)+1/e**2)) #
    corrected discharge coefficient
d0=sqrt((4*G)/(mu*pi*sqrt(2*rho_l*dp))) #
    corrected outer diameter
R=ratio1*0.5*d0 #
    corrected swirl radius in meter
dport=sqrt((2*R*d0)/(i*K)) #
    corrected inlet diameter in meter

#=====DETERMINE S VALUE=====
S=1 #
    guess value S
mu_ant=sqrt(1-mu**2*K**2)-S*sqrt(S**2-mu**2*K**2)-(log((1+sqrt(1-mu**2*K**2))/(S+sqrt(S**2-mu**2*K**2))))*mu**2*K**2
error_previous=mu-mu_ant
step=0.00001
run=True
while run==True: #
    iteration
    S=S+step
    mu_ant=sqrt(1-mu**2*K**2)-S*sqrt(S**2-mu**2*K**2)-(log((1+sqrt(1-mu**2*K**2))/(S+sqrt(S**2-mu**2*K**2))))*mu**2*K**2
    error=mu-mu_ant
    if abs(error)>abs(error_previous):
        step=step*-1
    if abs(error)<0.00001:

```

```

run=False
S_best_guess=S
error_previous=error

#=====DESIGN STEP 2=====
alpha=2*np.rad2deg(atan(((2*mu*K)/(sqrt((1+S_best_guess)**2-4*mu**2*K**2)))))) #
    spray angle in degrees
ds=R*2+dport #
    diameter swirl chamber in meter
dport1=dport/sqrt(cc) #
    define parameter dport'
ls=ls_ratio*dport1 #
    length of inlet in meters
if K_labda<4.5: #
    if K_labda<4.5 a ratio of 0.75 is used
    l=0.75*d0 #
        lenght of outlet in meter
elif K_labda>4.5: #
    if K_labda>4.5 a ratio of 0.375 is used
    l=0.375*d0 #
        length of outlet in meter

#=====DETERMINE SMD=====
theta=np.deg2rad(0.5*alpha) #
    determine half angel in rad
Fn=G/sqrt(rho_l*dp) #
    Determine Fn parameter
h0=(0.00805*Fn*sqrt(rho_l))/(d0*cos(theta)) #
    Determine h0 parameter in meter
U0=sqrt((2*dp)/rho_l) #
    determine injection velocity
#convert to different units->
U0=U0*100 #
    from meter to cm
h0=h0*100 #
    from meter to cm
rho_l=rho_l*10**-3 #
    from kg/m^3 to g/cm^3
rho_a=rho_a*10**-3 #
    from kg/m^3 to g/cm^3
Dl=((h0**4*sigma**2)/(U0**4*rho_l*rho_a)**(1/6)*cos(theta)*0.9615)*(((h0**2*rho_a
**4*U0**7)/(72*rho_l**2*sigma**5))**(1/3)*cos(theta)*2.6*mu_l+1)**0.2)
Dl=Dl/100 #
    to meter
SMD=1.89*Dl #
    SMD in meter
#convert back to si units->
U0=U0/100 #
    from cm to meter
h0=h0/100 #
    from cm to meter
rho_l=rho_l*10**3 #
    from g/cm^3 to kg/m^3
rho_a=rho_a*10**3 #
    from g/cm^3 to kg/m^3

#=DETERMINE LIQUID SHEET THICKNESS=
ratio_t_r0=(1-sqrt(1-mu*cos(np.deg2rad(alpha*0.5))))/(cos(np.deg2rad(alpha*0.5))) #
    determine ratio thickness and r0
Delta=ratio_t_r0*0.5*d0 #
    determine sheet thickness in meter

```

```

#=====STORING INFORMATION=====

if j==0:
    for j=0 condition
        SMD_list_0.append(SMD*10**6)
        d0_list_0.append(d0*1000)
        dp_list.append(dp*10**-5)
elif j==1:
    for j=1 condition
        SMD_list_1.append(SMD*10**6)
        d0_list_1.append(d0*1000)
elif j==2:
    for j=2 condition
        SMD_list_2.append(SMD*10**6)
        d0_list_2.append(d0*1000)
elif j==3:
    for j=3 condition
        SMD_list_3.append(SMD*10**6)
        d0_list_3.append(d0*1000)

dp=dp+deltadp
#=====GENERATING LABELS=====
print("Start_showing_graphs")
label0="mass_flow: ", G_list[0], "kg/s"
label1="mass_flow: ", G_list[1], "kg/s"
label2="mass_flow: ", G_list[2], "kg/s"
label3="mass_flow: ", G_list[3], "kg/s"

label0=str(list(label0))
label1=str(list(label1))
label2=str(list(label2))
label3=str(list(label3))

#=====PLOTTING THE INFO=====
plt.subplot(211)
plt.plot(dp_list, SMD_list_0, label=label0)
plt.plot(dp_list, SMD_list_1, label=label1)
plt.plot(dp_list, SMD_list_2, label=label2)
plt.plot(dp_list, SMD_list_3, label=label3)
plt.legend(loc='upper_right')
plt.ylabel('SMD_[micrometer]')
plt.xlabel('Delta_pressure_[bar]')
plt.grid()

plt.subplot(212)
plt.plot(dp_list, d0_list_0, label=label0)
plt.plot(dp_list, d0_list_1, label=label1)
plt.plot(dp_list, d0_list_2, label=label2)
plt.plot(dp_list, d0_list_3, label=label3)
plt.legend(loc='upper_right')
plt.ylabel('outlet_diameter_[mm]')
plt.xlabel('Delta_pressure_[bar]')
plt.grid()
plt.show()

```

C.2.2. SPRAY ANGLE AS FUNCTION OF FILLING FACTOR

A graph is made that to explore how the filling factor influences the spray angle

"""

```

Written by T. Borsboom at 02-10-2020
script will determine geometrical and performance parameters for
a pressure simplex swirl injector.
"""
from math import *
import numpy as np
import matplotlib.pyplot as plt

ratio1_list=[]
theta_list=[]
#=====FLUID PROPERTIES=====
rho_l=1400 #density
    liquid in kg/m^3
v=8.9214*10**-7 #kinematic
    viscosity in m^2/s
mu_l=1.249 #dynamic
    viscosity in cp
sigma=80 #surface
    tenstion dyne/cm
ratio1=1
ratio1_step=0.1
while ratio1 < 10.0:
    print(ratio1)
    #=====DESIGN PARAMETERS=====
    #efficiency of
        filling [-]
e=0.244
G=0.005 #mass
    flow inkg/s
rho_a=1.225 #
    density ambient gas (air) kg/m^3
dp=2*10**5 #
    Pressure drop in pa
i=1 #
    number in inlets[-]
#ratio1=4 #
    factor between R and r0
phi=1.05 #ratio
    of viscous and ideal flow
cc=0.875 #
    contraction coeficient
ls_ratio=2.25 #ratio
    of the length of the port and dport1 var

#=====FIRST DESIGN STEP=====
K=((1-e)*sqrt(2))/(e*sqrt(e)) #K
    factor
mu=e*sqrt((e)/(2-e)) #
    discharge coeficient mu
d0=sqrt((4*G)/(mu*pi*sqrt(2*rho_l*dp))) #
    outlet diameter in meter
R=ratio1*0.5*d0 #swirl
    radius in meter
dport=sqrt((2*R*d0)/(i*K)) #inlet
    diameter in meter

#=====CHECK VISCOSITY=====
B=R/(0.5*dport) #
    determine the B factor
Re=(4*G)/(pi*rho_l*v*sqrt(i)*dport) #

```

```

    determine the Reynolds number
labda=10**(25.8/(log10(Re))**2.58-2) #
    determine labda
K_labda=K/(1+(labda/2)*(B**2/i-K))
c2=(2/labda)*(phi**1.5-1) #check
    2
c1=(B**2/i-K) #check
    1
if c1<c2: #case
    viscosity can be neglected
    condition=1
elif c1>c2: #case
    viscosity has to be taken into account
    condition=2
    K=K_labda #
        corrected K
#=====DETERMINE NEW EPSILON VALUE=====
K_ant=((1-e)*sqrt(2))/(e*sqrt(e))
error_previous=K-K_ant
step=0.00001
run=True

while run==True:
    e=e+step
    K_ant=((1-e)*sqrt(2))/(e*sqrt(e))
    error=K-K_ant
    #print(error)
    if abs(error)>abs(error_previous):
        step=step*-1
    if abs(error)<0.001:
        run=False
        e_best_guess=e
        error_previous=error
    e=e_best_guess
    mu=1/(sqrt(K**2/(1-e)+1/e**2)) #
        corrected discharge coefficient
    d0=sqrt((4*G)/(mu*pi*sqrt(2*rho_l*dp))) #
        corrected outer diameter
    R=ratio1*0.5*d0 #
        corrected swirl radius in meter
    dport=sqrt((2*R*d0)/(i*K)) #
        corrected inlet diameter in meter

#=====DETERMINE S VALUE=====
S=1 #guess
    value S
mu_ant=sqrt(1-mu**2*K**2)-S*sqrt(S**2-mu**2*K**2)-(log((1+sqrt(1-mu**2*K**2))/(S+sqrt(S
**2-mu**2*K**2))))*mu**2*K**2
error_previous=mu-mu_ant
step=0.00001
run=True
while run==True: #
    iteration
    S=S+step
    mu_ant=sqrt(1-mu**2*K**2)-S*sqrt(S**2-mu**2*K**2)-(log((1+sqrt(1-mu**2*K**2))/(S+sqrt(S
**2-mu**2*K**2))))*mu**2*K**2
    error=mu-mu_ant
    if abs(error)>abs(error_previous):
        step=step*-1
    if abs(error)<0.00001:
        run=False

```

```

        S_best_guess=S
        error_previous=error

#=====DESIGN STEP 2=====
alpha=2*np.rad2deg(atan((2*mu*K)/(sqrt((1+S_best_guess)**2-4*mu**2*K**2)))) #spray
    angle in degrees
ds=R*2+dport #
    diameter swirl chamber in meter
dport1=dport/sqrt(cc) #
    define parameter 'dport'
ls=ls_ratio*dport1 #
    length of inlet in meters
if K_labda<4.5: #if
    K_labda<4.5 a ratio of 0.75 is used
    l=0.75*d0 #
        length of outlet in meter
elif K_labda>4.5: #if
    K_labda>4.5 a ratio of 0.375 is used
    l=0.375*d0 #
        length of outlet in meter

#=====DETERMINE SMD=====
theta=np.deg2rad(0.5*alpha) #
    determine half angle in rad
Fn=G/sqrt(rho_l*dp) #
    Determine Fn parameter
h0=(0.00805*Fn*sqrt(rho_l))/(d0*cos(theta)) #
    Determine h0 parameter in meter
U0=sqrt((2*dp)/rho_l) #
    determine injection velocity
#convert to different units->
U0=U0*100 #from
    meter to cm
h0=h0*100 #from
    meter to cm
rho_l=rho_l*10**-3 #from
    kg/m^3 to g/cm^3
rho_a=rho_a*10**-3 #from
    kg/m^3 to g/cm^3
Dl=((((h0**4*sigma**2)/(U0**4*rho_l*rho_a))**(1/6)*cos(theta)*0.9615)*(((h0**2*rho_a**4*U0
**7)/(72*rho_l**2*sigma**5))**(1/3)*cos(theta)*2.6*mu_l+1)**0.2)
Dl=Dl/100 #to
    meter
SMD=1.89*Dl #SMD
    in meter
#convert back to si units->
U0=U0/100 #from
    cm to meter
h0=h0/100 #from
    cm to meter
rho_l=rho_l*10**3 #from
    g/cm^3 to kg/m^3
rho_a=rho_a*10**3 #from
    g/cm^3 to kg/m^3

#DETERMINE LIQUID SHEET THICKNESS=
ratio_t_r0=(1-sqrt(1-mu*cos(np.deg2rad(alpha*0.5))))/(cos(np.deg2rad(alpha*0.5))) #
    determine ratio thickness and r0
Delta=ratio_t_r0*0.5*d0 #determine sheet thickness in meter

ratio1_list.append(ratio1)

```

```

theta_list.append(alpha)
ratio1=ratio1+ratio1_step

plt.plot(ratio1_list , theta_list)
plt.xlabel('filling_facvort_[-]')
plt.ylabel('spray_angle_[deg]')
plt.show()

```

C.3. TOLERANCES ANALYSES

In this section the python scripts are provided that is used to analyse the effect of relaxing the tolerances.

C.3.1. TOLERANCES SWIRL INJECTOR

```

from math import *
import numpy as np
"""
d0=1.7*10**(-3)
dp=2.1*10**(-3)
ds=8.51*10**(-3)
"""
d0=1.1*10**(-3)
dp=1.3908*10**(-3)
ds=5.6871*10**(-3)

i=1
e=0.472
G=0.005
R=(ds-dp)/2
ratio1=R/(0.5*d0)
#R=ratio1*0.5*d0
K=(2*R*d0)/(i*dp**2)
K_labda=4.625292339497171

cc=0.875
rho_a=1.225
rho_l=1400
v=8.9214*10**-7 #kinematic
    viscosity in m^2/s
mu_l=1.249 #dynamic
    viscosity in cp
sigma=80
phi=1.05
ls_ratio=2.25

#=====DETERMINE NEW EPSILON VALUE=====
K_ant=K
e_step=0.000001
K=((1-e)*sqrt(2))/(e**1.5)
error_previous=K_ant-K

run=True
while run==True:
    e=e+e_step
    K=((1-e)*sqrt(2))/(e**1.5)
    error=K-K_ant
    #print(error)
    if abs(error)>abs(error_previous):
        e_step=e_step*-1
    if abs(error)<0.0001:

```

```

run=False
e_best_guess=e
error_previous=error
e=e_best_guess
mu=e*sqrt((e)/(2-e))
Pressure_drop=((4*G)/(d0**2*mu*pi))**2/(2*rho_l)

#=====DETERMINE S VALUE=====
S=1 #guess
value S
mu_ant=sqrt(1-mu**2*K**2)-S*sqrt(S**2-mu**2*K**2)-(log((1+sqrt(1-mu**2*K**2))/(S+sqrt(S**2-mu
**2*K**2))))*mu**2*K**2
error_previous=mu-mu_ant
step=0.00001
run=True
while run==True: #iteration
    S=S+step
    mu_ant=sqrt(1-mu**2*K**2)-S*sqrt(S**2-mu**2*K**2)-(log((1+sqrt(1-mu**2*K**2))/(S+sqrt(S
**2-mu**2*K**2))))*mu**2*K**2
    error=mu-mu_ant
    if abs(error)>abs(error_previous):
        step=step*-1
    if abs(error)<0.00001:
        run=False
        S_best_guess=S
        error_previous=error

alpha=2*np.rad2deg(atan((2*mu*K)/(sqrt((1+S_best_guess)**2-4*mu**2*K**2)))) #spray
angle in degrees
#ds=R*2+dp #diameter
swirl chamber in meter
dport1=dp/sqrt(cc) #define
parameter dport'
ls=ls_ratio*dport1 #length of
inlet in meters
if K<4.5: #if K_labda<4.5
    a ratio of 0.75 is used
    l=0.75*d0 #length of
    outlet in meter
elif K>4.5: #if K_labda>4.5
    a ratio of 0.375 is used
    l=0.375*d0
#ds=R*2+dp
#=====DETERMINE SMD=====
theta=np.deg2rad(0.5*alpha) #determine
half angel in rad
Fn=G/sqrt(rho_l*Pressure_drop) #Determine Fn parameter
h0=(0.00805*Fn*sqrt(rho_l))/(d0*cos(theta)) #Determine
h0 parameter in meter
U0=sqrt((2*Pressure_drop)/rho_l) #determine injection
velocity
#convert to different units->
U0=U0*100 #from
meter to cm
h0=h0*100 #from
meter to cm
rho_l=rho_l*10**3 #from kg/m
^3 to g/cm^3

```

```

rho_a=rho_a*10**-3 #from kg/m
    ^3 to g/cm^3
DI=((h0**4*sigma**2)/(U0**4*rho_l*rho_a)**(1/6)*cos(theta)*0.9615)*(((h0**2*rho_a**4*U0**7)
/(72*rho_l**2*sigma**5))**(1/3)*cos(theta)*2.6*mu_l+1)**0.2)
DI=DI/100 #to meter
SMD=1.89*DI #SMD in
    meter
#convert back to si units->
U0=U0/100 #from cm
    to meter
h0=h0/100 #from cm
    to meter
rho_l=rho_l*10**3 #from g/cm
    ^3 to kg/m^3
rho_a=rho_a*10**3 #from g/cm
    ^3 to kg/m^3

#=DETERMINE LIQUID SHEET THICKNESS=
ratio_t_r0=(1-sqrt(1-mu*cos(np.deg2rad(alpha*0.5))))/(cos(np.deg2rad(alpha*0.5))) #determine
    ratio thickness and r0
Delta=ratio_t_r0*0.5*d0
print("For_the_following_dimensions->")
print("outlet_diameter",d0*1000,"mm")
print("swirl_chamber",ds*1000,"mm")
print("inlet_port_diameter",dp*1000,"mm")

print("====_Results_====")
print("Discharge_coefficient",mu,"[-]")
print("value_K_factor",K,"[-]")
print("Pressure_drop",Pressure_drop/100000,"Bar")
print("SMD:_",SMD*10**(6), "micrometer")
print("spray_angle:_",alpha, "degrees")
print("Injection_velocity:_",U0, "m/s")
print("Sheet_thickness:_",Delta*1000, "mm")
print("Ratio_swirl_radius_and_r0:",ratio_l,"[-]")
if K<K_labda:
    print("viscous_effects_should_be_taken_into_account_in_the_dimensions")
if K>K_labda:
    print("The_assumption_to_neglect_the_viscous_hold_for_the_dimensions")

```

C.3.2. TOLERANCES JET INJECTOR

```

from math import *
import numpy as np
import matplotlib.pyplot as plt
#====FLOW PROPERTIES=====
rho_l=789.4 #kg/m^3
v=1.58348*10**-6 #m^2/s
mu_l=1.25*10**-3 #Pa s
sigma=22*10**-3 #n/m

#====DESIGN PARAMETERS=====
G=0.00056779 #kg/s
#dP=2.2*10**5 #Pa
#mu=0.3247
mu_g=18.13*10**-6 #kg/m^3 ambient
rho_a=1.225

dt=0.001 #time step

```

```

t=0.001 #start time
Ta=293 #ambient temp

#tollerentias
cd=0.0939
d0=0.8*10**(-3)
l=3.6*10**(-3)

l_d0_ratio=l/d0
dP=((4*G)/(cd*pi*d0**2))**2/(2*rho_l)
A=3.0+l_d0_ratio/3.6 #coefficient for spray angle
theta=2*np.rad2deg(atan((4*pi)/A*sqrt(rho_a/rho_l)*sqrt(3)/6))
j=d0/8 #lenght scale
U_l=sqrt(2*dP/rho_l)
We_fj=(rho_l*U_l**2*j)/sigma
SMD=We_fj**-0.74*133*j
print("Following parameter->")
print("outlet_diameter", d0*1000,"mm")
print("outlet_lenght", l*1000,"mm")
print("discharge_coeficient", cd,"[-]")
print("====_Results_====")
print("Pressure_drop:_",dP/100000,"bar")
print("Spray_angle:_",theta,"degrees")
print("SMD:_",SMD*1000000,"micrometer")
print("Injection_velocity:_",U_l,"m/s")

```


D

MIXING LOCATIONS

In this appendix the images are provided of the mixing locations for the different configuration at different initial pressures.

D.1. CONFIGURATION 1

Obtained results from the *left* image of [Figure D.1](#) : mixing distance is 48.6 mm from injector head and the spray angle of the swirl injector has a value of 70 degrees. Obtained results from the *right* image of [Figure D.1](#): mixing distance is 53.4 mm from injector head and the spray angle of the swirl injector has a value of 68 degrees.

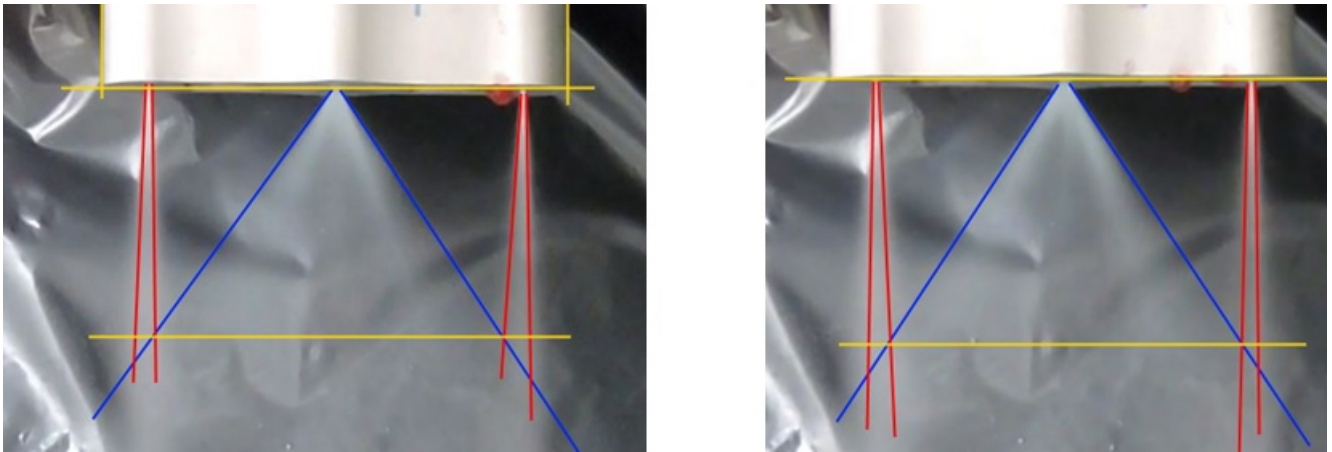


Figure D.1: Configuration 1 at an initial pressure of 3 bar

Obtained results from the *left* image of [Figure D.2](#) : mixing distance is 54.2 mm from injector head and the spray angle of the swirl injector has a value of 69 degrees. Obtained results from the *right* image of [Figure D.2](#): mixing distance is 50.1 mm from injector head and the spray angle of the swirl injector has a value of 73 degrees.

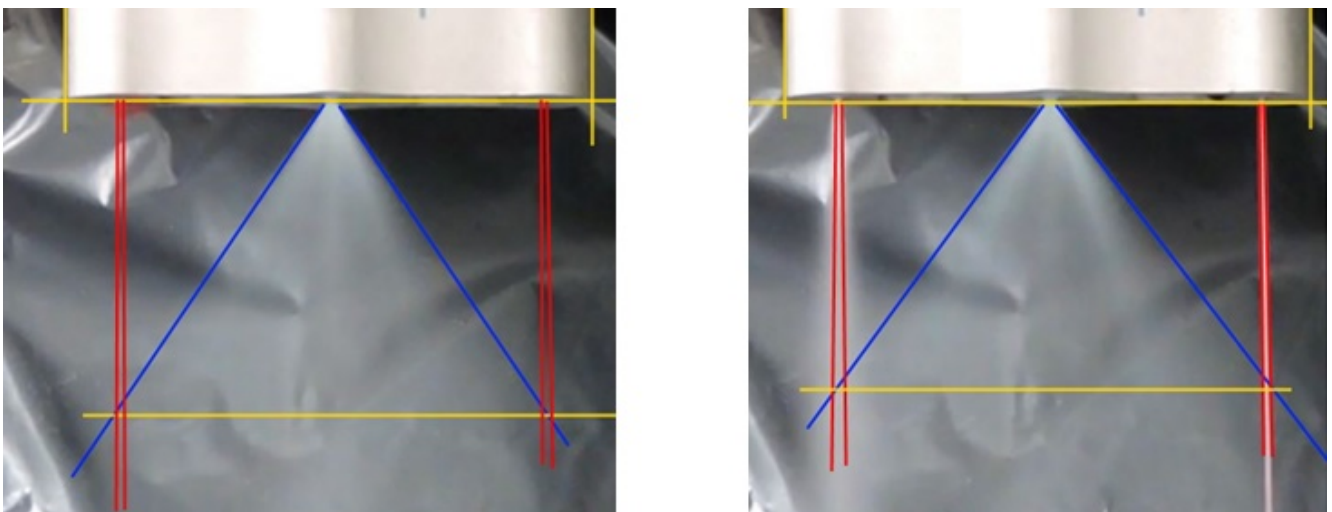


Figure D.2: Configuration 1 at an initial pressure of 5 bar

Obtained results from the *left* image of [Figure D.3](#) : mixing distance is 51.5 mm from injector head and the spray angle of the swirl injector has a value of 71 degrees. Obtained results from the *right* image of [Figure D.3](#): mixing distance is 49.6 mm from injector head and the spray angle of the swirl injector has a value of 72 degrees.

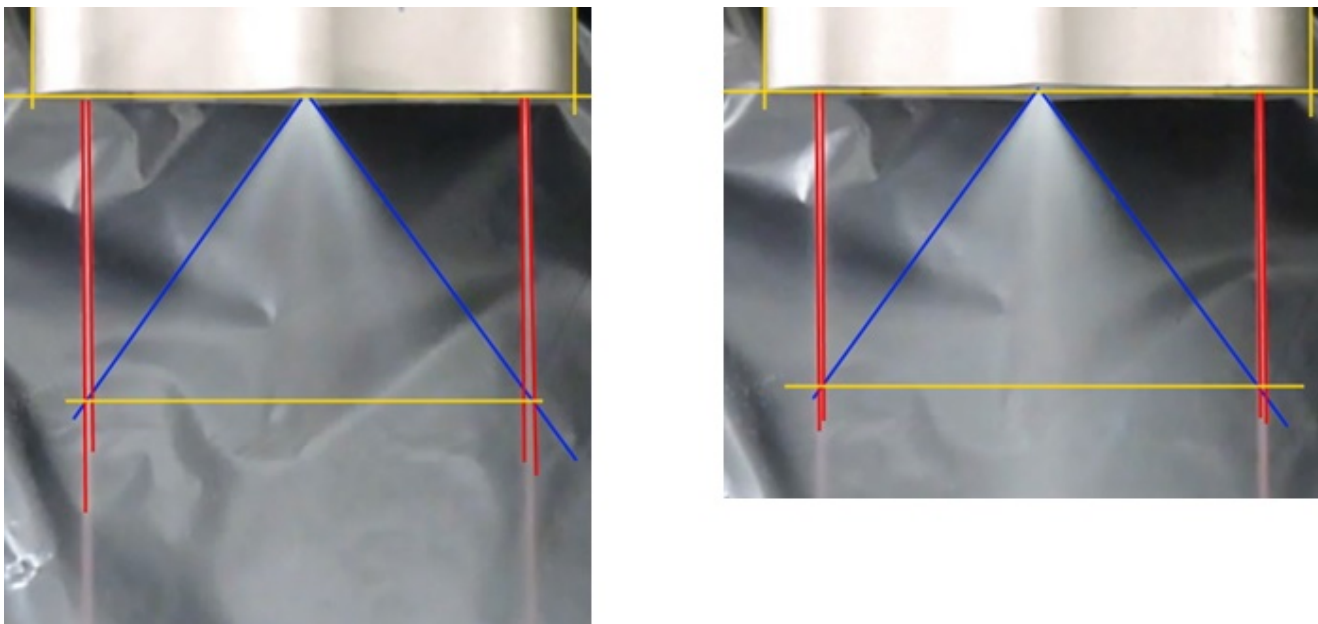


Figure D.3: Configuration 1 at an initial pressure of 7 bar

D.2. CONFIGURATION 2

Obtained results from the *left* image of [Figure D.4](#) : mixing distance is 49.7 mm from injector head and the spray angle of the swirl injector has a value of 72 degrees. Obtained results from the *right* image of [Figure D.4](#): mixing distance is 52.9 mm from injector head and the spray angle of the swirl injector has a value of 70 degrees.

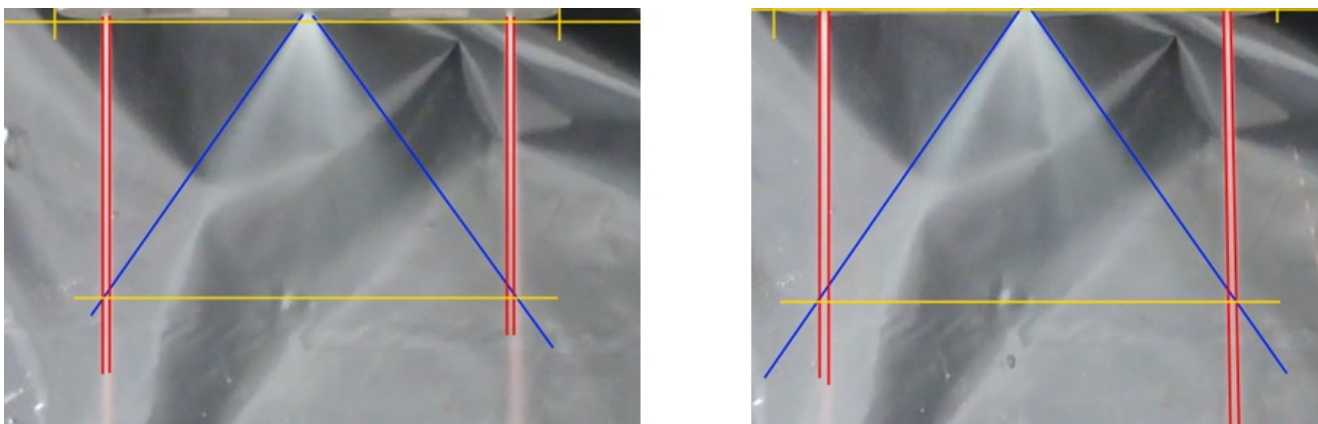


Figure D.4: Configuration 2 at an initial pressure of 3 bar

Obtained results from the *left* image of [Figure D.5](#) : mixing distance is 51.3 mm from injector head and the spray angle of the swirl injector has a value of 68 degrees. The middle red line located at the left of the jet injector indicates the symmetry line. Obtained results from the *right* image of [Figure D.5](#): mixing distance is 54.5 mm from injector head and the spray angle of the swirl injector has a value of 72 degrees.

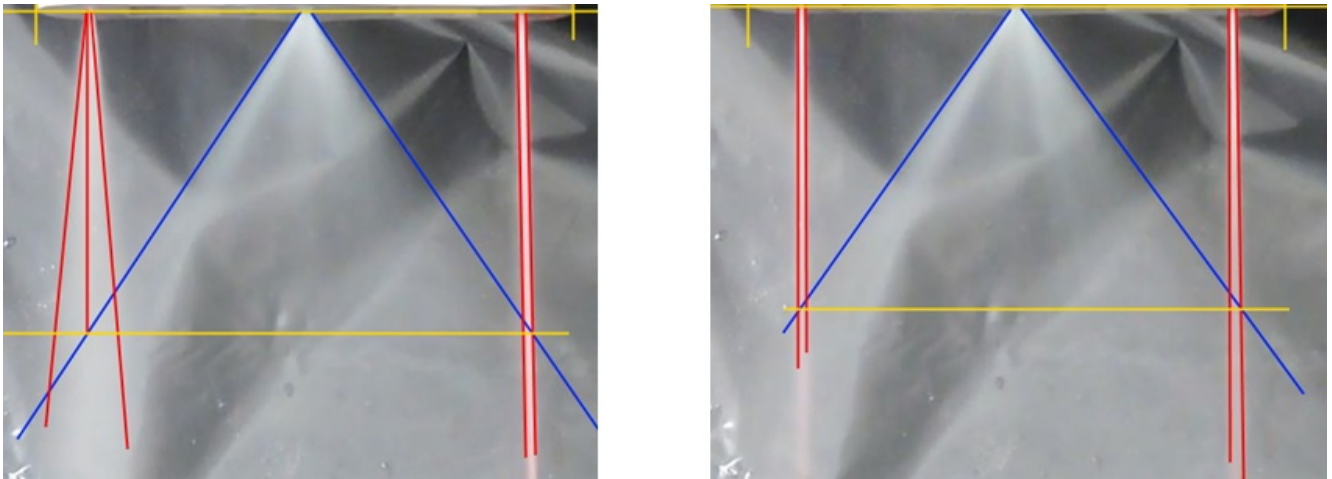


Figure D.5: Configuration 2 at an initial pressure of 5 bar

Obtained results from the *left* image of [Figure D.6](#) : mixing distance is 53.0 mm from injector head and the spray angle of the swirl injector has a value of 73 degrees. Obtained results from the *right* image of [Figure D.6](#): mixing distance is 50.5 mm from injector head and the spray angle of the swirl injector has a value of 66 degrees.

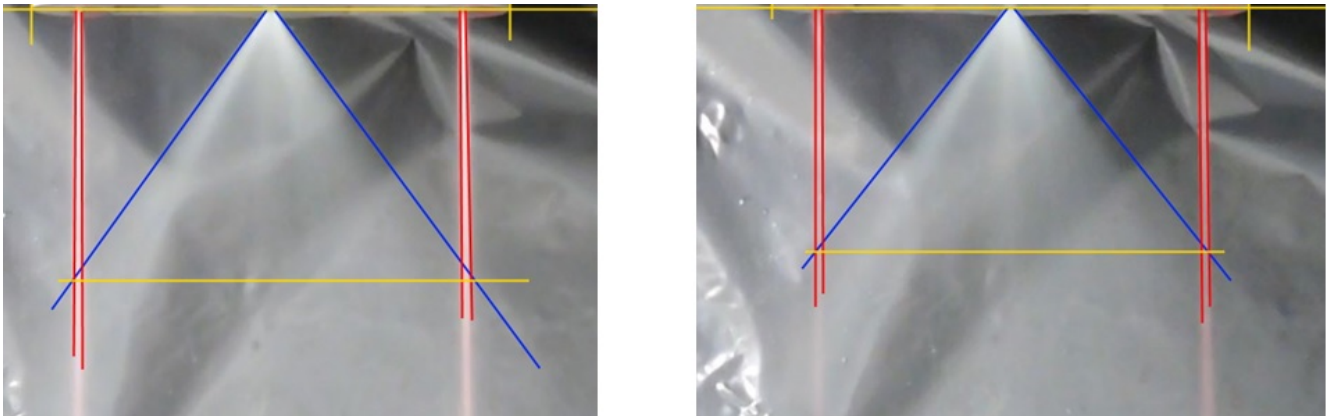


Figure D.6: configuration 2 at an initial pressure of 7 bar

D.3. CONFIGURATION 3

Obtained results from the *left* image of [Figure D.7](#) : mixing distance is 49.5 mm from injector head and the spray angle of the swirl injector has a value of 70 degrees. Obtained results from the *right* image of [Figure D.7](#): mixing distance is 54.0 mm from injector head and the spray angle of the swirl injector has a value of 68 degrees.

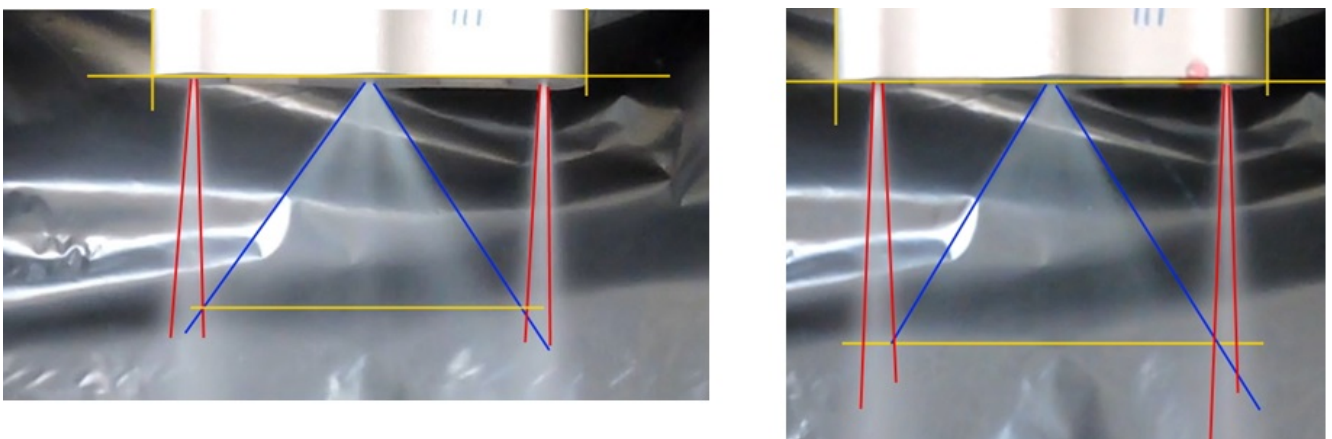


Figure D.7: Configuration 3 at an initial pressure of 3 bar

Obtained results from the *left* image of [Figure D.8](#) : mixing distance is 59.7 mm from injector head and the spray angle of the swirl injector has a value of 67 degrees. Obtained results from the *right* image of [Figure D.8](#): mixing distance is 57.7 mm from injector head and the spray angle of the swirl injector has a value of 67 degrees.

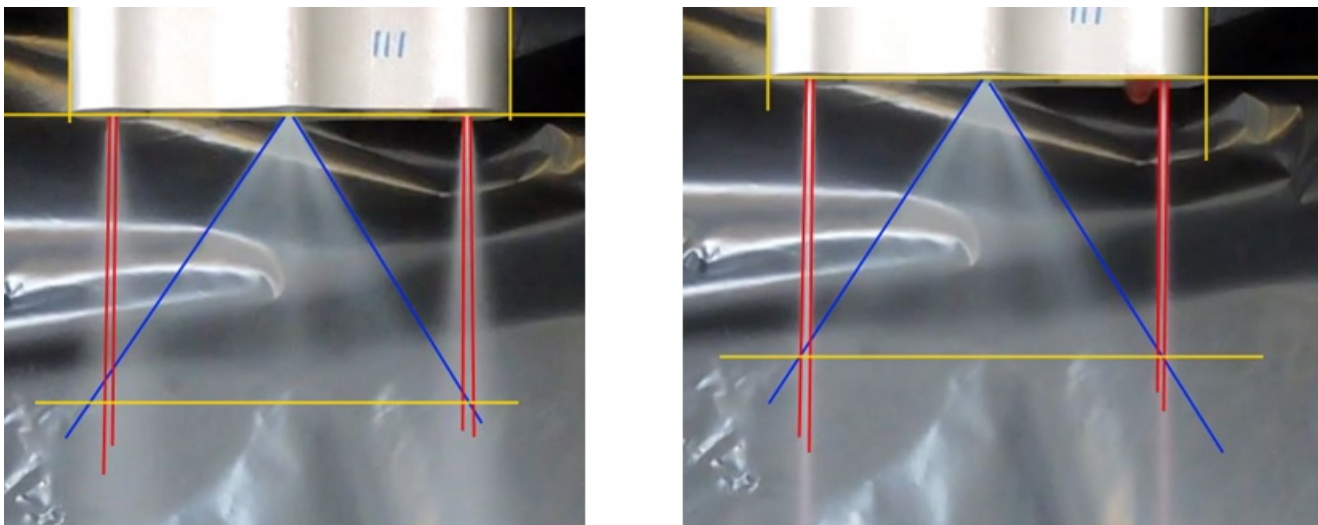


Figure D.8: Configuration 3 at an initial pressure of 5 bar

Obtained results from the *left* image of [Figure D.9](#) : mixing distance is 57.5 mm from injector head and the spray angle of the swirl injector has a value of 67 degrees. Obtained results from the *right* image of [Figure D.9](#): mixing distance is 57.5 mm from injector head and the spray angle of the swirl injector has a value of 67 degrees.

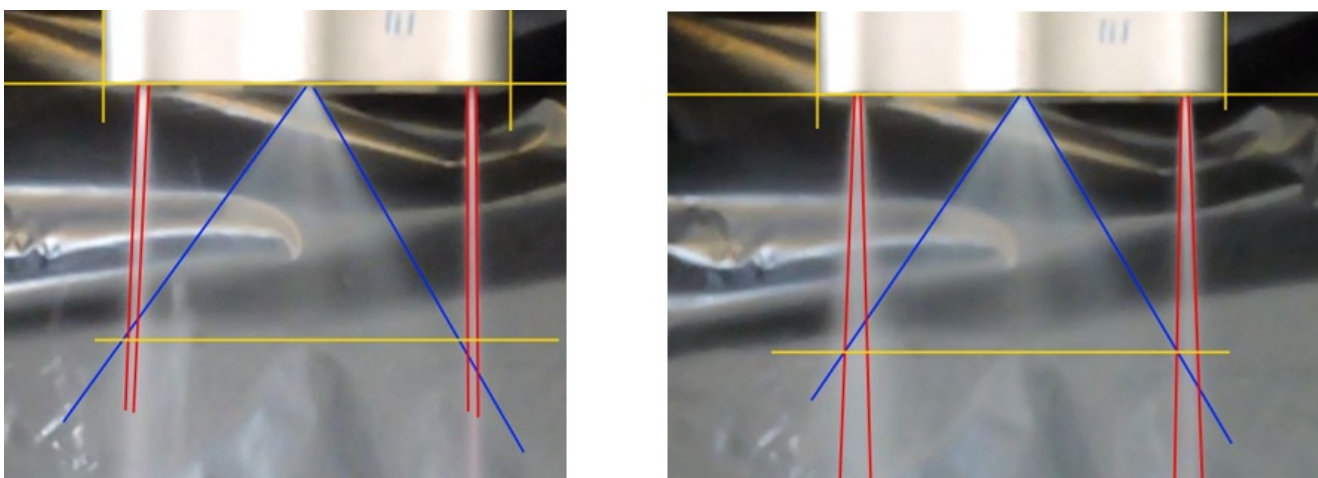


Figure D.9: Configuration 3 at an initial pressure of 7 bar

D.4. CONFIGURATION 4

Obtained results from the *left* image of [Figure D.10](#) : mixing distance is 44.7 mm from injector head and the spray angle of the swirl injector has a value of 73 degrees. Obtained results from the *right* image of [Figure D.10](#): mixing distance is 47.7 mm from injector head and the spray angle of the swirl injector has a value of 70 degrees.

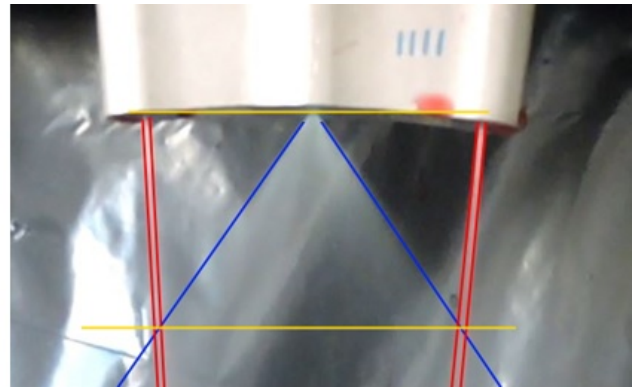
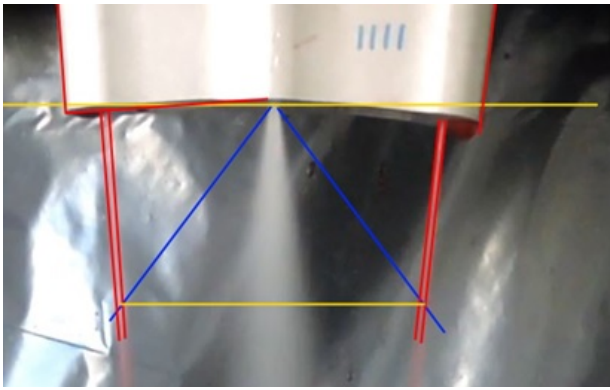


Figure D.10: Configuration 4 at an initial pressure of 3 bar

Obtained results from the *left* image of [Figure D.11](#) : mixing distance is 46.7 mm from injector head and the spray angle of the swirl injector has a value of 70 degrees. Obtained results from the *right* image of [Figure D.11](#): mixing distance is 45.7 mm from injector head and the spray angle of the swirl injector has a value of 70 degrees.

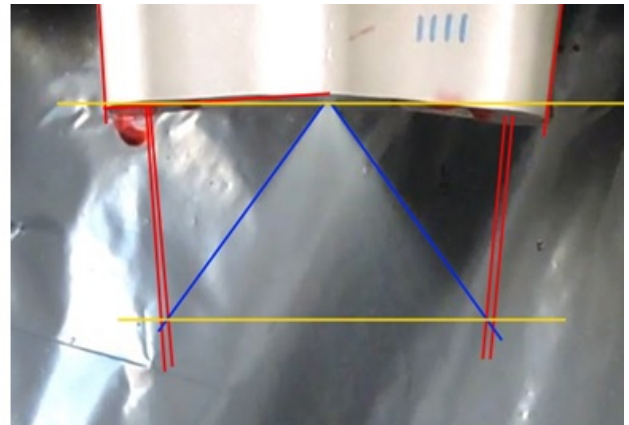
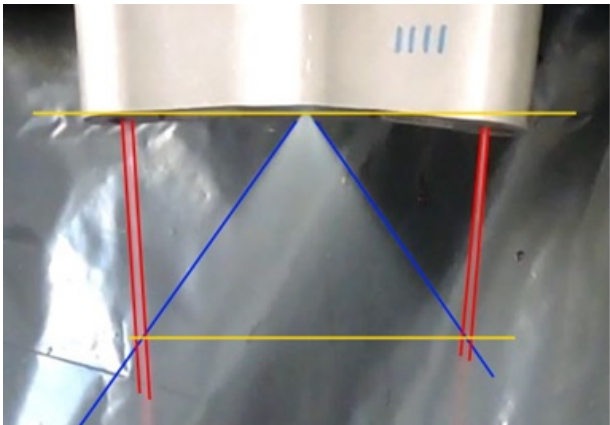


Figure D.11: Configuration 4 at an initial pressure of 5 bar

Obtained results from the *left* image of [Figure D.12](#) : mixing distance is 47.6 mm from injector head and the spray angle of the swirl injector has a value of 70 degrees. Obtained results from the *right* image of [Figure D.12](#): mixing distance is 47.6 mm from injector head and the spray angle of the swirl injector has a value of 70 degrees.

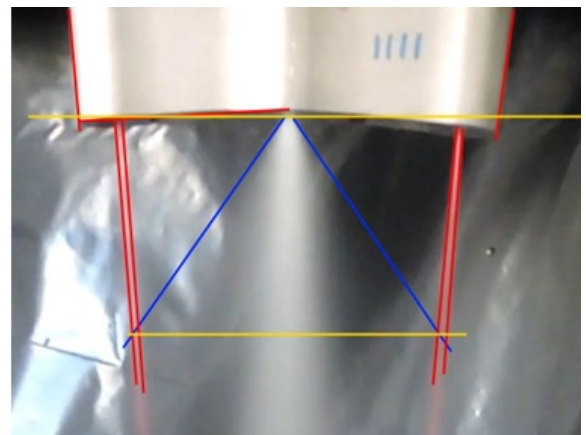
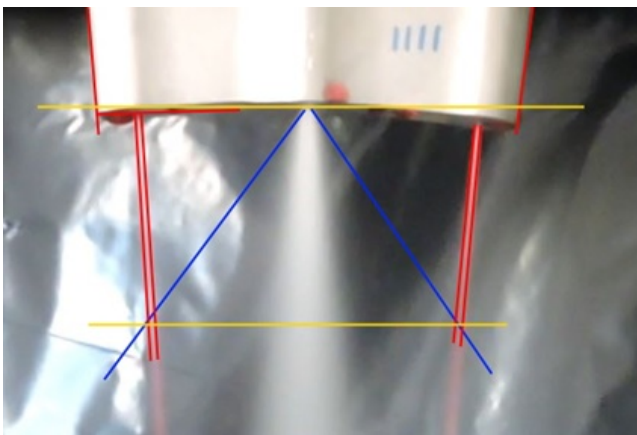


Figure D.12: Configuration 4 at an initial pressure of 7 bar

E

TEST PROCEDURES

1) PRESSURIZATION TEST SETUP

1. Check if **Compressed air/nitrogen valve 1 is closed**
2. Check if **Compressed air/nitrogen valve 2 is closed**
3. Check if H_2O_2 **valve is closed**
4. Check if **ETOH valve is closed**
5. Open supply line compressed air
6. listen for sissing sound that indicates a leakage
7. **Test setup is now pressurized**

2A) FILLING OPERATION H_2O_2 TANK

1. Check if **Compressed air/nitrogen valve 1 is closed**
2. Check if H_2O_2 **valve is closed**
3. Check pressure gauge to check if propellant tank is pressurized
4. **Open H_2O_2 valve** to depressurize the H_2O_2 tank
5. **Close H_2O_2 valve** to depressurize the H_2O_2 tank
6. Check pressure gauge to check if propellant tank is depressurized
7. **remove closing plug** of H_2O_2 tank
8. use syringe to fill the H_2O_2 tank
9. **insert closing plug** of H_2O_2 tank
10. check fitting closing plug
11. **Open Compressed air/nitrogen valve 1** to pressurize the H_2O_2 tank
12. H_2O_2 **Tank is now filled**

2B) FILLING OPERATION ETOH TANK

1. Check if **Compressed air/nitrogen valve 2 is closed**
2. Check if **ETOH valve is closed**
3. Check pressure gauge to check if propellant tank is pressurized
4. **Open ETOH valve** to depressurize the ETOH tank
5. **Close ETOH valve** to depressurize the ETOH tank
6. Check pressure gauge to check if propellant tank is depressurized
7. **remove closing plug** of ETOH tank
8. use syringe to fill the ETOH tank

9. **insert closing plug** of ETOH tank
10. check fitting closing plug
11. **Open Compressed air/nitrogen valve 2** to pressurize the ETO tank
12. **ETOH tank is now filled**

3A) CONDUCTING EXPERIMENT MONO PROPELLANT MODE

1. **Complete filling operation of H_2O_2 tank procedure**
2. check if **Compressed air/nitrogen valve 1** is **open**
3. set pressure regulator to desired pressure
4. check setting high speed camera
5. **Start** high speed camera
6. **Open H_2O_2 valve**
7. When propellant is depleted, **close H_2O_2 valve**
8. **Save** footage high speed camera

3B) CONDUCTING EXPERIMENT DUAL PROPELLANT MODE

1. **Complete filling operation of H_2O_2 tank and ETOH tank procedures**
2. check if **Compressed air/nitrogen valve 1** and **Compressed air/nitrogen valve 1** are **open**
3. set pressure regulators to desired pressure
4. check setting high speed camera
5. **Start** high speed camera
6. **Open H_2O_2 valve** and **Open ETOH valve**
7. When propellants are depleted, **close H_2O_2 valve** and **ETOH valve**
8. **Save** footage high speed camera

4) PURGING TEST SETUP

1. Complete filling procedures H_2O_2 tank and ETOH tank with deionized water
2. **Open H_2O_2 valve** and **Open ETOH valve**
3. check if the propellant tanks with deionized water is depleted
4. **Close H_2O_2 valve** and **Close ETOH valve**
5. repeat above steps 3 times
6. Dry test setup with nitrogen

5) DEPRESSURIZE TEST SETUP

1. Check if **Compressed air/nitrogen valve 1** is **closed**
2. Check if **Compressed air/nitrogen valve 2** is **closed**
3. Check if **H_2O_2 valve** is **closed**
4. Check if **ETOH valve** is **closed**
5. Close supply line compressed air

6. **Open Compressed air/nitrogen valve 1**
7. **Open Compressed air/nitrogen valve 2**
8. **Open H_2O_2 valve**
9. **Open ETOH valve**
10. check pressure gauges if test setup is depressurized
11. **Close Compressed air/nitrogen valve 1**
12. **Close Compressed air/nitrogen valve 2**
13. **Close H_2O_2 valve**
14. **Close ETOH valve**
15. **Test setup is now depressurized**

EMERGENCY PROCEDURES - TANKS CANNOT BE DEPRESSURIZED

Two possible options can be used to depressurize the propellant tanks:

1. Closing plug located in "T-joint" between the pressure regulator and pressure gauge
2. Closing plug located at the propellant tanks

EMERGENCY PROCEDURES - CHEMICAL SPILLAGE

1. Use deionized water to dilute the chemical spillage
2. Use paper towel to absorb the diluted chemical spillage

F

OVERVIEW CONDUCTED EXPERIMENTS

In this appendix an overview of the conducted experiments are provided, categorized for the different test objectives.

F.1. ATOMAZATION BEHAVIOUR

Deionized water was used to study the atomization behavior for the different injector configurations at an initial tank pressure of 3 bar. For the majority of the experiments, the high-speed camera is set to a frame rate of 67500 frames per second (fps). For some experiments, this frame rate is reduced to 6400 fps to observe the general aspects of the atomization process. This reduction in frame rate is specified in the column "Notes". In this column it is also specified where the spray patterns are studied. See [Table E1](#), for the overview of the conducted experiments.

Table E1: Overview of the conducted experiments to study the atomization behaviour

Test ID	Configuration	Injector	Notes
1	1	swirl	frame rate adjusted to 6400 fps
2	1	swirl	frame rate adjusted to 6400 fps
3	1	swirl	spray pattern is studied
4	1	swirl	spray pattern is studied
5	2	swirl	spray pattern is studied
6	2	swirl	spray pattern is studied
7	3	swirl	spray pattern is studied
8	3	swirl	spray pattern is studied
9	4	swirl	spray pattern is studied
10	4	swirl	spray pattern is studied
11	4	jet	frame rate adjusted to 6400 fps
12	4	jet	frame rate adjusted to 6400 fps
13	1	jet	spray pattern is studied
14	1	jet	spray pattern is studied
15	2	jet	spray pattern is studied
16	2	jet	spray pattern is studied
17	3	jet	spray pattern is studied
18	3	jet	spray pattern is studied
19	4	jet	spray pattern is studied
20	4	jet	spray pattern is studied

F.2. ATOMIZATION PERFORMANCE

In this section the overview of the conducted experiments are provided in [Table F2](#). The high-speed camera is set to a frame rate of 67500 fps for all the conducted experiments associated to the performance study.

Table F2: Overview of the conducted experiments to study the atomization behaviour

Test ID	Working liquid	Tank pressure [bar]	Configuration	Injector
21	Hydrogen peroxide	3	4	swirl
22	Hydrogen peroxide	3	4	swirl
23	Hydrogen peroxide	7	4	swirl
24	Hydrogen peroxide	7	4	swirl
25	Ethanol	3	1	jet
26	Ethanol	3	1	jet
27	Ethanol	3	2	jet
28	Ethanol	3	2	jet
29	Ethanol	3	3	jet
30	Ethanol	3	3	jet
31	Ethanol	3	4	jet
32	Ethanol	3	4	jet
33	Ethanol	7	2	jet
34	Ethanol	7	2	jet

F.3. MIXING PROCESS

Dionized water was used to study the mixing process between the atomized flow of the jet and swirl injectors. The P600 Nikon camera was used to study location where the mixing process occurs. Deionized water was used as a working liquid. In the column "Notes" it is specified where the timing of opening the ball valves were incorrect, as explained in [Chapter 7](#). The overview of the conducted experiments is provided in [Table F5](#).

Table F3: Overview of the conducted experiments to study the mixing process

Test ID	Tank pressure [bar]	Configuration	Notes
35	3	1	
36	3	1	
37	3	2	faulty timing
38	3	2	
39	3	3	
40	3	3	
41	3	4	faulty timing
42	3	4	faulty timing
43	5	1	
44	5	1	
45	5	2	
46	5	2	

Table E4: Overview of the conducted experiments to study the mixing process continued

Test ID	Tank pressure [bar]	Configuration	Notes
47	5	3	faulty timing
48	5	3	
49	5	4	
50	5	4	faulty timing
51	7	1	
52	7	1	
53	7	2	
54	7	2	
55	7	3	
56	7	3	
57	7	4	faulty timing
58	7	4	faulty timing

The mixing process is also studied with a high-speed camera with a frame rate of 76500 fps, after studying the location of the mixing process. See [Table E5](#) for an overview of the used configurations and initial tank pressures to conduct these experiments.

Table E5: Overview of the conducted experiments to study the mixing process with the high-speed camera

Test ID	Tank pressure [bar]	Configuration
59	3	2
60	3	2
61	3	4
62	3	4
63	5	2
64	5	2
65	5	4
66	5	4
67	7	2
68	7	2
69	7	4
70	7	4

F.4. HEATING ELEMENT

Deionized water which is supplied to the fourth injector configuration with an initial tank pressure of 5 bar. The interaction with the heating element is filmed with a high-speed camera with a frame rate of 6400 fps. In the column "Notes" the used configuration of the heating elements are discussed. When applicable, the used current level is also included in this column. See [Table F6](#) for the overview of the conducted experiments.

Table F6: Overview of the conducted experiments to study the interaction between the atomized flow and heating element

Test ID	Injector	Notes
71	swirl	heating element configuration 1 for mono mode
72	swirl	heating element configuration 1 for mono mode
73	swirl	heating element configuration 2 for mono mode
74	swirl	heating element configuration 2 for mono mode
75	swirl	heating element configuration 3 for mono mode
76	swirl	heating element configuration 3 for mono mode
77	jet + swirl	heating element configuration 1 for bi-propellant mode
78	jet + swirl	heating element configuration 1 for bi-propellant mode
79	jet + swirl	heating element configuration 2 for bi-propellant mode
80	jet + swirl	heating element configuration 2 for bi-propellant mode
81	jet + swirl	heating element configuration 3 for bi-propellant mode
82	jet + swirl	heating element configuration 3 for bi-propellant mode
83	jet + swirl	heating element configuration 3 at a current of 1.5 A
84	jet + swirl	heating element configuration 3 at a current of 1.5 A
85	jet + swirl	heating element configuration 3 at a current of 2.0 A
86	jet + swirl	heating element configuration 3 at a current of 2.0 A
87	jet + swirl	heating element configuration 3 at a current of 2.5 A
88	jet + swirl	heating element configuration 3 at a current of 2.5 A
89	jet + swirl	heating element configuration 3 at a current of 3.0 A
90	jet + swirl	heating element configuration 3 at a current of 3.0 A